Supramolecular aspects, ion recognitions, metal complexes and antimalarial activity of quinoline derivatives

A Dissertation submitted to the

Indian Institute of Technology Guwahati as

partial fulfillment for the Degree of

Doctor of Philosophy in Chemistry

Submitted by

Prithiviraj Khakhlary

Department of Chemistry

Indian Institute of Technology Guwahati

August 2015

Supramolecular aspects, ion recognitions, metal complexes and antimalarial activity of quinoline derivatives

A Dissertation submitted to the
Indian Institute of Technology Guwahati as
partial fulfillment for the Degree of
Doctor of Philosophy in Chemistry

Submitted by

Prithiviraj Khakhlary

Department of Chemistry

Indian Institute of Technology Guwahati

August 2015

Dedicated to My Family

&

Friends…

Statement

I hereby declare that this thesis entitled "**Supramolecular aspects, ion recognitions, metal complexes and antimalarial activity of quinoline derivatives**" is the outcome of research work carried out by me under the supervision of Prof. Jubaraj B. Baruah, at the Department of Chemistry, Indian Institute of Technology Guwahati, India.

In keeping with the general practice of reporting scientific observations, due acknowledgement has been made whenever work described here has been based on the findings of other investigators.

IIT Guwahati
August, 2015

Prithiviraj Khakhlary

Certificate

This is to certify that Prithiviraj Khakhlary has been working under my supervision since August, 2010 as a regular registered Ph. D. student. I am forwarding his thesis entitled "**Supramolecular aspects, ion recognitions, metal complexes and antimalarial activity of quinoline derivatives**" being submitted for the Ph. D. (Science) Degree of this Institute.

I certify that he has fulfilled all the requirements according to the rules of this institute regarding the investigations embodied in his thesis and this work has not been submitted elsewhere for a degree.

IIT Guwahati
August, 2015

Prof. Jubaraj B. Baruah

Acknowledgements

This thesis might not have seen through its completion unless I had the support and encouragement of numerous people around me. Today, when I bring it to an end, I would like to express few words of appreciation to the people who actually made this thesis a reality and an unforgettable experience for me.

First and foremost, with a deepest sense of gratitude, I wish to express my sincere thanks to my supervisors, Prof. Jubaraj B. Baruah whose timely help during my crucial phase of my career has made possible to achieve this target. The enlightening experience of doing science under his guidance can hardly be described in words. The numerous discussions and interactions I had with him expanded my horizons to hitherto unknown frontiers of science and knowledge. I am indebt to this wonderful person for all that he has given me and above all for motivating me towards scientific research. My everlasting gratitude goes towards him.

I would like to thank Prof. Annie K. Powel of Karlsruhe Institute of Technology, Germany for magnetic measurements and Dr. Robyn Lynne van Zyl of Faculty of Health Sciences; WITS Research Institute for Malaria, University of the Witwatersrand, South Africa for antimalaria studies which are included in this thesis.

I would like to acknowledge my sincere gratitude to all my doctoral committee members for their insightful advices and valuable suggestions. I am also grateful to the entire faculty and staff in the Department of Chemistry, Indian Institute of Technology Guwahati for providing a wonderful work atmosphere throughout this period.

I would like to thank my lab mates Dr. W. Marjit Singh, Dr. Rupam Sarma, Dr. Devendra Singh, Dr. Dipjyoti Kalita, Dr. Babulal Das, Dr. Bhaskar Nath, Dr. Bigyan R. Jali, Jayanta, Nithi, Krapa, and Arup whom I had an opportunity to work with. No words can express my thankfulness for giving me their time and companionship, which made the time spent in the laboratory and outside pleasant and memorable. I would like to give my special thanks to my friends Kalpada, Mrinalda, Pojulda, Yova, Bhupen, Veihotelou, Biju, Soumik, Pronob, Dipankar, Parash, Probinda, Monuj and all my

batch mates for their timely help, support and for the wonderful time we shared during this period.

The financial support from University grant commission (UGC), New Delhi for the research fellowship is duly acknowledged.

I would also like to acknowledge all my teachers for their love and blessings and motivation.

Finally, my Ph. D. endeavor could not be completed without the endless love, unending support, tolerance and blessings from my parents and my sister. They are the main soul and inspiration for each and every step that I achieve in my life.

Prithiviraj Khakhlary

Preview

This thesis deals with studies on synthesis, characterization, metal complexes, ion/s recognition properties and antimalaria activity of quinoline derivatives. The content of the thesis is divided into six chapters.

A general introduction to various aspects of quinoline derivatives in pharmaceutical applications, molecular/ion recognition properties and metal complexes of quinoline derivatives are discussed in chapter 1. This includes a brief discussion on their pharmaceutical applications and supramolecular aspects. The selective recognition of various types of molecular/ion by quinoline derivatives are discussed in this chapter. Further, various metal complexes of quinoline derivatives are included. In the later part of this chapter scope of the work is presented based on the discussions of earlier results.

Chapter 2 of the thesis discuses various aspects of synthesis, characterization and properties of Zinc (II), Manganese (II) and Cobalt (II) 8-oxyquinolate cluster. The work presented in this chapter also includes magnetic properties of cobalt and manganese 8-oxyquinolate clusters.
The reactions of zinc halides with 8-hydroxyquinoline (hydroxQ) in equi-molar ratio were carried out in different solvents. Respective solvates of tetra nuclear complexes of zinc-oxyquinolate were obtained as shown in Scheme 1.1. The reaction used for synthesis of these complexes (**2.1-2.4)** is given in Equation 1.1.

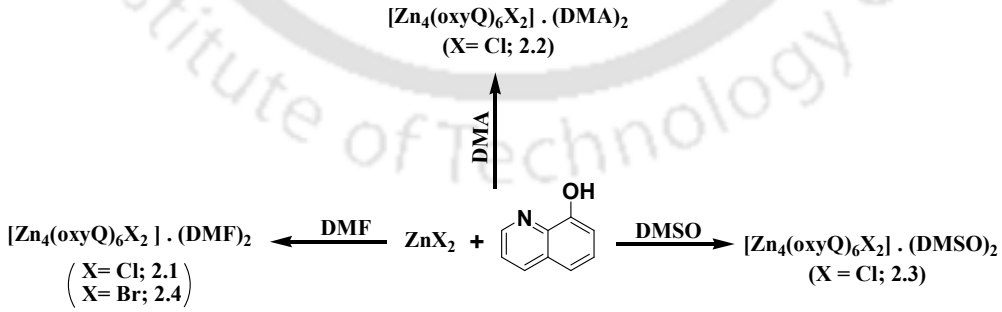

Scheme 1.1: Synthesis of zinc complexes **2.1**, **2.2, 2.3** and **2.4.**

$$6\text{hydroxQ} + 6ZnX_2 + 2\ \text{solvent} \rightarrow [Zn_4(oxyQ)_6X_2].(\text{solvent})_2 + 2H_2[ZnX_4] + 2HX \quad \ldots\ldots(1.1)$$

X = Cl, Br.

From the crystal structure it is clear that the clusters **2.1-2.4** are isostructural and in each complex, zinc ions are in two different types of environments (Figure 1.1). Zinc centers holding halide ions are penta coordinated while the other centers are hexa coordinated.

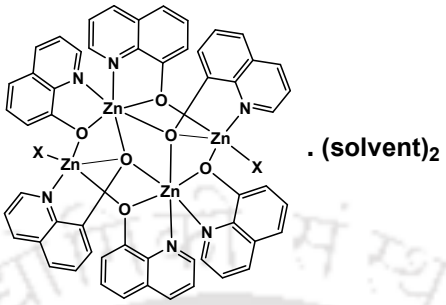

Where X = Cl or Br, solvent = DMF, DMA or DMSO.

Figure 1.1: Tetranuclear zinc-8-oxyquinolate complex.

These complexes can be used for reversible uptake of moisture. For example, de-solvated complex **2.1**, on standing under ordinary atmospheric condition at room temperature, slowly absorbs moisture to yield hydrated form. The anhydrous form was regenerated upon heating the hydrated sample. Since, reversible adsorption of water was observed by these complexes, the surface area of the complexes **2.1** and **2.4** were determined. Surface areas of complex **2.1** and complex **2.4** are 8.933m²/g and 6.172 m²/g respectively.

Use of aqueous solvent in the reaction of zinc chloride with 8-hydroxyquinoline did not yield the corresponding hydrated tetranuclear zinc-8-oxyquinolate complex, however yielded a tetra-chlorozinc complex and it was formed through a disproportionation reaction as illustrated in Equation 1.2.

$$2\ \text{hydroxQ} + 2ZnCl_2 + 2H_2O \rightarrow (\text{HhydroxQ})_2[ZnCl_4] + Zn(OH)_2 \ldots\ldots (1.2)$$

From this reaction $(\text{HhydroxQ})_2[ZnCl_4]$ (**2.5**) was isolated and characterized by determining crystal structure (Figure 1.2a). This mono nuclear complex has hydroxyquinolinium cation. Advantage of this reaction was taken to prepare a composite material consists of zinc oxide with complex **2.5**. Fluorescence emissions of these complexes have been detailed in this chapter. The reaction of 8-hydroxyquinoline with zinc halide was affected by methylpyridine ligand. A molecular complex $[Zn(oxyQ)_2(3mepy)].[Zn(oxyQ)_2(3mepy)_2].3H_2O$ (Where 3mepy = 3-methylpyridine) (**2.6**) was obtained from the reaction of 8-hydroxyquinoline with zinc chloride

in the presence of 3-methylpyridine. The two neutral components of this molecular complex were found to be devoid of chloride ion (Figure 1.2b).

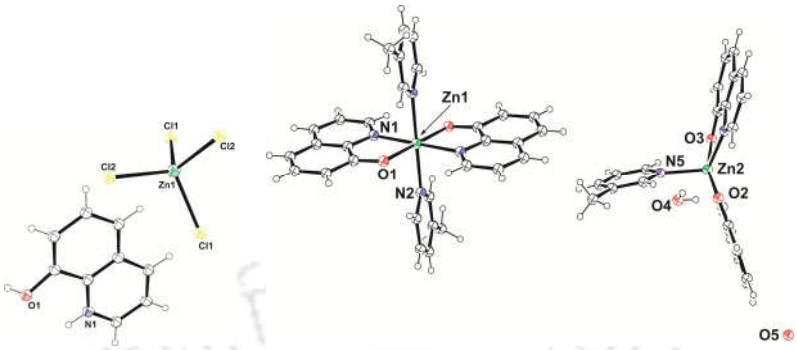

(a) (b)

Figure 1.2: (a) Structure of complex **2.5** and (b) Structure of molecular complex **2.6** (ORTEP drawn with 35 % probability).

This molecular complex is comprised of two mono nuclear complexes $[Zn(oxyQ)_2(3mepy)]$ and $[Zn(oxyQ)_2(3mepy)_2]$. The five coordinated complex adopts a distorted square pyramid structure, whereas the six coordinated has a distorted octahedral geometry around zinc ion.

Tetra nuclear 8-oxyquinolate cobalt (II) or manganese (II) complexes were prepared by the reaction of 8-hydroxyquinoline with their respective metal salts (Scheme 1.2). The results obtained from reactions of 8-hydroxyquioline with mercury and lead are compared.

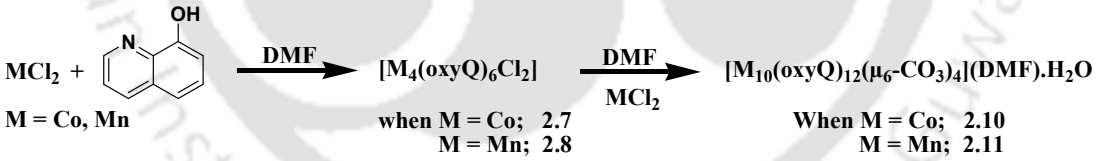

Scheme 1.2: Synthesis of tetra nuclear and deca nuclear cobalt and manganese clusters.

These tetra nuclear complexes under solvothermal condition further react with cobalt (II) chloride or manganese (II) chloride respectively in dimethylformamide to give their respective deca nuclear cluster having a composition $[M_{10}(oxyQ)_{12}(\mu_6\text{-}CO_3)_4](DMF).H_2O$. The deca nuclear clusters were formed by inclusion of carbonate ions that formed *in situ*. Carbonate ligands in the cluster are discerned by spectroscopic tools in addition to X-ray structure determination. Structure of the cobalt deca nuclear cluster (**2.10**) is shown in Figure 1.3a. Coordination environments showing core of metal ions in the crystal structure of **2.10** is shown in figure 1.3b.

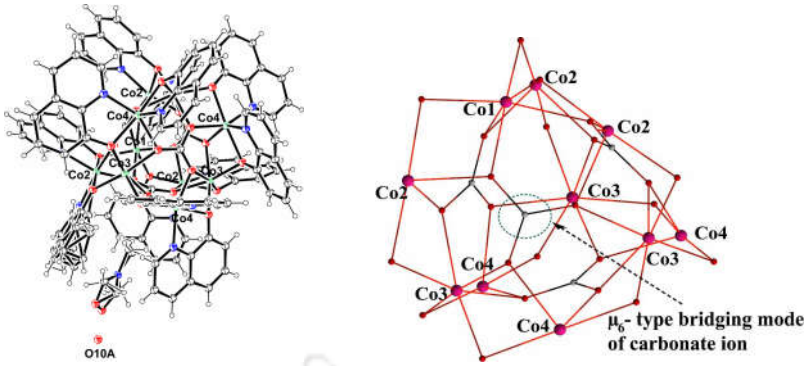

(a) (b)

Figure 1.3: (a) Structure of cluster **2.10** (drawn with 35 % thermal ellipsoids). (b) Core of deca nuclear cobalt cluster (quinoline rings are not shown for clarity of the structure).

Deca nuclear clusters contain four carbonate anions each acts as μ_6-bridge to connect six metal ions. Two sets of cobalt ions on the basis of coordination are observed; one set is in N2O4 type of hexa coordinated environment and the other one is in O6 type of octahedral environment as in this set, five cobalt ions linked to three oxygen atoms of bridging carbonates and three oxygen atoms of bridging oxyquinolates. Magnetochemistry of these clusters (**2.7**, **2.10** and **2.11**) show antiferromagnetic coupling between the metal centers.

In chapter 3 of the thesis synthesis, characterization, anion-π interactions and selective ions recognition by a nitroso derivative of 8-hydroxyquinoline **3.1**, are presented. Relevance of anion-π interactions in chloride (**3.2**), bromide (**3.3**), perchlorate (**3.4**) and nitrate (**3.5**) salts of 5-(hydroxyimino)quinolin-8-one are discussed.

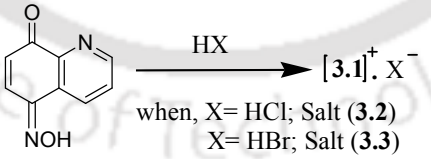

3.1

when, X= HCl; Salt (**3.2**)
X= HBr; Salt (**3.3**)
X= $HClO_4$; Salt (**3.4**)
X= HNO_3; Salt (**3.5**)

Scheme 1.3: Synthesis of the salts **3.2-3.5**.

The crystal structures of salt **3.2** and salt **3.3** are isostructural; halide ions are sandwiched between two planar aromatic rings of the cations. Distance between anion and centroid of π-cloud of cation in the salt **3.2** and salt **3.3** are 3.374 Å and 3.465 Å respectively. These distances

are within permissible distances for chloride-π interactions. Perchlorate salt **3.4** has a layer like structure in which perchlorate ions are held on top of π-cloud of cations. Anions are at suitable distance to have anion-π interactions. Distance between oxygen atom and centroid of π-cloud on cation is 3.253Å, suggests a separation conducive for anion-π interaction.

Structures of nitrate salt of 5-aminoquinoline **3.6,** 4-hydroxyquinazoline **3.7** and that of 8-hydroxyquinoline **3.8** are compared with nitrate salt **3.5**. Two arrangements of nitrate anions with respect to cations are discerned. Nitrate anions are sandwiched between aromatic planes of cations in nitrate salts of **3.1** or 4-hydroxyquinazoline; whereas nitrate anions are oblique with respect to aromatic plane of counter cation in nitrate salts of **3.1** and 5-aminoquinoline (Figure 1.4).

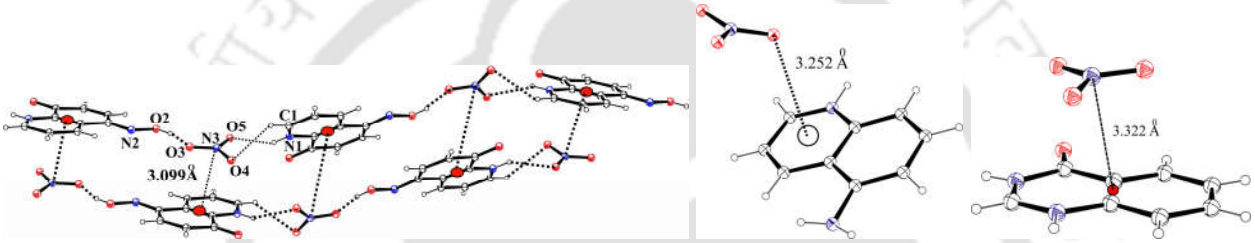

(a) (b) (c)

Figure 1.4: Anion-π interactions in (a) nitrate salts **3.5** (b) 5-aminoquinolinium nitrate (**3.6**) and (c) 4-hydroxyquinazolinium nitrate (**3.7**) salts.

They appear in different planes from cations and distance between centroid of anion and cation is 3.099 Å which is shorter than the conventional anion-π distances.

A solution study based on changes in by UV-visible absorptions caused by the adding various acids to **3.1** was carried out to determine binding constants. Magnitudes of binding constants for salts follow order **3.4 > 3.3 > 3.5 >> 3.2**. A critical examination based on binding constants of a series of nitrate salts have shown that in solution anion-π interactions are too weak to show a distinction in binding constants due to large electrostatic interactions contributing to the salts.

However, it was found that the fluoride ions have extra ability to cause color change to a solution of **3.1** in dimethylsulphoxide which is not caused by ions other than acetate ions. Thus such color changes enabled to detect fluoride ions visually in absence of acetate ions over other ions. An increase of the absorption in the spectra at 437 nm with an appearance of a new absorption at 640 nm occurs on addition of a solution tetra butyl ammonium fluoride (TBAF) in DMSO (Figure

1.5a, 1.5b) to a solution of **3.1** was observed. This change passes through an isobestic point 356 nm showing one to one transformation between the two species.

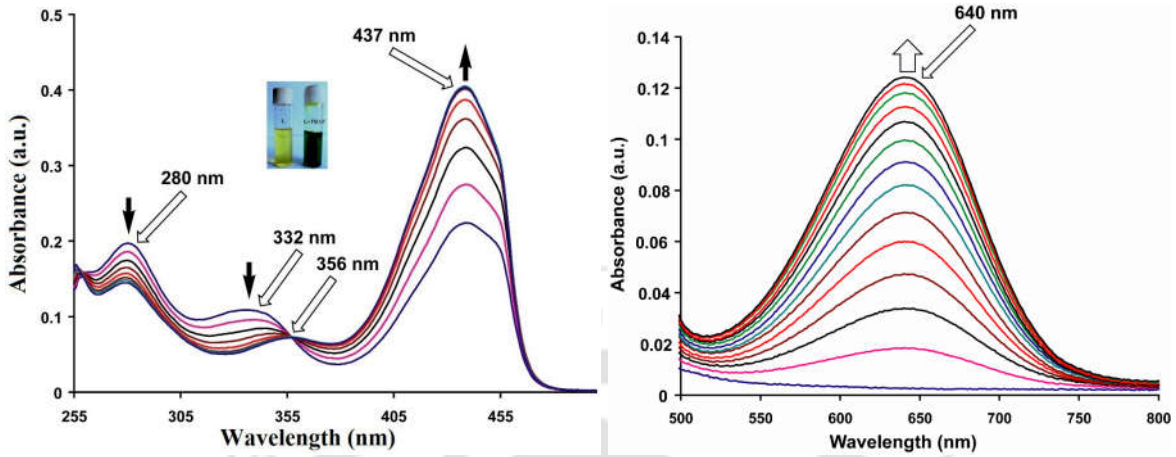

(a) (b)

Figure 1.5: (a) Changes in UV-visible spectra of compound **3.1** (10^{-5} M in DMSO) on addition of TBAF (0.1 to 1 equivalent from TBAF 10^{-4} M stock solution) in 250-500 nm region (inset is photographs of solutions of **3.1** in the absence and presence of TBAF) and (b) changes in absorption in 500-800 nm region of **3.1** (10^{-4} M in DMSO) on addition of TBAF (10^{-3} M in DMSO).

The fluoride ion quenches the fluorescence emission of **3.1**. However, no such changes were observed on addition of other ions such as chloride, bromide, iodide, nitrate, bisulphate and perchlorate, showing the specificity of **3.1** for fluoride ions. Moreover, discussion on the changes in visible spectra of the compound **3.1** on addition of zinc ions is included in the chapter. Similarly a host-guest complex (**3.9**) of tetra butyl ammonium fluoride with **3.1** was prepared and characterized. To discern the intermediate complex involved in this study zinc complex was used as model compound for studying interaction of fluorides is also presented in the chapter.

The Synthesis, characterization and structural study of polymorphs and salts of 4-nitro-N-(quinolin-8-yl)benzamide are discussed in Chapter 4. The polymorphs of 4-nitro-N-(quinolin-8-yl)benzamide (**4.1**) were obtained from crystallization in different solvents as shown in scheme 1.4.

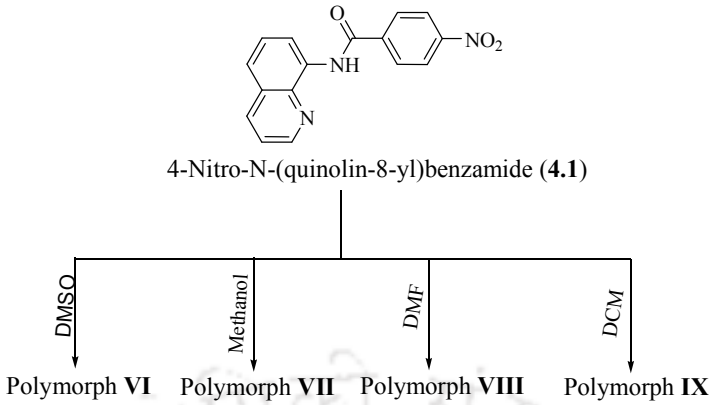

Scheme 1.4: Synthesis of polymorphs of **4.1**.

4-Nitro-N-(quinolin-8-yl)benzamide (**4.1**) adopts different conformers in neutral or protonated form of which may be guided by solvents or anions as illustrated in the Figure 1.6. In neutral form stabilization of any such conformer would lead to polymorph. Four polymorphs namely Polymorph **VI**, Polymorph **VII**, polymorph **VIII**, polymorph **IX** and a concomitant of polymorph **VIII** and **IX** were obtained by crystalllisation of **4.1** from DMSO, methanol, DMF, DCM and solvent mixture of *tert*-butanol and dimethylformamide respectively.

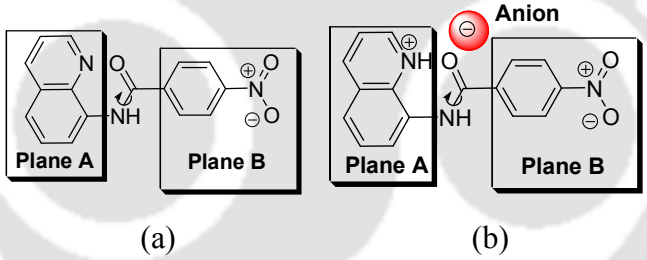

Figure 1.6: (a) The two aromatic planes in the **4.1** and (b) The salts of **4.1**, showing that the position of an anion can influence the torsion angle of protonated **4.1**.

The polymorph **VII** crystallizes in the monoclinic space group $P2_1/c$ with $Z = 4$. It has a chain like structure having $R^2_2(10)$ type of hydrogen bond motifs. The polymorph **VIII** belongs to monoclinic space group $P2_1/c$ with $Z= 4$. This polymorph forms head to tail chains and one of the oxygen atoms of the nitro group is involved in C-H···O interactions to yield a layered structure. Both the aromatic rings namely, the phenyl and the quinoline rings are nearly parallel to each other and they are placed within the proximity favorable to have π···π interactions. The crystals of polymorph **IX** belong to monoclinic *Cc* space group, it has $Z = 4$. The packing

pattern of polymorphs **VII** and **IX** are almost identical having double chain type structure. In terms of packing, the polymorph **IX** has a single chain structure, devoid of stacking. It also has a double chain structure but the position of the molecules in the lattice makes the difference. These interactions in **IX** result in the formation of $R^2_2(10)$ motifs (Figure 1.7). All the aromatic rings positioned on the one side of the chain are similar. Thus, it gives rise to an one dimensional chain like structure which is extended through $R^2_2(10)$ hydrogen bond motifs.

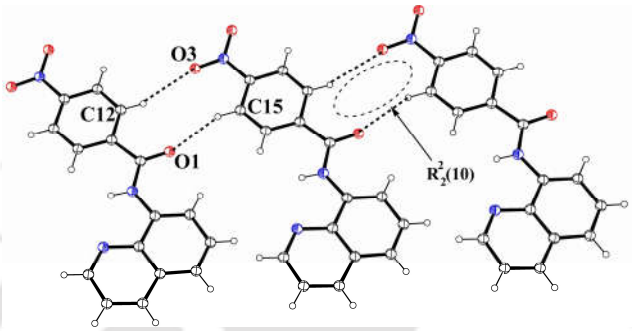

Figure 1.7: Packing pattern in polymorph **IX** with extended $R^2_2(10)$ cyclic hydrogen bonding (drawn in 35% ellipsoid).

The concomitant polymorph comprising of the polymorphs **VIII** and **IX** are obtained from a mixed solvent system of *tert*-butanol and DMF. Each solvent has different ability to interact with the nitro group and carbonyl groups of the **4.1**. Thus, the dispersive forces operating in solutions will vary with the ability of the solvent to solvate the molecules of **4.1** and thereby they adopt different structures in solution. From this study it is revealed that the crystallized products carry these signatures of the interacting molecules of **4.1** in solution by dispersive forces and adopt suitable orientations as per the guidance of the solute-solvent interactions which are discussed in details in the chapter.

Crystal structures of salts of **4.1** with sulphuric acid (H_2SO_4), hydrobromic acid (HBr) and nitric acid (HNO_3) were compared to show the role of anions in stabilization of a particular geometry. The salt **4.2** has an ethylsulphate anion which was generated *in-situ* by the reaction of sulphuric acid with ethanol. On analyzing these three salts it was found that the twist between the two planes was guide by the bulkiness of the corresponding counter ion. In case of salt **4.2** the phenyl ring with respect to quinoline ring was almost perpendicular to each other, this happens to accommodate the ethylsulphate anion in the lattice which has a relatively big size. Among the

bromide salt **4.3** and nitrate salt **4.4** the twist between the quinoline and the phenyl rings was found to be more in **4.3**. Sequence of twist between the two planes was **4.2** > **4.3** > **4.4.**

The chapter 5 deals with synthesis, characterization and antimalarial study of quinoline derivatives, their salts and cocrystal. This chapter contains discussion of structural features and the antimalarial activities of salts and co-crystals of aminoquinoline derivatives with different hydroxyaromatic acids and compared it with some neutral quinoline derivatives. The salts and cocrystal of aminoquinoline derivatives taken up for the study is listed in Chart 1.1. The solt/cocrystal generally enhances solubility, in our case we observe the same and also find that the antimalarial activities of the quinoline derivatives are improved on salt or cocrystal formation.

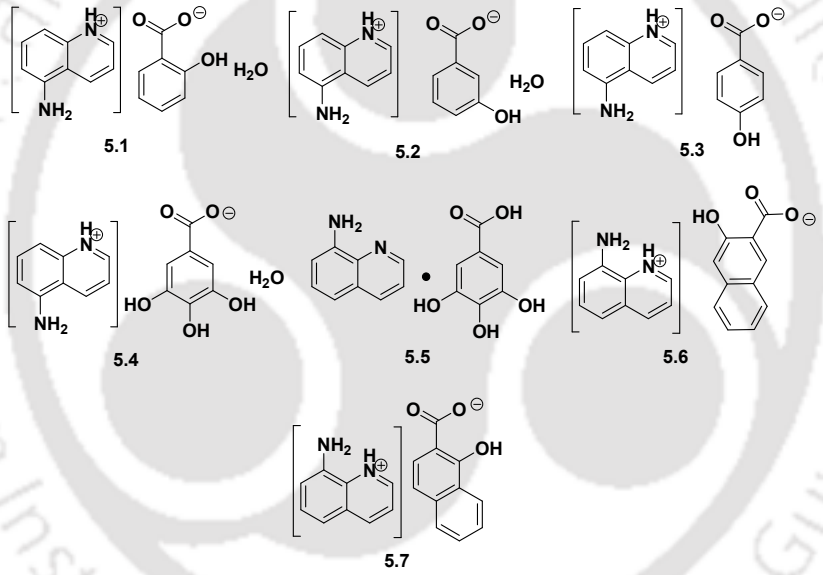

Chart 1.1: Salts and cocrystal of aminoquinoline derivatives.

Salts of 5-aminoquinoline with 2-hydroxybenzoic acid (**5.1**) and 3,4,5-trihydroxybenzoic acid (**5.4**) as well as of 8-aminoquinoline with 1-hydroxy-2-naphthoic acid (**5.7**) are prepared by the reaction of corresponding acid with amine, however the similar reaction of 8-aminoquinoline with 3,4,5-trihydroxybenzoic acid led to the formation of 1:1 cocrystal (**5.5**). Hydroxyaromatics acids were chosen as salts and cocrystal counterpart as they have definitive therapeutic applications. Each salts **5.1, 5.4**, **5.7** and as well as the cocrystal **5.5** showed potent antimalarial activity with IC_{50} values in 6-20 μM magnitude. Among the samples studied for antimalarial

activity, salts and cocrystal showed an enhancement in potency, whereas the covalently linked compounds showed minimal activity. Comparison of antimalarial values of salts and cocrystal with quinidine as standard is included in the chapter.

Chapter 6 deals with the synthesis, characterization, and metal recognition property of *bis*-quinoline amide derivatives. We have synthesized two of amide derivatives namely, compound **6.1** and compound **6.2** of quinoline and studied their metal ions recognition properties in solution state. Synthesis of the compound **6.1** and compound **6.2** are shown in the Scheme 1.6.

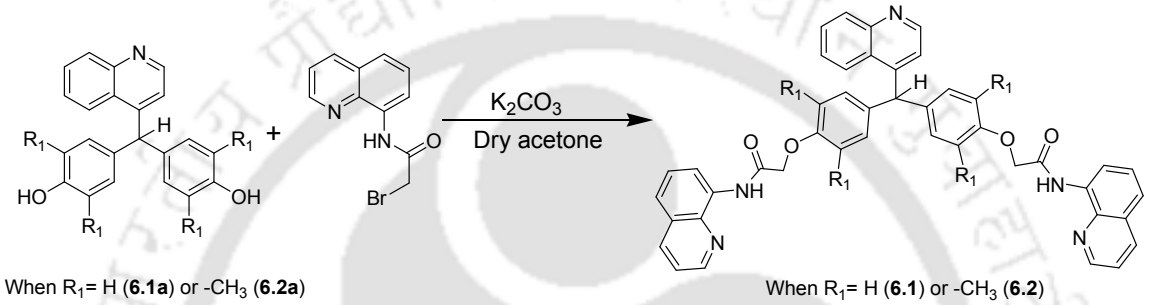

Scheme 1.6: Synthesis of compound **6.1** and **6.2**.

Compound **6.1** shows fluorescence emission at 397 nm on excitation at 310 nm, which on addition of Zn^{2+} ions get quenched and a new emission peak at 493 nm appeared. On further addition of Zn^{2+} ions, intensity of this emission peak reaches a maximum and beyond a critical concentration emission peak splits in to two new emission peaks appearing at 451nm and 551 nm (Figure 1.8a). Similar fluorescence titrations were carried out with Li^{+}, Na^{+}, K^{+}, Be^{2+}, Mg^{2+}, Ca^{2+}, Ni^{2+}, Co^{2+}, Mn^{2+}, Cd^{2+} and Hg^{2+} show insignificant changes in the fluorescence emssion. On the other hand, Cu^{2+} ions quench emission at 397 nm (Figure 1.8b). This occurs as a result of the electrons as well as energy transfer from the excited state of **6.1** to a low lying empty d-orbital of Cu^{2+} ions. A similar trend of fluorescence emission intensity changes as that of compound **6.1** was also observed in compound **6.2** by interactions with Zn^{2+} ions and Cu^{2+} ions. Major difference between the emission properties of these two compounds is in the splitting patterns of the fluorescence emission peak at higher zinc concentrations. Compound **6.2** showed single emission peak at longer wavelength (490 nm) on addition of Zn^{2+} ions with a shoulder at 400 nm and decrease of emission intensity of peak at 400 nm while on addition of Cu^{2+} ions.

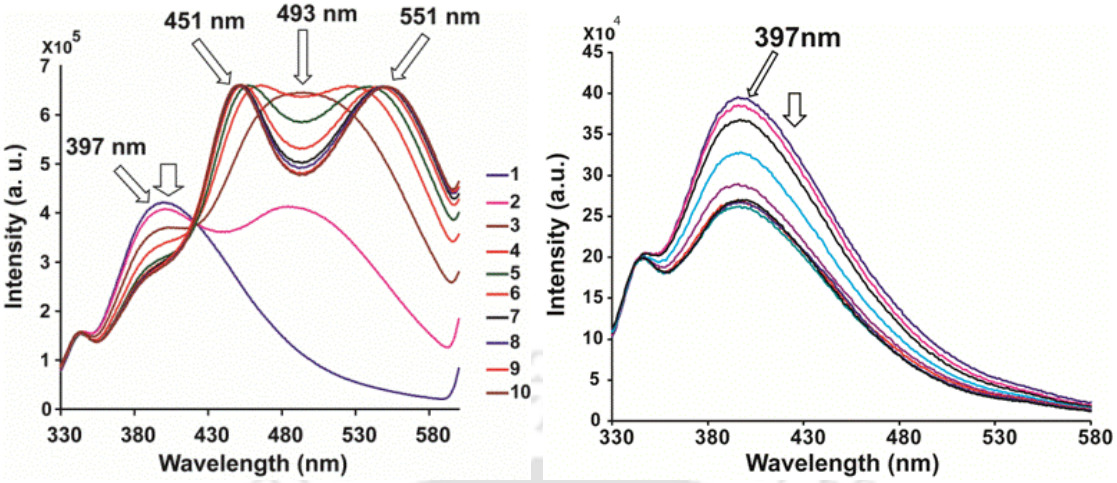

(a) (b)

Figure 1.8: The changes in the emission spectra of the compound **6.1** (10^{-5} M in methanol, 3 mL) on addition of the solutions of (a) Zn^{2+} ions and (b) Cu^{2+} ions (in each case 0.033 equivalent from a solution of methanol in aliquot).

The compound **6.1** and compound **6.2** have major difference in competitive sensing. The compound **6.2** unlike compound **6.1**, can sense Zn^{2+} ions as well as Cu^{2+} ions in presence of each other (Figure 1.9a and 1.9b) however, in the later case presence of Cu^{2+} ions suppress the Zn^{2+} ions sensing.

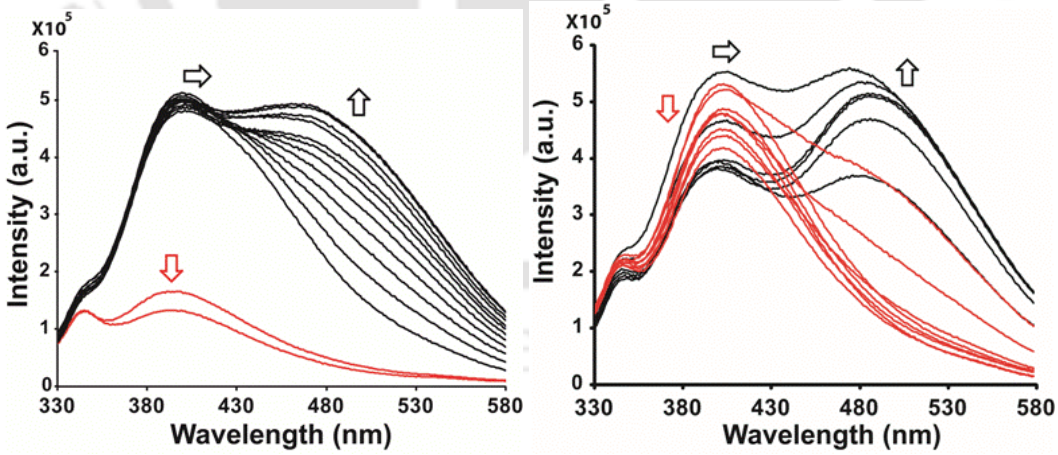

(a) (b)

Figure 1.9: (a) Changes in fluorescence of a solution of **6.2** (10^{-4} M in methanol) containing 1 equivalent cupric chloride (red lines), followed by addition of a solution of zinc chloride in 0.033 equivalent in aliquot (black lines). (b) Changes in fluorescence of a solution of **6.2** on addition of

zinc chloride 0.033 equivalent (six times, black lines) followed by addition of cupric chloride in 0.033 equivalent aliquots (red lines).

Addition of Zn^{2+} ions to a methanol solution of **6.1** increases the absorption at 252 nm and 360 nm at the cost of absorption at 303 nm and these changes pass through three isobestic points, at 245 nm, 280 nm and 331 nm. Similar changes were observed on addition of Cu^{2+} ions. Other ions like, Li^{+}, Na^{+}, K^{+}, Be^{2+}, Mg^{2+}, Ca^{2+}, Ni^{2+}, Co^{2+}, Mn^{2+}, Cd^{2+} and Hg^{2+} did not change absorption spectra of compound **6.1**. However, Cu^{2+} and Zn^{2+} ions were less effective to change the absorbance spectra of compound **6.2** compared to **6.1**. A coordination complex of Zn^{2+} or Cu^{2+} ions with **6.1** proposed based on the result obtained from isothermal microcalorimetric study has also been discussed.

A conclusion section is given at the thesis underlying the major overall findings from the present work; this is done to complement the conclusions that are given at the discussion of each chapter. Relevant literatures and experimental sections of each chapter are compiled after results and discussion in each chapter. The crystallographic parameters are given as an appendix and corresponding crystallographic information files are provided as soft copy attached to the thesis.

Table of Content: Page No.

Chapter 1

Introduction

1.1: General features of quinoline derivatives

Quinoline was first obtained from coal-tar in 1834 by F. Runge.[1] Later Gerhardt[2] extracted quinoline by distillation of cinchonine, quinine and other alkaloids reacting with caustic potash. Since then quinoline and its derivatives have found various applications and contributing to fundamentals of chemical sciences and related topics. Quinoline derivatives have various applications such as medicine,[3-8] catalyst,[9-12] electronics.[13-15]

Quinoline derivatives show potent drugs activities. Among them highly useful antimalarial drugs such as quinine, chloroquine, primaquine, quincrine, quinidin, and epiquinine

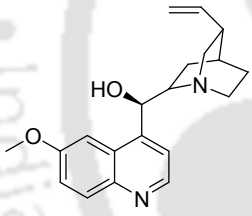

Quinine (1.1)

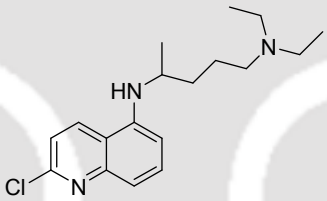

Chloroquine (1.2)

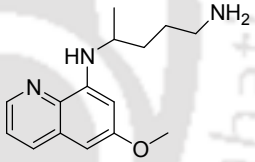

Primaquine (1.3)

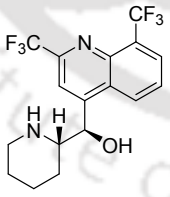

Melfaquine (1.4)

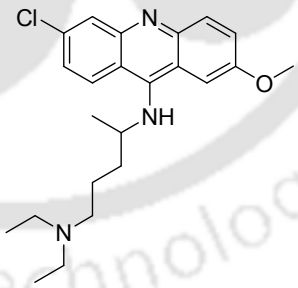

Quinacrine (1.5)

needs special mention. Malaria pigment hemozoin obtained from Plasmodium falciparum which is human malaria organism is consist of supramolecular assemblies of hemes. Hence there is necessity to understand interactions of hemozoin with quinoline drugs. Many other Quinoline derivatives show antimalarial, antibacterial and antifungal activities, some examples are listed in Table 1.1.

Table 1.1: Some biological active quinoline derivatives.

Anti- malarial drugs	Anti- bacterial	Anti- fungal
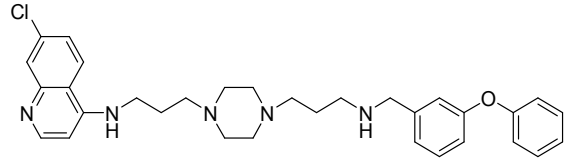 **(1.6)**	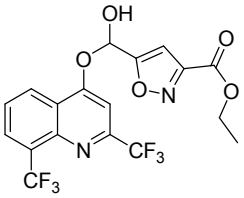 **(1.10)**	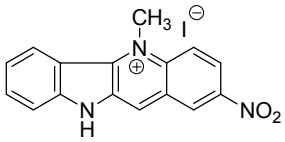 **(1.13)**
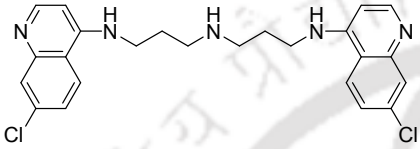 **(1.7)**	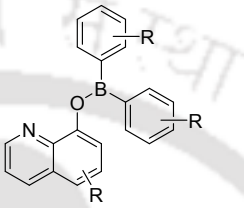 R = -4F, -4Cl, -3Cl, -4MeO **(1.11)**	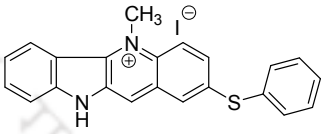 **(1.14)**
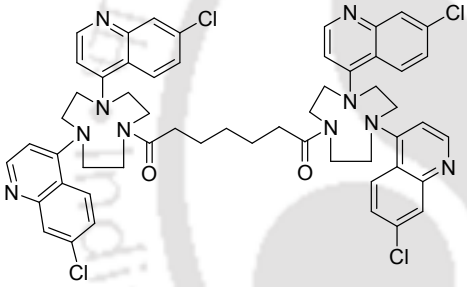 **(1.8)**	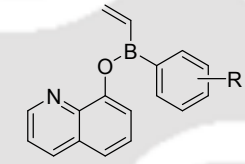 R = -H, -2Cl, -3Cl, -4Cl, -3F, -3CN **(1.12)**	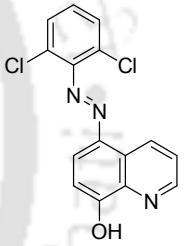 **(1.15)**
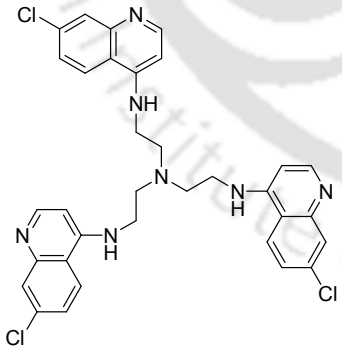 **(1.9)**		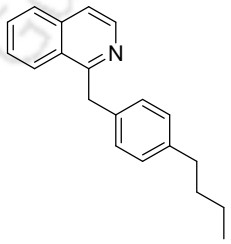 **(1.16)**

On the other hand, some quinoline derivatives such as 8-hydroxyquinoline is a common chelating agent to metal ions[16-18] and it is also used in organic light emitting diodes (OLED).[19-21] Quinoline derivatives are used routinely in analytical chemistry. Fluorescence properties

associated with quinoline derivatives are utilised to probe biological systems and molecular recognitions.

1.2: Supramolecular aspects of quinoline derivatives

Quinoline bears naphthalene skeleton in which one carbon atom of the ring is substituted by a nitrogen atom. Presence of nitrogen atom on the ring confers basicity. Nitrogen atom also makes the two fused rings non-equivalent, hence quinoilnes are dipolar molecules. There are two isomers of quinoline, possessing nitrogen at 1-position of the ring is called quinoline, whereas the iso-quinoline contains nitrogen atom at 2-position of the fused-ring.

Quinoline Isoquinoline

Quinoline is used as solvent and while crystallisation of many compounds from such solvent, different solvates having quinoline/s as solvated molecule/s are observed. For example quinoline form solvates with dicarboxylic acid **1.17** and depending on crystallisation conditions different compositions of solvates are observed.[22] In this particular case, two forms were identified, each of them has different packing patterns, and crystallized in different space groups. One form was obtained from a solution in quinoline, whereas the other from was obtained from a mixed solvent of pyridine and quinoline as shown in Scheme 1.1.

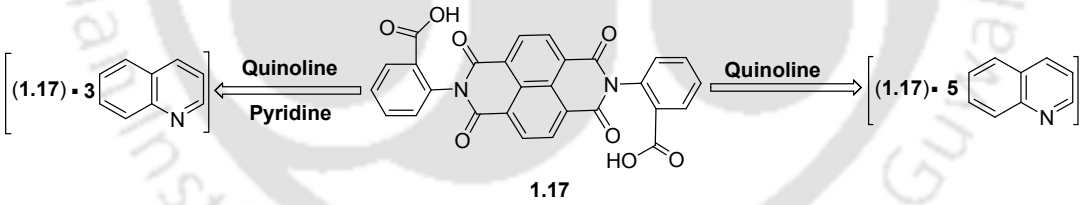

Scheme 1.1: Different quinoline solvates of **1.17**.

Some amide group tethered quinoline derivatives have ability to form gels.[23] Packing arrangements of such amides show different orientations around the guest molecules can be adopted depending on the substituent. As shown in Figure 1.1 head to head arrangement or head to tail arrangements by encapsulation of water molecule was observed from two different derivatives. In this Figure quinoline containing side of an asymmetric amide is considered as head and other side is considered as tail.

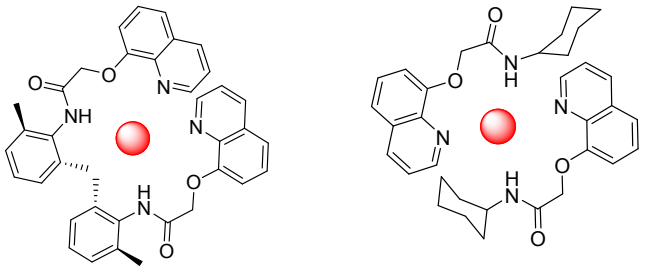

Head to Head arrangement **Head to Tail arrangement**

Figure 1.1: Head to head and head to tail arrangements of water assisted self-assemblies.

Similar molecules such as **1.18, 1.19, 1.20** and **1.21** recognise specific acid, which is reflected in changes in fluorescence emission of the quinoline derivative caused by different acids.[24] Compounds **1.18, 1.19** and **1.21** are responsive towards amino acids whereas receptors **1.20**, is not responsive towards amino acids, which suggest substrate selectivity to recognise amino acids.

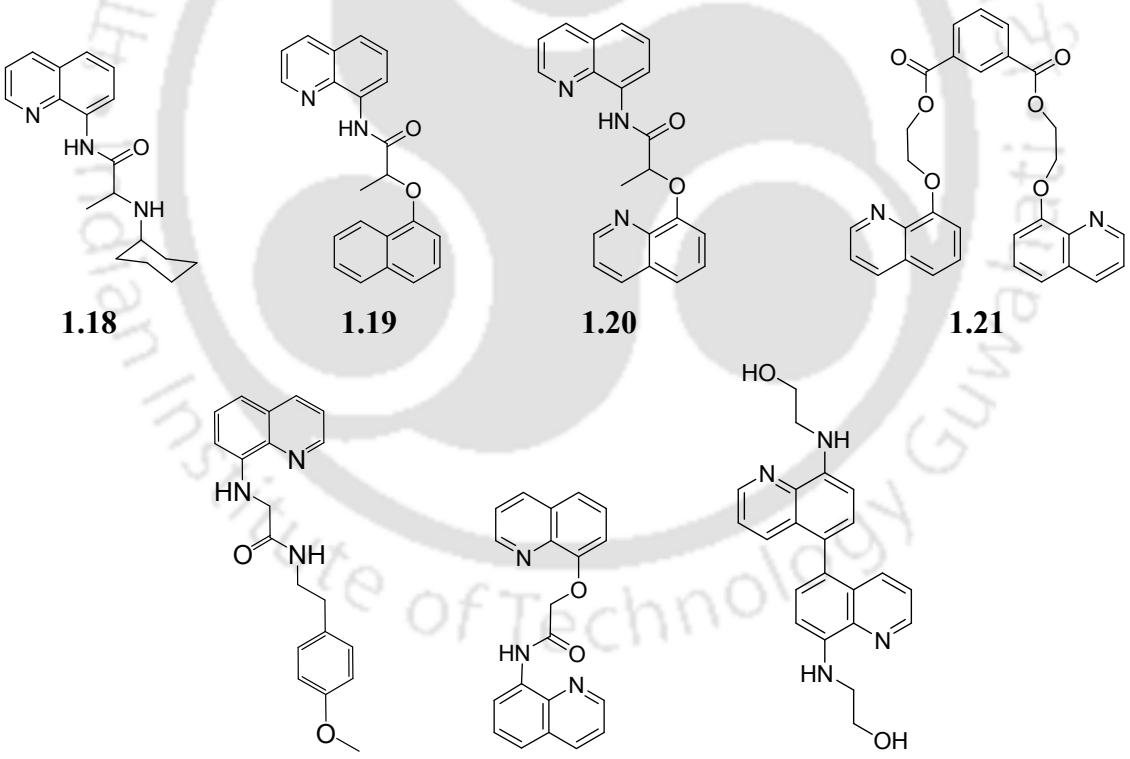

1.18 **1.19** **1.20** **1.21**

1.22 **1.23** **1.24**

Beside these, fluorescence response of compound **1.21** towards amino acid is opposite to that of response shown by compound **1.18** and **1.19.** This was explained on the basis of having a

template similar to crown ether in skeleton of compound **1.21.** Such unit favours binding towards NH_3^+ of zetterionic form of amino acid.

Self assembly of perchlorate salt of quinoline derivative **1.22** generates channel-like structure having pore of diameter 7.36 Å (Figure 1.2).[25] In this case very weak interactions such as C-H···π interactions[26] and C–H···O interactions[27] contribute significantly to stability of the assembly.

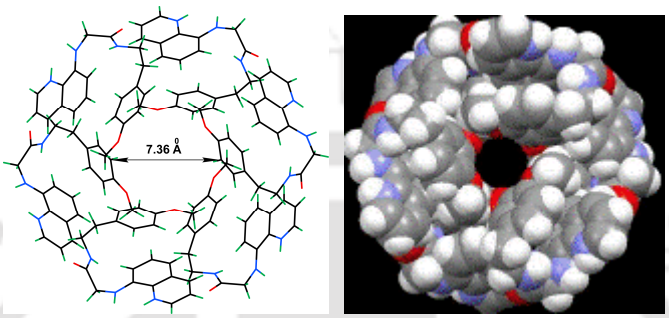

(a) (b)

Figure 1.2: (a) Self-assembly of perchlorate salt of **1.22** (perchlorate anions are omitted); (b) space-filled model showing the void.

Interesting aspect of quinoline derivative **1.23** is the formation of monoprotonated tetrafluoroborate salt on reaction with fluoroboric acid despite of having scope for formation of diprotonated salt. Perchlorate salt is a diprotonated **1.23** has two perchlorate anions per cationic unit (Scheme 1.2). Further to this, hydrolytic reaction of sodium tetrafluoroboarte in aqeous dimethylformamide in presence of **1.23** was observed. Such hydrolysis also results in formation of corresponding perchlorate salt.

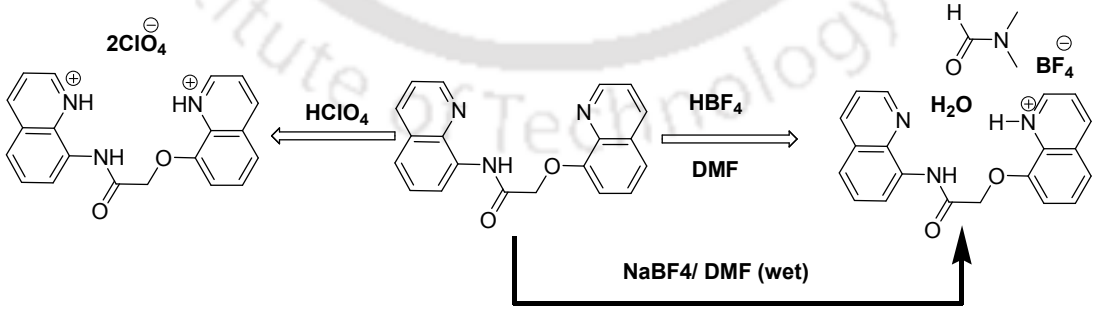

Scheme 1.2: Formation of perchlorate and tetrafluoroborate salts of **1.23**.

Biquinoline derivative **1.24** forms self assembly to adopt a single helical structure.[28] On treatment with perchloric acid it forms perchlorate salt which retains helical structure and in the helical structure perchlorate ion occupies the spaces in the folds.

Kemp's triacid (1, 3, 5-cyclohexyl tricarboxylic acid), **1.25** binds selectively 8-substituted quinoline. For example, it forms co-crystals with 8-aminoquinoline or 8-hydroxyquinoline through intermolecular hydrogen bonds; one example is depicted in Figure 1.3.[29]

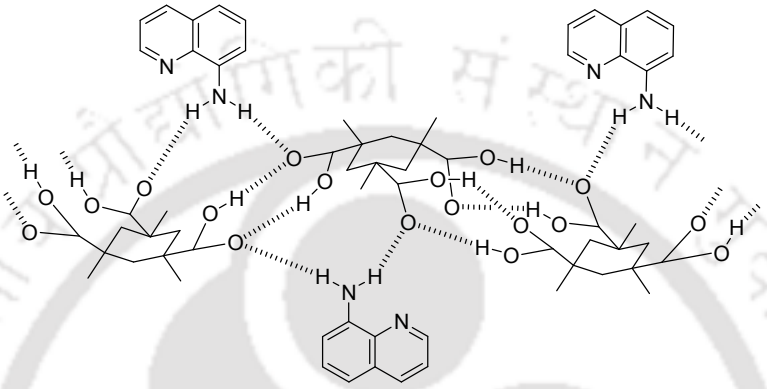

1.25

Figure 1.3: Cocrystal of Kemp's triacid with 8-aminoquinoline.

N-functionalised dicationic quinoline derivative, **1.27** has ability to bind anion much strongly than neutral analogue. Such observation is of interest as binding of cation at the inner core of **1. 27** is not sterically favourable, hence electrostatic attraction of anions to dicationic receptor of anion is a major factor to have higher anion binding over the neutral counterpart without N-methyl groups.[30]

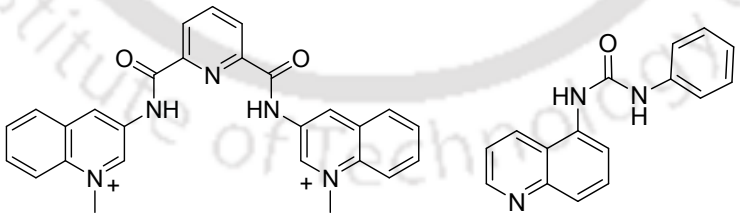

1.27 **1.28**

Proton transfer from 1-phenyl-3-(quinolin-5-yl)urea **1.28** helps to distinguish isomeric dicarboxylic acids such as maleic acid and fumaric acid[31] or positional isomers terephthalic acid and phthalic acid. One isomer of each pair shows distinct colour change on interaction with **1.28**. Proton transfer without proton transfer to form salt or co-crystal have been established by single crystal X-ray diffraction as well as by solid sate ^{1}H-NMR study.

Inter-linking between 2, 3-dihydroxynapthalene appended quinoline derivatives with boron atoms **1.29** is a good receptor for biphosphate anion (Figure 1.4). Colour changes of this compound **1.29** takes place selectively on formation of biphosphate.[32]

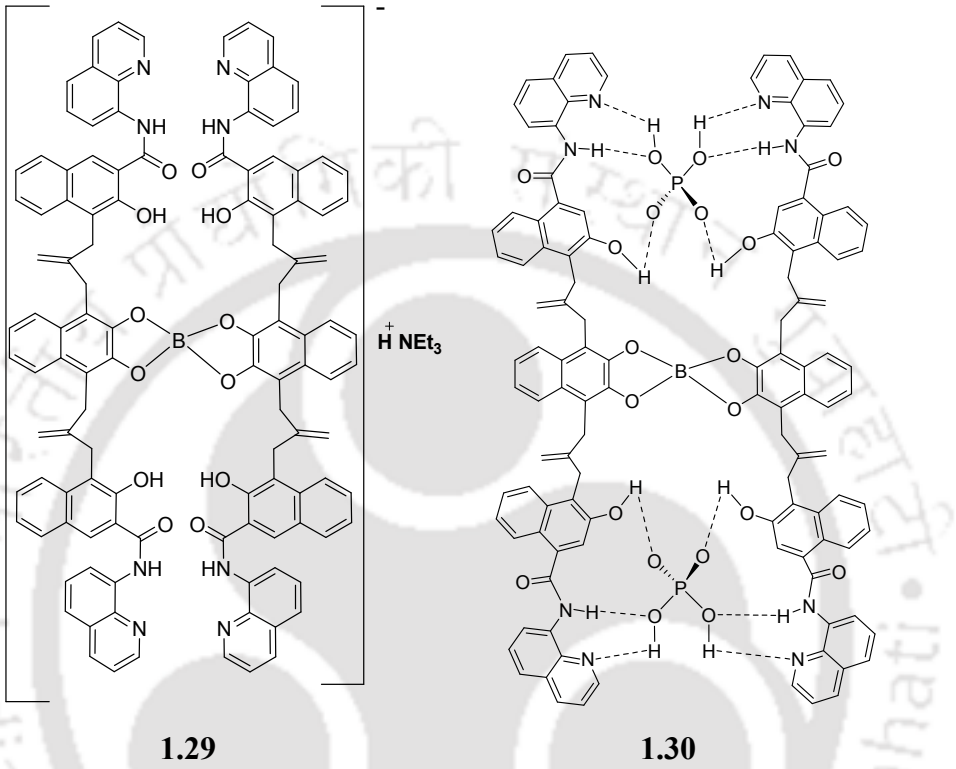

1.29 **1.30**

Figure 1.4: Boron complex **1.29** and its host-guest complex with biphosphate anion **1.30**.

Quinoline derivative **1.31** and **1.32** having multiple binding sites linked with both amide and ether linkage binds various carboxylic acids. Compound **1.31** distinguishes hydroxy dicarboxylic acids from their non-hydroxy analogues and also aliphatic dicarboxylic acids from aromatic diacids.[33] Compound **1.32** shows high affinity towards tartaric acid and while interacting with tartaric acid fluorescence emission of compound **1.32** drastically changes, it enables detection of tartaric acid among various acids. Reason for such recognition process was established from solution study and from crystal structure determination it is shown that complementary hydrogen bonds facilitates accommodation of tartaric acid within the arms of a scissor like geometry of molecule to form 1:1 host-guest complex **1.33**.[34]

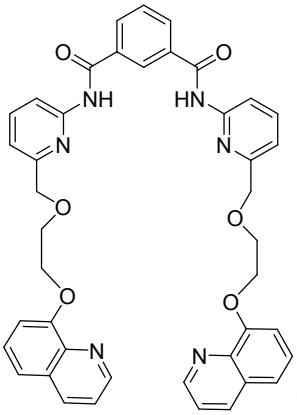

1.31

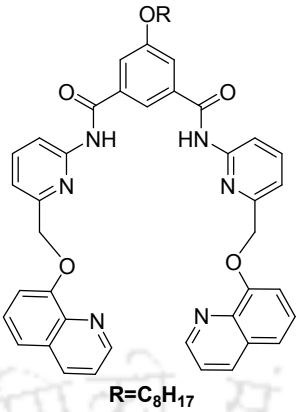

1.32

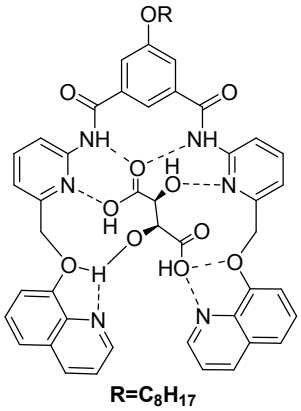

1.33

Nano-cage like structure is generated from interactions of dendritic molecule such as **1.34** with palladium ions (Scheme 1.3). This type of nano-cage is used for fluorescent detection of nucleosides.[35-36]

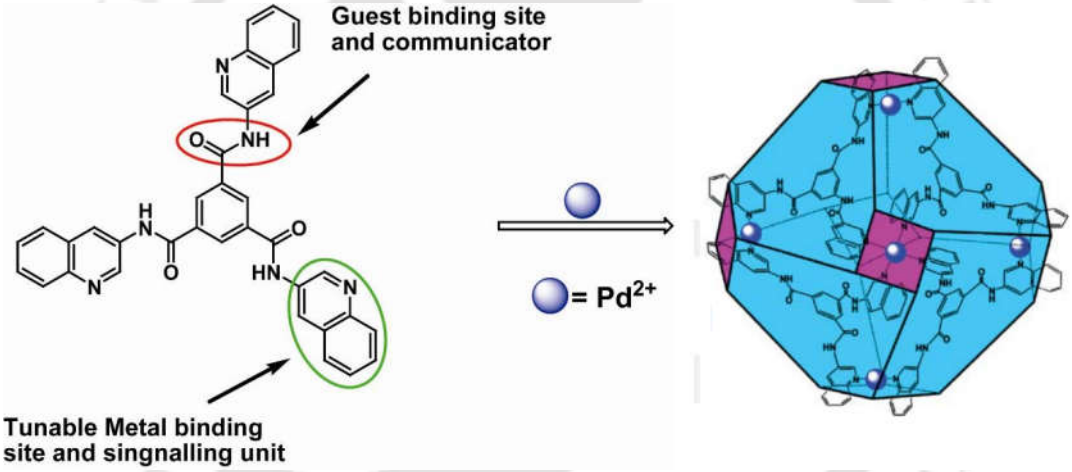

Scheme 1.3: Formation of nano cage from compound **1.34.**

There are large numbers of molecules in which quinoline unit is attached to another binding site or to functional molecules demonstrating a plethora of supramolecular chemistry. In next section, specific anion and cation binding properties of quinoline derivatives are discussed.

1.3: Quinoline derivatives in detection of cations

Quinoline derivatives are fluorescence active compounds; hence quinolines containing fluorescent receptors are very common. Generally design of quinoline based fluorescence receptors shows signal transduction through three mechanisms: [37-40] a) Photoinduced electron transfer (PET), b) intramolecular charge transfer (ICT) and c) fluorescence resonance energy

transfer (FRET). To exaplain these process we illustrate each case by taking illustrative case of each type.

Photoinduced electron transfer process requires use of spacer which generally has a separation distance between less than three intervening -CH_2- unit to connect a fluorescence group to an atom having nonbonding electron pair, such as nitrogen or sulfur atom (Figure 1.5),. Such atoms can transfer an electron to fluorescence group at excited state and result in fluorescence quenching. But when such electron pair is coordinated to a metal ion (or other cation), the electron transfer is prevented and fluorescence is enhanced.

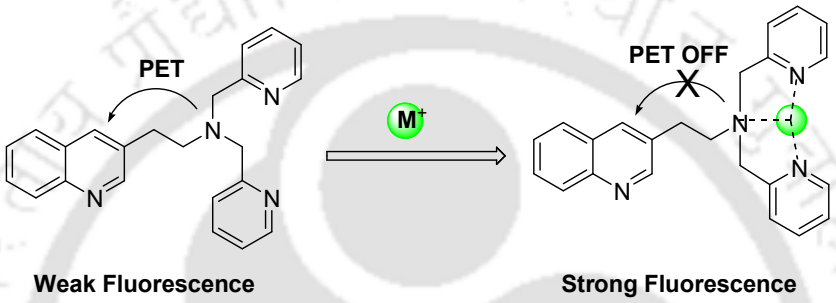

Figure 1.5: An illustration of photo electron transfer mechanism.

As an illustrative example of a system operating though PET mechism is the fluorescence changes on interaction of **1.35** with Zn^{2+} and Cu^{2+} ions. Compound **1.35** binds to Zn^{2+} or Cu^{2+} in different manner showing an efficient ratiometric OFF and ON response.[41] It adopts an imidic acid tautomeric form while binding to Zn^{2+} ion; and while binding to Cu^{2+} ion it forms of an deprotonated amide tautomer formed by loosing the proton from NH group as shown in the Scheme 1.4.

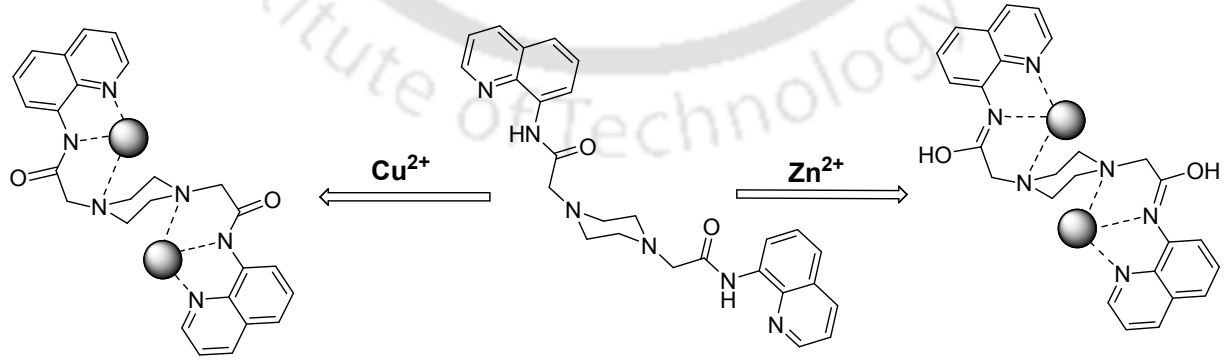

Scheme 1.4: Different binding mechanism of Zn^{2+} and Cu^{2+} ions with **1.35**.

In intramolecular charge transfer mechanism can be explained with a Scheme shown in Figure 1.6. In this Figure quinoline moiety attached to a conjugated system can be a coordinating site to a metal ion and an electron donating or electron withdrawing group and presence at a remote site can assist in pulling or pushing the electrons. This would result charge transfer to or from fluorophore at excited state. On complexation such effect is influenced by a metal ion; hence fluorescence can be modulated. Since the ICT mechanism operates through conjugation, the spacer part is not required.

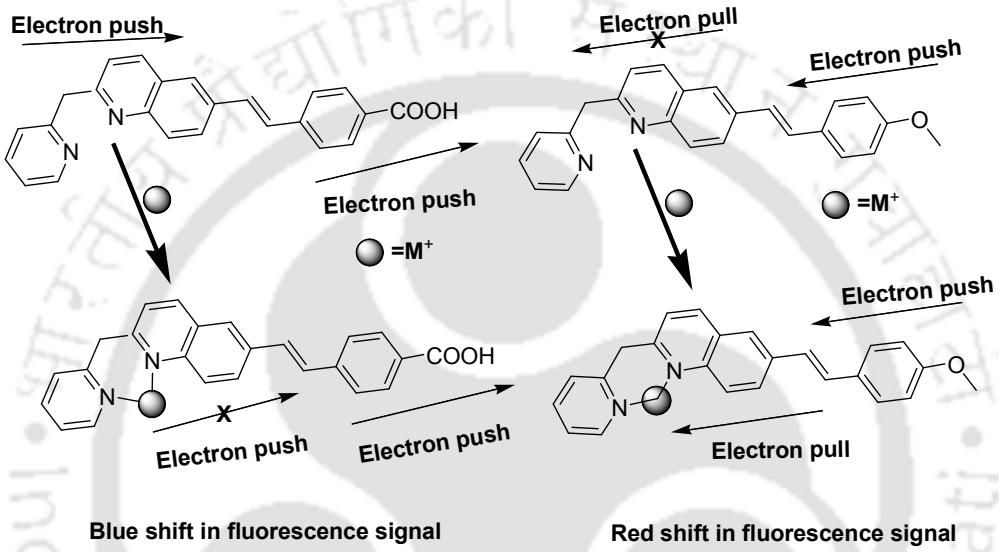

Figure 1.6: Model depicting intramolecular charge transfer mechanism.

ICT is observed in sensing of zinc ions by compound **1.36**, in which the N-methyl group has a role to push the electron to the ring taking the emission to a higher wavelength (Figure 1.7). Upon coordination of zinc ion to the nitrogen atom of the quinoline effects the emission spectra and appears at 620 nm, whereas uncoordinated compound **1.36** emits at 545 nm.[42]

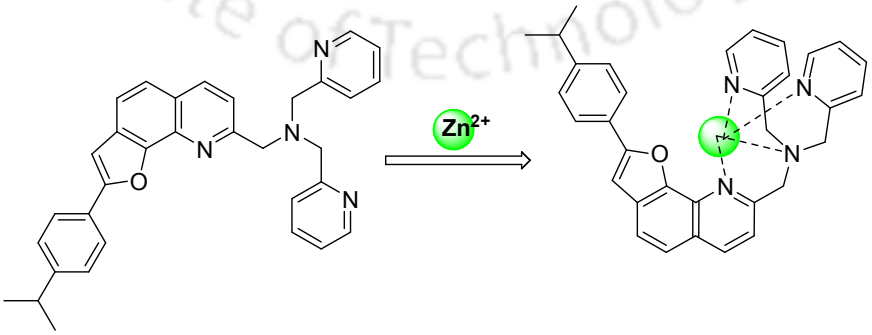

Figure 1.7: Intramolecular charge transfer mechanism in compound **1.36**.

On the other hand, fluorescence resonance energy transfer occurs in fluorescent molecules comprised of donor and acceptor components separated by a suitable distance with appropriate orientation to favor energy transfer between them. Thus, there must be a clear possibility of communication between a donor and an acceptor part. It involves non-radiative transfer of excitation energy from an excited donor to a proximal ground-state acceptor. Following conditions must be satisfied for observing FRET: a) Donor part should have sufficient lifetime for energy transfer. b) Distance from the donor to the acceptor must be less than 10 nm. c) The absorption spectrum of the acceptor fluorophore must overlap with fluorescence emission spectrum of the donor fluorophore (at least by 30%). d) Orientations of donor and acceptor dipole must be approximately parallel. FRET- may be observed in small molecule containing two fluorophores connected by a spacer through covalent links.

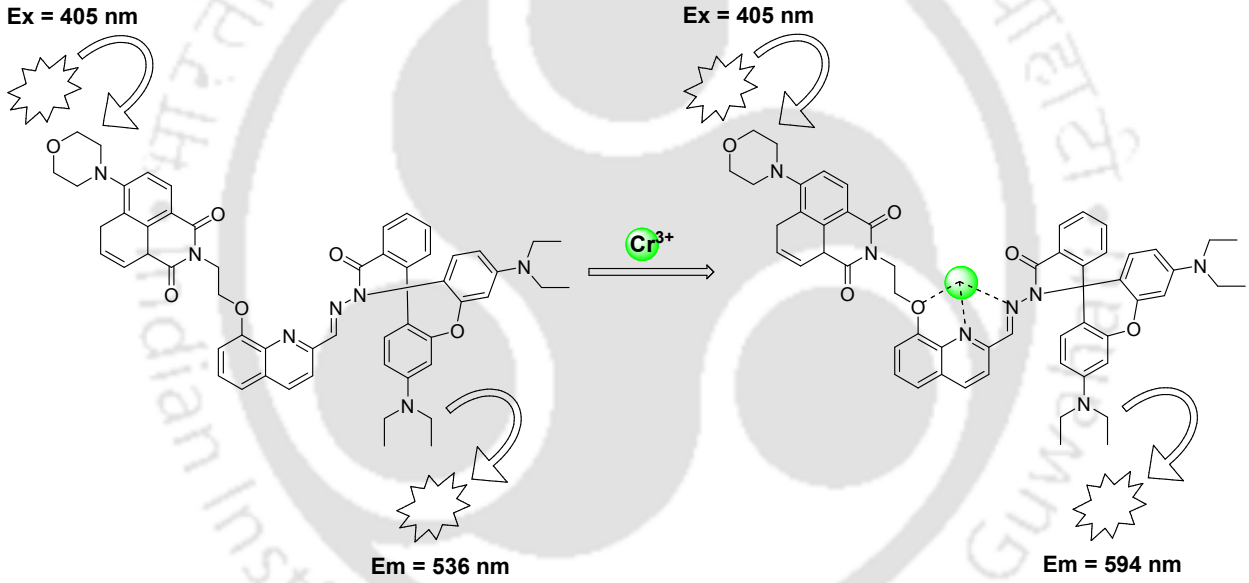

Figure 1.8: Fluorescence resonance energy transfer mechanism in compound **1.37** and changes caused by Cr^{3+} ion.

Based on the fluorescence resonance energy transfer mechanism ratiometric sensors have been designed.[43] For example, fluorescence quenching of compound **1.37** takes place on complexation with Cr^{3+} (Figure 1.8). In this case energy transfer is reflected as quenching of fluorescence. The fluorescence lifetime of the donor part of **1.37** is lower in absence of Cr^{3+} ions. There is an increase in acceptor fluorescence emission which occurs through a FRET mechanism. Since FRET is very sensitive to the distance between fluorophores, compound **1.37** on complexation

with Cr^{3+} brings the acceptor and donor moiety close and also provides favorable orientation for energy transfer. This shifts the emission to higher wavelength. It has been suggested that in this system distance of separation between donor and acceptor changes through coordination hence fluorescence changes may be used to estimate distance between fluorophores.

There are large numbers of examples on quinoline derivatives which have evolved over the years to detect various metal ions. Thus list of some quinoline derivatives used in detection of different metal ions are listed in table 1.2. Major challenge in this area is to identify water soluble molecules with specific signal response to an analyte. Further understanding on interference of other metal ions prior to development of a new analytical device is essential. Thus, major aspect of this research is directed towards screening of fluorescence responsive molecules and modulation of signals. There are also some studies directed to generate logic gates[44-45] and some are towards medical sides such as NMR imaging.[46]

Table 1.2: List of compounds with their respective metal ion/s detections.

Compound	Substituent	Compound No.	Metal ion/s
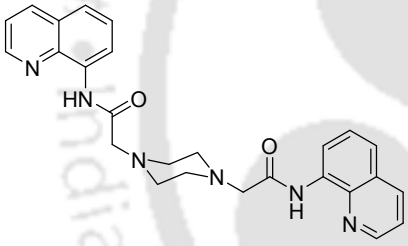		**1.35**	Zinc and Copper[41]
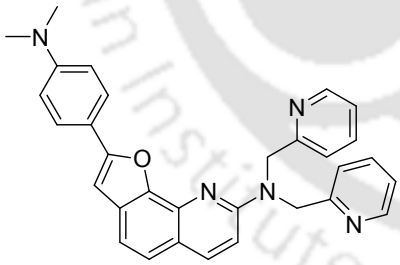		**1.36**	Zinc[42]
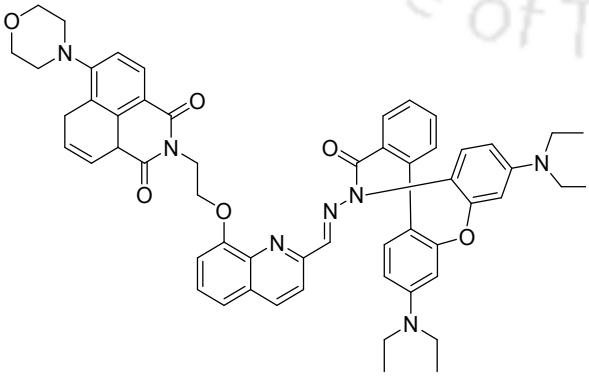		**1.37**	Chromium[43]

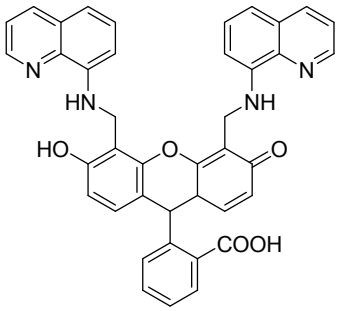		**1.38**	Zinc[51]
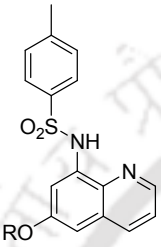	R= -CH_3	**1.39**	Zinc[46]
	R= -CH_2COOEt	**1.40**	Zinc[47]
	R= -CH_2COOH	**1.41**	Zinc[47]
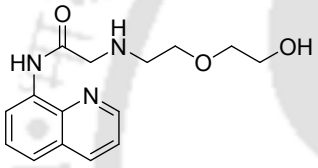		**1.42**	Zinc[48]
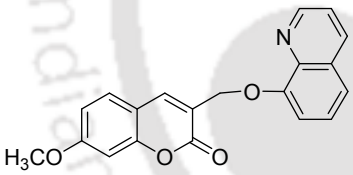		**1.43**	Zinc[53]
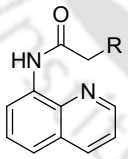	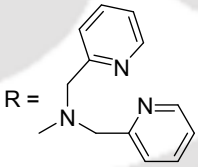	**1.44**	Zinc[49]
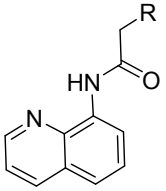	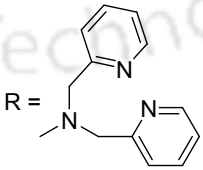	**1.45**	Zinc[50]
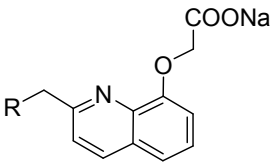	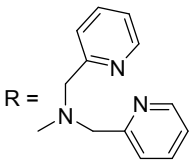	**1.46**	Zinc[49]

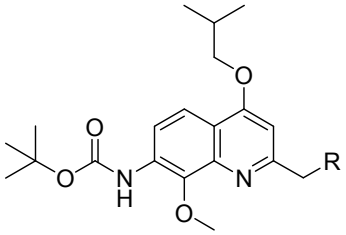	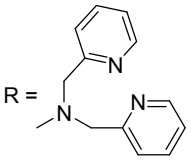	**1.47**	Cadmium and Zinc[54]
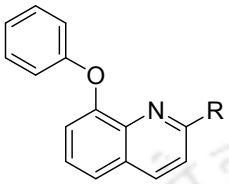	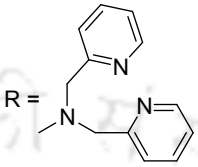	**1.48**	Zinc[56]
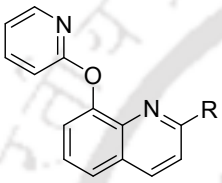	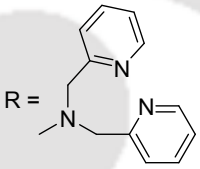	**1.49**	Zinc[56]
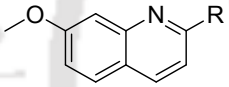	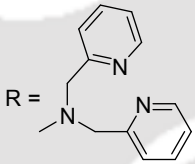	**1.50**	Zinc[58]
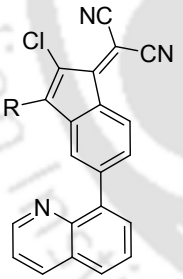	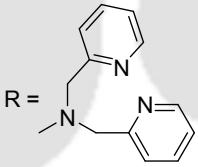	**1.51**	Copper[59]
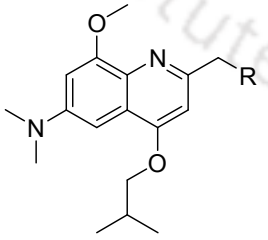	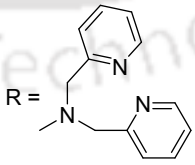	**1.52**	Cadmium and Zinc[60]
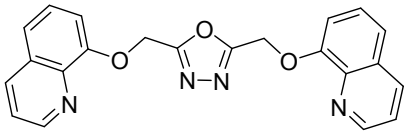		**1.53**	Cadmium[61]

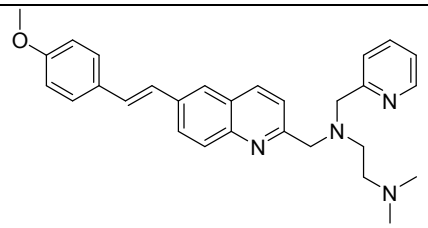	**1.54**	Cadmium[63]
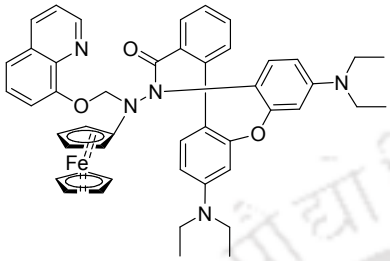	**1.55**	Mercury[64]
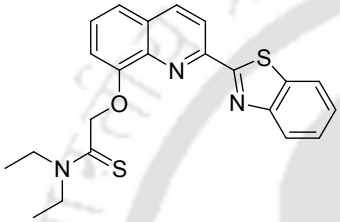	**1.56**	Mercury[65]
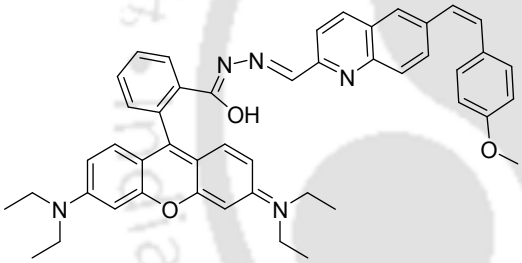	**1.57**	Iron[56]

Among various metal ions, detection of zinc ion has been an important issue from biological point of view. Quinoline receptors for zinc generate high interest as the mobile zinc ions in biology can be detected by quinoline derivatives. Various fluorogenic chelators for transition metal ions based on quinoline moieties, particularly 8-hydroxyquinoline and 8-aminoquinoline are found to be suitable for detecting Zn^{2+} ion in biological samples. Quinoline derivatives such as **1.40,**[47] **1.41**,[47] **1.42**[48] and **1.44**[49] can detect specifically Zn^{2+} ion in aqueous solution, hence they are of biological interest. A high selectivity water-soluble fluorescent sensor **1.45** demonstrates[50] femtomolar sensitivity for Zn^{2+} ion with a 14-fold enhanced quantum yield upon chelation to Zn^{2+} ion and also exhibits selectivity to zinc ion over other physiological relevant divalent metals in the presence of EDTA. Coordination of acetic carboxylic group significantly enhances the affinity for zinc ion. Compound **1.46** shows nanomolar affinity for zinc ions and

shows large fluorescence shifts with enhancement of fluorescence intensity.[49] Therefore, **1.38** has desired chemical and spectroscopic properties that satisfy the criteria for further biological and environmental applications. 8-aminoquinoline based chemosensor **1.38** exhibits 150-fold increase in fluorescence emission upon binding to Zn^{2+} and shows high selectivity for Zn^{2+} ions from other biologically relevant metal cations, toxic heavy metals.[51]

As mentioned earlier, selectivity of detection of a metal ion over other metal ions is important. There is large amount of work devoted in this direction. For example, compound **1.39** is selective[52] to quantify Zn^{2+} ions in the presence of high concentrations of Ca^{2+} and Mg^{2+} ions. As far as simultaneous multiple ions detection is concerned **1.43** was employed as a novel fluorescent probe for Co^{2+} and Ni^{2+} ions.[53]

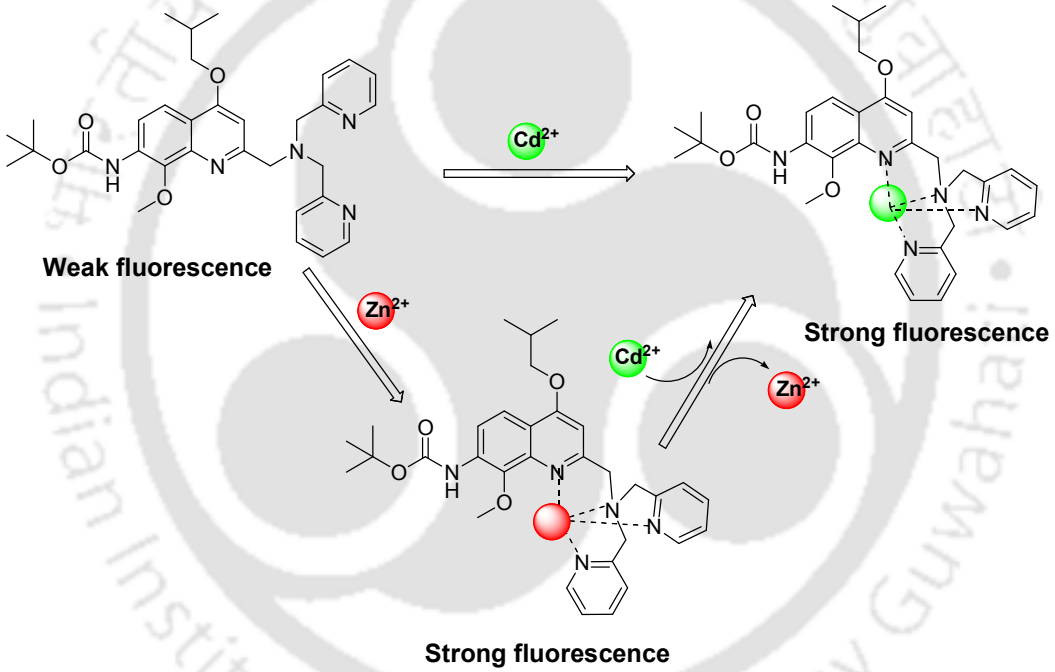

Figure 1.9: Process of sensing of Zn^{2+} or Cd^{2+} ions by **1.47**.

Ratiometric signal chelation enhanced fluorescence output for Cd^{2+} ion was observed when the bound Zn^{2+} ion was displaced by Cd^{2+} ion (Figure 1.9). These results demonstrated that **1.47** can act as a radiometric sensor for Zn^{2+} and also as a dual mode Cd^{2+}-selective sensor ratiometric displacement.[54] A turn-on fluorescent probe **1.57** for Fe^{3+} based on the rhodamine platform has been reported. Compound **1.57** shows high selectively for Fe^{3+} over Cr^{3+} ions.[55]

Compounds **1.48** and **1.49** show[57] a 4 to 6 fold enhancement in fluorescence intensity upon coordination of Zn^{2+} ions, and with slight enhancement upon addition of K^{+}, Mg^{2+} and Ca^{2+}. Oxygen atom present at 8-position and the quinoline nitrogen atom participate in the

coordination of Zn^{2+} ions, and that dipicolyl amine group endows the sensor with a high affinity for Zn^{2+} ions. The sensor **1.36** based on ICT process instead of PET process, can readily reveal changes in intracellular Zn^{2+} ions concentration.[42] Dual emissions and cell-permeable nature of **1.36** make it possible to study cellular Zn^{2+} in hippocampus in a ratiometric approach. Compound **1.50** is used for monitoring Zn^{2+} ions. It shows 14-fold fluorescence enhancement upon Zn ion addition.[57] It has nanomolar range sensitivity and high selectivity for Zn^{2+} ions which makes it favorable in biological applications as used for imaging Zn^{2+} in living cells with two-photon microscopy. Chemosensor **1.51** with conjugated backbone shows a 5-fold increase in the intensity of emission on interaction with Cu^{2+} ions.[58]

Interference of Cd^{2+} is a well-known problem for zinc fluorescence sensors and cadmium fluorescence sensors. 4-isobutoxy-6-(dimethylamino)-8-methoxyquinaldine sensor **1.52** based on the ICT mechanism exhibits very high sensitivity for Cd^{2+} and excellent selectivity response for detection Cd^{2+} over heavy and transition metal ions.[59] Structural study on zinc and cadmium complexes of **1.52** showed that the dipicolyl amine moiety plays main role to grasp metal ions, while 8-position methoxy oxygen helps to tune selectivity of the sensor. Furthermore, it demonstrates to be a ratiometric chemosensor to image intracellular, which is superior to intensity-based images of the sole emission channel.

Two 8-hydroxyquinoline units flanking semi-rigid oxadiazole moiety such as in **1.53** effectively chelate Cd^{2+} and show very high selectivity over other heavy and transition metal ions.[60] A Quinoline derivative of N', N'-dimethyl N''-(pyridin-2-ylmethyl)ethane-1, 2-diamine **1.54** is used as a probe for Cd^{2+} ions.[61] This probe shows a large red shift with significant enhancement of emission intensity on binding to Cd^{2+} ion and also exhibits higher selectivity for Cd^{2+} over Zn^{2+} ions.

Paramagnetic Fe^{3+} and Cr^{3+} ions are generally most efficient fluorescence quenchers, thus development of fluorescence chemosensors of these metal ions is a challenging job. FRET-based Cr^{3+} chemosensor **1.37**, showed gradually decrease in intensity of fluorescence emission and a new emission appeared at longer wavelength with increase in emission intensities.[43]

Some detection process of metal ions occurs due to chemical reactions; in such detection process one form of a fluorophore or chromphoric compound transforms selectively to another by specific metal ion. Such process was demonstrated in detection of mercury by compounds **1.55** and **1.56**. Compound **1.55** has 8-hydroxyquinoline connected rhodamine and ferrocene which are

chromophoric and electroactive respectively. In this example, compound **1.56** is capable to recognize Hg^{2+} ions through opening and closing rhodamine ring before and after binding.[62] Because of changes in interior electron density before and after binding, the electrochemical signals of ferrocene varies. On the other hand, hydroxyquinoline derivative **156** is highly sensitive to detect of Hg^{2+} ions. In this case, very efficient hydrolytic conversion of thioamide into amide takes place in the presence of Hg^{2+} ions.[63]

There are large numbers of examples on quinoline units connected to various supramolecular receptors to make them polyfunctional or to enhance selective binding abilities. Among these units crown ether, calix-arene, cyclotriveratrylene, porphyrin and aza-crown units are extensively used. Some examples of such receptors are given as **1.58**, **1.59**, **1.60**, **1.61** and **1.62**. Aza-crown based quinoline derivative **1.58** is a chemosensor of Zn^{2+} ions.[64]

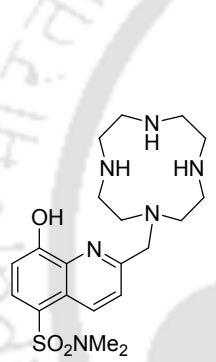

1.58

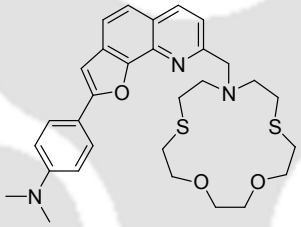

1.59

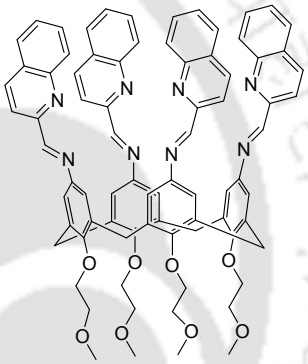

1.60

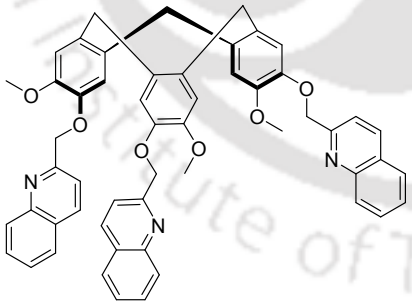

1.61

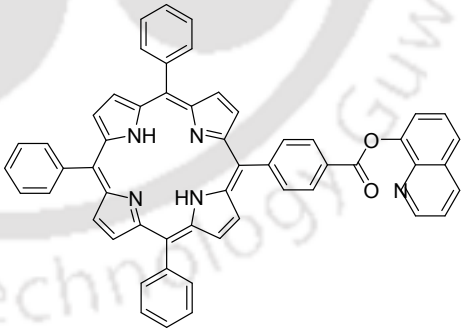

1.62

In this example, deprotonation of the hydroxy group of hydroxyquinoline moiety forms chelated complex with Zn^{2+} thus, the detection process is sensitive to pH. Compound **1.59** is used as an effective fluorescent sensor for silver ions. It shows a large Stokes shift of about 173 nm on interaction with silver ions and operates with an ICT mechanism.[65] Compound **1.60** is based on calix[4]arene and bears four iminoquinolines. It shows large enhancement of fluorescence

intensity on interaction with Cu^{2+} ions and shows a high selectivity toward Cu^{2+} over others metal ions.[66] Cyclotriveratrylene derivative **1.61** bearing three fluorogenic quinolinyl groups detect Cu^{2+} ions with very high efficiency.[67] In both these examples, quinoline moiety is responsible for fluorescence changes upon coordination of metal ions and cavity size controls selectivity of the sensors towards Cu^{2+} ions. Complexation of mercury ion to porphyrin unit quenches fluorescence of **1.62** and induces a new emission with enhancement of intensity at lower wavelength.[68]

Siderophore analogs based on tris(2-aminoethyl)amine (TREN) spacer **1.63** and **1.64** are good iron selective sensor molecules.

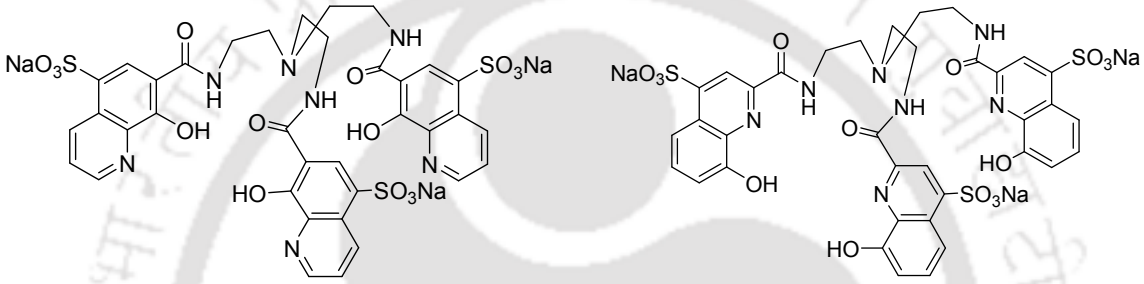

O-TRENSOX **N -TRENSOX**

1.63 **1.64**

Among these two compounds, O-TRENSOX **(1.63)** is more selective towards iron than N-TRENSOX (**1.64**), so it is used as iron sequestering agent.[69-70]

1.4: Quinoline derivatives as sensors for anions

Quinoline derivatives have provided wide ranges of templates to selectivity bind anions. Hydroxy-quinoline derivatives have been widely used in sensing fluoride ions.[71] Metal oxyquinolinate complexes usually of zirconium interact with fluoride ions (Figure 1.10).

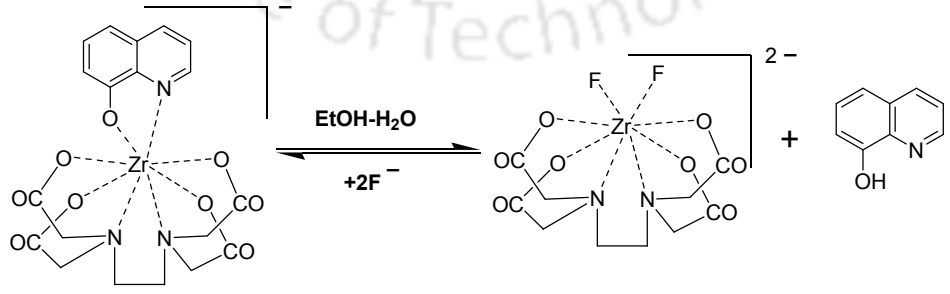

Figure 1.10: Fluoride sensing of zirconium oxyquinolate complex.

Selective reaction of fluoride ion with zirconium oxyquinolinate complex releases quinolinium ions which show colour change to detect fluoride ions**.**

Copper complex **1.65** has been found to shows high selectivity to bind acetate ions over other anions such as fluoride, chloride, bromide, iodide, DL-malate, L-mandelate, benzoate, isophthalate, phosphate, nitrate and sulphate (Figure 1.11).[72] Such selectivity with parent ligand without complexing to copper was not observed. This is due to coordination of ligand to copper ion, which makes an azacrown moiety to provide complementing binding site to an acetate ion.

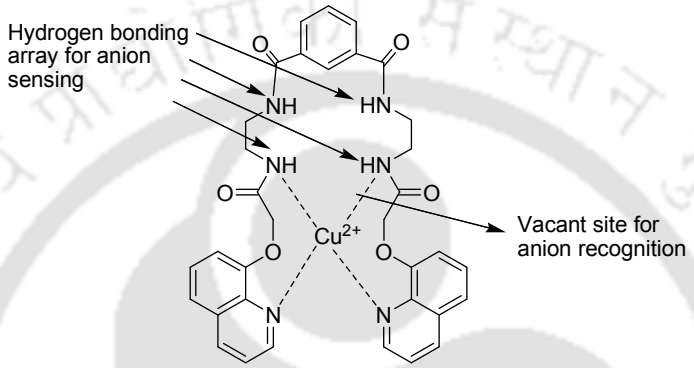

1.65

Figure 1.11: Binding sites for acetate ion in **1.65**.

Many anion selective compounds have been prepared based on quinoline moieties. Some of such compounds are listed in Table 1.3.

Table 1.3: List of compounds with their respective anion/s detections.

Compound	Compound No.	Anion/s
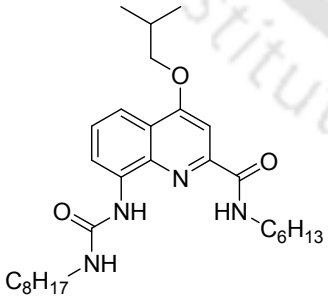	**1.66**	Fluoride[75]
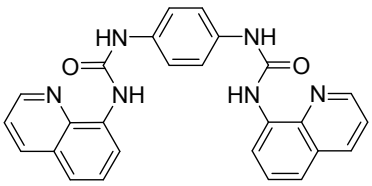	**1.67**	Bisulfate and fluoride[76]

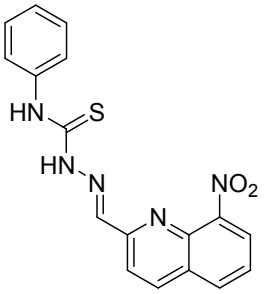	**1.68**	Acetate[77]
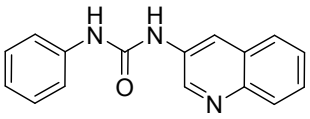	**1.69**	Fluoride[78]
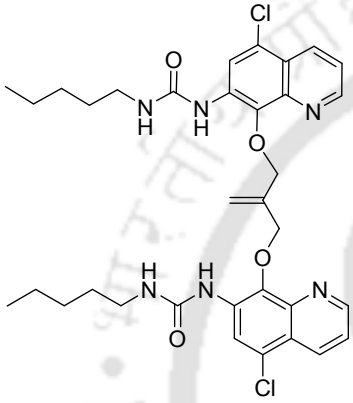	**1.70**	Fluoride[79]

Compound **1.66** is based on a quinoline backbone bearing urea as well as an amide moiety. It effectively binds halide anions in 1:1 ratio. It has a high selectivity for fluoride ions over the bigger anions.[73] Fluoride being a small anion most appropriately fit in the binding pocket formed by the three NH protons.[74] Simple aminoquinoline based *bis*-urea **1.67** is a receptor for anions, which effectively binds oxoanions and halides. Two quinoline rings present in the molecule allows it to form a cavity suitable to hold an anion. Compound has high affinity for bisulfate and fluoride ions. This is due to strong hydrogen-bond interactions between the host and anions.[75]

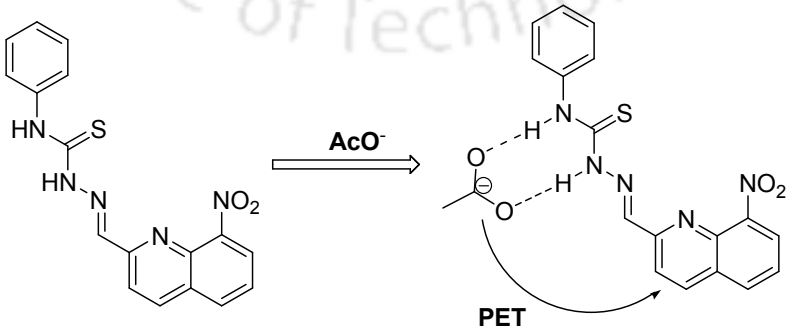

Scheme 1.5: Anion- induced flouroscent quenching sensor **1.68** based on PET mechanism.

A novel colorimetric and fluorescence anion sensor based on 8-nitroquinolyl-2-aldehyde phenyl-thiosemicarbazone **1.68** is used for observing naked-eye color change from colorless to yellow on complexation with acetate ions. However, fluorescence emission of this compound is quenched by acetate ions as due PET as shown in Scheme 1.5.[76]

N-Phenyl-N'-(3-quinolinyl)urea **1.69** is highly selective colorimetric and ratiometric sensor for fluoride ion, Sensing process operates through a proton transfer mechanism. By controlling pH the sensor can be reversibly used or recovered for several cycles with only a slight decay.[77]

Bis-ureidoquinoline sensor **1.70**, shows turn-on fluorescence changes in the presence of a fluoride anion and exhibits high selectivity for fluoride in presence of other anions.[78] Sensitive and selective changes caused by fluoride anion on fluorescence emission of **1.70** is attributed to hydrogen-bond interactions between two uriedo groups and fluoride anion.

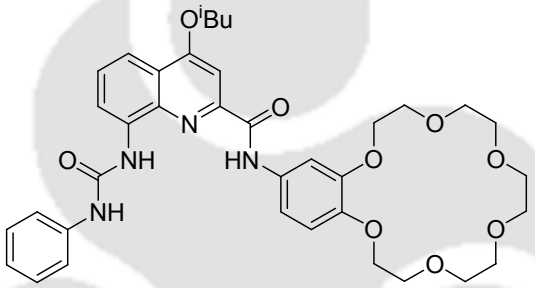

1.71

Receptor **1.71** has crown ether unit attached quinoline and urea moieties, it exhibits higher affinity for chloride ion over other halides. Such selectivity occurs due to presence of a preorganized cavity. The order of selectivity in detection by this receptor is $I^- < Br^- < Cl^-$. This trend is due to higher basicity of chloride ions and size of binding pocket in the receptor fits small anion.[79]

1.5: Metal complexes and coordination polymers of quinoline derivatives

Quinoline is similar to pyridine and it has vast coordination chemistry similar to pyridine. But, functionalized quinoline derivatives provides better scope to form metal complexes as more numbers of coordination sites can be added to such unit through fictionalization. In addition to this, functional group provides directionality and helps in anchoring multiple numbers of metal ions. Thus coordination chemistry of quinoline derivatives is very vast. In this section we attempt to describe some coordination features of identified functional group attached to quinoline

derivative to provide a glimpse of the versatility and possibility to expand such coordination chemistry.

Quinoline carboxylic acid ligands are commonly used to form metallo-organic frameworks.[80-87] Quinoline carboxylic acid can have similar coordination chemistry as that of pyridine carboxylic acids but the differences arises from larger conjugated π-systems, therefore π-π stacking interactions play more important role in the formation of such complexes. Quinoline molecule has week coordinating ability but in quinoline carboxylic acids, carboxylic acid unit helps to form chelated or bridging complexes. For example, 6-quinoline carboxylic acids bind to metal centres in various modes to form coordination polymers as illustrated in Figure 1.12.

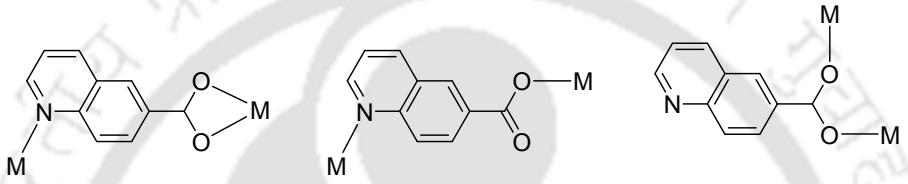

Figure 1.12: Binding modes of quinoline-6-carboxylic acid.

Quinoline-6-carboxylic acid forms two dimensional coordination polymers with Ni^{2+}, Co^{2+} and Cu^{2+} which have wave like net structures having porous packing pattern.[88]

8-quinolyloxy-acetic acid, **1.72** has a flexible tether holding carboxylate moieties, has multifunctional coordination sites. It can form chelate as well as bridging complex through N, O atoms of quinolyl and carboxylate group (Figure 1.13).[89-90] 8-Quinolyloxy-acetic acid forms a helix chain polymer with Cu^{2+} salt while it forms zig-zag chain polymers with $Ni^{2+}$and Co^{2+} salts.[91] Under hydrothermal condition it forms 1-D, 2-D, and 3-D coordination polymers with lanthanide ions, namely Eu^{3+} and Gd^{3+} along with some other auxiliary ligand.[92]

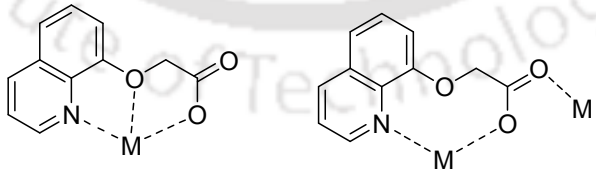

Figure 1.13: Binding modes of 8-quinolyloxy-acetate anion with metals.

Quinoline-2-hydroxy-6-carboxylic acid, **1.73** shows supramolecular features by hydrogen bonds of OH group to make interesting supramolecular motifs (Figure 1.14). Quinoline-2-hydroxy-6-carboxylic acid donot form coordination polymer as nitrogen atom does not take part in the

coordination with metal. This happens as ligand remains in keto form to give dinuclear complex with metal ions as instance with dysprosium.[93]

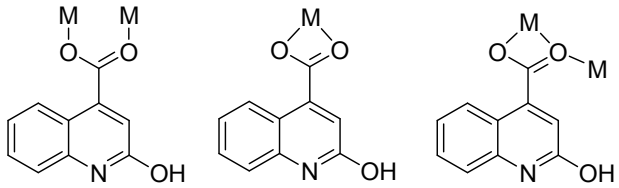

Figure 1.14: Binding modes of quinoline-2-hydroxy-6-carboxylic acid.

Bis(8-carboxamidoquinoline) binaphthol **1.74**,[94] is an interesting quinoline based ligand and it forms selective metal complexes with Zn^{2+} or Cu^{2+} ions which are illustrated in Figure 1.15.

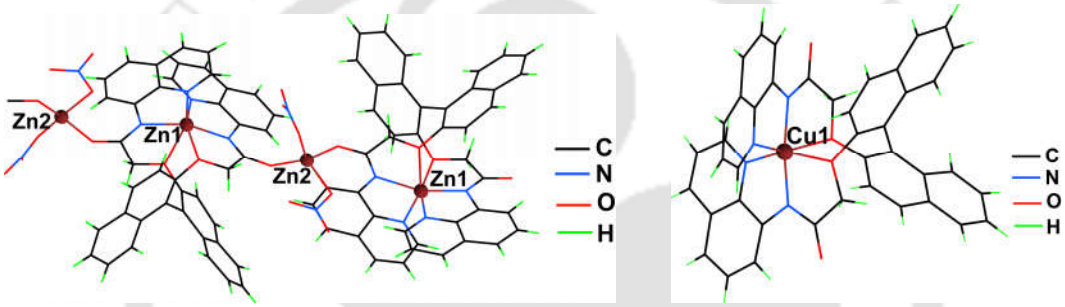

(a) (b)

Figure1.15: (a) Zinc complex and (b) Copper complex of **1.74**.

Erbium complex of hydroxyquinoline derivative **1.75** shows near infra red emission and find use as light emitting diode (Figure 1.16).[95]

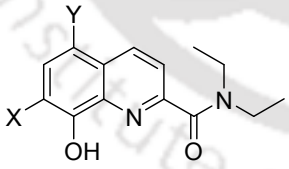

HL1: X,Y=H ; HL2: X= H,Y =Br ; HL3: X,Y =Br

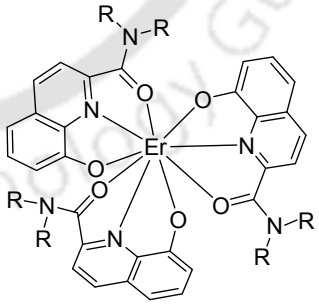

1.75 R = CH_2CH_3

Figure 1.16: Structure of **1.75** and its erbium complex.

Tetrapodal ligand **1.76** forms water soluble chelates with lanthanide ions, which are good sensitizer of NIR luminescence.[96-97]

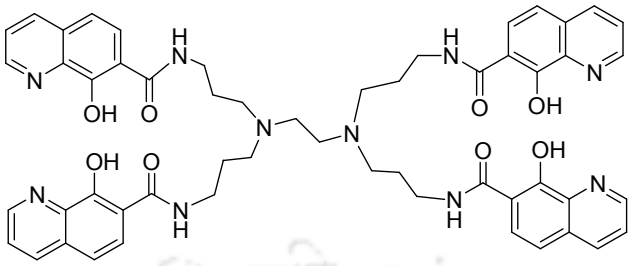

1.76

Reaction of 8-hydroxyquinoline along with 2-bromopropionic acid in presence of sodium hydroxide yields a coordination polymer **1.77**. The coordination polymer on treatment with perchloric acid exchanges anion to form a dinuclear complex **1.78**. The coordination polymer **1.77** can be also used for cadmium coordination polymer **1.79** (Scheme 1.6).[98]

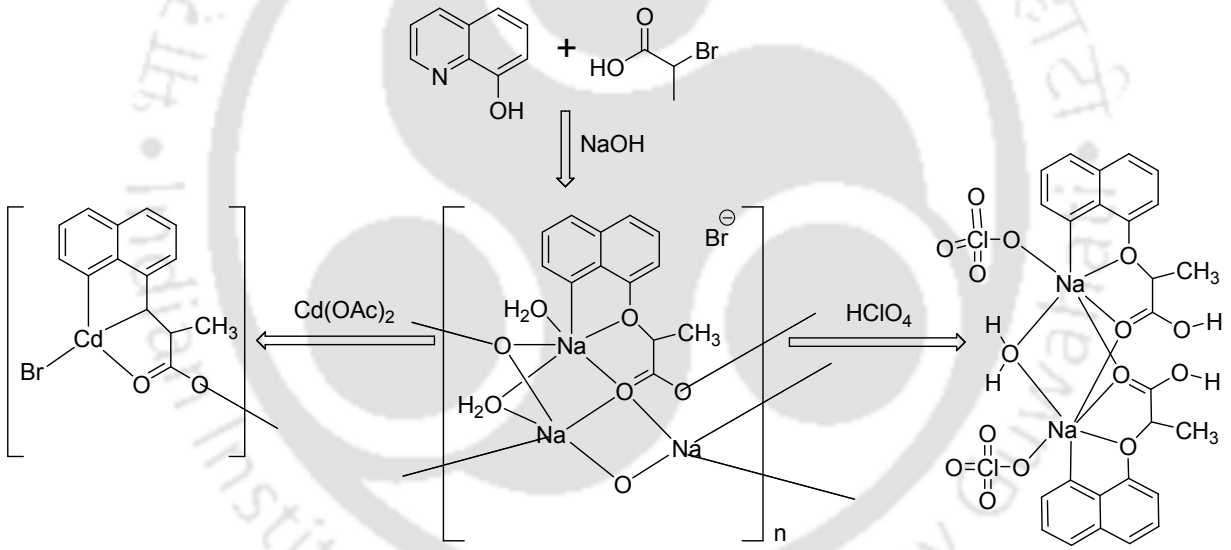

Scheme 1.6: Synthesis of the coordination polymer **1.77**, **1.79** and dinuclear complex **1.78**.

A series of dinuclear paddle-wheel like transition metal complexes of 2-phenylquinoline 4-carboxylic derivative **1.80** are reported. These complexes (Figure 1.17) exhibit antibacterial activities.[99]

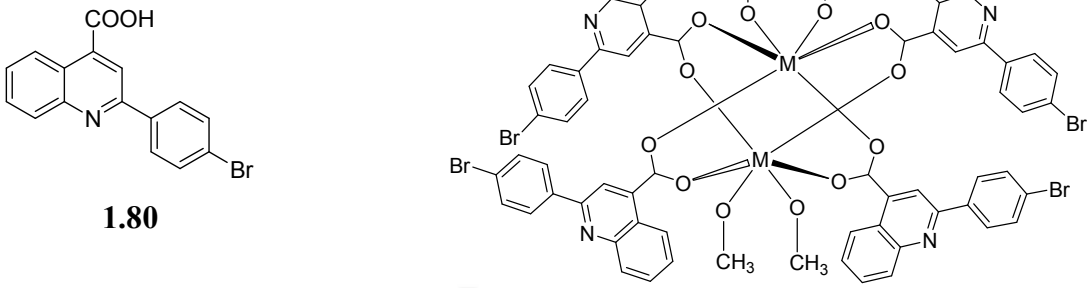

1.80

Figure 1.17: Metal complexes of **1.80**.

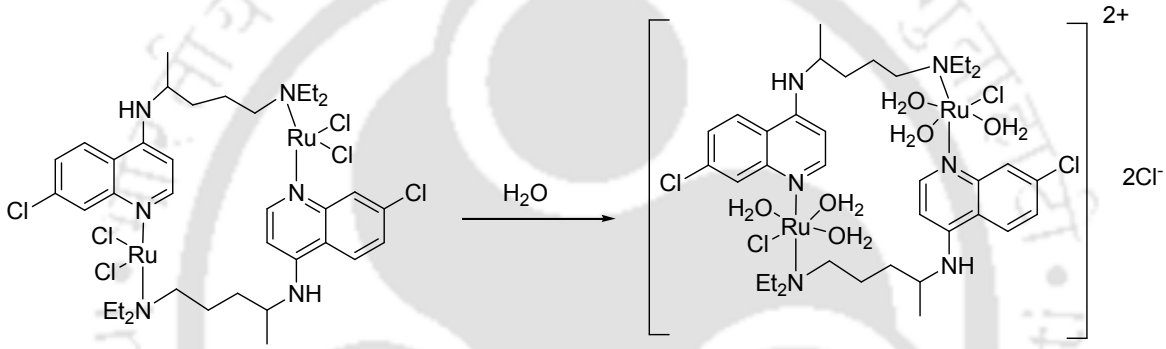

Scheme 1.7: Hydrolysis of ruthenium drug.

Ruthenium chloroquine complexes are drugs for malaria. The mechanism of antimalarial action[100] of ruthenium (II)-chloroquine complex $[RuCl_2(CQ)]_2$ **(1.86)** have suggested that $[RuCl_2(CQ)]_2$ undergoes hydrolyses in aqueous medium to form an ionic species, which is the active drug (Scheme 1.7).

The above discussions provide a platform for showing promising aspects of on quinoline derivatives with a broad spectrum of potential applications.

1.6: Scope of the present work

Among all the quinoline derivatives, 8-hydroxyquinoline is regarded as the second most important chelating agent after EDTA for cation analysis, although most indicators derived from it are not specific enough for the selective detection of specific metal ions.[101]

From the discussion made in earlier sections it is very clear that quinoline derivatives have can be the choice for many supramolecular studies. Quinoline group contains conjugated π-systems

which provide an important contribution in stabilization of the supramolecular assemblies by π-π interactions. The rare earth quinolines are known for their near-infrared luminescence properties, hence they find a wide applications in optoelectronic devices.[102] 8-Hydroxyquinolinate complexe of erbium(III) is known to exhibit infrared luminescence[103-105] and they are used for fabrication of near-infrared-emitting OLEDs.[106-107] Tris(8-hydroxyquinolinato)aluminum(III) exhibits intense green electroluminescence and is an active component in organic light-emitting diodes (OLEDs) operating in the visible region.[108-109] Heteroleptic aluminum(III) *bis*(2-methyl-8-quinolinolate)phenolate complexes show tunable, blue-to green emission.[110]

Many metal complexes of quinoline derivatives find importance biological activities. For example, manganese complexes quinoline derivatives, $[Mn(QA)Cl_2]$ and $[Mn(QA)(OAc)(H_2O)_2](OAc)$ (QA = 2-di(picolyl)amine- N-(quinoline-8-yl)acetamide)) are potential attenuators for absorption of Ca^{2+} in mitochondria and interfere with the metabolism of O_2 for cancer chemotherapy.[111]

Thus, looking at the potentials of these quinoline derivative in the field of supramolecular assemblies, host-guest interactions, biological activities and the properties of the its metal complexes, we have synthesized a number of quinoline derivatives and investigated various aspects including host-guest interactions, polymorphism, molecular recognition and coordination chemistry of these quinoline derivatives.

1.7: Reference

1. F. F. Runge, *Ann. Physik*, 1834, **31**, 68.
2. C**.** Gerhardt, *Annalen*, 1842, **42**, 310.
3. R. Klingenstein, P. Melnyk, S. R. Leliveld, A. Ryckebusch, C. Korth, *J. Med. Chem*., 2006, **49**, 5300.
4. K. C. Fang, Y. L. Chen, J. Y. Sheu, T. C. Wang, C. C. Tzeng, *J. Med. Chem*., 2000, **43**, 3809.
5. S. J. Benkovic, S. J. Baker, M. R. K. Alley, Y. H. Woo, Y. K. Zhang, T. Akama, W. Mao, J. Baboval, P. T. R. Rajagopalan, M. Wall, L. S. Kahng, A. Tavassoli, L. Shapiro, *J. Med. Chem.*, 2005, **48**, 7468.
6. L. Dassonneville, K. Bonjean, M. C. De Pauw- Gillet, P. Colson, C. Houssier, J. Q. Leclercq, L. Angenot, S. Y. Ablordeppey, *Bioorg. Med. Chem*., 2002, **10**, 1337.

7. R. Musiol, J. Jampilek, V. Buchta, L. Silva, H. Niedbala, B. Podeszwa, A. Palka, K, Majerz-Maniecka, B. Oleksynd, J. Polanskia, *Bioorg. Med. Chem.,* 2006, **14**, 3592.
8. K. Nakamoto, I. Tsukada, K. Tanaka, M. Matsukura , T. Haneda, S. Inoue, N. Murai, S. Abe, N. Ueda, M. Miyazaki, N. Watanabe, M. Asada, K. Yoshimatsu, K. Hata, *Bioorg. Med. Chem. Lett.,* 2010, **20**, 4624.
9. S. Aiki, A. Taketoshi, J. Kuwabara, T. Koizumi, T. Kanbara, *J. Organomet. Chem.*, 2011, **696**, 1301
10. E. Błaż, J. Pielichowski, *Molecules,* 2006, **11**, 115.
11. W. A. Ma, Z. X. Wang, *Organometallics*, 2011, **30**, 4364.
12. S. Zhang, W. H. Sun, T. Xiao, X. Hao, *Organometallics*, 2010, **29**, 1168.
13. L. H. Slooff, A. van Blaaderen, A. Polman, G. A. Hebbink, S. I. Klink, F. C. J. M. Van Veggel, D. N. Reinhoudt, J. W. Hofstraat, *J. Appl. Phys.,* 2002, **91**, 3955
14. R. J. Curry, W. P. Gillin, *Appl. Phys. Lett.,* 1999, **75**, 1380.
15. R. J. Curry, W. P. Gillin, *Synth. Met*., 2000, **35**, 111.
16. H. E. Zorel jr, C. A. Ribeiro, M. S. Crespi, *J. Mater. Sci. Lett.*, 2001, **20**, 621.
17. A. Y. Shen, C. P. Chenb, S. Raffler, *Life Sciences*, 1999, **64**, 813.
18. F. Chang, S. Park, H. Kim, *Bull. Korean Chem. Soc.*, 2008, **29**, 1327.
19. R. Katakura, Y. Koide, *Inorg. Chem*., 2006, **45**, 5730.
20. M. Cai, T. Xiao, R. Liu, Y. Chen, R. Shinar, J. Shinar, *Appl. Phys. Lett*., 2011, **99**, 153303.
21. N. Rolfe, P. Desai, P. Shakya, T. Kreouzis, W. P. Gillin, *J. Appl. Phys*., 2008, **104**, 083703.
22. D. Singh, J. B. Baruah, *Cryst. Growth Des*., 2012, **12**, 3169.
23. A. Karmakar, R. J. Sarma, J. B. Baruah, *CrystEngComm*., 2007, **9**, 379.
24. D. Kalita, H. Deka, S. S. Samanta, S. Guchait, J. B. Baruah *J. Mol. Struct*., 2009, **935**, 47.
25. D. Kalita, J. B. Baruah, *CrystEngComm.*, 2010, **12**, 1562.
26. Y. Furusho, Y.Tanaka, T. Maeda, M. Ikeda, E. Yashima, *Chem. Commun.,* 2007, 3174.
27. L. -S. Li, H. Jiang, B.W. Messmore, S. R. Bull, S. I. Stupp, *Angew. Chem. Int. Ed. Eng.*, 2007, **46**, 5873.
28. D. Kalita, J. B. Baruah, *Cryst. Growth Des*. 2011, **11**, 5131.
29. G. Smith, U. D. Wermuth, J. M. White, *Chem. Commun.*, 2000, 2349.
30. A. D. Gonzalez, H. Hopfl, F. Medrano, A. K. Yatsimirsky, *J. Org. Chem*., 2010, **75**, 2259.
31. D. Kalita, J. B. Baruah, *J. Mol. Struct.,* 2010, **969,** 75.

32. N. Kameta, K. Hiratani, *Chem. Commun*., 2005, 725.
33. K. Ghosh, S. Adhikari, A. P. Chattopadhyay, P. R. Chowdhury, *Beilstein J. Org. Chem.*, 2008, **4**, 52.
34. K. Ghosh, S. Adhikari; *Tetrahedron Lett*., 2006, **47**, 3577.
35. C. He, Z. Lin, Z. He, C. Duan, C. Xu, Z. Wang, C. Yan, *Angew. Chem. Int. Ed.* 2008, **47**, 877.
36. Y. Liu, X. Wu, C. He, R. Zhang, C. Duan, *Dalton Trans*., 2008, 5866.
37. A. P. de Silva, H. Q. Nimal Gunaratne, T. Gunnlaugsson, A. J. M. Huxley, C. P. McCoy, J. T. Rademacher, T. E. Rice, *Chem. Rev.,*1997, **97**, 1515.
38. M. Sarkar, S. Banthia, A. Patil, M. B. Ansari, A. Samanta, *New J. Chem.* 2006, **30**, 1557.
39. M. Sarkar, S. Banthia, A. Samanta, *Tetrahedron Lett.,* 2006, **47**, 7575.
40. S. Banthia, A. Samanta. *J. Phys. Chem. B,* 2006, **110**, 6437.
41. J. Jiang, H. Jiang, X. Tang, L. Yang, W. Dou, W. Liu, R. Fang, W. Liu, *Dalton Trans.*, 2011, **40**, 6367.
42. L. Xue, C. Liu, H. Jiang, *Chem. Commun.,* 2009, 1061.
43. Z. Zhou, M. Yu, H. Yang, K. Huang, F. Li, T. Yi, and C. Huang, *Chem. Commun.,* 2008 3387.
44. M. F. Budyka, N. I. Potashova, T. N. Gavrishova, V. M. Lee, *High Energ. Chem*., 2011, **45**, 281.
45. Z. Dong, X. Le, P. Zhou, C. Dong, J. Ma, *RSC Adv.***,** 2014, **4**, 18270.
46. C. G. Anklin, P. S. Pregosin, *Magn. Reson. Chem*., 1985, **23**, 671.
47. P. D. Zalewski, S. H. Millard, I. J. Forbes, O. Kapaniris, A. Slovotinek, W. H. Betts, A. D. Ward, S. F. Lincoln, I. Mahadevan, *J. Histochem. Cytochem*., 1994, **42**, 877.
48. Y. Zhang, X. Guo, W. Si, L. Jia, X. Qian, *Org. Lett*., 2008, **10**, 473.
49. J. Du, J. Fan, X. Peng, H. Li, S. Sun, *Sensors and Actuators B,* 2010, **144**, 337.
50. H. -H. Wang, Q. Gan, X. -J. Wang, L. Xue, S. -H. Liu, H. Jiang, *Org. Lett.*, 2007, **9**, 4995.
51. E. M. Nolan, J. Jaworski, K. -I. Okamoto, Y. Hayashi, M. Sheng, S. J. Lippard, *J. Am. Chem. Soc*., 2005,**127**, 16812.
52. C. J. Frederickson, E. J. Kasarskis, D. Ringo, R. E. Frederickson, *J. Neurosci.Methods,* 1987, **20**, 91.
53. W. Lin, L. Yuan, Z. Cao, J. Feng, Y. Feng, *Dyes and Pigments,* 2009, **83**, 14.
54. L. Xue, Q. Liu, H. Jiang, *Org. Lett.,* 2009, **11**, 3454.

55. S. X. Wang, X. M. Meng, M. Z. Zhu, *Tetrahedron Lett.,* 2011, **52**, 2840.
56. L. Xue, H. -H. Wang, X. -J. Wang, H. Jiang, *Inorg. Chem.,* 2008, **47**, 4310.
57. X. -Y. Chen, J. Shi, Y. -M. Li, F. -L. Wang, X. Wu, Q. -X. Guo, L. Liu, *Org. Lett.,* 2009, **11**, 4426.
58. E. Ballesteros, D. Moreno, T. Gomez, T. Rodriguez, J. Rojo, M. Garcia-Valverde, T. Torroba, *Org. Lett.*, 2009, **11**, 1269.
59. L. Xue, G. P. Li, Q. Liu, H. H. Wang, C. Liu, X. Ding, S. He, H. Jiang, *Inorg. Chem.,* 2011, **50**, 3680.
60. X. -L. Tang, X. -H. Peng, W. Dou, J. Mao, J. -R. Zheng, W. -W. Qin, W. -S. Liu, J. Chang, X. -J. Yao, *Org. Lett.,* 2008, **10**, 3653.
61. Y. Li, H. Chong, X. Meng, S. Wang, M. Zhu, Q. Guo, *Dalton Trans.*, 2012, **41**, 6189.
62. K. C. Song, J. S. Kim, S. M. Park, K. -C. Chung, S. Ahn, S. -K. Chang, *Org. Lett.* 2006, **8**, 3413.
63. H. Yang, Z. Zhou, K. Huang, M. Yu, F. Li, T. Yi, C. Huang, *Org. Lett.,* 2007, **9**, 4729.
64. S. Aoki, K. Sakurama, N. Matsuo, Y. Yamada, R. Takasawa, S. Tanuma, M. Shiro, K. Takeda, E. Kimura, *Chem. Eur. J.,* 2006, **12**, 9066.
65. H. -H. Wang, L. Xue, Y.-Y. Qian, H. Jiang, *Org. Lett.,* 2010, **12**, 292.
66. G. -K. Li, Z. -X. Xu, C. -F. Chen, Z. -T. Huang, *Chem. Commun.,* 2008, 1774.
67. T. Moriuchi-Kawakami, J. Sato, Y. Shibutani, *Anal. Sci.,* 2009, **25**, 449.
68. Z. -X. Han, H. -Y. Luo, X. -B. Zhang, R. -M. Kong, G. -L. Shen, R. -Q. Yu, *Spectrochim. Acta. A,* 2009, **72**, 1084.
69. P. Baret, C. G. Beguin, H. Boukhalfa, C. Caris, J. P. Laulhtre, J. L. Pierre, G. Serratrice, *J. Am. Chem. Soc*., 1995, **117**, 9760.
70. G. Serratrice, H. Boukhalfa, C. Beguin, P. Baret, C. Caris, J. L. Pierre, *Inorg. Chem.*, 1997**,** **36**, 3898.
71. R. S. Sujith, G. N. Rao, C. Janadhana, *Spectrochim. Acta.,* 2006, **65A**, 565.
72. S. Goswami, R. Chakrabarty, *Tetrahedron Lett*., 2009, **50**, 5994.
73. M. Albrecht, Triyanti, M. de Groot, M. Bahr, E. Weinhold, *Synlett.,* 2005, **13**, 2095.
74. Z. -H. Sun, M. Albrecht, R. Fröhlich, *Eur. J. Org. Chem.,* 2013, 3254.
75. T. H. Russ, A. Pramanik, M. E. Khansari, B. M. Wong, M. A. Hossain, *Nat. Prod. Commun.*, 2012, **7**, 301.

76. J. Shao, *Spectrosc Lett.*, 2012, **45**, 262.
77. C. Jia, B. Wu, L. Liang, X. Huang, X. Yang, *J. Fluoresc.,* 2010, **20**, 291.
78. Y. Jo, N. Chidalla, D. -G. Cho, *J. Org. Chem.,* 2014, **79**, 9418.
79. Z. -H. Sun, F. -F. Pan, Triyanti, M. Albrecht, G. Raabe, *Eur. J. Org. Chem*., 2013, 7922.
80. X. H. Bu, M. L Tong, H. C. Chang, S. Kitagawa, S. R. Batten, *Angew. Chem., Int. Ed.,* 2004, **43**,192.
81. H. S. Lin, P. A. Maggard, *Inorg. Chem.,* 2007, **46**, 1283.
82. D. Dobrzynska, L. B. Jerzykiewicz, J. Jezierska, M. Duczmal, *Cryst. Growth Des.*, 2005, **5**, 1945.
83. X. H. Bu, M. L. Tong, Y. B. Xie, J. R. Li, H. C. Chang, S. Kitagawa, J. Ribas, *Inorg. Chem.*, 2005, **44**, 9837.
84. X. H. Bu, M. L Tong, J. R. Li, H. C. Chang, L. J. Li, S. Kitagawa, *CrystEngComm.,* 2005, **7,** 411.
85. M. A. M. Abu-Youssef, A. Escuer, V. Langer, *Eur. J. Inorg. Chem.*, 2006, 3177.
86. M. A. M. Abu-Youssef, V. Langer, *Polyhedron*, 2006, **25**, 1187.
87. Z. F. Chen, P. Zhang, R. G. Xiong, D. J. Liu, X. Z. You, *Inorg. Chem. Commun.*, 2002, **5**, 35.
88. S. Hu, H. H. Zou, M. H. Zeng, Q. X. Wang, H. Liang. *Cryst. Growth Des.*, 2008, **8**, 2346.
89. X. N. Cheng, W. X. Zhang, X. M. Chen, *J. Am. Chem. Soc*., 2007, **129**, 15738.
90. Z. H. Wang, J. Fan, W. G. Zhang, J. Wang, *Acta Crystallogr. Sect. E*, 2008, **64**, m1446.
91. Y. H. Wang, R. F. Song, F. Y. Zhang, *J. Mol. Struct*., 2005, **752**, 104.
92. J. Fan, Z. H. Wang, M. Yang, X. Yin, W. G. Zhang, Z. F. Huang, R. H. Zeng, *Cryst Eng Comm.*, 2010, **12**, 216.
93. R. Feng, F. L. Jiang, M. Y. Wu, L. Chen, C. F. Yan, M. C. Hong, *Cryst. Growth Des.*, 2010, **10**, 2306.
94. L. Tang , J. Zhao, M. Cai, P. Zhou, K. Zhong, S. Hou, Y. Bian, *Tetrahedron Lett.,* 2013, **54**, 6105.
95. M. Albrecht, O. Osetska, J. Klankermayer, R. Fröhlich, F. Gumy, J. C. G. Bünzli, *Chem. Commun.,* 2007, 1834.
96. D. Imbert, S. Comby, A. S. Chauvin, J. C. G. Bunzli, *Chem. Commun*., 2005, 1432.
97. S. Comby, D. Imbert, A. S. Chauvin , J. C. G. Bu1nzli, *Inorg. Chem*., 2006, **45**, 732.

98. D. Kalita, R. Herbst-Irme, D. Stalke, J. B. Baruah, *Polyhedron,* 2012, **44**, 52.
99. Qin, F. -X. Li, L. Xue, N. Lei, Q. -L. Ren, D. -Y. Wang, H. -L. Zhu, *Acta Chim. Slov.,* 2014, **61**, 170.
100. S. Levy, S. J. Azoulay, *Cardiovas. Electrophysiol*., 1994, **5**, 635.
101. P. Jiang, Z. Guo, Coord. *Chem. Rev.*, 2004, 248, 205.
102. L. H. Slooff, A. van Blaaderen, A. Polman, G. A. Hebbink, S. I. Klink, F. C. J. M. Van Veggel, D. N. Reinhoudt and J. W. Hofstraat, *J. Appl. Phys.,* 2002, **91**, 3955.
103. R. Van Deun, P. Fias, K. Binnemans, C. Gorller-Walrand, *Phys. Chem. Phys*., 2003, **5**, 2754.
104. W. P. Gillin, R. J. Curry, *Appl. Phys. Lett*., 1999, **74**, 798.
105. S. W. Magennis, A. J. Ferguson, T. Bryden, T. S. Jones, A. Beeby, I. D. W. Samuel, *Synth. Met.,* 2003, **138**, 463.
106. R. J. Curry, W. P. Gillin, *Appl. Phys. Lett.,* 1999, **75**, 1380.
107. R. J. Curry, W. P. Gillin, *Synth. Met*. 2000, **111**, 35.
108. W. E. Ohnesorge, L. B. Rogers, *Spectrochim. Acta.,* 1959, **15**, 27.
109. K. Sano, Y. Kawata, T. I. Urano, Y. Mori, *J. Mater. Chem*., 1992, **2**, 767.
110. C. Pérez-Bolívar, V. A. Montes, P. Anzenbacher, Jr., *Inorg. Chem.*, 2006, **45**, 9610.
111. Z. -W. Wang, Q. -Y. Chen, Q. -S. Liu, *Transition Met Chem*., 2014, **39**, 917.

Chapter 2

Synthesis, characterization and properties of Zinc (II), Manganese (II) and Cobalt (II)-8-oxyquinolate clusters

Metal ions such as magnesium, zinc, cobalt, nickel, copper and molybdenum forms complexes with 8-hydroxyquinoline which finds application in analytical chemistry.[1] Depending on pH of the medium 8-hydroxyquinoline in separation of aluminum from beryllium and magnesium, and also in the separation of beryllium in the presence of aluminum, iron, titanium, and zirconium.[2] Beside these, metal complexes of 8-hydroxyquinoline are used in organic light emitting diodes (OLED).[3] 8-hydroquinoline can form different metal complexes with same metal ions, for instance, it forms mono nuclear bis(quinolinato)zinc complex from acidic reaction condition.[4] On the other hand, anhydrous zinc-quinolinate complex is polymeric, it can be prepared by recrystallisation of a hydrated form from gas phase.[5] The dehydration process is shown in Figure 2.1. There are also examples of tetra nuclear zinc oxyquinolinate complex having terminal carboxylate group. Such tetra nuclear complex can be easily converted into coordination polymer by attaching dicarboxylate in place of carboxylate group. An example of coordination polymer is shown in Figure 1.1b. In this coordination polymer tetruclear zinc-oxyquinolinate units are held by oxalate.[6-7]

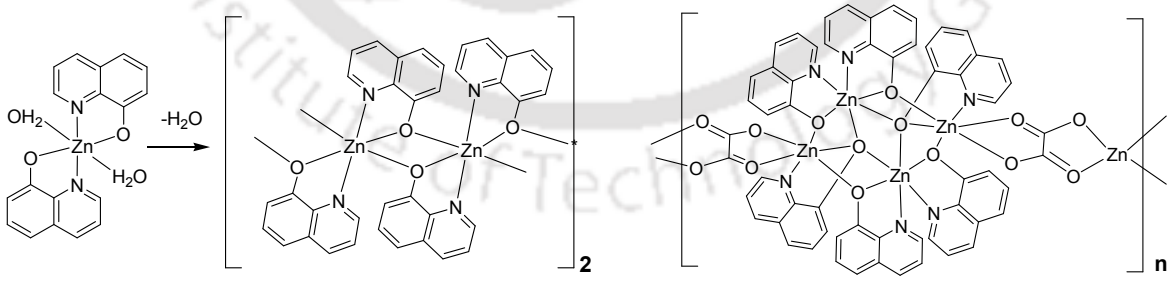

(a) (b)

Figure 2.1 (a) Conversion of mononuclear zinc complex to polynuclear complex by dehydration. (b) A coordination polymer of zinc-oxyquinolinate having oxalate bridges.

There are numbers of examples of other metal complexes in which 8-hydroxquiniline act as the sole ligand or it is a constituent of mixed ligand complex. In all these complexes 8-hydroxyquinoline binds through various binding modes such as (i) chelating, (ii) bridging with μ^2-oxy, (iii) chelating-bridging with μ^2- oxy, and (iv) chelating-bridging with μ^3- oxy (Figure 2.2).[8]

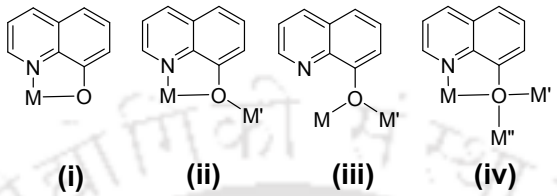

Where M and M' are metal ions

Figure 2.2: Binding modes of 8-hydroxyquinoline.

As far as tetranuuclear oxyquinolinate complexes are concerned they have close structural features to that of metalcarboxylate complexes.[9] In literature many examples of tetra nuclear zinc clusters such as $Zn_4O(acetate)_6$ has been used as molecular model for zinc oxide as this tetra nuclear zinc cluster has a central oxygen atom which hold four zinc atoms in tetrahedral coordination environment.[10] More importantly metallo-organic frameworks of such motifs are important, as porous materials have gas absorbing properties.[11-12] Although there was a report on tetra nuclear oxyquinolinate zinc complex,[6] however, no further work in this regard such as to find out their solvation arising due to packing patterns. On the other hand such chemistry has not been extended to other metal ions. Moreover, recently we have shown that 1,8-dicarboxynaphthoic acid which has some structural similarity to 8-hydroxyquinoline in terms of position of binding sites forms dinuclear, tetra nuclear or hexanuclear complexes with various metal ions depending on the ancillary lignads.[9] Thus we have chosen to study the synthesis, reactivity and various properties of teranuclear zinc-oxyquinolinate complexes.

2.1: Zinc (II) oxyquinolate complexes

Reaction of equimolar amount of 8-hydroxyquinoline with zinc chloride in different solvents such as hydroxyquinoline in dimethylformamide (DMF), dimethylacetamide (DMA) and dimethylsulfoxide (DMSO) respectively yielded corresponding solvates of tetra nuclear zinc-oxyquinolate complexes each having a general composition $[Zn_4(oxyQ)_6Cl_2\ ].(DMF)_2$ **(2.1),**

$[Zn_4(oxyQ)_6Cl_2].(DMA)_2$ (**2.2**) and $[Zn_4(oxyQ)_6Cl_2\ ].(DMSO)_2$ (**2.3**) as shown in the Scheme 2.1. On the other hand, the bromide containing zinc-oxyquinolate complex $[Zn_4(oxyQ)_6Br_2\ ].(DMF)_2$ (**2.4**) was synthesized by similar reaction between 8-hydroxyquinoline with zinc bromide.

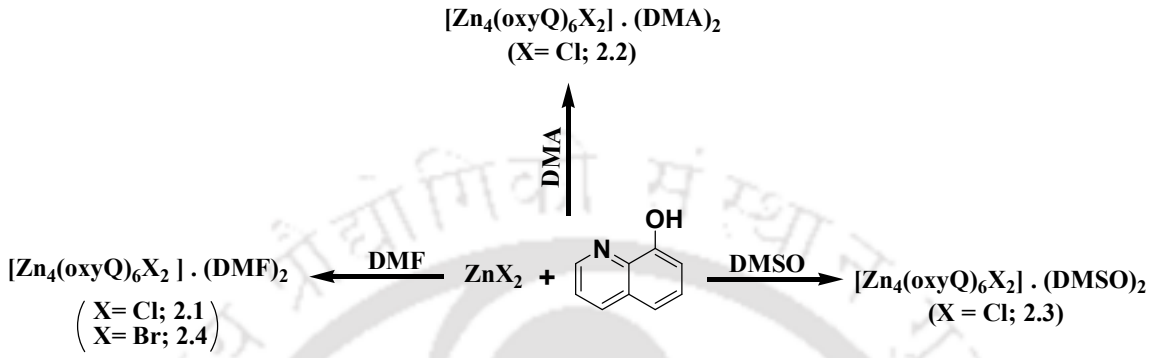

Scheme 2.1: Synthesis of zinc complexes **2.1**, **2.2, 2.3** and **2.4**.

All these complexes were characterized by FT-IR, elemental analysis, thermogravimetry, powder X-ray diffraction and single crystal structure determination. Each of these complexes has similar FTIR spectra, however they have unique characteristic powder x-ray diffractions pattern which makes them different from each other. Comparable diffraction pattern may suggest their similarity in packing patterns.

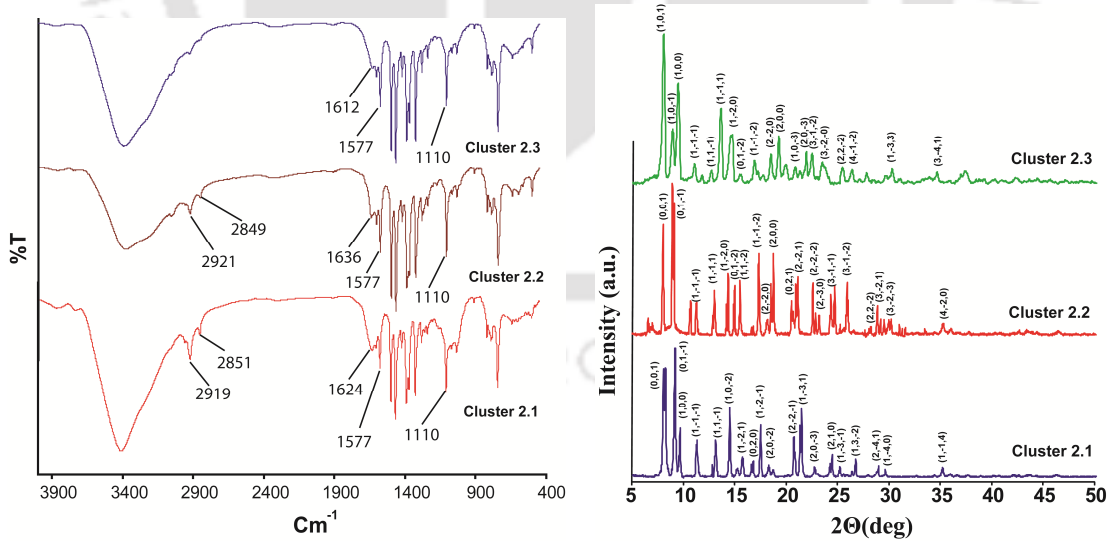

(a) (b)

Figure 2.3: (a) FT-IR spectra overlay and (b) Powder XRD pattern overlay of DMF solvate (**2.1**), DMA solvate (**2.2**) and DMSO solvate (**2.3**).

Although solid state IR spectra have shown distinction among the solvates, but each exchanges the solvent molecules with absorbed water while making KBr pallet, thus each shows strong OH stretching absorptions at 3397 cm^{-1}, 3362 cm^{-1} and 3376 cm^{-1}. DMF shows strong absorption at 1624 cm^{-1},[13] which is seen in the solvate **2.1**, DMSO shows a strong S-O stretching at 1105 cm^{-1},[14] in the DMSO solvate **2.3** there is an absorption at this region because of C-O stretching, hence could not be distinguished. However, the powder XRD were recorded which is shown in Figure 2.3. Indexing of Miller indices of powder X-ray diffraction patterns were done on the basis of the crystallographic information files of respective crystal structure that were determined by single crystal X-ray diffraction. When we compared the simulated powder patterns of these complexes with the experimental data it was confirmed that the experimental diffraction patterns matches with the simulated diffraction obtained from single crystal diffraction data, it implies high purity bulk materials.

Three tetra nuclear zinc-oxyquinolate complexes **2.1-2.3** are isostructural, each belong to *P-1* space group and have unit cell volume 1457.18 (14) $Å^3$, 1482.62 (15) $Å^3$, 1445.71 (18) $Å^3$ and 1470.82(16) $Å^3$ respectively. The respective crystal densities are 1.531 g/cm^3, 1.536 g/cm^3, 1.555 g/cm^3 and 1.617 g/cm^3. The complexes have similar tetra-nuclear zinc core as for the complex **2.1** shown in Figure 2.4a. Zinc ions in the complexes are in two different types of environments. The zinc sites holding halide ions are penta-coordinated while the other two zinc sites are hexa-coordinated. Hexa-coordinated zinc sites have zinc atoms coordinated to four oxygen atoms from independent oxyquinolates and two nitrogen atoms from two independent oxyquinolates giving a distorted octahedral geometry around the zinc atom. These octahedral centre have Zn2-O1 bond has distance of 2.103 Å, while Zn2-O2, Zn2-O3 and Zn2-N3 bonds have 2.136 Å, 2.109 Å and 2.081 Å respectively. Moreover the angle O1-Zn2-N1 and N1-Zn2-N3 are 79.5º and 98.2º respectively which imply a distorted octahedral geometry of hexa-coordinated sites of the complex. The basal plane is occupied by two O2 atoms, N1 and N3 atoms whereas O1 and O3 occupy the axial positions of the octahedral. Whereas, in case of penta-coordinated zinc sites three oxygen atoms from three independent oxyquinolines, a nitrogen atom and chloride anion coordinate to give trigonal bipyramidal environments. In these sites O1, N2 and O3 atoms form the base plane, while O2 and Cl1occupy axial positions. Bond angles of the equatorial plane are 107º, 117º and 118º respectively, whereas between the axial positions is171º. Zn-O bonds are in

the range of 2.0 to 2.31 Å and zinc nitrogen bonds are in the range of 2.08 to 2.10 Å, which are conventional bond distances observed in zinc oxyquinolate complexes.[4, 6]

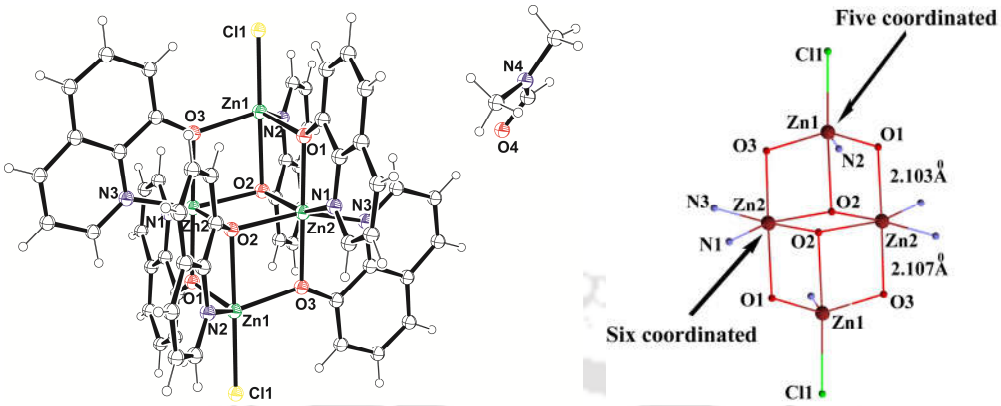

(a) (b)

Figure 2.4: (a) Structure of the complex **2.1** (drawn in 30% thermal ellipsoid), (b) Coordination environment in $[Zn_4(oxyQ)_6Cl_2]$ complex (drawn after removing organic part).

Table 2.1: Bond lengths and bond angles of the complexes **2.1**, **2.2** and **2.3**.

Bond	Length (Å)	Length (Å)	Length (Å)	Bond angle	Angle (°)	Angle (°)	Angle (°)
	Complex **2.1**	Complex **2.2**	Complex **2.3**		Complex **2.1**	Complex **2.2**	Complex **2.3**
Zn1-Cl1	2.28(11)	2.28(2)	2.28(2)	Cl1-Zn1-O1	108.47(8)	108.02(14)	109.83(13)
Zn1-O1	2.00(4)	2.00(5)	1.99(5)	Zn1-O2-Zn2	95.66(9)	95.63(17)	106.80(2)
Zn1-O2	2.31(2)	2.30(4)	2.32(4)	Cl1-Zn1-O2	171.98(8)	171.73(12)	171.33(12
Zn1-O3	2.00(3)	2.01(5)	2.01(5)	Cl1-Zn1-O3	106.40(8)	106.65(14)	105.23(13)
Zn1-N2	2.10(4)	2.10(6)	2.10(5)	Zn1-O2-Zn2a	96.99(10)	97.00(16)	97.82(15)
Zn2-O1	2.10(2)	2.10(4)	2.10(4)	Cl1-Zn1-N2	97.56(10)	97.26(18)	77.41(17)
Zn2-O2	2.13(3)	2.14(5)	2.12(5)	Zn2-O2-Zn2a	100.30(11)	100.29(15)	99.96(14)
Zn2 -N1	2.08(4)	2.08(6)	2.09(6)	Zn1-O3-Zn2a	107.04(13)	106.80(2)	96.68(16)

Comparisons of various metal ligand bond distances among the complexes **2.1-2.3** are listed in Table 2.1. This comparison of bond distances suggests that the tetra nuclear metal complexes have similar structure however, with a small but definite have effect on change of solvent of crystallization. The solvents have effects in the geometry of the tetra-nuclear complex in complexes **2.1-2.3**. Complexes **2.1** and **2.2** have DMF and DMA as solvent of crystallization, solvent belongs to homologous series, and accordingly there is less difference in the structure of the host part. However, complex **2.3** has DMSO as solvent of crystallization; it has a clear difference in the Zn1-O2-Zn2 bond angle at one face without significantly affecting analogous

bond on other faces. Thus, presence of DMSO solvent causes slight distortion of one face of the tetra nuclear complex.

Complex **2.4** has bromide ligands instead of chloride that are present in complex **2.1**; and structurally both are alike. Complex **2.1** and **2.4** both have DMF as solvent of crystallization but they posses different halide, former has two chlorides, whereas later has two bromides. It has Zn-Br distances 2.432Å. Other metal-ligand bond parameters are provided in appendix; despite these two complexes have structural similarities. However, there are differences between the two complexes for instances bond distance of Zn1-O2 is 2.313 Å in case of complex **2.1** whereas, this bond distance is slightly shorter in case of complex **2.4**, i.e. 2.285 Å. Again, distances of Zn1-O3 bond in former complex **2.1** is 2.007 Å whereas this bond is found to be slightly longer (i.e. 2.013 Å) in complex **2.4**. Moreover, differences in zinc-halide bond distances between the two complexes are also observed. The Zn-Cl distance is 2.283 Å whereas, the Zn-Br distance is found to be 2.4323 Å. The longer bond distance in case of Zn-Br bond can be attributed to the greater ionic radius of bromide ion compared to chloride ion. In both cases the halogens project away and do not interfere in the knitting of the tetra nuclear units. Due to differences in electro negativity of chloride and bromide ions, metal-oxygen bond distances of the site where the halides are attached get affected. This also influences packing patterns due to the difference present between the halides that play a vital role providing a definite shape to these complexes.

We have also examined packing patterns of these complexes and found that in each case they are guided by C-H···π and C-H···X interactions. Since the packing arrangements have similarities, one illustrative example to show such interactions is shown in Figure 2.5a and 2.5b. Figure 2.2a shows C-H···π interactions between C-H bond opposite to nitrogen atom 8-hydroxyquinoline ring and Figure 2.2b illustrates C-H···X interactions. It is a well known fact that interplay of weak interactions such as C-H···π[15] and C-H···X[16] interactions greatly contributes to their stability in solid state. In complex **2.1**, C11-H···Cl1 has hydrogen bond donor-acceptor distance $d_{H11\cdots Cl1}$ 2.819 Å and angle < C11-H11···Cl1, 130.1°; which suggest a considerably weak interaction but these bond parameters are within admissible limit to have a C-H···X interaction. Distance between the centriod of π-cloud of quinoline to the H of C3-H3 bond is 2.92 Å. This separation is also favorable for C-H···π interactions.

Solvent molecules such as DMF, DMA and DMSO as solvated species contribute to stability of their respective crystal lattice by involving in C-H···O and other X-H···O interactions (where X

= N, O, halogen etc.). In the present cases, solvent molecules are held loosely by very weak hydrogen bond interactions. Dimethylformamide in complex **2.1** has C-H···O as well as C-H···π interactions with the host molecule to be anchored in crystal lattice.

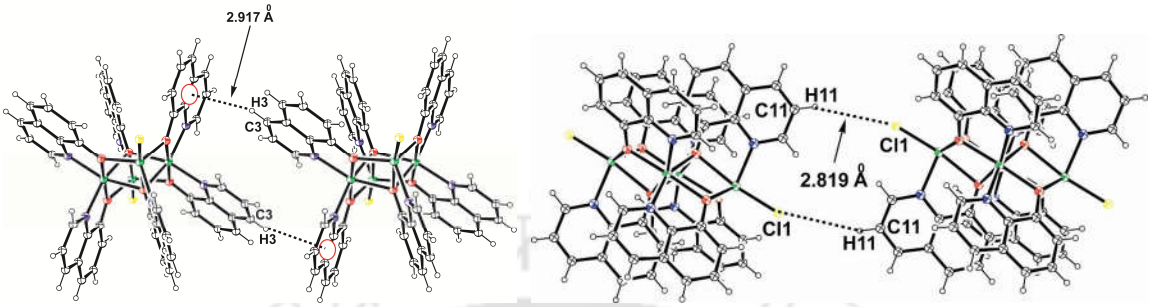

(a) (b)

Figure 2.5: (a) The C-H···π interactions and (b) C-H···Cl interactions in the complex **2.1**.

Structurally these clusters are very interesting, as tetra nuclear zinc carboxylates picks up oxygen atom to form Zn_4O unit, in such structures an oxy-anion holds four zinc ions.[12] Generally oxy-anion in these complexes is picked up from moisture during synthesis of the complexes. This is especially true in case of methyl-phenylcarboxylate tetra nuclear cluster of zinc, in which careful reaction condition could not help in exclusion of oxide.[12] On the other hand, due to such difficulties many zinc carboxylate clusters are prepared either in inert condition or using organometallic route. Such difficulties were also reported from our group[17] where it is observed that tetra nuclear benzthizaolate complex of zinc also adopts a structure in which oxyanion gets incorporated. For comparison the structure and coordination geometry of the complex is given in Figure 2.6.[12]

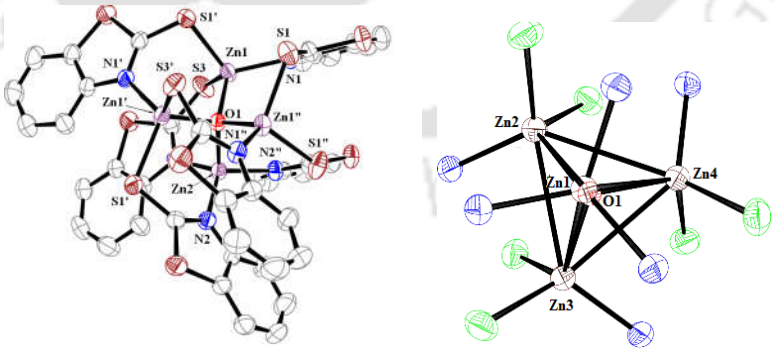

(a) (b)

Figure 2.6: (a) Structure of bezthiozolatezincoxy cluster (b) Coordination environment of the Zn_4O cluster.

Zinc clusters of Zn_4O family act as building blocks for the constructions of various types of porous frameworks which show selective gas absorption.[11] Due to weak binding with solvent molecules, the complexes **2.1-2.4** lose their solvent molecules at relatively low temperature, which are reflected in their thermal analysis. Since these tetra nuclear complexes are relatively large in size, their packing patterns themselves should result in voids in between them and make them suitable for physisorption study. Thermograph of the DMF solvate **2.1** is shown in Figure 2.7a suggests weight loss at 90-137 °C due to loss of two molecules of DMF (theoretical 10. 9% and found 8.9 %) and compound is thermally stable up to 350 °C. Thermal decomposition in case of solvates can be correlated by Scheme 2.2.

$$[Zn_4(oxyQ)_6Cl_2].(solvent)_2 \rightarrow [Zn_4(oxyQ)_6Cl_2] \rightarrow [Zn_4(oxyQ)_3(OH)(O)Cl_2]$$

Scheme 2.2: The thermal decomposition of the complexes **2.1-2.3**.

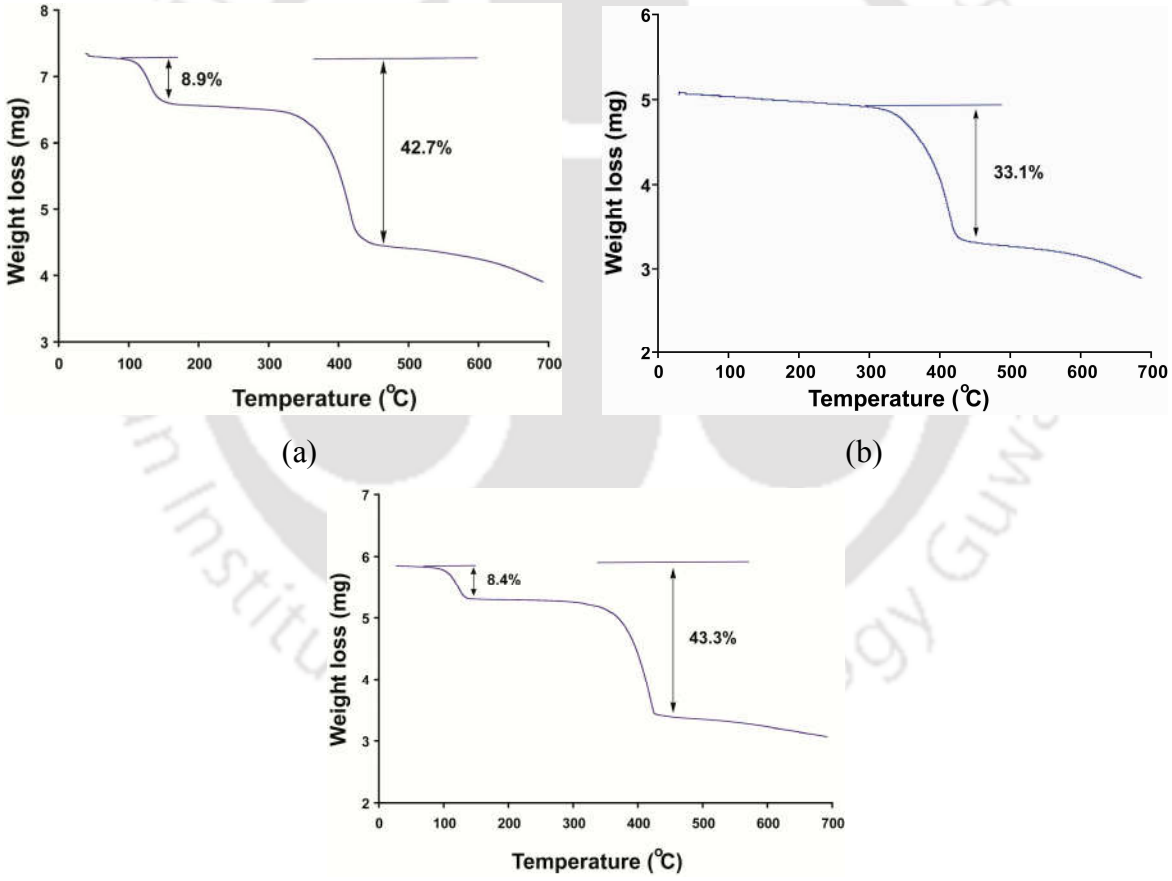

Figure 2.7: Thermogram of (a) complex **2.1**, (b) Sample prepared by heating complex **2.1** at 200°C followed by cooling to room temperature and (c) De-solvated sample of **2.1** after exposing to moisture for a day (Heating rate in each case 5°C per minute).

It involves two steps; first is loss of solvent, followed by decomposition of the complex to lose three 8-hydroxyquinolate units. For complex **2.1**, the calculated weight loss to form a composition $[Zn_4(oxyQ)_3(OH)(O)Cl_2]$ is 41.1% whereas found weigh loss in the temperature of 350-450°C is 42.7 %. The complex **2.4** also has shown a similar trend of thermal decomposition as complex **2.1**. Complex **2.1** on heating at 200°C resulted de-solvated complex, which on standing under ordinary atmospheric condition at room temperature slowly absorbs moisture to yield hydrated form. The water absorption process is reversible. Process is illustrated by three thermograms of the complex after and before heating at 200°C (Figure 2.7). Complex **2.1** heated at 200°C on standing at room temperature absorb moisture; this process is reflected in the weight loss in the thermogram of the de-solvated sample after exposing to moisture (Fig. 2.7c). Similar phenomenon of absorption of atmospheric moisture is also shown by complex **2.4**. The de-solvation and exchange of solvent by water molecules can be monitored by change in color of the sample. For example initial brownish green color of the sample changes to orange on heating which returns to greenish color on accepting water as illustrated in the photograph of the sample shown in Figure 2.8.

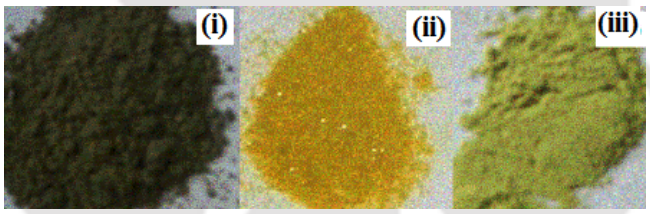

Figure 2.8: Photograph of the powdered sample (i) complex **2.4**, (ii) de-solvated complex **2.4** by heating at 200 °C for 1h and (c) sample after keeping de-solvated complex **2.4** overnight in a closed chamber saturated with moisture.

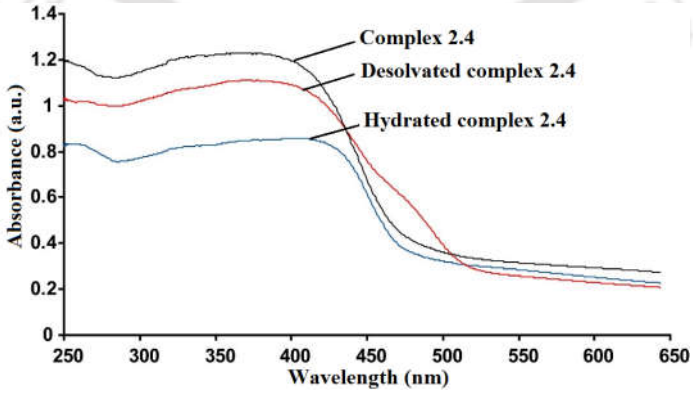

Figure 2.9: Changes in solid state absorbance spectra of complex **2.4** on removal of solvent and absorption of moisture from atmosphere.

The visible spectra of solid samples of **2.4** were recorded and shown as Figure 2.9. Anhydrous form has a shoulder at 475 nm in addition to the parent absorption of solvated form at 400 nm. Such phenomenon of colour changes is due to variations in the π-stacking interactions between the included guests in the host framework, which are involved in ligand to ligand charge transfer transitions.[18] In the present case the complexes **2.1** and **2.4** have strong C-H···π interactions, which may be affected by removal of solvent of crystallization, which is reflected in color of the complexes. Generally formation of zinc complexes are guided by solvents;[19-20] thus the stability of solvates by the tetra-nuclear core in complexes **2.1** and **2.4** are of synthetic interest.[21-22]

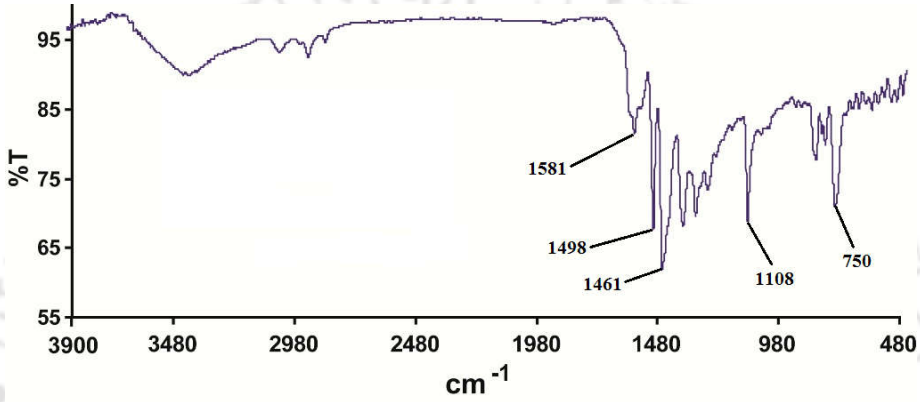

Figure 2.10: FT-IR spectra of **2.4** on heating at a temperature of 480 °C.

The IR spectra of the complex **2.4** showed the IR-stretching frequencies of the oxyquinolate part after it was heated to 480 °C (Figure 2.10). This suggests that upto a temperature of 480 °C, a portion of the oxyquinolate ligand remains with the zinc ions.

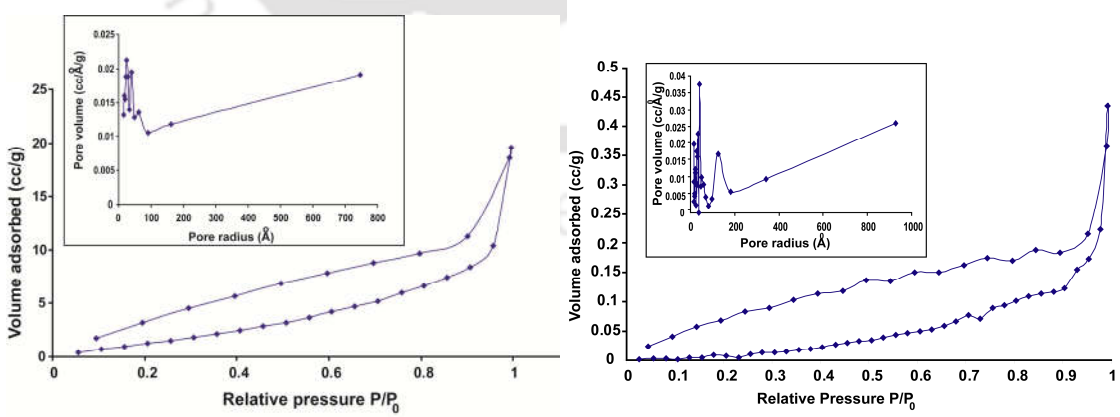

(a) (b)

Figure 2.11: Nitrogen gas adsorption isotherm at 77 K for (a) complex **2.1** and (b) complex **2.4**; pore size distribution (inset).

Since reversibility of water binding was observed by these complexes and they also have relatively high thermal stability, the surface area of the complexes **2**.**1** and **2**.**4** were determined. They follow type 2 of nitrogen adsorption plot[23] showing reversibility in nitrogen adsorption (Figure 2.11). The surface areas for complex **2.1** and **2.4** are 8.933 m^2/g and 6.172 m^2/g respectively.

As mentioned earlier, formation of zinc oxyquinolate complex is largely influenced by reaction conditions. Accordingly we also observed an interesting observation in this direction. We found that when 8-hydroxyquinoline reacts with zinc chloride in water a white crystalline precipitate was formed. When we determined the structure of this complex by X-ray single crystal diffraction we found that the complex has a composition $(HhydroxQ)_2[ZnCl_4]$ (**2.5**). Complex **2.5** has hydroxyquinolinium cation outside coordination sphere of tetrachloro-zincate. This result was surprising to us, as the reaction was carried out in neutral condition using zinc chloride salt without additional acid. It may be also mentioned that to form tetrachloro zincate anions acidic condition is required.[24-25] Hence, we felt that there must be a hydrolytic equilibrium as illustrated in equation 2.3, to generate the corresponding complex **2.5**. In such a process hydroxyquinolinium cation, tetra-chloro zincate and zinc hydroxide should be present in the solution. Thus the entire reaction is guided by water as solvent.

$$2\ hydroxQ + 2ZnCl_2 + 2H_2O \rightarrow (HhydroxQ)_2[ZnCl_4] + Zn(OH)_2$$

Where, hydroxQ = 8-hydroquinoline

Equation 2.3: Reaction of zinc chloride with 8-hydroxyquinoline in water.

It was not possible to for us to demonstrate the formation of zinc hydroxide in solution by a direct method. Thus we adopted an indirect method. It is a well known fact that zinc hydroxide forms zinc oxide on heating. Zinc oxide has its characteristic powder XRD pattern which is available in literature. Based on these, we took the reaction mixture containing equimolar amounts of hydroxyquinoline and zinc chloride in water, on completion of the reaction the solvent was evaporated. Crude reaction mixture which is supposed to be comprised of complex **2.5** and zinc hydroxide was heated at 120°C for 12 h and the powder XRD pattern of the solid was recorded. When we compared powder XRD of this sample with powder XRD pattern we observed that powder XRD pattern has the desired peaks of zinc oxide (Figure 2.12). Zinc oxide peaks are marked with downward arrows in Figure 2.12. Thus, zinc oxide was formed during

heating of the crude mixture which must have been formed from dehydration of zinc hydroxide. Literature suggests that conventionally zinc oxide is obtained on heating zinc hydroxide around 100 °C for overnight.[26]

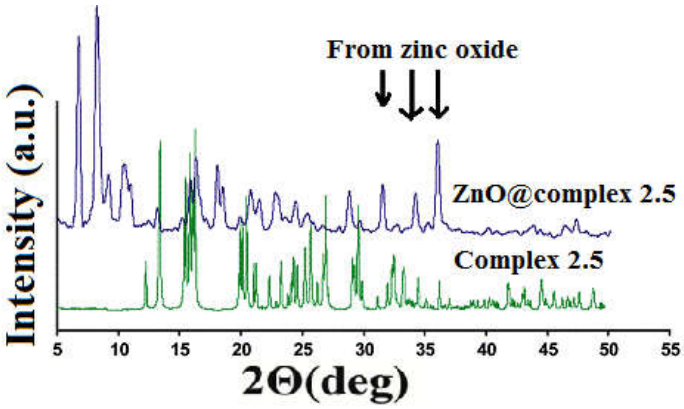

Figure 2.12: Powder XRD pattern of complex; bottom: **2.5**, top: Crude precipitate from the reaction of zinc chloride with 8-hydroxyquinoline in water which was heated at 120 °C for 12 h.

Complex **2.5** was characterized by determining its structure by single crystal diffraction. The compound has a tetrachloro zincate with conventional distorted tetrahedral geometry (Figure 2.13a). In this complex we found that it comprises of a tetrachloro-zincate complex unit which has a tetrahedral geometry around zinc ion, and two 8-hydroxyquinolium cations. Tetrachloro-zinc complex holds six 8-hydroxyquinolium cations.

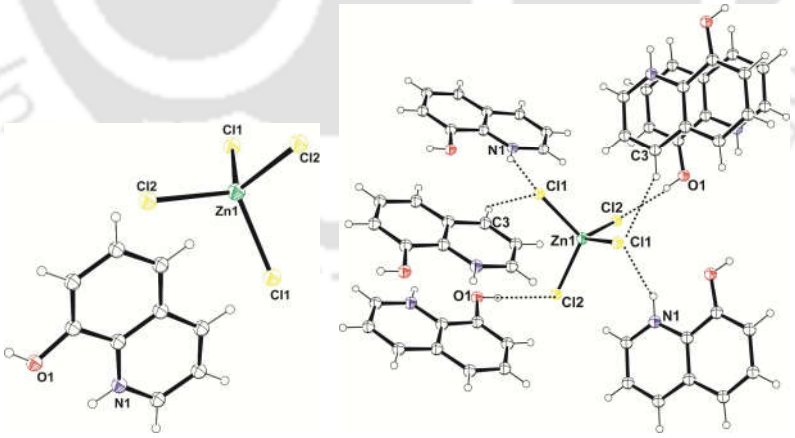

(a) (b)

Figure 2.13: (a) Structure of complex **2.5** (drawn in 35% thermal ellipsoid) (b) Hydrogen bonds environment around $ZnCl_4$.

Two Cl1 anions hold two 8-hydroxyquinolium cations each by bifurcated hydrogen bonds, namely N-H···Cl and C-H···Cl, whereas, Cl2 anion is attached through O-H···Cl hydrogen bond to hold one 8-hydroxyquinolium cation each (Figure 2.13b). Distances of N-H···Cl, C-H···Cl and O-H···Cl are 2.353 Å, 2.706 Å and 2.295 Å respectively. Complex **2.5** does not decompose at 150 °C, hence the zinc oxide observed was not from this part of the reaction mixture. $[ZnCl_4]^{2-}$ anions are often formed in the reactions of zinc chloride with hydrochloric acid, however, formation of tetrachloro zincate from a reaction of zinc chloride with 8-hydroxyquinoline without additional acid is noteworthy. On the other hand, $Cs_2[ZnCl_4]$ anion[27] has Zn-Cl bond distances ~2.25Å with Cl-Zn-Cl angles varying from 106-115 °. Zinc chloride bond distances in the complex are Zn1-Cl1, 2.2632(14); Zn1-Cl2, 2.2771(13); and Cl1-Zn1-Cl2 bond angle is 111.88(5) °.

Complex **2.5** has less thermal stability; it decomposes at a temperature about 250 °C. Thermogram of complex **2.5** shown in Figure 2.14 shows that it loses 45.8 % weight in the range of 250-350 °C. This weight loss corresponds to loss of a hydroxyquinoline and two hydrochloric acid molecules (theoretical weight loss 43.7 %). On further heating, it loses weight in the temperature range of 450 °C to 700 °C to give a residue having composition $ZnClO_{0.5}$ (theoretical weight loss 78.9 %, experimental weight loss 79.2 %). This suggests that when $(HhydroxQ)_2[ZnCl_4]$ is heated, it forms a complex $[(oxQ)ZnCl_2]$; which above 450 °C forms dinuclear Zn_2OCl_2.

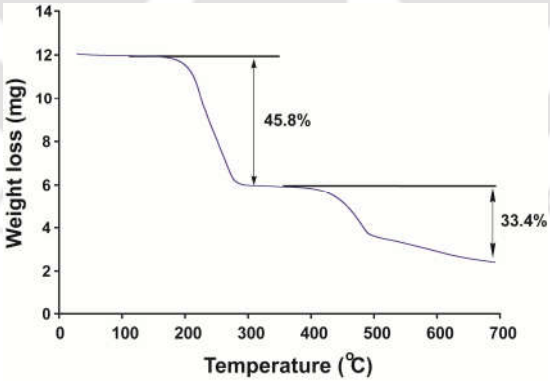

Figure 2.14: Thermogram of the complex **2.5**.

We have studied reactions of 8-hydroxyquinoline with zinc chloride in presence of different 3-methylpyridine. This reaction surprisingly gave a molecular complex **2.6**. Molecular complex **2.6** is comprised of two neutral mono nuclear complexes. Both the constituent complexes of this

molecular complex were devoid of chloride ions. These two neutral complexes $[Zn(oxyQ)_2(3mepy)]$ and $[Zn(oxyQ)_2(3mepy)_2]$ (Where 3mepy = 3-methylpyridine) (Figure 2.15a) crystallised together as an assembly. Structurally such complexes are very interesting; however there are only few examples of such complexes in literature.

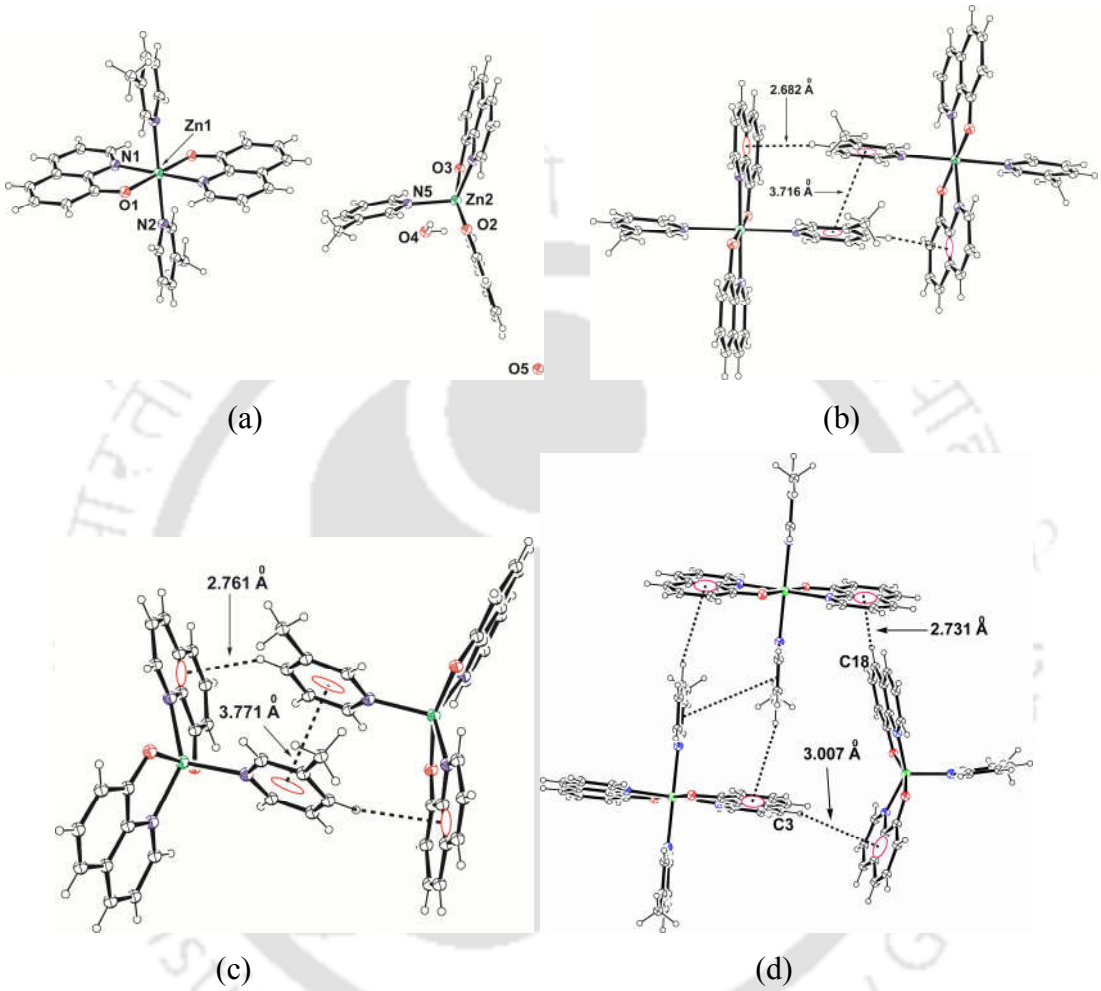

Figure 2.15: (a) Structure of molecular complex **2.6** (ORTEP with 35 % thermal ellipsoids), (b) Hexa-coordinated molecules of **2.6**, (c) Penta-coordinated molecules of **2.6** and (d) Weak interactions between penta- and hexa-coordinated parts of complex. Some of the selected bond distance (Å) Zn1-O1, 2.053(3); Zn1-N1, 2.145(4); Zn1-N2, 2.275(4); Zn2-N3, 2.076(4); Zn2-O2, 2.062(4); Zn2-O3, 2.059(4); Zn2-N4, 2.903(4); Zn2- N5, 2.080(5); and selected bond angles (°) are O1-Zn1-N1, 80.90(17); O1-Zn1-N2, 88.99(17); N1-Zn1-N2, 91.33(15); N3-Zn2-N5,103.22(19); N4-Zn2-N5, 115.0(2); O2-Zn2-O3, 162.20(16); O2-Zn2-N3, 80.97(18); O2-Zn2 -N4, 91.20(17); O2-Zn2-N5, 101.5(2); O3-Zn2-N3, 96.26(17); O3-Zn2-N4, 80.08(17); O3-Zn2-N5, 96.26(19); N3-Zn2-N4, 141.80(17).

Our research group have shown such molecular complexes in metal complexes of carboxylates.[28] Molecular complexes between trinuclear and dinuclear combination of zinc complexes; and between tetra-coordinate and hexa-coordinate zinc complex have been reported earlier.[29] To best of our knowledge the present example is only example in literature on molecular complexes of zinc 8-oxyquinolate. Two complexes involved in this molecular complex have different coordination geometry around each zinc ion. One part $[Zn(oxyQ)_2(3mepy)]$ adopts distorted square pyramid structure, whereas other part $[Zn(oxyQ)_2(3mepy)_2]$ has distorted octahedral geometry. The penta coordinated zinc complex has two oxyquinolates in chelating mode and a methylpyridine. Oxyquinolates occupy basal plane of square pyramid, whereas 3-methylpyridine coordinating through nitrogen atom occupies axial position as shown in Figure 2.15a. The hexa coordinated part having octahedral structure is highly symmetric with a mirror plane bisecting the half of the complex (Figure 2.15a). This complex has two 3-methylpyridine molecules occupying two axial positions of the octahedron while two oxyquinolates occupy the basal plane. Bond distances and bond angles contributing to **2.6** are listed in the caption of Figure 2.15. Comparing axial Zn-N bonds in two geometries namely Zn1-N2, (2.27 Å) and Zn2-N5, (2.08 Å) it may be suggested that 3-methylpyridine molecule is tightly bound in penta coordinated geometry than hexa coordinated geometry. To examine reasons for stability of molecular complex **2.6**, we have looked at weak interaction Schemes in the complex. We can characterize the complex by taking three different types of interaction Schemes operating to hold (a) penta coordinated-penta coordinated complexes, (b) hexa coordinated-hexa coordinated complexes and (c) penta coordinated-hexa coordinated complexes in crystal lattice. First two sets of interactions result in layered arrangements of same kind of molecules, whereas third set of interactions contribute to self-assembling of layers. Interactions between similar coordinated complexes are mainly through π-π and C-H···π interactions, while in the third case it is merely C-H···π interactions.

In general many coordination polymers of zinc show photoluminescence properties.[30-32] Fluorescence emission spectra of each solid sample of the complexes by exciting at 390 nm are shown in the Figure 2.16. 8-Hydroxyquinoline in solid state has fluorescence emission at 480 nm. Observed trend in change in emission intensity has no clear correlation with solvent of crystallisation. DMA and DMF solvates show relatively lower intensity with respect to 8-hydroxyquinoline; whereas DMSO solvate it occurs at 495 nm which shows slight enhancement

of fluorescence with emission shift towards higher wavelength. These observations clearly points out that there is an interstitial role of solvent to guide the fluorescence of the complexes. Similar observations of change of fluorescence intensities in zinc metallo-organic frameworks with inclusion of aromatic compounds were observed.[18] Molecular complex **2.6** shows the highest emission, whereas the DMF and DMA solvates have the lowest emission. Interestingly, a dual emission in the case of the sample of ZnO doped into the complex **2.5** was observed, which was studied in the form of ZnO@complex **2.5** (Figure 2.16b). Zinc oxide encapsulated complex has emission at 575 nm which is relatively at higher wavelength and it also has another emission peak relatively at lower wavelength (450 nm), with respect to 8-hydroxyquinoline (480 nm) or complex **2.5** (495 nm). There are examples of composite materials showing dual fluorescence, which have practical applications, thus the observation at such high wavelength is of definite interest.[33-34]

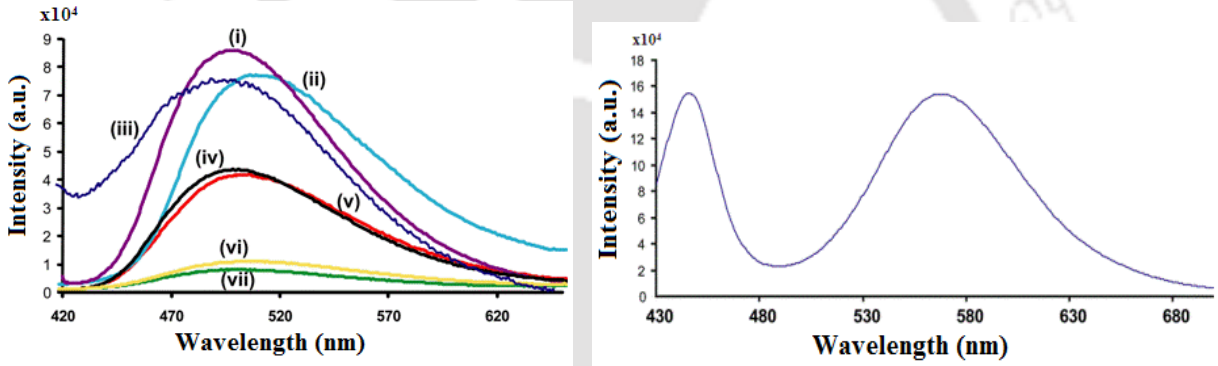

(a) (b)

Figure 2.16: Fluorescence emission of the solid samples of complex (i) **2.6**; (ii) **2.3**; (iii) 8-hydroxyquinoline**;** (iv) **2.5**; (v) **2.4**; (vi) **2.2**; (vii) **2.1** (λ_{ex} = 390 nm). (b) The fluorescence emission of ZnO@complex **2.5**.

2.2: Cobalt (II) and manganese (II) oxyquinolate complexes

We studied reaction of 8-hydroxyquinoline with other metal ions such as cobalt and manganese ions with an anticipation that such metal ions will give paramagnetic complexes. The paramagnetic manganese and cobalt clusters generally show novel magnetic properties including single molecular magnet.[35-36] Thus a reaction of cobalt (II) chloride with 8-hydroxyquinoline yielded a tetra nuclear complex **2.7** which has a composition $Co_4(oxyQ)_6Cl_2$. The complex is isostructural with tetra nuclear zinc complexes. Structure of the complex is

shown in Figure 2.17. Complex **2.7** is highly disordered containing two chloride ligands attached to two cobalt ions.

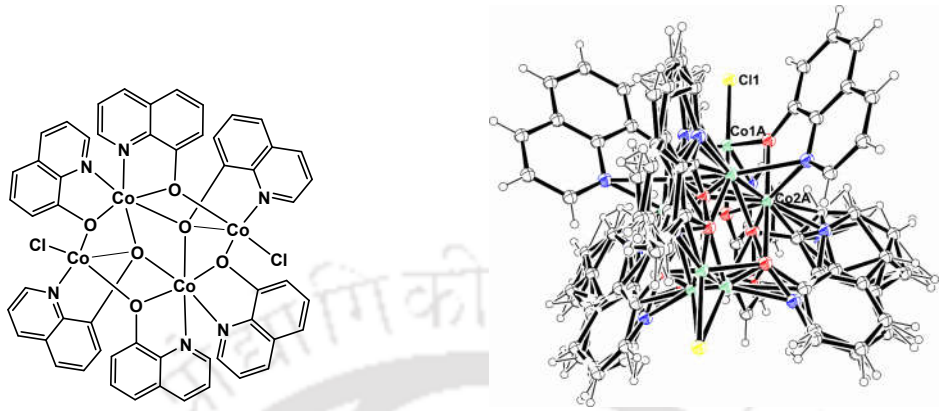

(a) (b)

Figure 2.17: (a) Structure of complex **2.7**, (b) ORTEP diagram of complex **2.7** (drawn in 35 % thermal ellipsoid).

Two cobalt ions are in the N2O4 type hexa-coordinated distorted octahedral environment whereas other two cobalt ions are in the NO3Cl type penta-coordinated environment. Tetra nuclear cobalt (II) complexes having single and double sets of coordination environments are reported earlier.[37] In some cases both the sets cobalt atoms are in distorted octahedral geometry, however in other cases cobalt atoms are in distorted octahedral and square pyramidal geometry.[37] Since the complex **2.7** is highly disorder, hence during the initial refinement, large peaks were found ca. 1 Å from the cobalt atoms, which were large enough to refine as oxygen atoms with realistic temperature factors, but which were both chemically and structurally unrealistic. It was noted that when these "ghost peaks" and the cobalt atoms were taken together they formed regular hexagons or equilateral triangles perpendicular to the Cl···Cl axis, and that this axis was coincident to the sixfold or threefold axes of these hexagons and triangles. Furthermore, the eight ghost peaks could be arranged into two sets of four, each of which had peak-peak distances very similar to the Co-Co distances. Given also the almost exact trigonal symmetry of the external shape of the molecule, the presence of a threefold whole-molecule disorder was clear. Assignment of the cobalt atoms and "ghost peaks" all as partial-occupancy cobalt atoms, with the total occupancy of each set of three cobalt atoms restrained to unity and a common temperature factor assigned to each set of three cobalt atoms, showed relative occupancies of ca. 64 : 19 : 17. The temperature factors of the cobalt atoms were then restrained to be similar, rather

than constrained to be equal. Refinement of the organic ligands using isotropic atoms of occupancy 0.64, with the quinoline ring systems each constrained to two fused regular hexagons (AFIX 116) allowed most of the atoms of the minor components of the ligands to be located. Refinement of these, again using AFIX 116, with similarity restraints to all C-O distances and the oxygen atoms restrained to lie in the plane of their respective quinoline rings, was relatively straightforward. The C, N and O atoms of the major ligand components could then be refined anisotropically, with similarity restraints (SIMU) applied to the thermal parameters of partial atoms closer than 0.4 Å to each other. In the final refinement, the relative occupancies were fixed to values adding up to exactly unity, and the structure refined to convergence. Some relevant bond distances and bond angles of the complex are listed in Table 2.2.

Table 2.2: Bond parameters of the complex **2.7**.

Bond	Length (Å)	Bond angle	Angle (°)
Co1-O2	1.61	Cl3-Co1-O2	102.26
Co1-O3	1.80	Cl3-Co1-O3	105.14
Co1-N1	2.18	Cl3-Co1-N1	100.45
Co2-O3	2.20	O2-Co1-O3	102.23
Co2-N3	2.14	O2-Co1-N1	127.78
Co1-Cl3	2.31	O3-Co1-N1	116.10

A similar reaction of 8-hydroxyquinoline with manganese chloride resulted a complex which has identical IR spectra as that of complex **2.7**, thus it may be suggested to be a tera nuclear manganese complex (**2.8**). It has similar pattern PXRD diffraction patterns with tetra nuclear cobalt complex **2.7**.

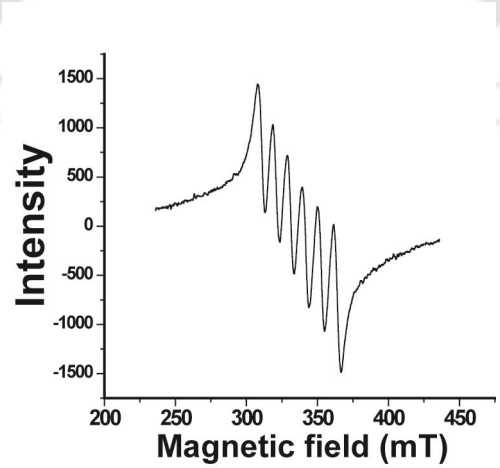

Figure 2.18: EPR spectra of complex **2.8**.

Solid state epr spectra of complex **2.8** shows metal centre to be a di-positive manganese as there are lines for five unpaired electrons of manganese (II) ions and $g_{average}$ value is found to be 1.992 (Figure 2.18). However, when we tried to crystallize this complex, manganese (II) got oxidized to give a mono nuclear tris(oxyquinolate)-manganese (III) complex **2.9**. This complex was characterized by determining its crystal structure which is shown in Figure 2.19a. Complex has a distorted octahedral geometry where two axial positions are occupied by two oxygen atoms from two independent oxyquinolate whereas the basal plane is occupied by one oxygen atom and three nitrogen atoms. It is a diamagnetic complex. Furthermore in our laboratory similar reaction with 8-hydroxyquinoline is extended to heavy metal such as lead (II) and mercury (II), interestingly a tetra nuclear complex of lead (II)-oxyquinolate was obtained having metal centers of different arrangements compared to tetra nuclear zinc and cobalt complexes discussed above (Figure 2.19b).

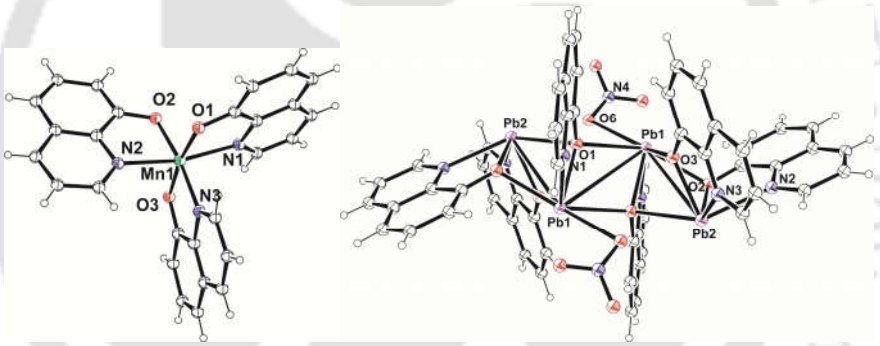

(a) (b)

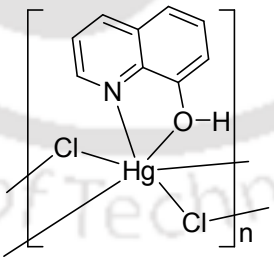

(c)

Figure 2.19: (a) Structure of manganese tris(oxyquinolate) complex, (b) Tetra nuclear lead-oxyquinolate complex and (c) Coordination polymer of mercury-oxyquinolate complex.

In case of reaction with mercury chloride under solvothermal condition gives a coordination polymer of mercury(II)-oxyquinoline chloride; in which chloride anions act as bridging ligand to

extend the coordination polymer (Figure 2.19c). These examples establishes the versatile nature of 8-hydroxyquinoline to form different metal complexes with metal ions under different reaction conditions.

There are many low nuclearity metallacycles of first row transition metals which transform to higher nuclearity clusters depending on ancillary ligands[38] or having carbonate as anchoring ligand on uptaking carbon dioxide from air.[39-40] We studied the reactivity of complexes **2.7** and **2.8** with additional amount of their respective metal chloride in dimethyformamisde, we found that in both case deca nuclear complexes $[Co_{10}(oxyQ)_{12}(\mu_6\text{-}CO_3)_4](DMF)\cdot H_2O$ (**2.10**) and $[Mn_{10}(oxyQ)_{12}(\mu_6\text{-}CO_3)_4](DMF)\cdot H_2O$ (**2.11**) were formed as illustrated in equation 2.4.

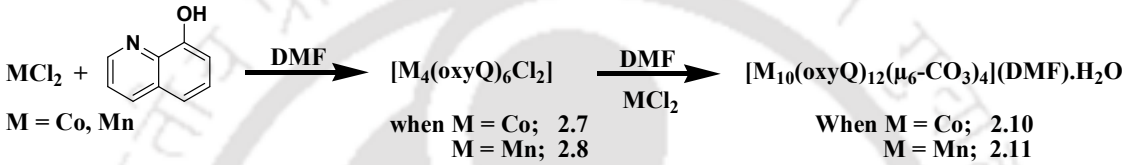

Eqaution 2.4: Synthesis of deca nuclear complexes

These complexes are formed by picking up of carbonate ligand which may be from the atmospheric carbon dioxide. There are examples of the formation of copper and nickel carbonate clusters by uptaking of atmospheric carbon dioxide.[40] Moreover, there are examples in literatures that under drastic conditions of high pressure and temperature can oxidize dimethylformamide to give formate anion, which can act as ligand to hold metal centers to give stable metal cluster.[41-44] Such complexes have formate anion included in respective clusters, but we have carbonate anion in our clusters. Moreover dimethylammonium cation formed *in situ,* can also be obtained form decomposition DMF molecule which many cases helps charge neutralization of metal clusters.[45-47] We have not observed any part having ammonium cation. Thus, clusters **2.10** and **2.11** can be thought of formed by the reaction of respective tetra nuclear complex with additional metal salt and by uptaking carbonate anions formed *in situ*. Under inert reaction conditions or in the absence of additional cobalt chloride, a deca nuclear cluster was not formed. A deca nuclear cluster was also not formed in a similar solvothermal reaction carried out in dimethylsulphoxide or in dimethylsulphoxide saturated with carbon dioxide as a solvent. A control experiment, with addition of sodium carbonate to the reaction mixture in dimethylsulphoxide did not give deca nuclear cluster. And also any decomposed product from DMF such as dimethylamine in the reaction mixture was not observe when analyzed by GC-MS, thus trace amounts of carbon

dioxide from the atmosphere under hydrothermal conditions could be responsible for the formation of deca nuclear cluster; nonetheless, without DMF as a solvent the deca nuclear cluster was not observed. Carbonate ligands in these clusters are discerned by spectroscopic tools in addition to X-ray structure determination. The presence of carbonate ligands in deca nuclear cluster **2.10** was also confirmed chemically, as it liberated carbon dioxide upon addition of dilute hydrochloric acid; the liberated gas was analyzed by a chemical test with lime water. Deca nuclear cluster **2.10** contains as many as four carbonate anions and each anion acts as a μ_6-bridge[40] to connect six cobalt ions. The binding mode of one of the carbonate ligands in deca nuclear cluster **2.10** to knit metal ions within the cluster is shown in Figure 2.20a. Five cobalt (II) ions of the cluster are individually coordinated to two oxyquinolate chelating ligands. These chelating oxyquinolate ligands are also involved in the μ_2-oxyquinolate bridge to connect neighboring cobalt ions. This set of cobalt ions of the cluster is anchored to two independent oxygen atoms of two carbonate ligands. Thus, these cobalt ions are in the N2O4 type of an octahedral environment. On the other hand, there are other five cobalt ions linked to three oxygen atoms of bridging carbonates and three oxygen atoms of bridging oxyquinolates. This makes an O6 octahedral environment around these cobalt (II) ions (Figure 2.20b). A representative skeleton of the deca nuclear clusters **2.10** and **2.11** is shown in Figure 2.20c.

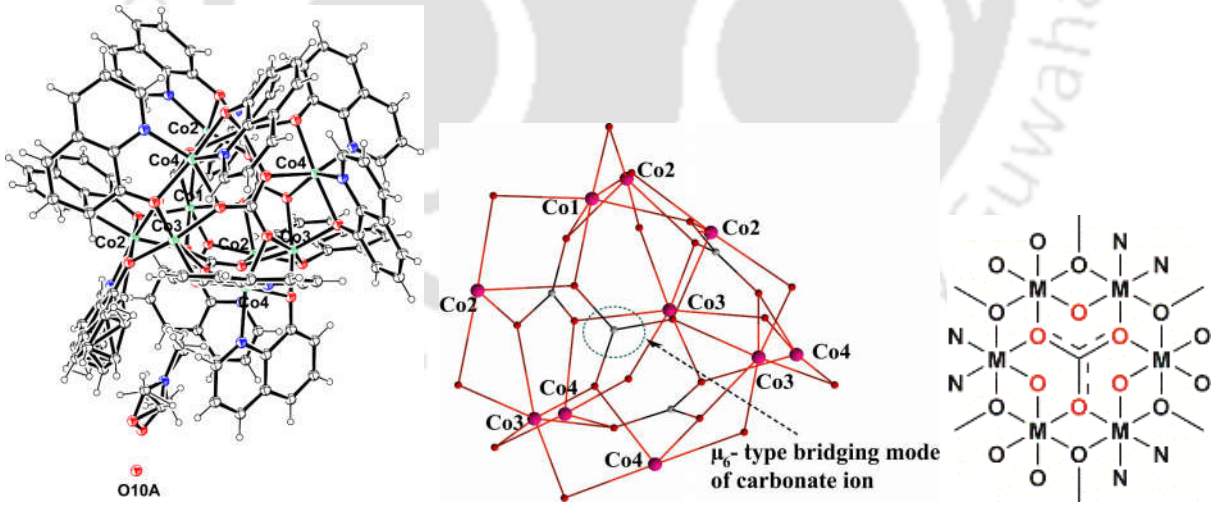

(a) (b) (c)

Figure 2.20: (a) ORTEP diagram of cluster **2.10** (drawn in 35 % thermal ellipsoids), (b) core of deca nuclear cobalt cluster (oxyquinoline rings are not shown for clarity of the structure) and (c) bridging mode of one of the carbonate ligand to hold six metal ions in deca nuclear metal clusters **2.10** and **2.11**.

Table 2.3: Bond parameters of clusters **2.10** and **2.11**.

Bond	Length (Å)		Bond angle	Angle (°)	
	Cluster **2.10**	Cluster **2.11**		Cluster **2.10**	Cluster **2.11**
M1-O1	2.06(4)	2.130(5)	O1-M1-O2	77.67(16)	78.72(2)
M1-O2	2.16(4)	2.244(5)	O1-M2-O2	78.30(16)	80.00(2)
M2-O1	2.08(4)	2.147(5)	O1-M2-O4	176.98(17)	173.39(2)
M2-O2	2.11(4)	2.170(5)	O1-M2-N1	79.12(19)	76.63(3)
M2-O4	2.09(5)	2.124(6)	O1-M2-N2	97.71(19)	97.49(3)
M3-O6	2.14(4)	2.221(5)	O2-M2-O4	101.74(17)	103.30(2)
M3-O7	2.05(4)	2.104(6)	O2-M2-N1	155.59(2)	154.49(3)

Carbonate ligand can adopt various coordination modes; the coordination of carbonate can be dependent on ancillary ligands and oxidation state of metal ions.[32] For instances, carbonate anion shows μ_2-type of binding mode to hold two nickel metal centre, while μ_3-type to give tri nuclear copper carbonato complex[48] and tetra nuclear nickel-carbonato complex in which carbonate anion act as bridging ligand to give a butterfly topology[40] and it also shows μ_6-type mode to dodeca nuclear copper cluster.[39] These metal-carbonato clusters are important from the magnetic property point of view. Magnetic behavior of the metal-carbonato complexes depend on the type of the coordination of the bridging carbonato ligand.[48] Examples of tri nuclear and dodeca nuclear copper-carbonato complexes formed by uptaking carbon dioxide from air are shown in Figure 2.21.

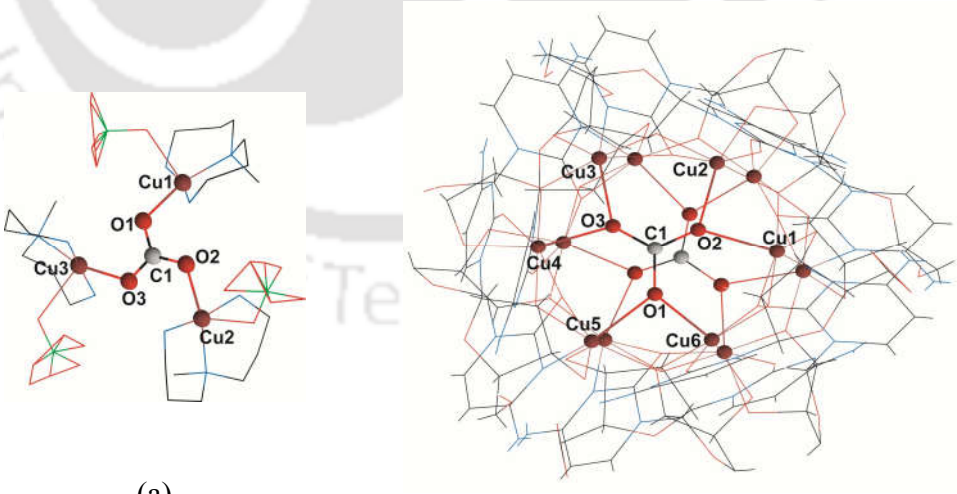

(a) (b)

Figure 2.2: Structure of (a) tri nuclear copper complex, (b) dodeca nuclear copper complex containing carbonate anion ligand.

The presence of solvated molecules of dimethylformamide in clusters **2.10** and **2.11** were confirmed by thermogravimetry analysis. In thermogram of cluster **2.10** there is a 3.51 % weight loss in the region of 135ºC to164ºC (Figure 2.22a) which is due to loss of solvent of crystallization (theoretical weight loss for a water molecule and a DMF molecule is 3.25 %) and decomposition of cluster **2.10** starts at a temperature of 264 °C. Whereas in case cluster **2.11** a 3.42 % weight loss was observed in the region of 144 °C to 190 °C (Figure 2.22b) due to loss of solvent of crystallization (theoretical loss = 3.30%). Decomposition of deca nuclear cluster **2.11** starts at 302 °C.

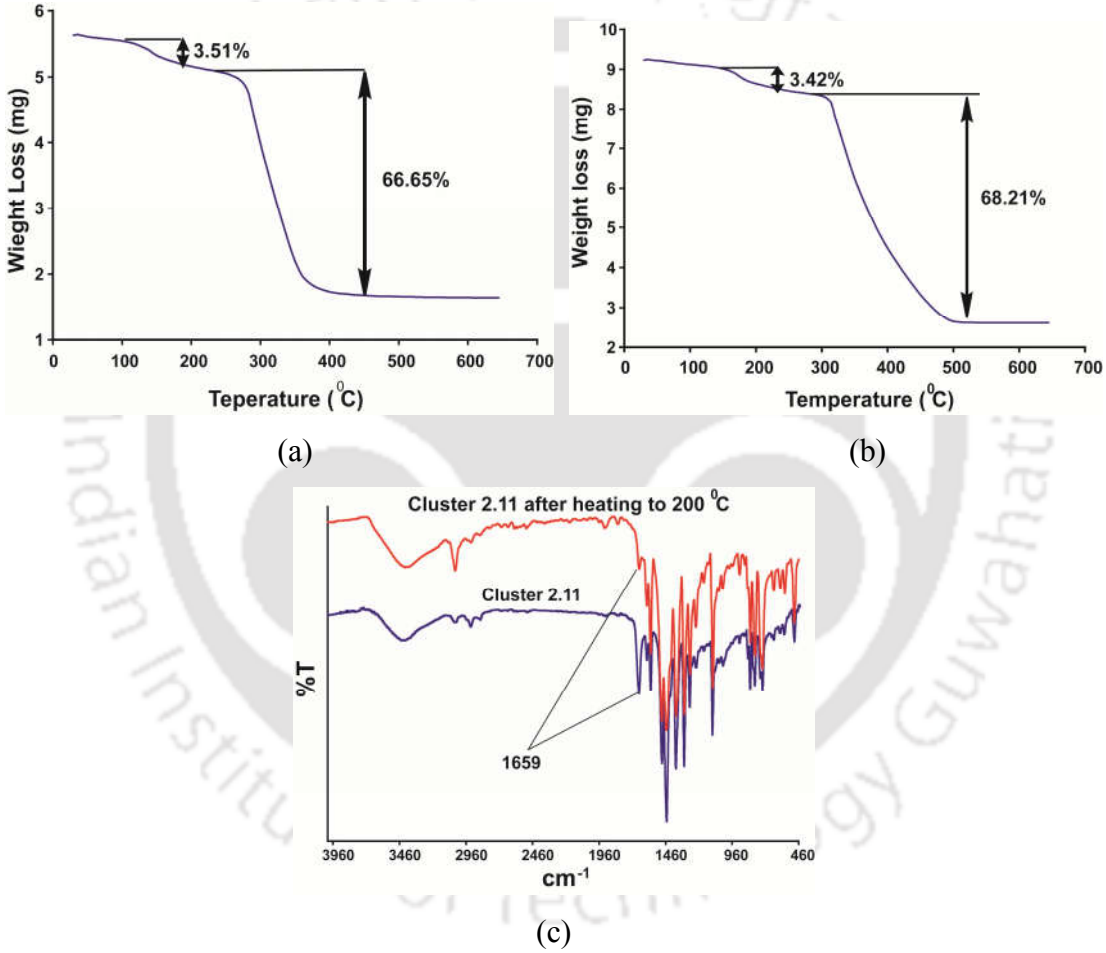

Figure 2.22 Thermogram of cluster (a) **2.10** and (b) **2.11** (each heating rate 5 °C per minute); (c) FT-IR spectra of cluster **2.11** before and after heating at 200 °C.

Loss of DMF molecule is also visible from the FT-IR spectra of manganese cluster, it has a C=O stretching signal from DMF at 1659 cm^{-1}, on heating at 200°C there is decrease in intensity of this signal (Figure 2.22c).

2.3: Magnetic study of complex 2.7, cluster 2.10 and cluster 2.11

An anti-ferromagnetic coupling between metal ions was reflected in temperature dependent magnetic properties of these complexes.

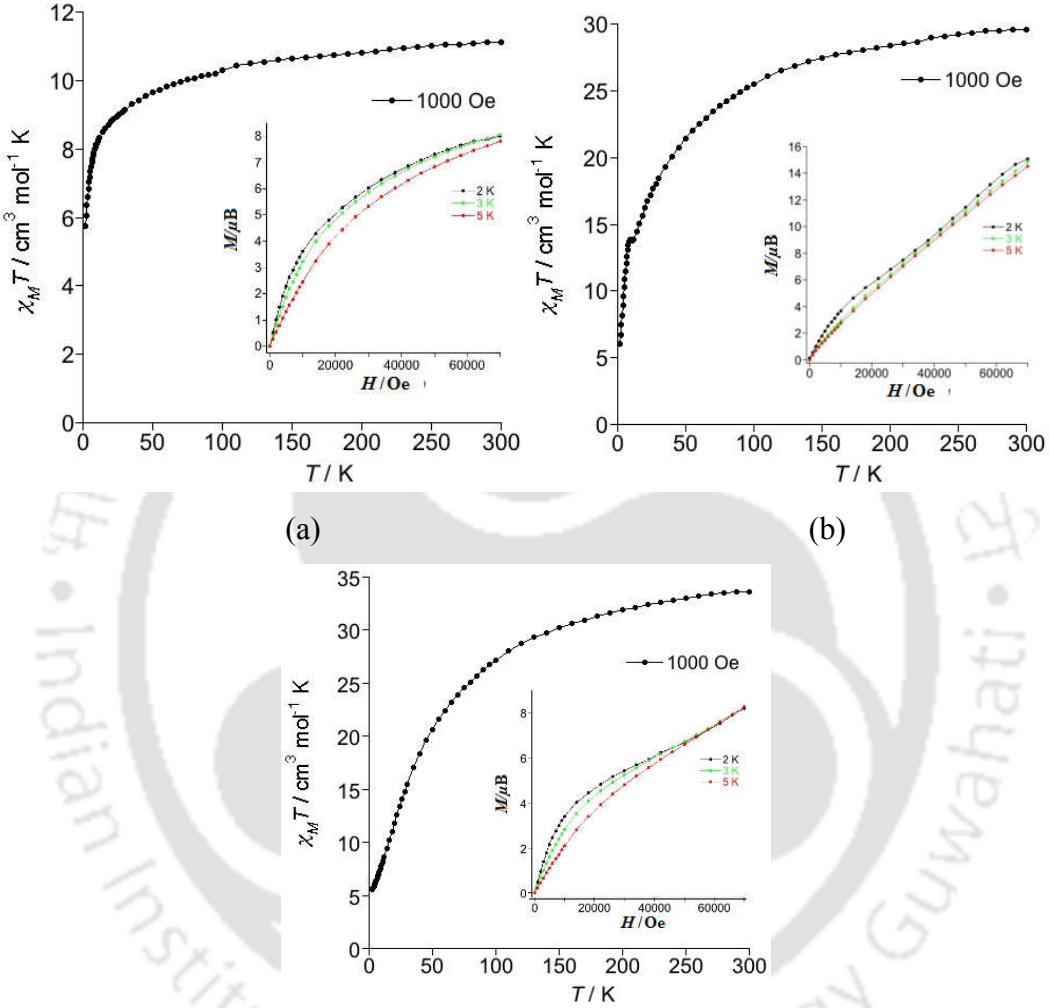

Figure 2.23: Plots of χMT *vs* T and M *vs* H (inset) for (a) complex **2.7**, (b) cluster **2.10** and (c) cluster **2.11**.

For the tetra nuclear cobalt complex **2.7** at 1000 Oe, the $\chi_M T$ value at 300 K was 11.16 cm^3 mol^{-1} K, (where χM being the magnetic molar susceptibility per tetra nuclear cobalt unit) which is close to the spin only value (S = 3/2 and g_{Co} = 2.1; 2.7 < $\chi_M T$ < 3.4 cm^3 mol^{-1} K per ion) expected for four non interacting high-spin cobalt (II) ions. This behavior is common for cobalt

(II) complexes, and can be attributed to the orbital contribution of cobalt (II).[49] The $\chi_M T$ values of complex **2.7** show a continuous decline to a minimum value of 5.71 cm^3 mol^{-1} K at 2 K (Figure 2.23a), which is in accordance with the anti-ferromagnetic behavior of cobalt (II) ions. *M vs. H* plots of the complex **2.7** show a saturation value 8.08μ_B per formula unit at 2 K and 7 T (inset of Figure 2.23a),, which is lower than the saturation value of 12μ_B for the spin-only cobalt (II) ion (S = 3/2 and g_{Co} = 2.1). This behaviour also supports an anti-ferromagnetic coupling between cobalt (II) ions in 1 unit.

Magnetic properties investigated by measuring $\chi_M T$ of the deca nuclear cobalt cluster **2.10** in the 2-300 K temperature range at 1000 Oe (where χM being the magnetic molar susceptibility per deca nuclear cobalt unit) is shown in Figure 2.23b. The measured $\chi_M T$ value at 300 K, 29.67 cm^3 mol^{-1} K, lies within the expected range for ten high-spin non-interacting cobalt (II) ions: S = 3/2 and g_{Co} = 2.1; 2.7 < $\chi_M T$ < 3.4 cm3 mol^{-1} K per ion,[49] with paramagnetic ions exhibiting a significant orbital contribution to their magnetic moment. On lowering temperature, the $\chi_M T$ value first smoothly decreases at 9 K ($\chi_M T$ = 13.87 cm^3 mol^{-1} K), and finally decreases more abruptly down to 2.0 K ($\chi_M T$ = 6.02 cm^3 mol^{-1} K). Decrease of $\chi_M T$ from room temperature to 13 K is ascribed to the effect of spin-orbit coupling (cobalt (II) ion exhibiting $^4T_{1g}$ ground term) and also to strong anti-ferromagnetic interactions between cobalt (II) ions. *M vs. H* plots of cluster **2.10** show a value 15.12μ_B per formula unit at 2 K and 7 T (inset of Figure 2.23b), which is much lower than the saturation value of 30μ_B for the spin-only cobalt (II) ion (S = 3/2 and g_{Co} = 2.1). This behavior also supports a strong anti-ferromagnetic coupling between cobalt (II) ions in the deca nuclear cobalt (II) core.

The plot of $\chi_M T$ *vs.*T under a 1000 Oe external field in the temperature range of 300-2 K for the deca nuclear manganese cluster **2.11** is shown in Figure 2.23c. The room-temperature $\chi_M T$ value for cluster **2.11** is 33.62 cm^3 mol^{-1} K, which is lower than the spin only value of 43.70 cm^3 mol^{-1} K for ten high-spin non-interacting manganese (II) ions (typically the manganese (II) ion has a S = 5/2 state and g_{Mn} = 2.0).[50] As the temperature is lowered, the $\chi_M T$ value decreases gradually down to 2 K, where the value has a minimum of 5.51 cm^3 mol^{-1} K at 2 K. This behavior indicates a strong anti-ferromagnetic interaction between manganese (II) ions in the deca nuclear manganese unit. The *M vs. H* plot of cluster **2.11** at different temperatures (2 K-5 K) is shown in the inset of Figure 2.23c. At 2 K, an increase of magnetization was observed with a value of 8.24μ_B at 7 T, which is much lower than the saturation value 50.0μ_B, expected for a spin-only

value of ten high-spin non-interacting manganese (II) ions (S = 5/2 and g_{Mn} = 2). This behavior also supports a strong anti ferromagnetic coupling between manganese (II) ions in the core of the deca nuclear cluster.

2.4: Conclusion

In conclusion, we synthesized a number solvates of tetra nuclear zinc-oxyquinolate complexes, salt of tetrachlorozincate complex with hydroxyquinolium cation and molecular complex of zinc oxyquinolate complex upon 1:1 molar ration reactions of zinc chloride with 8-hydroxyquinoline in different solvents. These zinc complexes show interesting features for example complexes **2.1** and **2.4** reversibly absorb atmospheric moisture on standing at room temperature which reflects on the color of metal complexes. The hydrolytic instability of zinc chloride has helped in precipitation of a tetrachlorozincate complex along with zinc hydroxide. This has enabled us to prepare zinc oxide within the matrix of the complex **2.5**. The formation of a molecular complex of two mono nuclear zinc-oxyquinolate complexes in 3-methylpyridine with complexes having different coordination environment has provided a unique example of molecular complex of zinc. Deca-nuclear of cobalt (II) and manganese (II) clusters prepared from their respective tetra-nuclear intermediate by trapping carbonate ions formed *in situ,* provided avenues to construct new clusters. Tetra nuclear cobalt (II) complex as well as deca nuclear clusters of cobalt (II) and manganese (II) show strong anti-ferromagnetic property, which opens possibilities for synthesis of new magnetic materials with analogous ligands.

2.5: Experimental

The detailed synthetic methodologies for synthesis of the metal complexes are described. Analytical data are provided with each complex. The instrumental details and crystallographic parameters are provided in Appendix.

Synthesis of complex 2.1:

To a solution of 8-hydroxyquinoline (0.31 g, 2 mmol) in methanol (20 mL) zinc chloride (0.28 g, 2 mmol) was added and stirred for 15-20 mins. A white precipitate was formed which was filtered and recrystallised from DMF to obtain the complex 2.**1**. Yield ~ 45 % (with respect to zinc). IR (KBr, cm^{-1}): 3392(s), 2919(w), 2851(w), 1624(m), 1577(m), 1499(s), 1467(s), 1421(w),

1389(s), 1371(s), 1327 (s), 1283 (w), 1240 (w), 1109(s), 1033(w), 820(w), 783(w), 742 (m), 620 (w). Elemental analysis: Calculated for $C_{57}H_{43}N_7O_7Cl_2Zn_4$; C: 53.89%, N: 7.72%, H: 3.41%; found, C: 53.81%, N: 8.12%, H: 3.55 %.

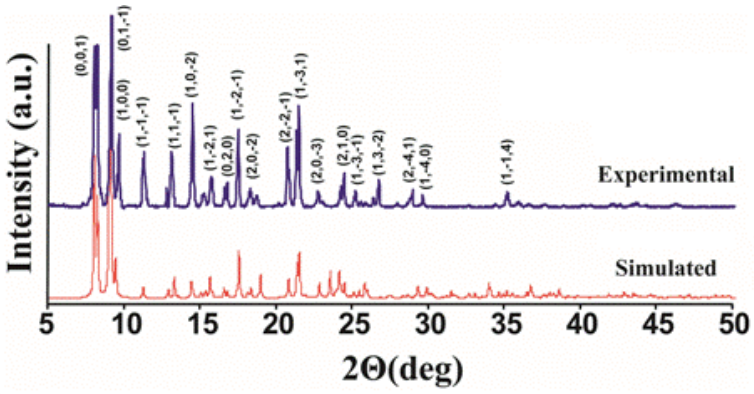

Figure 2.24: Powder XRD pattern of complex **2.1**.

Synthesis of complex 2.2:

To a solution of 8-hydroxyquinoline (0.31 g, 2 mmol) in methanol (20 mL) zinc chloride (0.28 g, 2 mmol) was added and stirred for 15-20 mins. A white precipitate was formed which was filtered and recrystallised from DMA to obtain the complex 2.**2**. Yield ~ 48 % (with respect to zinc). IR (KBr, cm^{-1}): 3372 (s), 2919 (w), 2851 (w), 1628 (m), 1602 (m), 1577 (m), 1499 (s),1466 (s), 1421 (w), 1389 (s), 1371 (s), 1327 (s), 1282 (w), 1240 (w), 1109 (s), 1031 (w), 820 (w), 785 (w), 742 (m), 640 (w), 596 (w), 502 (w). Elemental analysis: Calculated for $C_{57}H_{43}N_7O_7Cl_2Zn_4$; C: 53.89%, N: 7.72%, H: 3.41%; found, C: 53.56%, N: 8.15%, H: 3.48 %.

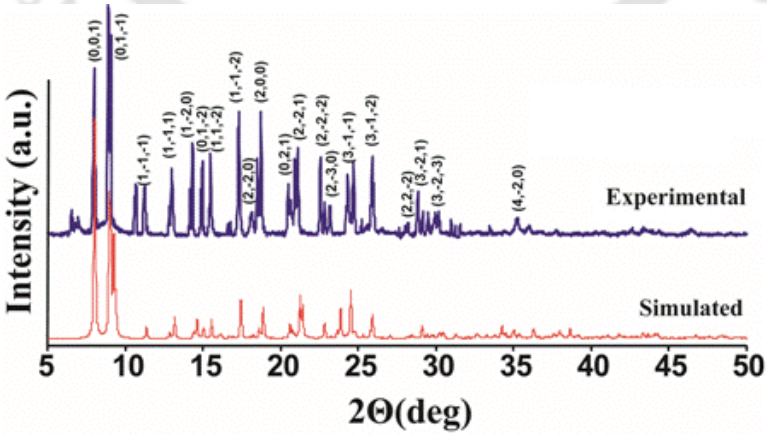

Figure 2.25: Powder XRD pattern of complex **2.2**.

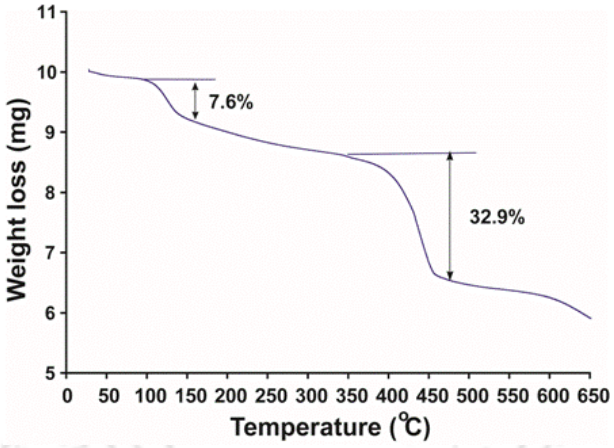

Figure 2.26: TGA thermogram (heating rate 5 ºC/minute) of complex **2.2**.

Synthesis of complex 2.3:

To a solution of 8-hydroxyquinoline (0.31 g, 2 mmol) in methanol (20 mL) zinc chloride (0.28 g, 2 mmol) was added and stirred for 15-20 mins. A white precipitate was formed which was filtered and recrystallised from DMSO to obtain the complex 2.**3**. Yield ~ 45 % (with respect to zinc). IR (KBr, cm^{-1}): 3378 (s), 2918 (w), 1618(m), 1603 (m), 1577 (m), 1500 (s), 1467 (s), 1399 (w), 1390 (s), 1371(s), 1327(s), 1283 (w), 1241(w), 1110 (m) 1033 (w), 850 (w), 820 (w), 780 (w), 743 (s), 640 (w), 502(w). Elemental analysis: Calculated for $C_{57}H_{43}N_7O_7Cl_2Zn_4$; C: 53.89%, N: 7.72%, H: 3.41%; found, C: 53.86%, N: 8.23%, H: 3.51 %.

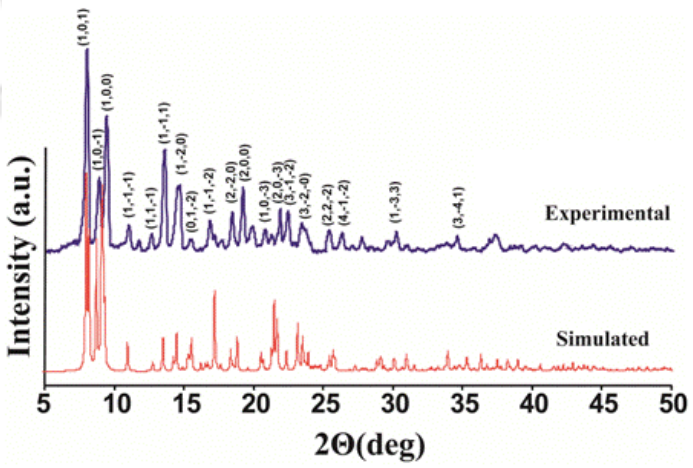

Figure 2.27: Powder XRD pattern of complex **2.3**.

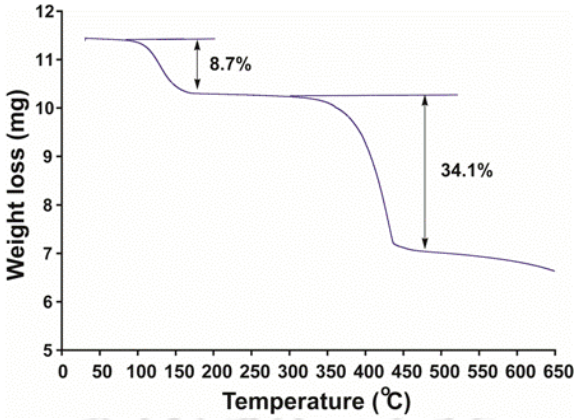

Figure 2.28: TGA thermogram (heating rate 5 ºC/minute) of complex **2.3**.

Synthesis of complex 2.4:

To a solution of 8-hydroxyquinoline (0.31 g, 2 mmol) in methanol (20 mL) zinc bromide (0.28 g, 2 mmol) was added and stirred for 15-20 mins. A white precipitate was formed which was filtered and recrystallised from DMF to obtain the complex **2.4**. Yield ~ 45 % (with respect to zinc). IR (KBr, cm^{-1}): 3190 (s), 1644 (m), 1601(m), 1577 (m), 1499 (s), 1456 (s), 1421(w), 1373(s), 1325(s), 1280 (w), 1137 (w), 1105(s), 1067 (w), 1032 (w), 909 (w), 821(m), 787 (m), 742 (m), 641(w), 600 (w), 545 (w), 499 (w).

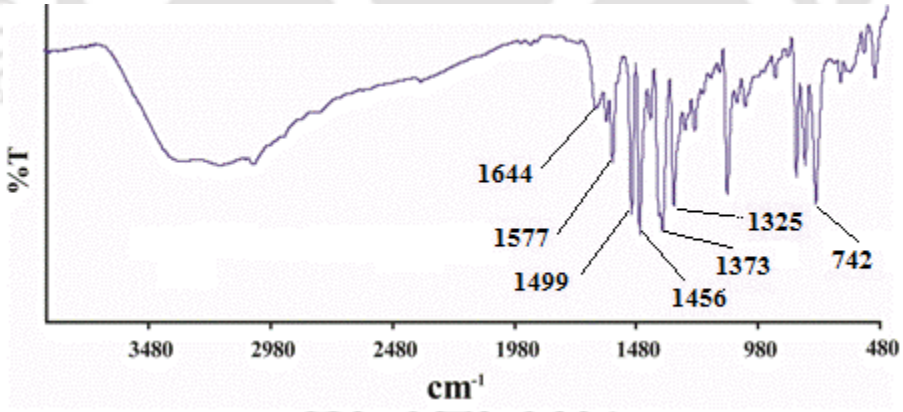

Figure 2.29: FT-IR (KBr, cm^{-1}) spectra of complex **2.4**.

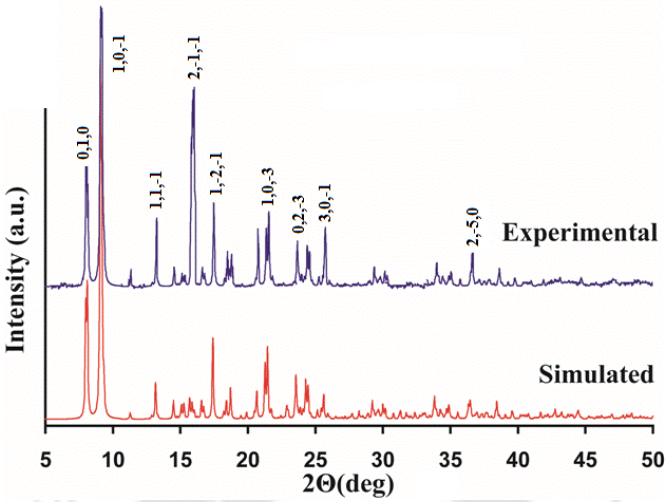

Figure 2.30: Powder XRD pattern of complex **2.4**.

Synthesis of 2.5:

To a solution of 8-hydroxyquinoline (0.31 g, 2 mmol) in methanol (20 mL) zinc chloride (0.28 g, 2 mmol) was added and stirred for 15-20 mins. A white precipitate was formed which was filtered and recrystallised from water to obtain the complex **2.5**. Yield ~ 35% (with respect to zinc). IR (KBr, cm^{-1}): 3453 (w), 3056 (w), 2933 (w), 2539 (w), 1627 (w), 1581 (m), 1531 (w), 1499 (s), 1467 (s), 1428 (w), 1382 (s), 1359 (s), 1324 (s), 1276 (m), 1241 (m), 1228 (w), 1180 (w), 1106(s), 1022 (s), 916 (w), 823 (s), 786 (s), 755 (s), 646 (w), 553(w), 514 (m).

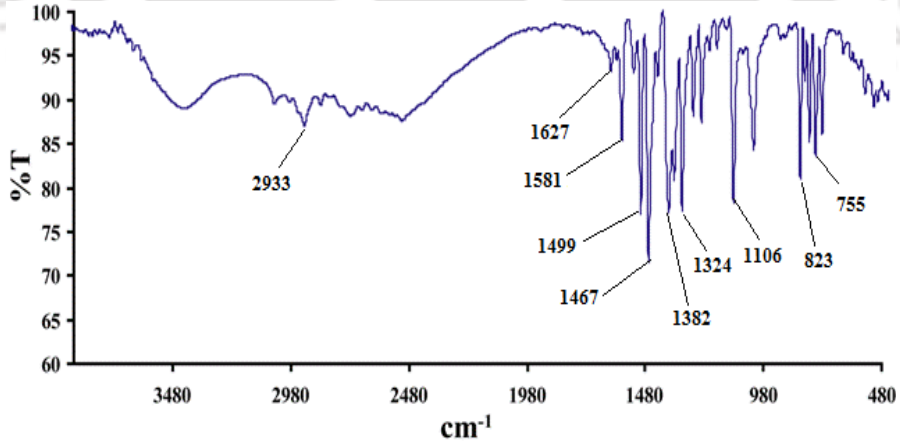

Figure 2.31: FT-IR (KBr, cm^{-1}) spectra of complex **2.5**.

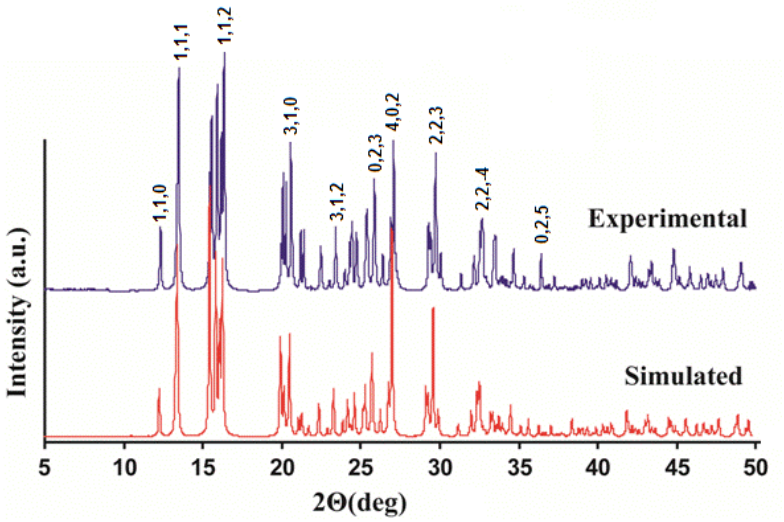

Figure 2.32: Powder XRD pattern of complex **2.5**.

Synthesis of 2.6:

To a solution of 8-hydroxyquinoline (0.31 g, 2 mmol) in methanol (20 mL) zinc chloride (0.28 g, 2 mmol) was added and stirred for 15-20 minutes. A white precipitate was formed which was filtered and recrystallised from 3-picoline to obtain the complex **2.6**. Yield ~ 60% (with respect to zinc). %. IR (KBr, cm^{-1}): 3323 (s), 3044 (w), 1581(m), 1571 (s), 1495 (m), 1464 (s), 1422 (w), 1389 (s), 1327 (s), 1283 (w), 1232 (w), 1109 (m), 1056 (w), 1031 (w), 821 (m), 791 (m), 735 (m), 705 (w), 640 (w), 500 (w). ^{1}HNMR (400 MHz, DMSO-d_6): 8.78 (t, J = 2.8 Hz, 3H), 8.36 (q, J = 1.6 Hz, 4H), 7.57 (q, J = 4 Hz, 3H), 7.44 (q, J = 8 Hz, 2H), 7.29 (d, J = 8 Hz, 2H), 7.02 (d, J = 7.2 Hz, 3H), 2.29 (s, 6H).

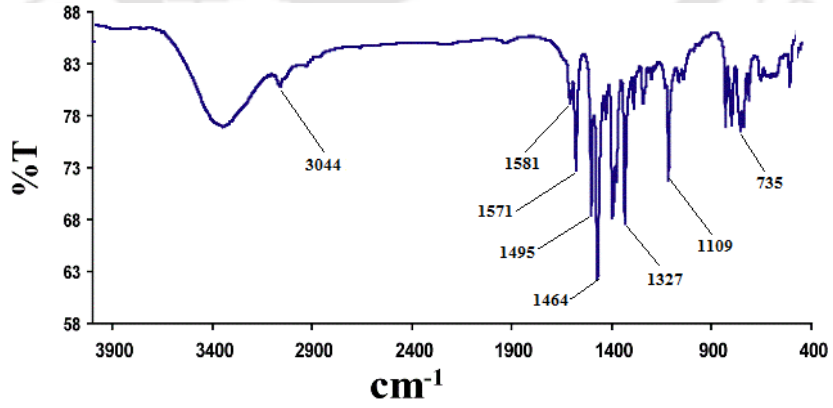

Figure 2.33: FT-IR (KBr, cm^{-1}) spectra of complex **2.6**.

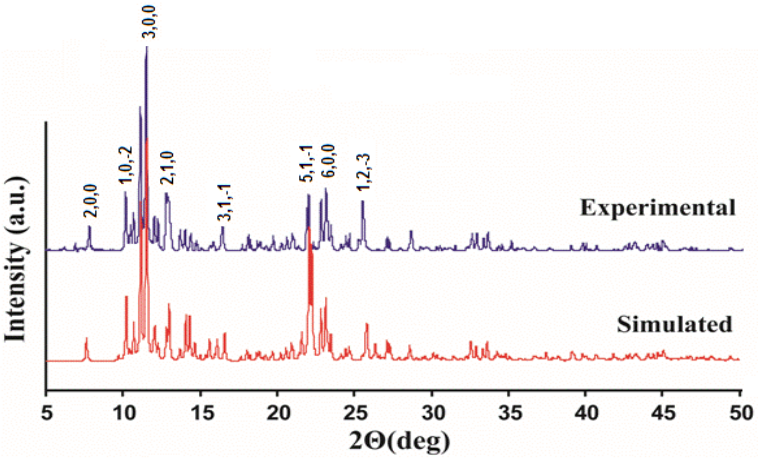

Figure 3.34: Powder XRD pattern of complex **2.6**.

Synthesis of 2.7:

A mixture of 8-hydroxyquinoline (0.31 g, 2 mmol), $CoCl_2.6H_2O$ (0.28 g, 2 mmol) and dimethylformamide (10 mL) was stirred for 15 minutes. The resulting solution was transferred to a Teflon-lined autoclave and kept under autogenous pressure at 160 °C for 2 days. After slow cooling to room temperature, pink block crystals of tetra nuclear cobalt cluster were obtained. Isolated yield based on cobalt 45 %. Elemental analysis: calculated for $C_{54}H_{36}Cl_2Co_4N_6O_6$, C: 55.36 %, N: 7.17 %, H: 3.10%; found C: 52.31 %, N: 7.62 %, H: 3.16 %. IR (KBr, cm-1): 3048 (w), 1658 (w), 1603 (w), 1577 (s), 1499 (s), 1465 (s), 1424 (s), 1379 (s), 1316 (s), 1269 (s), 1233 (w), 1177 (w), 1107 (s), 1032 (w), 908 (w), 826 (m), 789 (m), 756 (m), 733 (m), 645 (w), 600 (w), 507 (w).

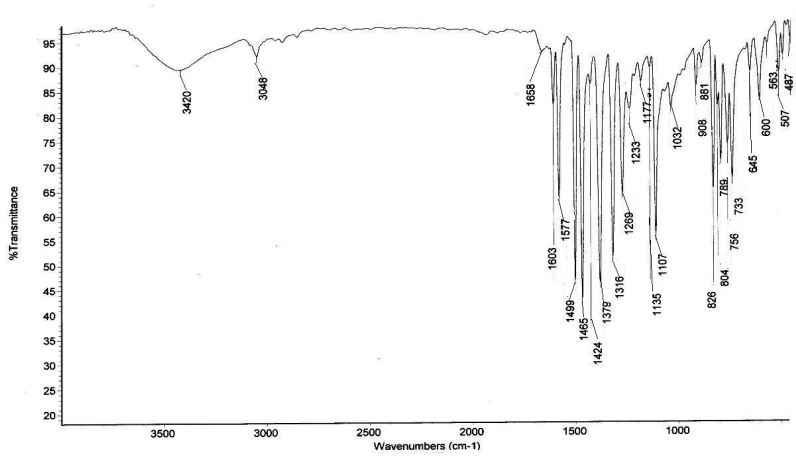

Figure 2.35: FT-IR (KBr, cm^{-1}) spectra of **2.7**.

Synthesis of 2.8:

A mixture of 8-Hydroxyquinoline (0.31 g, 2 mmol), $MnCl_2 \cdot 6H_2O$ (0.42 g, 2 mmol) and dimethylformamide (10 mL) was stirred for 15 minutes. The resulting solution was then transferred to a Teflon-lined autoclave and kept under autogenous pressure at 160 °C for 2 days. After slow cooling of the solution to room temperature, pink block crystals of tetra nuclear cobalt cluster were obtained. FT-IR (cm^{-1}): 3391(w), 3056 (w), 2923 (w), 1650 (w), 1599 (w), 1572 (s), 1494 (s), 1460 (s), 1422 (m), 1373 (s), 1315 (s), 1269 (s), 1232 (m), 1101 (s), 903 (m), 825 (s), 785 (m), 742 (s), 732 (s), 629 (m), 616 (m), 524 (m), 514 (m), 406 (w).

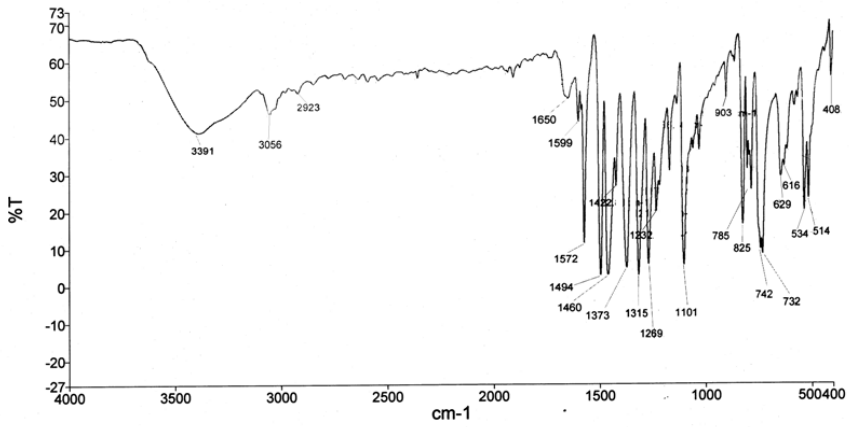

Figure 2.36: FT-IR (KBr, cm^{-1}) spectra of **2.8**.

Synthesis of 2.10:

A mixture of **2.7** (0.40 g, 3 mmol) and $CoCl_2 \cdot 6H_2O$ (0.23 g, 1 mmol) in DMF (10 mL) was stirred for 15 minutes. The resulting solution was then transferred to a Teflon-lined autoclave and kept under autogenous pressure at 160 °C for 2 days. After slow cooling of the solution to room temperature, pink block crystals of deca nuclear cobalt cluster were obtained in 72% yield. Elemental analysis: Calculated for $C_{121}H_{95}N_{15}O_{28}Co_{10}$; C: 51.97 %, N: 7.51 %, H: 3.42 %; found C: 51.68 %, N: 7.77 %, H: 3.31 %. IR (KBr, cm^{-1}): 3042 (w), 2925 (w), 1659 (s), 1602 (w), 1574 (s), 1492 (s), 1460 (s), 1379 (s), 1321 (s), 1278 (m), 1227 (w) 1108 (s), 1027 (w), 906 (w), 824 (m), 788 (m), 745 (m), 648 (w), 602 (w), 570 (w), 499 (w). Raman (KBr, cm-1): 3064 (w), 1580 (s), 1363 (s), 740 (w).

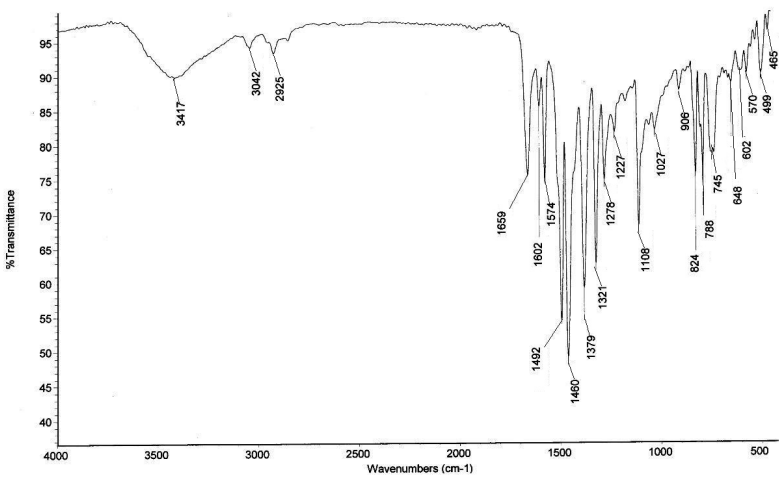

Figure 2.37: FT-IR (KBr, cm^{-1}) spectra of **2.10**.

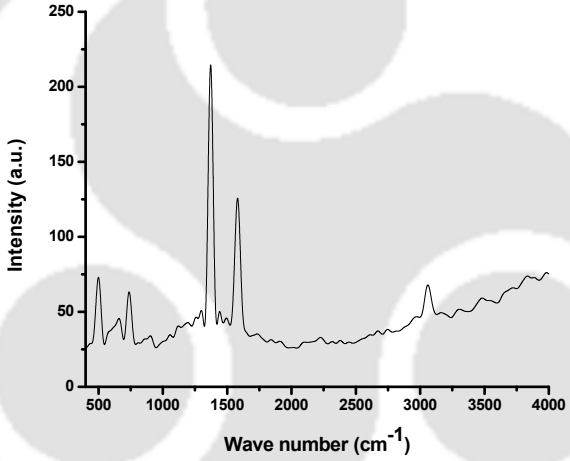

Figure 2.38: RAMAN (KBr, cm^{-1}) spectra of **2.10**.

Synthesis of 2.11:

A yellowish precipitate (0.40 g) obtained from a reaction $MnCl_2 \cdot 4H_2O$ (0.20 g, 1 mmol) with 8-hydroxyquinoline (0.16g, 1 mmol), analogously to the synthesis of tetra nuclear cobalt complex **2.7** was taken with $MnCl_2 \cdot 4H_2O$ (0.20 g, 1 mmol) in dimethylformamide (10 mL) was stirred for 15 minutes. The solution was transferred to a Teflon-lined autoclave and kept under autogenous pressure at 160 °C for 2 days. After slow cooling to room temperature yielded pink block crystals of deca nuclear manganese cluster 3 in 68% yield. Elemental analysis: calculated for $C_{121}H_{95}N_{15}O_{28}Mn_{10}$; C: 52.72 %, N: 7.67 %, H: 3.47 %; found C: 52.11 %, N: 8.48 %, H: 3.52 %. IR (KBr, cm^{-1}): 3419 (w), 3041 (w), 2924 (w), 1660 (m), 1601 (w), 1572 (m), 1487 (s), 1452

(s), 1383 (s), 1321 (s), 1278 (m), 1230 (w), 1172 (w), 1107 (s), 1058 (w), 1029 (w), 904 (w), 824 (m), 789 (m), 748 (m), 731 (m), 646 (w), 601 (w), 567 (w), 492 (w). Raman (KBr, cm^{-1}): 3054 (w), 1572(s), 1361(s), 870 (s).

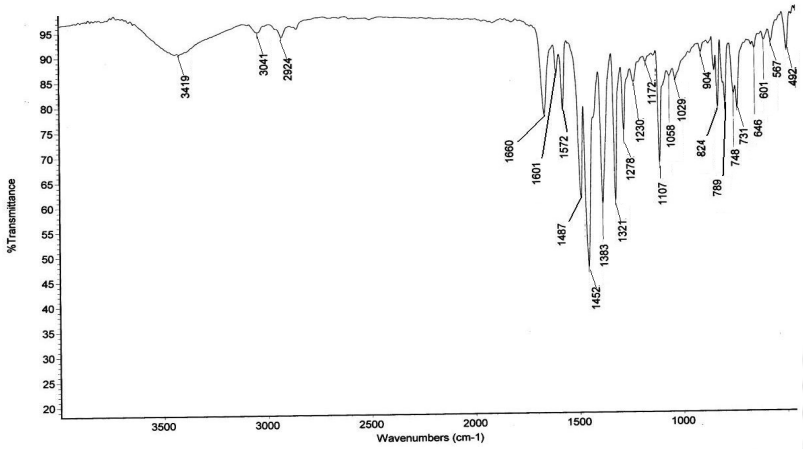

Figure 2.39: FT-IR (KBr, cm^{-1}) spectra of **2.11**.

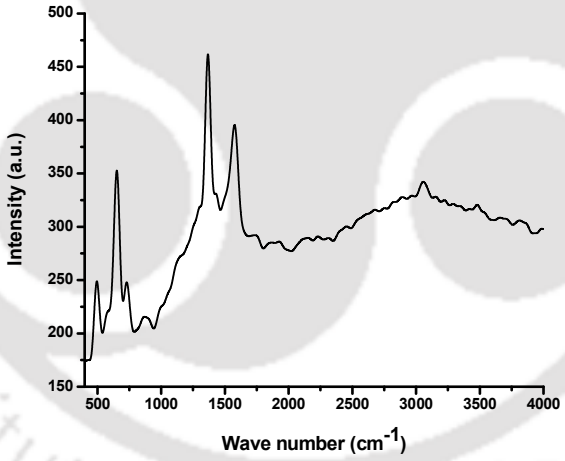

Figure 2.40: RAMAN (KBr, cm^{-1}) spectra of **2.11**.

2.6: Reference

1. H. R. Fleck, A. M. Ward, *Analyst*, 1933, **58**, 388.
2. H. B. Knowles, *J. Res. Nat. Bureaue of Standards*, 1935, **15**, 87.
3. R. J. Curry, W. P. Gillin, *Synth. Met*., 2000, **111**, 35.
4. L. L. Merritt, R. T. Cady, B. W. Mundy, *Acta Cryst.,* 1954, **7**, 473.
5. Y. Kai, M. Morita, N. Yasuoka, N. Kasai, *Bull. Chem. Soc. Jpn*., 1985, **58**, 1631.

6. E. Sattarzadeh, G. Mohammadnezhad, M. M. Amini, S. W. Ng, *Acta Cryst.,* 2009, **E65,** m712.
7. J. Wang, Q. Wang, Y. Sun, Y. Wang, G. Zhao, Y. Cui, *J. Serb. Chem. Soc.,* 2011, **76,** 529.
8. H. -B. Xu, J. -G. Deng, L. -Y. Zhang, Z. -N. Chen, *Cryst. Growth Des*., 2013, **13**, 849.
9. J. K. Nath, Y. Lan, A. K Powell, J. B. Baruah, *Z. Anorg. Allg. Chem.,* 2013*,* **639,** 2250**.**
10. R. Bertonncello, M. Bettinelli, M. Casarin, A. Gulino, E. Tondello, A. Vittadini, *Inorg. Chem.,* 1992, **31**, 1558.
11. H. Chun, H. Jung, *Inorg. Chem.,* 2009, **48**, 417.
12. C. Redshaw, S. Jana, C. Shang, M. R. J. Elsegood, X. Lu, Z. X. Guo, *Organometallics,* 2010, **29**, 6129.
13. N. A. A. El-Kanzi, *IJOC,* 2012, **2**, 352.
14. F. A. Cotton , R. Francis, W. D. Horrocks Jr., *J. Phys. Chem.*, 1960, **64**, 1534.
15. J. L. F. da Silva, A. P. Ferreira, M. M. Marques, S. G. Harjivan, M. F. M. da Piedadeab, M. T. Duarte, *CrystEngComm*., 2011, **13**, 1638.
16. O. Takahashi, Y. Kohno, M. Nishio, *Chem. Rev.,* 2010, **110**, 6049.
17. A. Goswami, N. Phukan, J. B. Baruah, *Cogent Chemistry,* 2015, **1**: 1060046.
18. S. Pramanik, C. Zheng, X. Zhang, T. J. Emge, J. Li, *J. Am. Chem. Soc.,* 2011, **133**, 4153.
19. A. Karmakar, J. B. Baruah, *Polyhedron,* 2008, **27**, 3409;
20. R. Sarma, D. Kalita, J. B. Baruah, *Dalton Trans.,* 2009, 7428.
21. W. Bury, I. Justyniak, D. Prochowicz, A. Rola-Noworyta, J. Lewinski, *Inorg. Chem.,* 2012, **51,** 7410;
22. W. M. Singh, J. B. Baruah, *Dalton Trans.,* 2009, 2352.
23. K. S. W. Sing, D. H. Everett, R. A. W. Haul, L. Moscou, R. A. Pierotti, J. Rouquerrol,
1. T. Siemieniewska *Pure and Appl. Chem.*, 1985, **57,** 603.
24. W. T. A. Harrison, *Acta Cryst*., 2005, **E61**, m1951.
25. M. J. Mayoral, P. Ovejero, J. A. Campo, J. V. Heras, E. Pinilla, M. R. Torres, M. Cano, *Inorg. Chem. Commun.,* 2009, 12214.
26. A. Cingolani, S. Galli, N. Masciocchi, L. Pandolfo, C. Pettinari, A. Sironi, *Dalton Trans.,* 2006*,* 2479.
27. J. A. McGinnety, *Inorg. Chem.,* 1974, **13**, 1057.
28. A. Karmakar, R. J. Sarma, J. B. Baruah, *Inorg. Chem. Commun.,* 2006, **9,** 1169.

29. N. Phukan, J. B. Baruah, *RSC Advances,* 2013, **3**, 1151.
30. J. Cui, Z. Lu, Y. Li, Z. Guo, H. Zheng, *Chem. Commun.,* 2012, **48,** 7967.
31. A. Lan, K. Li, H. Wu, D. H. Olson, T. J. Emge, W. Ki, M. Hong, J. Li, *Angew. Chem. Int. Ed. Eng.,* 2009, **48,** 2334.
32. A. J. Fletcher, K. M. Thomas, M. J. Rosseinsky, *J. Solid State Chem.,* 2005, **178**, 2491.
33. V. V. Shynkar, A. S. Klymchenko, E. Piemont, A. P. Demchenko, Y. Mely, *J. Am. Chem. Soc.,* 2004, **108**, 8151.
34. A. S. Klymchenko, A. P. Demchenko, *J. Am. Chem. Soc.,* 2002, **124**, 12372.
35. Z. -G. Li, G. -H. Wang, H. -Q. Jia, N. -H. Hu, J. -W. Xu, *CrystEngComm.***,** 2008,**10**, 173.
36. S. K. Ritter, *Chem. Eng. News*, 2004, **82**, 29.
37. H. -H. Chen, J. Yang, Y. -Y. Liu, J. -F. Ma, *CrystEngComm*., 2013, **15**, 5168.
38. R. Sessoli, H. -L. Tsai, A. R. Schake, S. Wang, J. B. Vincent, K. Folting, D. Gatteschi, G. Christou, D. N. Hendrickson, *J. Am. Chem. Soc*., 1993, **115**, 1804.
39. D. Armentano, N. Marino, T. F. Mastropietro, J. Martinez-Lillo, J. Cano, M. Julve, F. Lloret, G. De Munno, *Inorg. Chem*., 2008, **47**, 10229.
40. A. Escuer, R. Vicente, S. B. Kumar, F. A. Mautner, *J. Chem. Soc*., *Dalton Trans*., 1998, 3473.
41. J. Juillard, *Pure Appl. Chem*., 1977, **49**, 885.
42. H. Li, W. Shi, K. Zhao, Z. Niu, X. Chen, P. Cheng, *Chem. Eur. J.,* 2012, **18**, 5715.
43. X. -Y. Wang, L. Gan, S. -W. Zhang, S. Gao, *Inorg. Chem.,* 2004, **43**, 4615.
44. M. -L. Sun, X. Zhang, Y. -Y. Huang, Q. -P. Lin, Y. -Y. Qin, Y. -G. Yao, *New J. Chem.,* 2014, **38**, 55.
45. W. Chen, J. -Y. Wang, C. Chen, Q. Yue, H. -M. Yuan, J. -S. Chen, S. -N. Wang, *Inorg. Chem.,* 2003, **42**, 944.
46. J. Martinez-Lillo, D. Armentano, N. Marino, L. Arizaga, R. Chiozzone, R. Gonzalez, C. Kremer, J. Cano, J. Faus, *Dalton Trans.,* 2008, 4585.
47. J. Qian, F. Jiang, L. Zhang, K. Su, J. Pan, Q. Li, D. Yuan, M. Hong, *Chem. Commun.,* 2014, **50**, 1678.
48. A. Escuer, R. Vicente, E. Penalba, X. Solans, M. Font-Bardia, *Inorg. Chem*., 1996, **35**, 248.
49. F. Lloret, M. Julve, J. Cano, R. Ruiz-Garcia, E. Pardo, *Inorg. Chim. Acta*, 2008, **361**, 3432.

50. D. F. Li, S. Parkin, G. B. Wang, G. T. Yee, A. V. Prosvirin, S. M. Holmes, *Inorg. Chem*., 2005, **44**, 4903.

Chapter 3

Synthesis, characterization, anion–π interactions and selective ion recognition by 5-nitrosoquinolin-8-ol

Among various weak π-interactions, anion-π interaction is an important interactions contributing to self-assembling of supramolecular systems. This weak interaction plays vital role in the fields of non covalent synthesis,[1-2] self-replication,[3-5] supramolecular catalysis,[6-8] and functional non covalent devices.[9-10] Anion-π interaction occurs between electron deficient aromatic system and anion.[11-16] Generally such interaction requires favorable geometrical orientation of anion at an appropriate distance with respect to a π-cloud.[17-18] Such interaction may occurs through common processes (i) nesting, (ii) perching and (iii) encapsulation that are often come across in host-guest chemistry.[19-25] Some arrangements of anions with π-clouds to show anion-pi interactions are shown Figure 3.1.

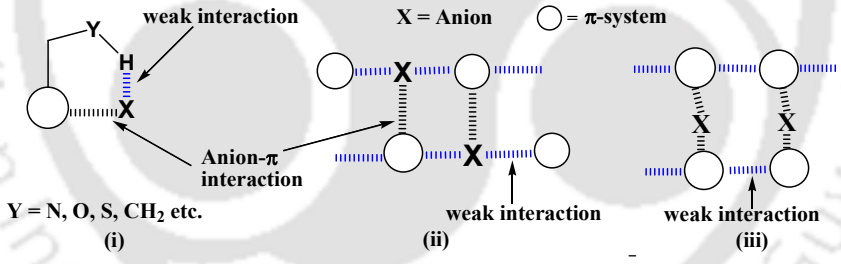

Figure 3.1: Arrangement of anions over π- cloud for anion- π interactions.

In the first case the anion is held in an appropriate position to have a favorable anion-π interaction with a support present in the host molecule by other weak non-covalent interactions such as hydrogen bonds. An example of a salt showing such interaction is shown in the Figure 3.2. In second type, the anions are placed in alternate places in between the host molecules to have least repulsions between similar types of ions. Such arrangements of π-aromatic rings containing organo-cation have not been explored.

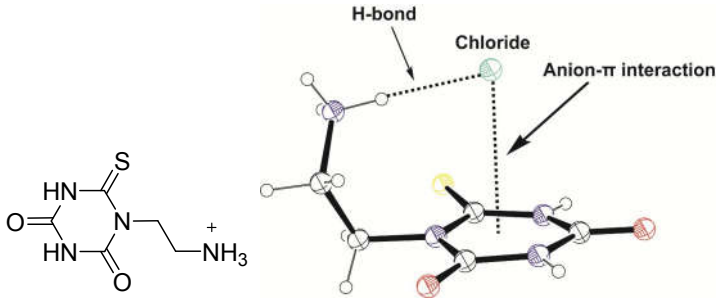

(a) (b)

Figure 3.2: (a) Ethylene ammonium thiocyanuric acid and (b) chloride-π interaction in its chloride salt.

Whereas, in the third case as illustrated by schematic diagram shown in Figure 3.1(iii) anions are sandwiched between host molecules. This type of arrangement is observed in nitrate anions in which anions are held within aromatic host to possess cage-like structures.[26] There are also other examples such as in encapsulation of iodide anion between two molecules of 1,4,5,8,9,12-hexaazatriphenylene hexacarbonitrile as illustrated in Figure 3.3b.

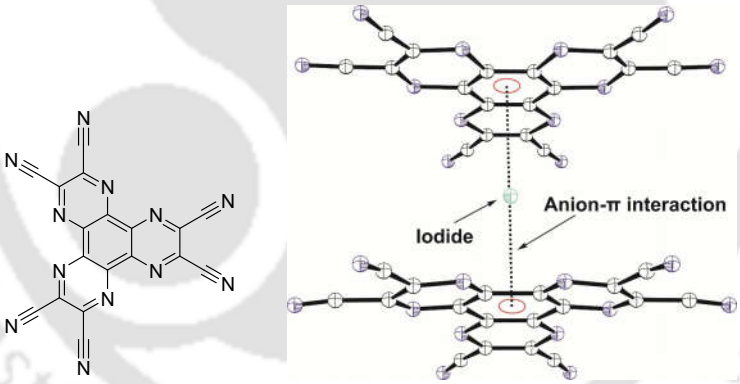

(a) (b)

Figure 3.3: (a) 1,4,5,8,9,12-Hexaazatriphenylene hexacarbonitrile (b) Encapsulation of iodide ions showing iodide-π interactions.

As mentioned, anion-π interactions are observed between anions and electron deficient π-systems. Since there are large number of quinoline based compounds that are used for anion recognitions, we were interested to develop quinoiline based systems for specific binding to anions. It is a well known fact that quinoline moiety provides a basis for π-π interactions. Hence they can be a template for anion-π interactions provided they are made electron deficient and

polarity in such structure is retained. Keeping these points in the mind, we have chosen 5-nitrosoquinolin-8-ol (**3.1**) a nitroso derivative of 8-hydroxyquinoline which is a basic system suitable to form various salts with acids. 5-nitrosoquinolin-8-ol can remain as keto or enol form as shown in Figure 3.4. The solid state structure of the compound determined by single crystal x-ray spectroscopy,[27] have shown that it adopts a keto form which can be named as 5-(hydroxyimino)quinolin-8-one (**3.1**) and its crystal packing shows that it forms a lamellar structure. Thus, a salt of this compound should help in sandwiching anions in between the laminar interactions of the host cations. Literature survey has shown that the structural aspects of the salts of **3.1** have not been explored so far. So we set our study to understand structures of different salts of **3.1** and its interaction with acids in solution.

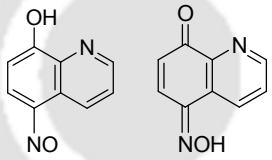

Figure 3.4: Enol and keto forms of **3.1**.

Compound **3.1** was synthesized by nitrosation reaction of 8-hydroxyquinoline following reported procedure.[28] The compound **3.1** reacts with various acids and accordingly chloride salt **3.2**, bromide salt **3.3**, nitrate salt **3.4** and perchlorate salt **3.5** were prepared by adding respective mineral acid to the methanolic solution of compound **3.1** and recrystallised as shown in Scheme 3.1.

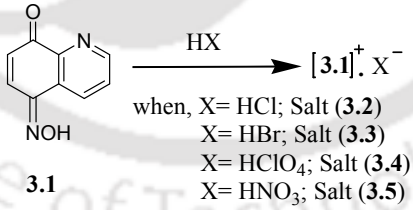

3.1

Scheme 3.1: Salts of compound 5-(hydroxyimino)quinolin-8-one (**3.1**).

3.1: Anion-π interactions in salts of compound 3.1

3.1.1: Structural study

Chloride salt **3.2** and bromide salt **3.3** are isostructural, as they have the same structure, but different cell dimensions nor the same chemical composition. Both the crystals of the salts belong to monoclinic, $P2_1/m$ space group with unit cell volumes 455.61and 481.09 respectively.

They also fulfill other conditions of isostructurality by having comparable variability in the atomic coordinates. Structure of chloride salt is shown in Figure 3.6a. In this structure chloride ions are sandwiched between two planar aromatic rings of the cations. Chloride ions and cations are placed in alternate positions so as to have maximum electrostatic interactions between the oppositely charged species. Further to this, the packing arrangements of ions are such that they have minimum repulsion between similar ions. Similar arrangements were also found in case of bromide salt **3.3**. Distance between anion and centroid of π-cloud of cation of the chloride salt **3.2** is 3.374 Å; whereas such distance in bromide salt **3.3** is 3.465 Å. These distances are within permissible distances for anion-π interactions of both the types anions.[29-32] For example in the crystal structure of bromide salt of 2,3,4,5,6-pentafluoro-*N*-(propan-2-ylidene)benzenamine, where layers of cations and anions run along parallely. The bromide anions are hold in the crystal lattice by C-H···Br, N-H···Br and anion-π interaction (Figure 3.5).[33] In this case the distance between the bromide anion and centroid of the phenyl ring was reported to be 3.440 Å.

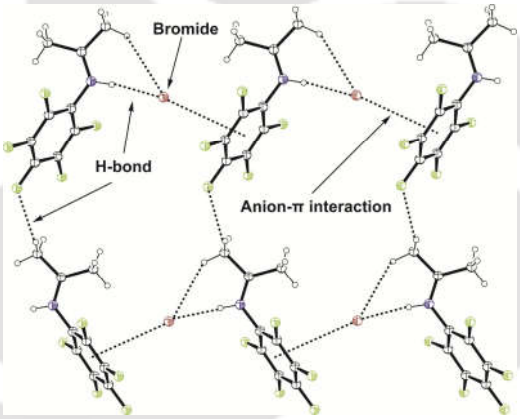

Figure 3.5: Bromide-π interaction in bromide salt of 2,3,4,5,6-pentafluoro-N-(propan-2-ylidene)benzenamine.

The self-assemblies of the salts **3.2** and **3.3** are guided by C-H···O, N-H···X and O-H···X (where 'X' represents the halide ion) interactions. Through the interplay of electrostatic interactions and weak interactions a layered structure is formed in each of these salts. The layered structure in case of chloride salt extends along c-axis plane (Figure 3.6b) and along b-axis plane in bromide salt (Figure 3.6c). Pertinent hydrogen bond parameters of salts **3.2** and **3.3** are listed in Table 3.1. It is clear from the hydrogen bonds in Table 3.1 that both the salts have similar hydrogen bonds to stabilize their respective self-assemblies. However, the N-H···X and O-H···X bond

distances were observed to be different between the two salts. In case of chloride salt **3.2** the N-H···X and O-H···X bonds distances are 2.27 Å and 2.19 Å respectively while, in case of bromide salt **3.3** theses are respectively 2.43 Å and 2.35 Å.

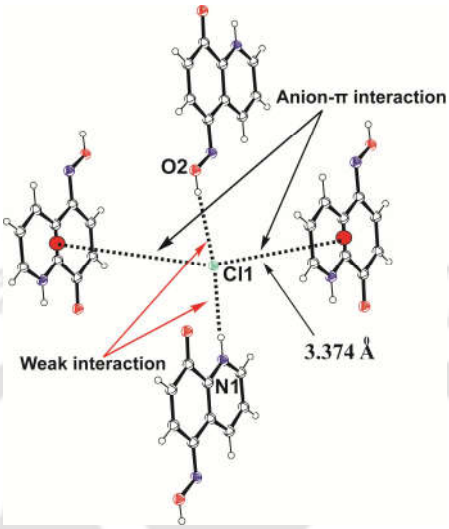

(a)

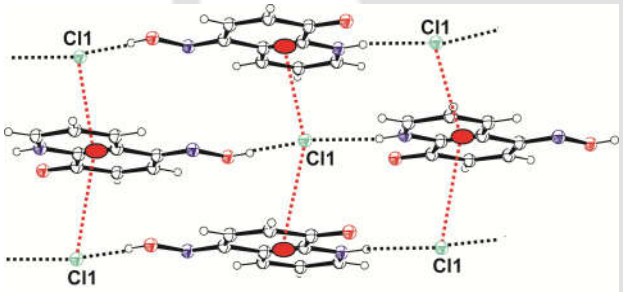

(b)

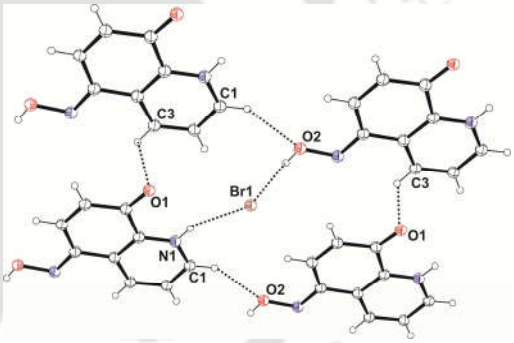

(c)

Figure 3.6: (a) Interactions of chloride with four different cations in salt **3.2**, (b) Hydrogen-bonds and anion-π interactions in salt **3.2** showing a layered structure and (c) hydrogen bonds in structure of salt **3.3**.

The longer N-H···X and O-H···X bonds distances in bromide salt **3.3** compared to chloride salt **3.2** can be attributed to the less electronegativity of bromide anion due to its higher ionic radius compared to chloride anion. Coordination environment of halide is distorted square planar geometry, where a halide ion holds two cations by anion-π interaction and while other two cations are hold by N-H···X and O-H···X type of hydrogen bonds.

Table 3.1: Hydrogen-bond parameters of salts **3.2-3.5**.

Compound No.	D-H···A	d_{D-H}(Å)	$d_{H\cdots A}$(Å)	$d_{D\cdots A}$(Å)	∠ D-H···A(°)
Salt **3.2**	N1-H···Cl1 [1-x,-1/2+y,1-z]	0.86(3)	2.27(3)	3.07(2)	157(3)
	O2-H···Cl1 [2-x,-1/2+y,1-z]	0.82(5)	2.19(2)	3.00(2)	159(2)
	C1-H···O2 [x,y,-1+z]	0.93(3)	2.59(2)	3.34(4)	137(5)
	C3-H···O1[1+x,y,z]	0.93(3)	2.33(3)	3.02(6)	130(9)
Salt **3.3**	N1-H···Br1 [1-x,-1/2+y,1-z]	0.86(3)	2.43(2)	3.24(6)	157(10)
	O2-H···Br1 [-x,-1/2+y,-z]	0.82(3)	2.35(9)	3.37(9)	143(8)
	C1-H···O2 [-1+x,y,z]	0.93(3)	2.59(3)	3.38(3)	143(9)
	C3-H···O1 [x,y,1+z]	0.93(3)	2.32(7)	3.04(4)	133(6)
Salt **3.4**	N1-H···O6 [1/2-x, 1/2+y, 1/2-z]	0.86(6)	2.00(2)	2.83(12)	161(3)
	C7-H···O3 [x,y,-1+z]	0.93(3)	2.71(2)	3.36(3)	128 (4)
	O2-H···O4 [1/2-x, 1/2-y, -z]	0.82(3)	2.25(4)	2.83(10)	129(5)
Salt **3.5**	O2-H···O3 [1-x,1-y,1-z]	0.82 (2)	1.89 (2)	2.66(19)	156(3)
	N1-H···O4 [-x,-1/2+y,1/2-z]	0.86(3)	2.36(4)	2.96(2)	128(2)
	N1-H···O5 [-x,-1/2+y,1/2-z]	0.86(3)	2.18(2)	2.97(2)	154(3)
	C7-H···O3[1-x,-1/2+y,1/2-z]	0.93(3)	2.57(3)	3.22(2)	128(6)
	C1-H···O4 [-x,-1/2+y,1/2-z]	0.93(3)	2.59(3)	3.08(2)	114(5)
	C2-H···O5 [-x,1-y, 1-z]	0.93(2)	2.45(5)	3.35(2)	165(2)

Crystal structure of the salt **3.4** comprises of a cation of **3.1** and a perchlorate anion in the asymmetric unit. One oxygen atom of perchlorate ion is crystallographically disordered; this atom is shown to have equal sharing of electron densities among two equivalent positions (Figure 3.7a).

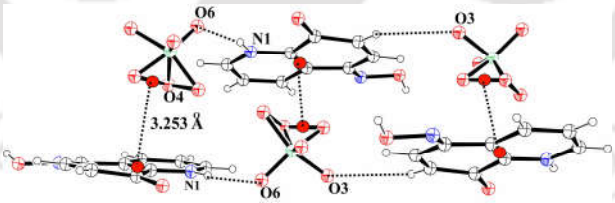

(a)

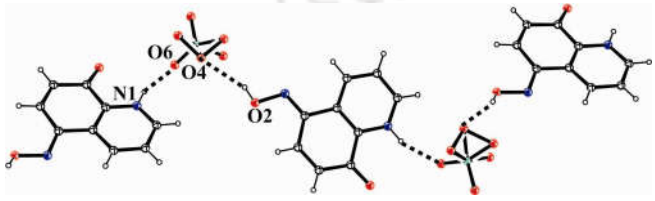

(b)

Figure 3.7: (a) Anion- π interactions in salt **3.4** and (b) hydrogen bonds between perchlorates and cations.

Perchlorate salt **3.4** has also a layer like packing pattern where the ions interact through weak hydrogen bonding such as N-H···O, O-H···O and C-H···O bonds as shown in the Figure 3.7b. In this case also anions are in a suitable distance from cations to have a favorable anion-π interaction. The layer of ions that extends through is hold by anion-π interaction. Distance between oxygen atom and centroid of π-cloud of cation is 3.253Å, suggests a separation conducive for anion-π interaction.

Nitrate salt **3.5** of compound **3.1** has a composition of $[\mathbf{H(3.1)}]^{+}.\mathbf{NO_3}^{-}$. In its crystal lattice nitrate anion is hydrogen bonded to four neighboring cations of compound **3.1** as shown in Figure 3.8a. Two oxygen atoms O4 and O5 of a nitrate ion are involved in two bifurcated hydrogen bonds formed by N1-H···O4, N1-H···O5 interactions and C1-H···O4, N1-H···O4 interactions. C3-H bond of a cation interacts with O5 atom of nitrate anion. There are weak C7-H···O3 and C6-H···O4 interactions between cations. The oxygen atom, O3 of nitrate anion is hydrogen-bonded to an O-H group of protonated **3.1**. A view along *b*-crystallographic axis shows wave-like layers of anions and cations indulging in anion-π interactions that hold the two lines of ions to extend along. Nitrate anions are found to be sandwiched between cations analogous to the case observed in chloride and bromide salts. Crystallographic *a*-axis of the lattice is related by a 2_1-screw axis (Figure 3.8b). Positions of nitrate ions are oblique with respect to cations, they appear in different planes from cations and distance between centroid of anion and cation is 3.099 Å which is favorable for anion-π interaction.[11-16] Literature suggest that nitrate ion held within concave aromatic host shows anion-π interaction;[31] there are also examples of nitrate ions possessing O···π interactions with π-cloud of a host[32] and nitrate ion placed over naphthalenedimide ring shows weak π-anion interaction.[34-35]

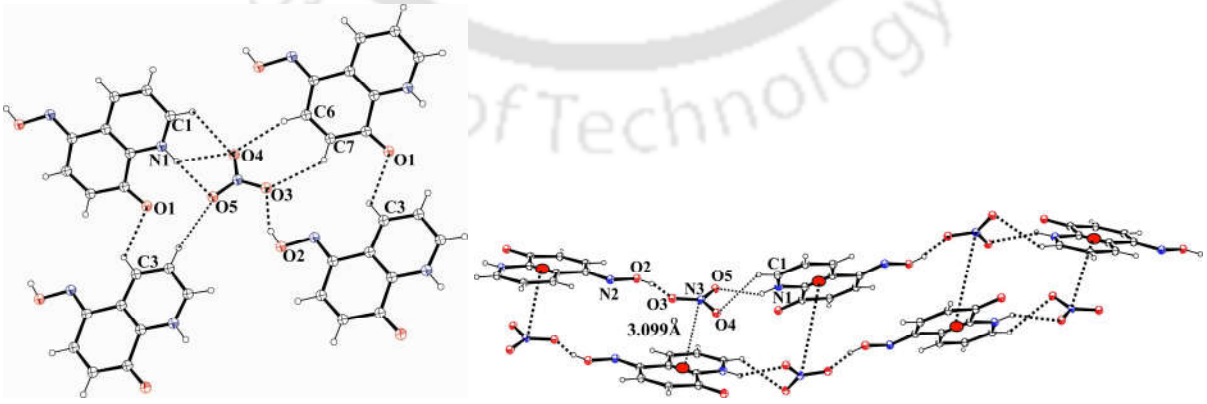

(a) (b)

Figure 3.8: (a) Hydrogen bonds and (b) anion-π interaction in layered structure of salt **3.5**.

Pyridine tethered macrocycle shows anion-π interaction with nitrate ion.[34] A shorter anion-π distance was observed in case of salt **3.5** compared to anion-π distances in conventional cases,[34] it is attributed to electrostatic interactions present among the ions playing a primary role in the tight packing.

Since there are other orientations of a nitrate anion to place over a π-cloud such as shown in Figure 3.9 exist, we chose to make a comparison of other salts of quinoline derivatives such as 5-aminoquinoline, 4-hydroxyquinazoline and 8-hydroxyquinoline. It may be mentioned that the nitrate salt of 8-hydroxyquinoline was reported in literature.[36]

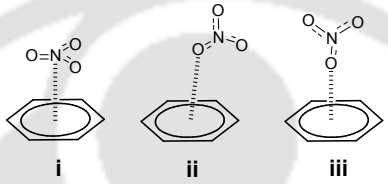

Figure 3.9: Modes of interaction of nitrate anion with π-cloud.

Structures of nitrate salts, namely 5-aminoquinolinium nitrate (**3.6**), 4-hydroxyquinazolineium nitrate (**3.7**) and 8-hydroxyquinolinium nitrate (**3.8**) were analyzed. Crystals of 5-aminoquinolinium nitrate salt belongs to monoclinic, $P2_1/c$ space group. In its crystal lattice each nitrate ion is surrounded by three 5-aminoquinolinium cations has C-H···O and N-H···O interactions as shown in Figure 3.10a. There are several bifurcated hydrogen bonds involved in holding nitrate anion by cations which have C-H···O or N-H···O bonds. C1-H bond of a 5-aminoquinolinium cation forms bifurcated hydrogen bond with two oxygen atoms of nitrate anion. There are two other C-H···O interactions namely C8-H···O3 and C3-H···O1 to hold the cations and anions. N1-H bond act as pivot for bifurcated hydrogen-bonds, N1-H···O2 and N1-H···O3 bonds, whereas one of hydrogen atom of N2-H is involved in two hydrogen bonds namely N2-H···O1 and N2-H···O3. In case of **3.6**, nitrate anions are slightly oblique from plane of aromatic rings of the cations; with oxygen atom to π-centroid distance of 3.252 Å (Figure 2.10c). 4-Hydroxyquinazolinium nitrate (**3.7**), crystallized in monoclinic space group $P2_1/c$. Each nitrate anion in lattice is surrounded by three 4-hydroxyquinazolinium cations (Figure 3.10b). There are two $R_2^2(7)$ types of hydrogen bonds, involving C1-H···O3, N2-H···O4 and C1-H···O4, N1-H···O2 interactions. On the other hand, there is a C3-H···O3 interaction between the nitrate ion and cation (Table 3.2).

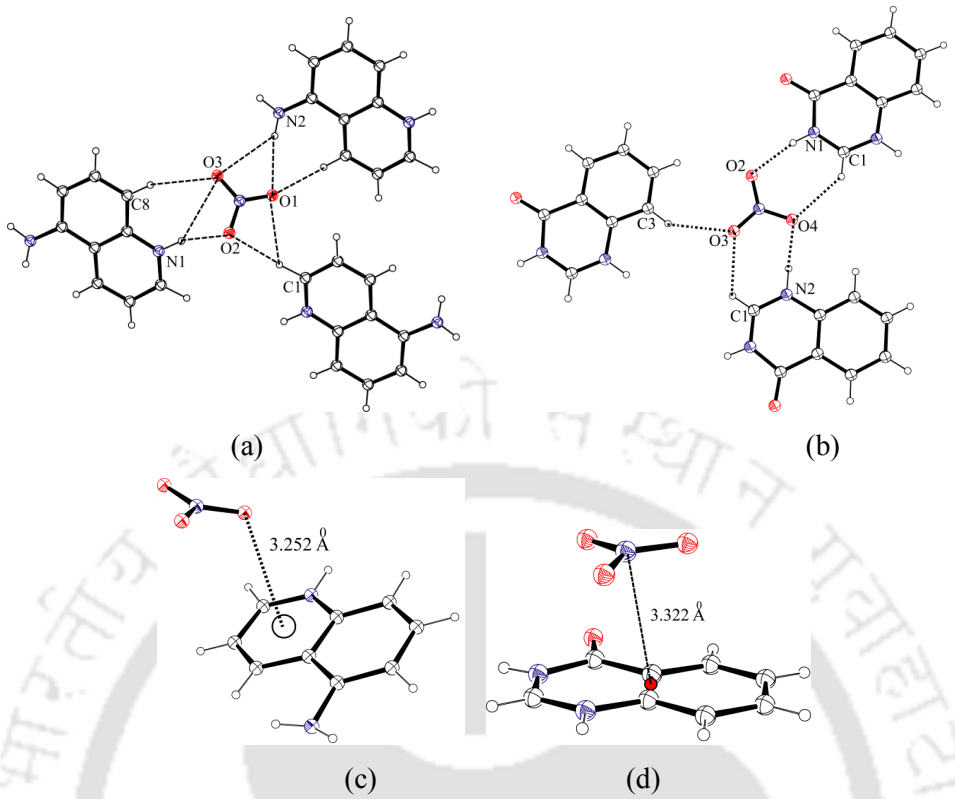

Figure 3.10: Hydrogen bonded assemblies of nitrate salts of (a) 5-aminoquinolinium and (b) 4-hydroxyquinazolinium. Anion-π interactions in nitrate salt (c) **3.6** and (d) **3.7**.

These interactions generate layer-like structure in which nitrate ions and cations are in same plane. As a result π-stacking interactions between cations and anions take place. Stacking interactions present in **3.7** are similar to salt **3.5**. Distance between parallel pair of cation and anion was found to be 3.322 Å (Figure 3.10d).

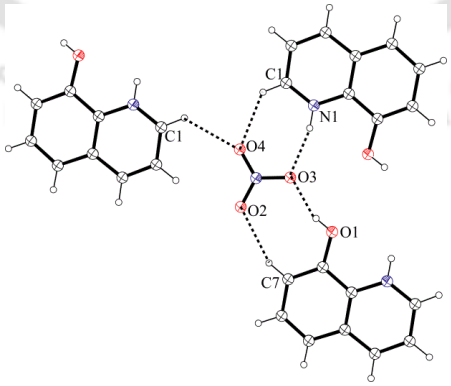

Figure 3.11: A portion of nitrate salt of 8-hydroxyquinoline to show complementary hydrogen bonds in self assembly.

In case of nitrate salt of 8-hydroxyquinoline (**3.8**) similar types of hydrogen bonds were observed as observed in case of **3.6** and **3.7**; however this system is devoid of anion-π interaction. It shows a lamellar structure and each nitrate anions are held between three quinolinium cations as shown in Figure 3.11. In this acse complementary hydrogen bonding of nitrate anion with OH and C-H bonds of hydroxyquinolinium cation plays the key role in stabilization of such structure.

Table 3.2: Hydrogen-bond parameters of **3.6** and **3.7**.

Compound No.	D-H···A	d_{D-H}(Å)	$d_{H\cdots A}$(Å)	$d_{D\cdots A}$(Å)	∠ D-H···A(°)
Salt **3.6**	N1-H···O2 [-1+x,1+y,z]	0.97(3)	1.79(3)	2.72(3)	162(3)
	N2-H···O1 [-1/2+x,1/2+y,z]	0.87(3)	2.27(3)	3.12(4)	168(3)
	C1-H··· O1 [1-x,2-y,-z]	1.07(3)	2.54(3)	3.24(4)	122.6(19)
	C1-H··· O2 [1-x,2-y,-z]	1.07(3)	2.23(3)	3.28(4)	167(2)
	C8-H···O3 [1+x,y,z]	0.98(4)	2.59(5)	3.39(5)	138(2)
	C3-H···O1 [-1+x,y,z]	0.94(7)	2.47(2)	3.21(5)	134(3)
Salt **3.7**	N1-H ··· O2 [-1+x,y,z]	0.86(8)	1.94(6)	2.78(3)	168(11)
	N2-H ··· O4 [x,1/2+y,1/2-z]	0.96(2)	1.85(2)	2.80(3)	178(2)
	C1-H··· O4 [-1+x,y,z]	0.93(4)	2.37(6)	3.11(3)	136(2)
	C1-H··· O3 [-x,1/2+y,1/2-z]	0.93(5)	2.38(9)	2.99(3)	124(3)
	C3-H··· O3 [-1+x,1+y,z]	0.93(3)	2.39(5)	3.22(3)	149(9)

We find that in two of the three nitrate salts studied have possibilities to show anion-π interactions. However the anion-π distances are longer than the distance observed in salt **3.5**. A comparison of nitrate-π interactions is listed in Table 3.3; it is seen that distance of anion-π interaction in the present study is shorter from most of the cases.

Table 3.3: Comparison of nitrate-π interactions in different systems.

System	Anion-π distance (Å)
Salt **3.5**	3.09
Salt **3.6**	3.25
Salt **3.7**	3.32
calix[4]pyrrole derivative	3.20[37]
2,4,6-Tris(di-2-picolylamino)-1,3,5-triazine	3.51[38]
Triazine derivative	3.45[39]
bis(arylethynyl)pyridine derivative	3.59[40]
Hexafluorobenzene derivative	3.32[41]
Naphthalene anhydride derivative	2.79[16]

3.1.2: Fluorescence study of 3.1-3.5

Quinoline derivatives are fluorescent probes on the other hand we observed compound **3.1** to be weakly fluorescent. So it was of our interest to find out the fluorescence emission of these salts in solid state to find out any significant difference caused by anion. Solid state fluorescence emissions were recorded for compound **3.1** as well as its salts **(3.2-3.5)** on excitation at 350 nm, it was observed that intensities at 504 nm were different for each sample. Relative fluorescence emission intensities of salts and parent compound is, nitrate salt ≈ perchlorate salt > bromide salt > 5-(hydroxyimino)quinolin-8-one > chloride salt as shown in Figure 3.12a. It was found that nitrate and perchlorate quenches fluorescence emission, however halides enhances. Thus there is a definite effect of anions to cause such changes in emission property. Moreover, we have recorded fluorescence emission of compound **3.1** and its salts in the liquid state by exciting at a wavelength of 350 nm. We observed two emission maximum for **3.1** at wavelength around 390 nm and 410 nm (Figure 3.12b). Salts have similar emission maximum at wavelength 438 nm, however with different intensities among each other. This trend of different emission intensities among the salts can be compared with trend of emission differences observed in solid state emission. From this comparison of solid state and solution sate emission, it can be suggested that anion-π interaction is active even in solutions of these salts.

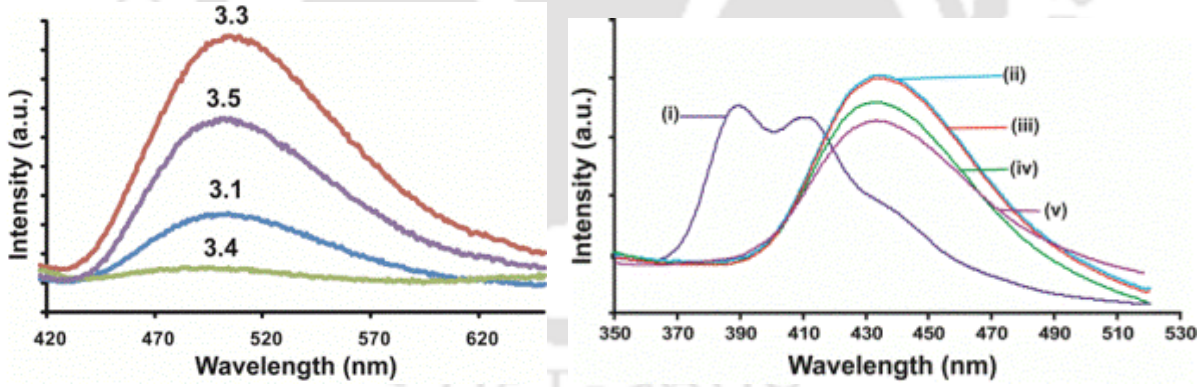

(a) (b)

Figure 3.12: Fluorescence emission spectra of **3.1** and different salts (λ_{ex} = 350 nm) in (a) solid sample and (b) solution in methanol; i) **3.1**, (ii) salt **3.2**, (iii) salt **3.3**, (iv) salt **3.5** and (v) salt **3.4**.

3.1.3: Absorbance study

Changes in UV-visible absorptions of **3.1** by various acids were monitored. Compound **3.1** shows absorption maximum at 279 nm, 328 and 445 nm, which on addition of solution of

mineral acid increases the intensity of former absorbance, whereas the absorbance at 445 nm disappears in each case. In case of addition of hydrochloric and nitric acids the absorbance at 279 nm increases with splitting of the peak into two new absorbance peaks at 260 nm and 268 nm as shown in Figure 3.13.

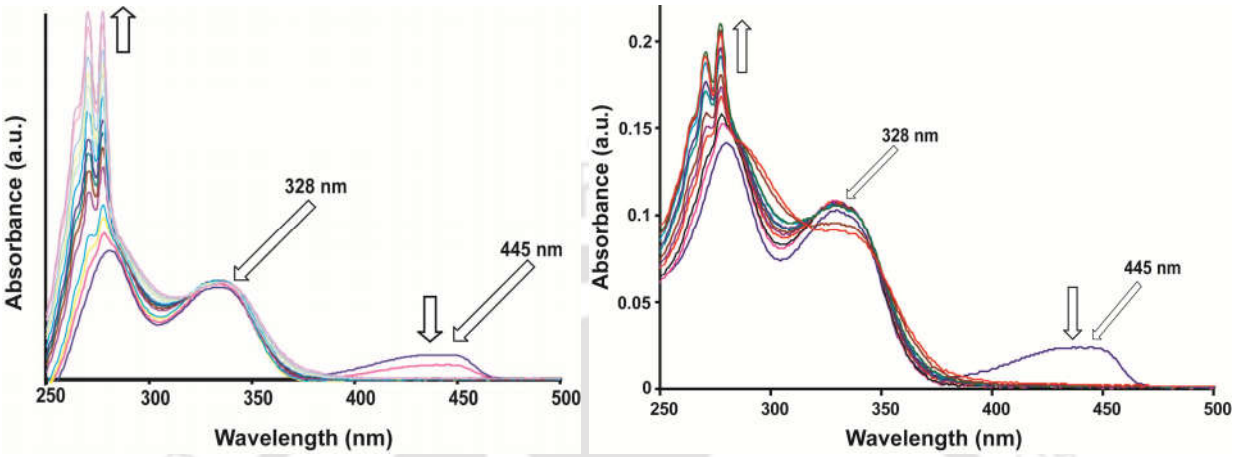

(a) (b)

Figure 3.13: UV-visible spectra of **3.1** in methanol (10^{-5} M) on addition of (a) HCl and (b) HNO_3 (10 μL in each aliquot of 10^{-3} M solution in methanol).

From the changes in absorption on addition of solutions of mineral acids to the solution of **3.1** binding constants were determined by using Benesi-Hildebrand equation.[42] Magnitudes of binding constants for salts follow order **3.4 > 3.3 > 3.5 >> 3.2**.

For a direct comparison among nitrate salts, UV-absorptions of compounds 5-aminoquinoline, 4-hydroxyquinazoline and 8-hydroxyquinoline with different amounts of nitric acid were monitored. Addition of nitric acid increases the intensity of π-π* transition at 214 nm of 5-aminoquinoline and 4-hydroxyquinazoline, however in case of 8-hydroxyquinoline on addition of nitric acid absorbance at 214 nm increases along with growth of a new peak at 253 nm as shown in Figure 3.14. Binding constants determined from changes in absorptions on addition of solution nitric acid to respective compounds for salt **3.5**, **3.6**, **3.7** and **3.8** were determined by using Benesi-Hildebrand equation, which are 2.44×10^2 M^{-1}, 4.18×10^3 M^{-1}, 3.73×10^3 M^{-1} and 5.42×10^3 M^{-1} respectively. Thus, *p*Ka values for salts are 2.38, 3.62, 3.57 and 3.73. Magnitudes of binding constants are of the order **3.8 > 3.6 > 3.7 >> 3.5**. Salts **3.6-3.8** have structural similarities; hence the differences between their binding constants are nominal. This also suggests that magnitudes of anion-π interactions are small.

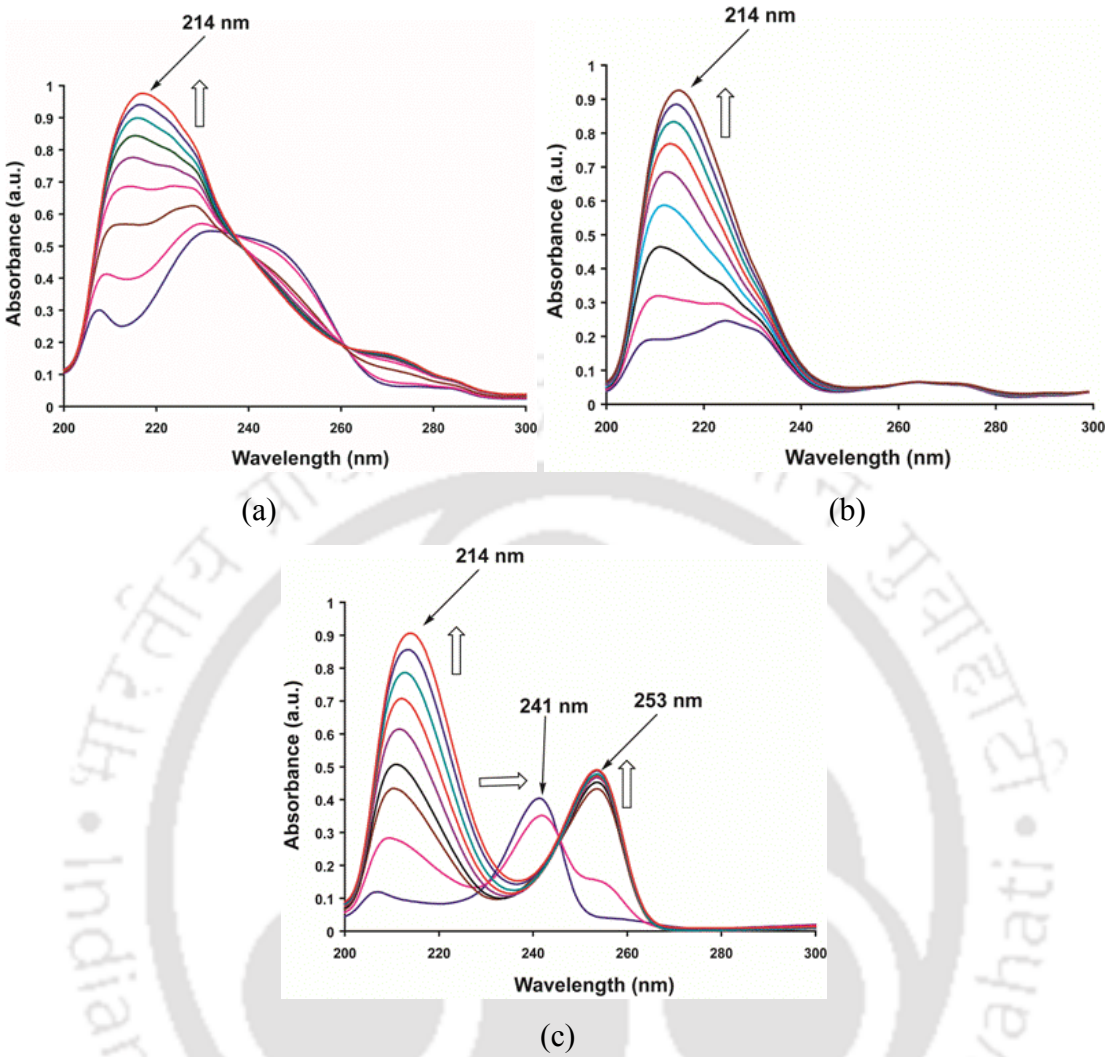

Figure 3.14: Changes in the UV-visible spectra of (a) 8-aminoquinoline; (b) 4-hydroxyquinoxaline and (c) 8-hydrxyquinoline in methanol (10^{-5} M, 3 mL) on addition of 10 µL in each aliquot of 10^{-3} M solution HNO_3 in methanol.

On the other hand, in solid state salt **3.8** does not show anion-π interaction, but it shows highest binding constants among three structurally related salts. Binding constant of salt **3.6** is higher than salt **3.7**. Hence, anion-π interaction could be a cause for difference in optical properties.

A critical examination based on binding constants of a series of nitrate salts have shown that in solution anion-π interactions are too weak to show a distinction in binding constants due to large electrostatic interactions contributing to the salts.

3.1.4: ^{1} H- NMR study

When ^{1}H-NMR spectra were recorded for each salt it was observed that chemical shifts for the aromatic ring protons were different among each other, which suggested salts exist as ion-pairs in solution. In solution, each salt shows ^{1}H-NMR peak due to O-H assigned as *f* (Figure 3.15) which was assigned on the basis of its presence in the parent compound. This hydrogen peak disappears on deuterium exchange. ^{13}C-NMR of the nitrate salt shows a peak at 181.4 ppm which is assigned to carbonyl carbon showing the compound remains in keto form. Chemical shift of ring protons differ from case to case and thus suggests a role of anion on chemical shifts. This implies diamagnetic contribution of anion to π-cloud of cation varies with counter anion suggesting interactions between the counter ions.

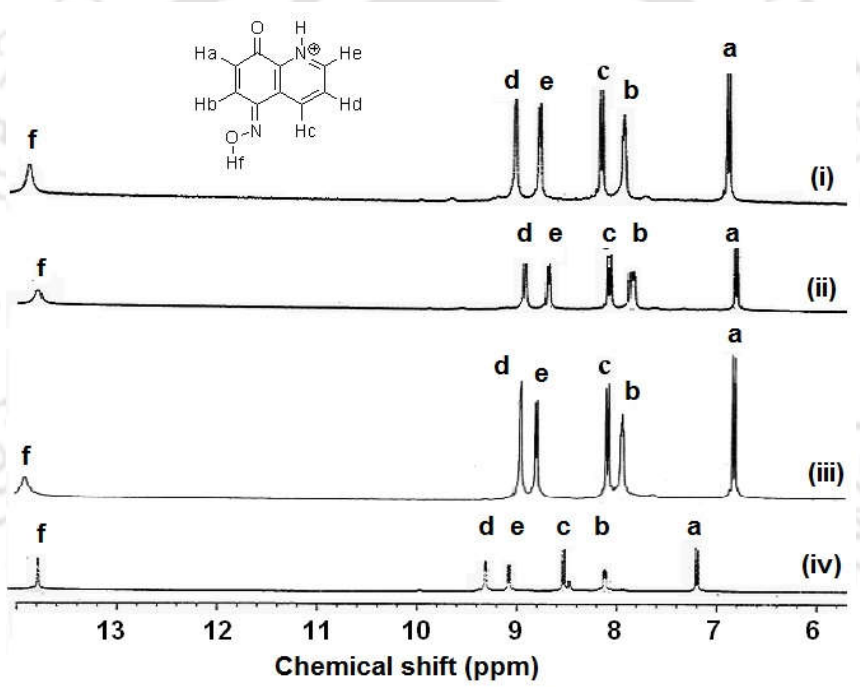

Figure 3.15: ^{1}H-NMR spectra (400MHz, DMSO-d_6) of (i) salt **3.2** (ii) salt **3.3**, (iii) salt **3.4** and (iv) salt **3.5** (only peaks in the range of 6-13.8 ppm are shown for clarity).

3.1.5: DFT calculation

DFT calculation was done for **3.1**, **3.2** and **3.5** and it can be seen that highest occupied molecular orbital (HOMO) shows absence of overlap between chloride and cation in salt **3.2** (Table 3.4). But, lowest unoccupied molecular orbital (LUMO) shows possibility of an overlap region. Thus covalent contribution for anion π-interaction at ground state has less significance in this salt.

However, in case of salt **3.5** we observe that symmetry of highest occupied molecular orbital (HOMO) are such that it has no orbital overlap between anion and cation. The order of energy gaps between the HOMO and LUMO follow as **3.1** > **3.2** > **3.5**.

Table 3.4: Molecular orbitals of **3.1**, **3.2** and **3.5**.

System	Molecular orbitals	Energy gap (eV)
3.1	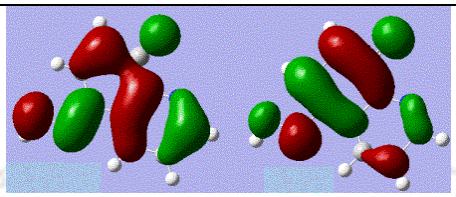 HOMO LUMO	0.146
3.2	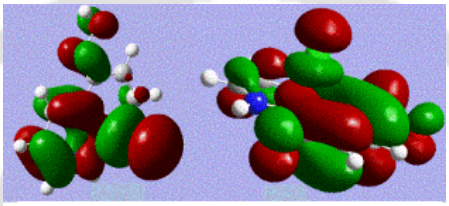 HOMO LUMO	0.110
3.5	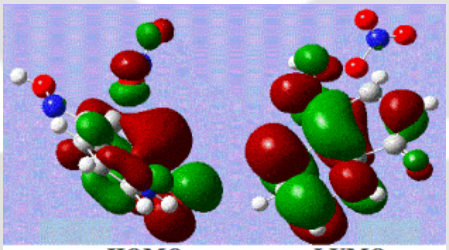 HOMO LUMO	0.091

3.2: Interaction of fluoride with 3.1

We found that interaction of tetrabutyl ammonium fluoride (TBAF) with **3.1** yielded dark blue crystalline compound which was a host-guest complex of TBAF with **3.1** (Figure 3.16a). Single crystals were grown from a DMSO solution of **3.1** with TBAF in 1:1 ratio and we obtained blue crystals (Figure 3.14b), which were analyzed by single crystal analysis. Since, the colors of two crystals are different from each other, this occurrence can be thought of sensing fluoride ions by **3.1** in solid state; **3.1** has pale yellow crystal, while with fluoride anion it gives a dark blue crystal. Asymmetric unit of the supramolecular adduct has two molecules each of **3.1** and TBAF which are symmetrically independent. Both the symmetry independent **3.1** molecules are in keto-forms, among which one of the **3.1** molecules is crystallographically disordered. The C8-O1 bond distance is 1.24 Å, it suggest it to be a C=O bond, supporting a keto form.

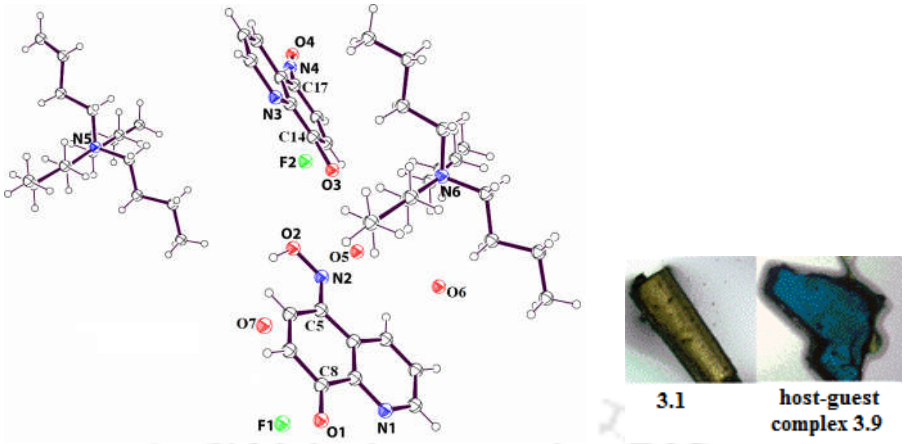

(a) (b)

Figure 3.16: (a) Host-guest complex **[(3.1).TBAF·1.5H_2O]** (drawn with 35% thermal ellipsoid) and (b) optical micrograph **3.1** and host-guest complex **3.9**.

On the other hand, C5-N2 bond distance is 1.35 °A which is supportive of a conjugated C=N bond. Comparing the structure with the reported structure of **3.1**[28] and its salts it is found to be consistent with a keto-form.

3.2.1: Selective interaction of fluoride ions with 3.1

Molecular recognition is an important subject, since it helps in selective detection of small biologically important molecules as well as environmentally hazardous components such as free ions.[43] Thus, variety of synthetic receptors have been designed for the selective detection of free ions.[44] As inorganic fluorides are used in treatment of diseases,[45-48] while its high concentration in drinking water is dangerous for human health.[49-51] Thus, there is a definite need for reagents that can be used for detection and estimation of fluoride ions.[52-55] Fluoride ions have ability to deprotonate hydroxy group[56-60] and such property may be compared with basic metal salts. For this property of fluoride ion, many sensors containing hydroxyl group[61] are used for selective detection of fluoride ions as deprotonation of hydroxyl group induces a change in optical signals. Moreover the compounds containing oxime moiety can also act as a selective sensor for fluoride ions. For example fluoride sensor containing oxime moiety attached to a pyrene ring can visually detect fluoride ions.[62-63] Recently, in our group compounds containing both oxime moiety as well as phenol group were used as sensor for fluoride ions.[64] It was observed that these compounds visually detect fluoride ions by formation of cocrystal or salts with the fluoride ions.

As mentioned above that **3.1** has possibility to adopt keto or enol form; it has the possibility of having phenolic group or oxime moiety where both can be good sensor for fluoride ions.

Thus, we have observed that on addition of a solution of TBAF to a solution of **3.1** in dimethysulphoxide causes a drastic color change by turning the solution to green. Colour change was caused specifically by TBAF among the other salts namely tetrabutylammonium chloride, bromide, iodide, perchlorate, nitrate or bisulphate. This enabled visual detection of fluoride ions and distinguishing them from other analogous salts. On addition of TBAF to a solution of **3.1** increased the absorption at 437 nm and a new absorption peak at 640 nm was developed (Figure 3.17a and 3.17b).

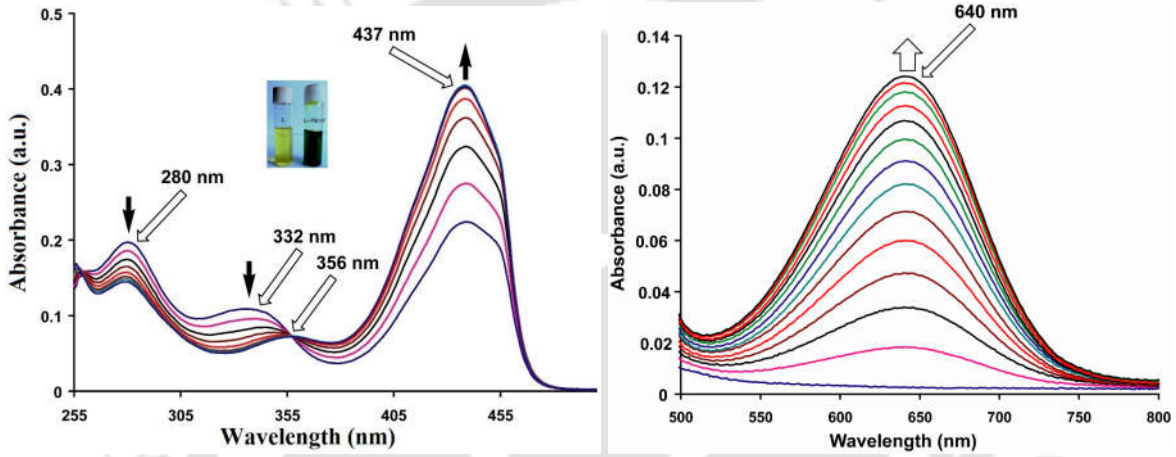

(a) (b)

Figure 3.17: (a) Changes in UV-visible spectra of compound **3.1** (10^{-5} M in DMSO) on addition of TBAF (0.1 to 1 equivalent from TBAF 10^{-4} M stock solution) in 250-500 nm region (inset is photographs of solutions of **3.1** in the absence and presence of TBAF) and (b) changes in absorption in 500-800 nm region of **3.1** (10^{-4} M in DMSO) on addition of TBAF (10^{-3} M in DMSO).

This change in absorption passed through an isobestic point at 356 nm. Formation of an isobestic point showed one to one transformation between two species in solution. From such change in absorbance intensity of new absorption maxima, fluoride ions could be detected over a concentration range spreading from 10^{-2} to 10^{-7} M of stock solutions of TBAF. Zirconium oxyquinolate based analytes[65-66] detect fluoride ions in the concentration range 10^{-4} to 10^{-7} M. On the other hand, acetate ions generally interferes in detection of fluoride ions,[67-68] in our case also we found interference of ammonium acetate in fluoride detection. Since acetate ions and

fluoride ions had similar effects on visible spectra of **3.1**, it may be suggested that change in color of **3.1** occurred from deprotonated species or through proton transfer to form ion-pairs in host-guest complex.

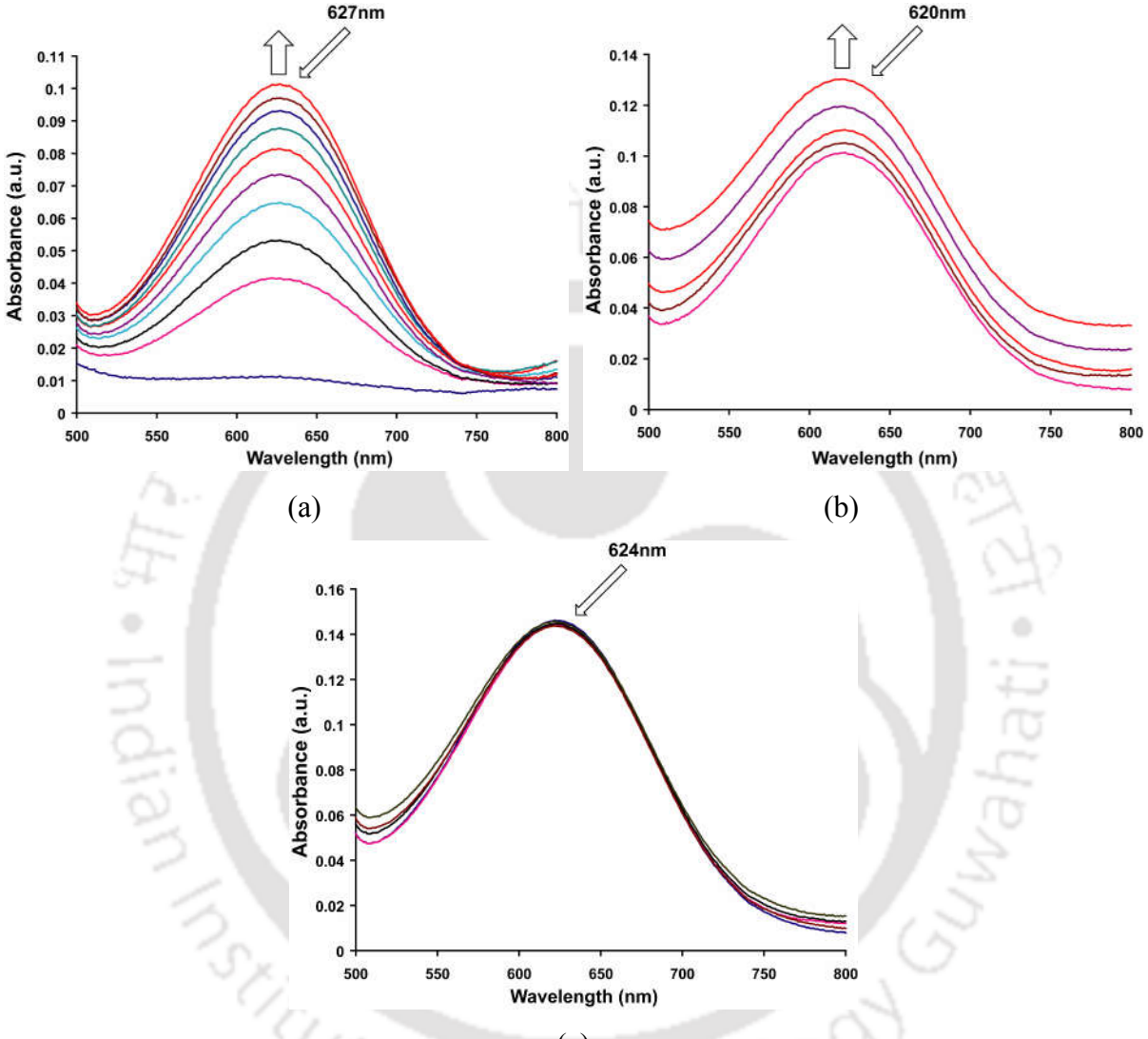

Figure 3.18: Visible absorption spectra of **3.1** (10^{-4} M in DMSO) on addition of 30 μL of TBAF (10^{-3} M in DMSO) at pH condition (a) 4.0, (b) 7.0 and (c) 9.2.

When we carried out similar titration study at different pH such as 4.0, 7.0 and 9.2, it was observed that on addition of TBAF to the solution of compound **3.1** at pH 4.0, new absorption peak appears at 627 nm (Figure 3.18a). Appearance of this absorbance in visible region enables **3.1** to detect fluoride ions barely with naked eye. In case of neutral pH absorbance at 620 nm get intensify on addition of TBAF (Figure 3.18b). However, compound **3.1** showed dark green

(absorbance at 624 nm) color in basic medium (pH = 9.2) disabling detection of fluoride ions, as the absorbance does not show any changes on addition of TBAF (Figure 3.18c). Thus, detection of fluoride ions by a solution of **3.1** was possible under near-neutral pH but not in basic medium.

To understand this phenomenon, ^{1}H-NMR study was carried out by analyzing signals of compound **3.1** that appear in region 6-14 ppm. We compared ^{1}H-NMR spectra of **3.1** titrated with different amounts of TBAF. Comparisons of ^{1}H-NMR signals in this region from different ratios of **3.1** and TBAF are shown in Figure 3.19a. Signals appearing in aliphatic region (1-3 ppm) from -CH_2- and -CH_3 groups of tetrabutylammonium cations in each case was checked, these signals did not change with different compositions. Signal of OH at 13.4 ppm disappeared on addition of TBAF, which suggested a possible deprotonation by fluoride ions or formation of host-guest complex of **3.1** with TBAF.

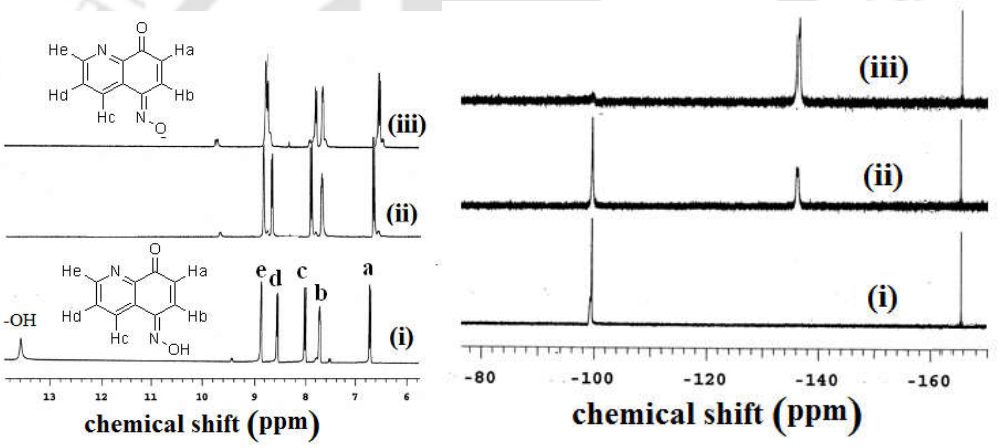

(a) (b)

Figure 3.19: (a) ^{1}H-NMR spectra in the region of 6 ppm to14 ppm obtained during titration of **3.1** (DMSO-d_6) with TBAF: (i) **3.1**, (ii) **3.1** with 0.25 equivalent of TBAF and (iii) **3.1** with 0.5 equivalent of TBAF. (b) ^{19}F-NMR spectra in the region of -80 ppm to -160 ppm of a solution of (i) TBAF (DMSO-d_6) and (ii-v) TBAF on adding different amounts of **3.1** (reference C_6F_6 at -164.9 ppm).

With increase in concentration of TBAF, proton signals Ha and Hb overlapped, which indicated its transformation of **3.1** to keto-form to form a host-guest complex [Figure 3.19a(ii)]. Ion-pair involving fluoride ions with phenols[55] were reported earlier in literature. Oximes are also known to form host-guest complexes with tetrabutyl ammonium fluoride.[62-63] ^{1}H-NMR titration carried

out by addition of triethylamine to a solution of **3.1**, showed similar disappearance OH signal at 13.4 ppm due to deprotonation of **3.1** by triethylamine. Addition of triethylamine or a base to a solution of **3.1** caused a similar color change as that of fluoride ions, thus there is resemblance between these two processes, yet fluoride ions being weak base capable of forming host-guest complex with **3.1** (vide crystallography). It is suggested to form ion pair through proton transfer to yield conjugated species equivalent to the one caused by simple deprotonation by acetate.

The ^{19}F-NMR spectra of TBAF had a signal at -98.1 ppm, this signal disappeared on addition of **3.1** with emergence of a new peak at -134.6 ppm, this indicated that fluoride ions interacted with **3.1** (Figure 3.19b). New peak appearing at -134.6 ppm was broadened on increased in concentrations of **3.1**; this could be due to fast exchange of fluoride ions between keto-enol forms. Chemical shift of hydrofluoric acid is generally dependent on solvents.[69] Thus, ^{19}F signal at -134.6 is attributed to ionic fluoride ions.

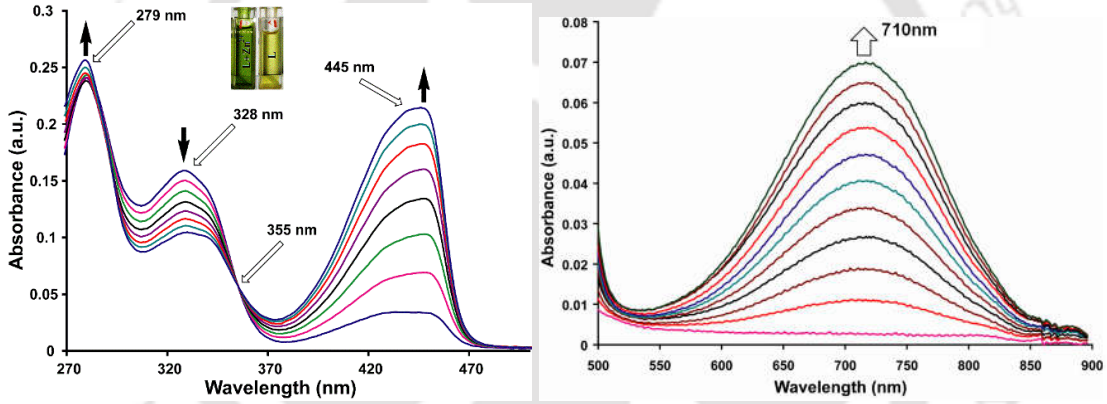

(a) (b)

Figure 3.20 (a) Changes in the UV-visible absorption spectra of **3.1** (10^{-5} M in methanol) on addition of Zn^{2+} ions in 0.1 to 0.7 equivalent (10^{-4} M in methanol). Inset is the photographs of a methanol solution of **3.1** in absence and presence of Zn^{2+} ions. (b) Increase in absorbance at 710 nm on addition of zinc chloride (10^{-3} M in methanol, 10 µL in each aliquot) to a solution of **3.1** (10^{-4} M in methanol) in the region of 500-900 nm.

When a solution of zinc chloride was added to a solution of **3.1** in methanol, the absorbance of peaks at 445 nm and 279 nm of **3.1** were increased with an appearance of new absorbance in visible region with absorbance at 710 nm, while the absorbance peak at 328 nm decreases. These changes pass through an isobestic point at 355 nm (Figure 3.20a). However, other metal chloride salts such as Mn^{2+}, Cd^{2+}, Fe^{2+}, Cu^{2+}, Ni^{2+}, Al^{3+} etc. cause insignificant changes in the visible

spectra of **3.1** compared to zinc chloride. Job's plot from absorption versus mole fraction of zinc ions and **3.1** shows formation of a zinc complex approximately in 1:2 metals to ligand ratio.

3.3: Complexation of 3.1 with zinc ions

Accordingly, crystalline 1:2 complex namely di-aqua-*bis*(5-nitroso-8-oxyquinolinato)zinc (II) **3.10** was obtained from reaction of **3.1** with zinc chloride was characterized by determining crystal structure (Figure 3.21a). On checking the morphology of zinc complex **3.10** a clear difference in color was observed from the parent compound **3.1**.

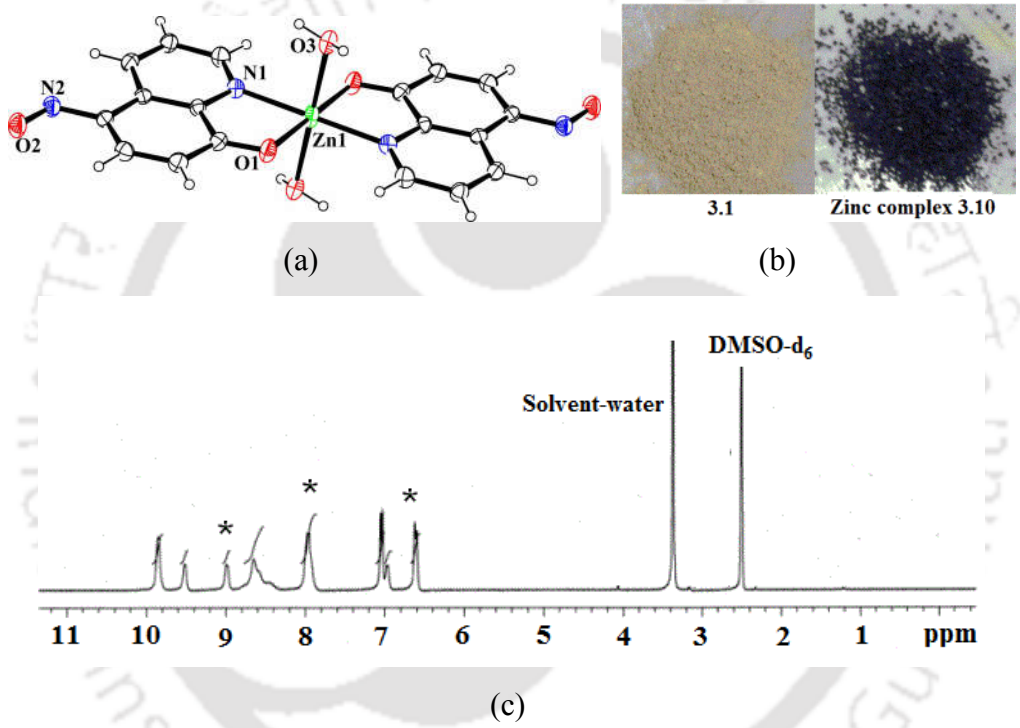

Figure 3.21: (a) Structure of di-aqua-bis(5-nitroso-8-oxyquinolinato)zinc (II) **3.10**, (ORTEP drawn with 30 % thermal ellipsoid), (b) optical micrograph **3.1** and zinc complex **3.10** (c) ^{1}H-NMR spectra of zinc complex **3.10**. Selected bond distances, Zn1-N1, 2.075(3) Å; Zn1-O1, 2.105(2) Å; Zn1-O3, 2.207(3) Å and bond angles, N1-Zn1-O1, 100.07(9)°; N1-Zn1-O3, 89.71(10)°.

As from the Figure 3.21b it can be seen that the compound **3.1** is pale yellow whereas, the zinc complex **3.10** is black in color which enables to distinguish them in the their solid state. Complex has a distorted octahedral geometry with two apical positions occupied by two aqua ligands. Irrespective of metal to ligand ratio used in the reaction this zinc complex could be obtained,

however this complex **3.10** on redissolution in DMSO solution dissociates to give double the number of peaks of parent ligand in ^{1}H-NMR spectra (Figure 3.21c).

Both the fluoride anion and Zn^{2+} ion could change the UV-visible spectra of solution of compound **3.1**. So, we carried out competitive experiments between the fluoride and zinc ions. When zinc chloride was added to a solution containing **3.1** and fluoride ions, the absorbance peak at 640 nm shifted to 710 nm with small decrease in intensity of the absorption (Figure 3.22a). This can be attributed to the formation of zinc-5-nitroso-8-oxyquinolinato complex; which absorbs at 710 nm, with the decomposition of host-guest complex formed between the **3.1** and TBAF.

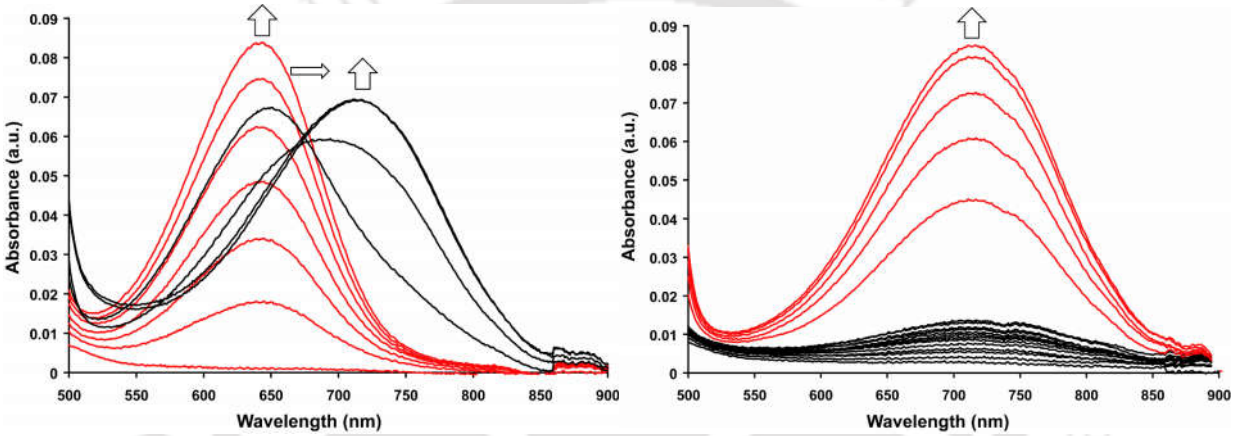

(a) (b)

Figure 3.22: (a) Changes in the visible absorbance of **3.1** (10^{-4} M in DMSO) at 640 nm on addition of solution of TBAF (10^{-3} M in DMSO) (red); the black lines show the shifting to 710 nm on addition of $ZnCl_2$ (10^{-3} M in DMSO) 10 µL in each aliquot. (b) Increase in absorbance of **3.1** (10^{-4} M in DMSO) on addition of $ZnCl_2$ solution at 710 nm (black) redlines shows increase in absorbance on further addition of TBAF (10^{-3} M in DMSO) solution (10 µL in each aliquot).

However, when TBAF was added to a solution of **3.1** containing Zn^{2+} ions the absorbance at 710 nm get intensified rather than shifting towards the lower wavelength (Figure 3.21b). In this case it can be thought as fluoride ions increase the basicity of the solutions containing **3.1** and Zn^{2+} ions which facilitates deprotonation of more **3.1** and as result the concentration of zinc-5-nitroso-8-oxyquinolinato complex increases, which increases the absorbance at 710 nm.

As we have seen in absorption study the spectra of **3.1** changes in similar pattern on addition of zinc ions or fluoride ions. In order to distinguish the sensing of these two ions, we carried

fluorescence titration of solution of **3.1** with different ions. A solution of **3.1** shows a fluorescence emission peak at 556 nm on excitation at 475 nm, which on addition of fluoride ions get quenched (Figure 3.23a). Similar titrations were also carried for other anions, such as tetrabutylammonium salts of chloride, bromide, iodide, perchlorate, nitrate or bisulphate. However, no such significant changes in the emission spectra of **3.1** were observed. This shows the selectivity of **3.1** towards the fluoride ion over the other anions studied. The fluorescence quenching is due to internal charge transfer between fluoride and the ligand, which is commonly caused by fluoride ions.[70] Binding constant of fluoride ion with **3.1** is calculated as 2.66×10^5 M^{-1} by Benesi–Hildebrand equation from the changes in intensity of emission caused by TBAF.

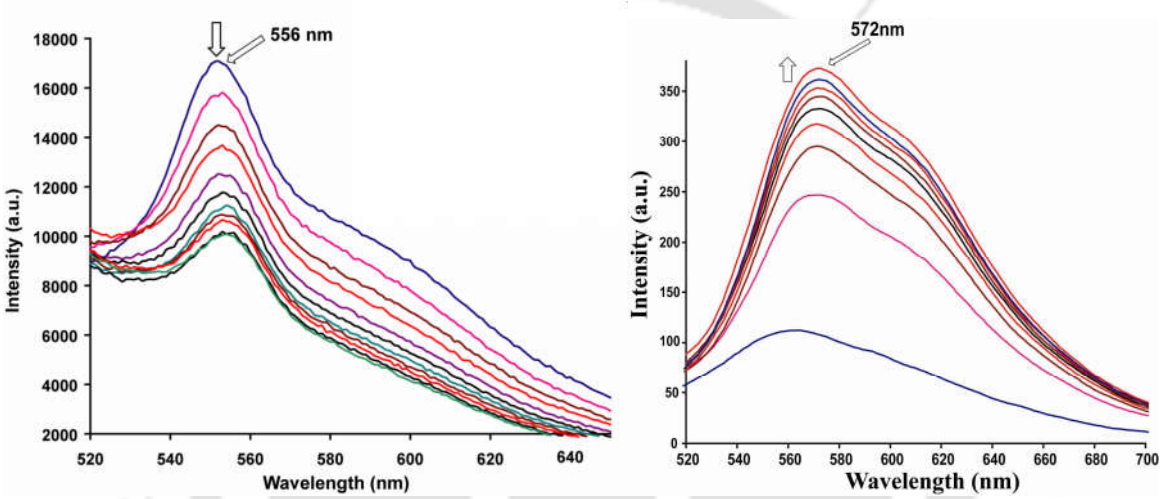

(a) (b)

Figure 3.23: (a) Fluorescence emission (λ_{ex} = 475 nm) of compound **3.1** (10^{-4} M in DMSO) on addition of TBAF in 10 µL (10^{-3} M in DMSO). (b) Change in fluorescence emission of **3.1** (λ_{ex} =475 nm; 10^{-4} M in methanol) on addition of zinc chloride (in 10 µL from 10^{-3} M in methanol in each aliquot).

On the other hand, methanolic solution of compound **3.1** showed a fluorescence emission peak at 572 nm on excitation at 475 nm. Intensity of this emission peak was enhanced and shifted by 12 nm on addition of Zn^{2+} ions (Figure 3.23b). Opposite trends in changes of fluorescence emission by fluoride and zinc ions enabled to distinguish these ions in independent experiments. Fluorescence titrations of **3.1** with different metal ions in methanol showed increase in fluorescence emission by cadmium (II) or aluminium (III) ions. Whereas, addition of solutions of paramagnetic ions such as Mn^{2+}, Fe^{2+}, Co^{2+}, Ni^{2+} and Cu^{2+}ions decreases the fluorescence

intensity. Similar fluorescence titrations performed with Na^{+}, K^{+}, Be^{2+}, Mg^{2+}, Ca^{2+} and In^{+3} ions showed no significant changes in the emission spectra of **3.1**. Binding constants of **3.1** with metal ions were in order of Zn^{2+} >> Cu^{2+} > Co^{2+} > Fe^{2+} > Ni^{2+} > Mn^{2+} > Cd^{2+} > Al^{3+}. Relative binding constants are illustrated as bar diagram shown in Figure 3.24.

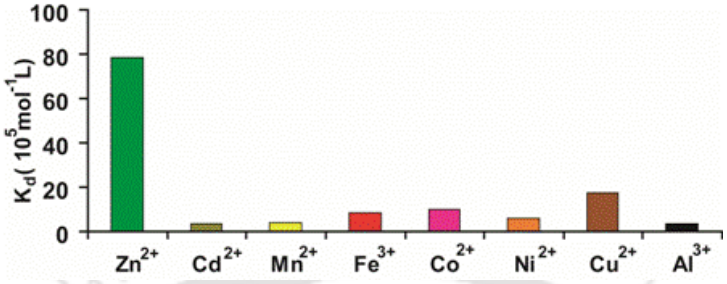

Figure 3.24: Bar graph showing binding constants of **3.1** with different metal ions.

Zinc ion has highest binding constant 7.87 × 10^6 M^{-1} relative to the other metal ions. Among the quenchers, Cu^{2+}ions are most effective and have a binding constant 17.45 × 10^5 M^{-1}. Paramagnetic Cu^{2+}ions generally causes quenching of fluorescence, which can attributed to transfer of energies or electrons from **3.1** to low lying empty d-orbital of Cu^{2+}ions.[71]

Metal complexes of quinoline derivatives are known for their ability to detect fluoride ions. Keeping this in mind we too carried a study to detect different anions by zinc complex **3.10**. Interestingly, it was observed that when a solution of TBAF in DMSO was added to the solution of **3.10** in DMSO, the absorbance at 718 nm shifts to 676 nm with a decrease in absorption. This changes passes through an isobestic point at 660 nm as shown in the Figure 3.25. This happens due to replacement of **3.1** from the metal complex by fluoride ions.

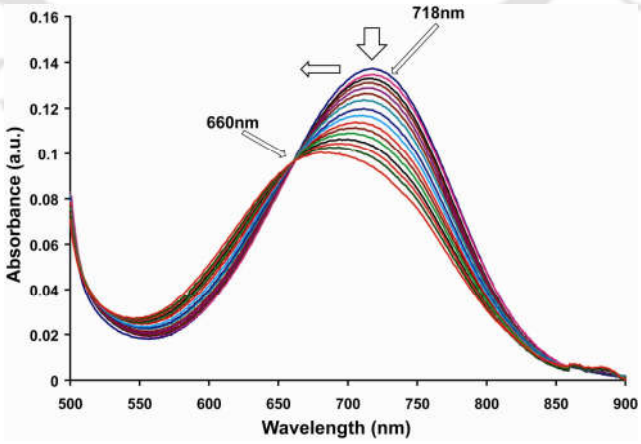

Figure 3.25: Changes in absorbance spectra of zinc complex (10^{-4} M in DMSO) on addition of TBAF (10^{-3} M in DMSO).

As mentioned above, addition of zinc chloride to a solution of **3.1** in presence of TBAF shifs absorption peak at 640 nm to 710 nm and absorption at 710 nm of a solution of **3.1** with zinc chloride increases on addition of TBAF. Thus the zinc complex can be constructed or dislodged by adequate concentration of fluoride ions and **3.1**. Other tetrabutylammonium salt such as chloride, bromide, perchlorate or nitrate does not change visible spectra of the complex **3.10** at this pH. This shows selective nature of zinc complex **3.10** towards the fluoride anions over the other anions.

3.4: Conclusion

It is found that anions are suitably placed to interact with the π-cloud of cations in layered structures of quinolinium salts **3.2-3.8**. Sandwiching of nitrate ions between cations in salts **3.5** and **3.7** are observed, whereas nitrates ions occupy oblique with respect to cation in salt **3.6**. Salt **3.5** show exceptionally shorter anion-π distance compared to the conventional distances. These salts remain as strong ion pair in solution. Thus, anion-π interactions are too weak to show a distinction in binding constants due to large electrostatic interactions contributing to the salts in solutions.

Moreover, host-guest of **3.1**with fluoride ion and a mononuclear complex of zinc are isolated and characterized. The bond distances of compound **3.1** in the adduct **3.9** confirmed that it remains in its keto form in solid state. Fluoride ions could be visually distinguished from numbers of anions at slightly acidic pH. Fluoride as well as acetate ions quench fluorescence emission of **3.1** which distinguishes them from other common neutral anions. Several cations can enhance intensity of fluorescence emission of **3.1** independently but zinc ions are special to show sharp enhancement of fluorescence intensity. Several metal ions bring about quenching of fluorescence which enables zinc ions to be distinguished from other cations. The difference in color of host-guest complex **3.9** and zinc complex **3.10** from the parent compound **3.1** enables fluoride ions and zinc ions to detect in solid state.

3.5: Experimental

The detailed synthetic methodologies for synthesis of the metal complexes are described. Analytical data are provided with each complex. The instrumental details and crystallographic parameters are provided in Appendix.

Synthesis of 3.1:

8-hydroxyquinoline (0.725 g, 5 mmol) was added to a solution of conc. sulphuric acid (0.3 mL) in distilled water (20 mL) with vigorous stirring at 15-18 ^{0}C. A solution of sodium nitrite (0.367 g) in water (10mL) was added dropwise over 30-40 minute at a reaction temperature of 18-20 ^{0}C. The mixture obtained was held at this temperature for 3h. The reaction product was neutralized at temperature not exceeding 25 ^{0}C with 24% solution of sodium hydroxide to pH 8-9 and then acidified to pH 5-6 with glacial acetic acid. The precipitate was filtered off, washed with distilled water (3 X 50 mL), then dried and recrystallised from 1:1 acetone-DMF solvent mixture. IR (KBr, cm^{-1}): 3436 (w), 3056 (w), 2933 (w), 2814 (w), 2702 (m), 1656 (s), 1601 (w), 1581 (w), 1459 (m), 1388 (w), 1331 (w), 1316 (w), 1131 (m), 1095 (w), 977 (s), 823 (w), 792 (w), 692 (w). ^{1}HNMR (DMSO-d$_6$): 13.4 (s, 1H), 8.87 (t, J = 0.8 Hz, 1H), 8.57 (d, J = 8.4 Hz, 1H), 8.03 (d, J = 10.8 Hz, 1H), 7.74 (q, J = 4.8 Hz, 1H), 6.75 (d, J = 10.4 Hz, 1H).^{13}C-NMR (DMSO-d$_6$): 183.42, 151.57, 145.19, 144.70, 131.85, 131.27, 130.44, 127.41, 125.93.

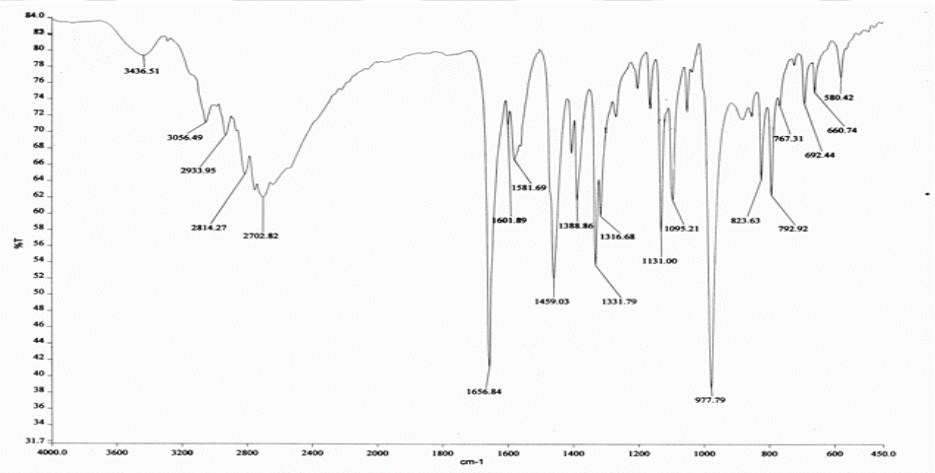

Figure 3.26: FT-IR (KBr, cm^{-1}) spectra of **3.1**.

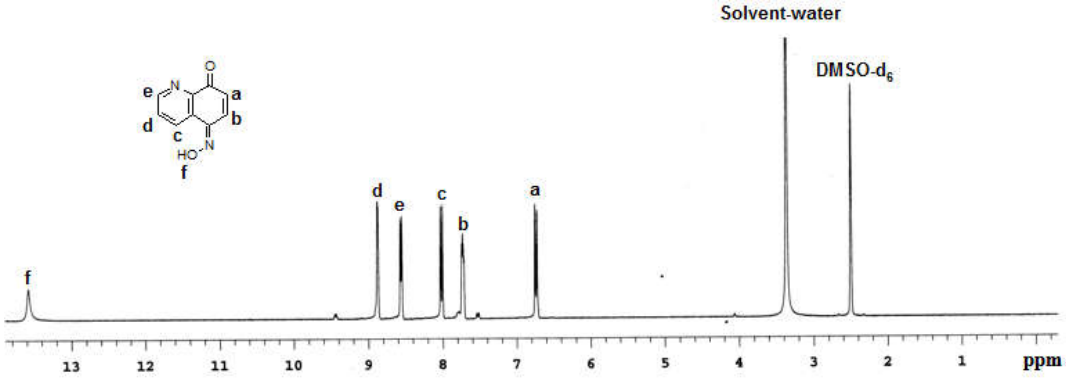

Figure 3.27: ^{1}H-NMR (400 MHz, DMSO-d$_6$) spectra of **3.1**.

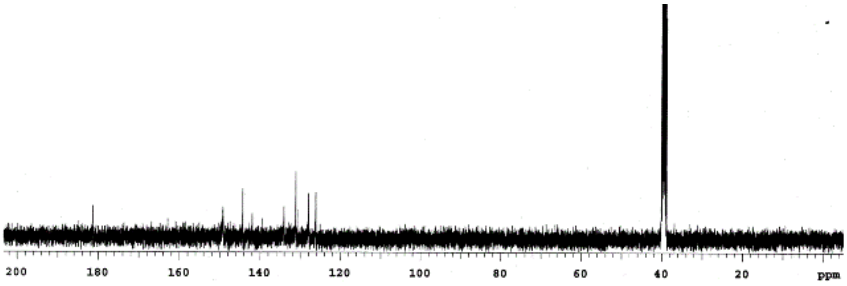

Figure 3.28: ^{13}C-NMR (400 MHz, DMSO-d_6) spectra of **3.1**.

Synthesis of 3.2:

The chloride salt of **3.1** was prepared by reacting **3.1** (0.173 g, 1 mmol) in DMF (15 mL) with 1 mL of HCl. On standing the chloride salt crystallizes. Yield ~ 93%. IR (KBr, cm^{-1}): 3447 (s), 2919(w), 2816 (w), 2746 (w), 1676 (m), 1659 (m), 1618 (m), 1582 (w), 1526 (w), 1326 (w), 1304 (w), 1276 (w), 1102 (w), 1080 (w), 991 (w), 822 (w), 803(w), 667 (w). ^{1}HNMR (DMSO-d_6, 400MHz), 13.79 (s, 1H), 8.90 (q, J = 1.2Hz, 1H), 8.65 (d, J = 8.4Hz, 1H), 8.06 (q, J = 4.4 Hz, 1H), 7.82 (d, J = 10.4 Hz, 1H), 6.79 (d, J = 10.4 Hz, 1H), 3.15 (s,1H).

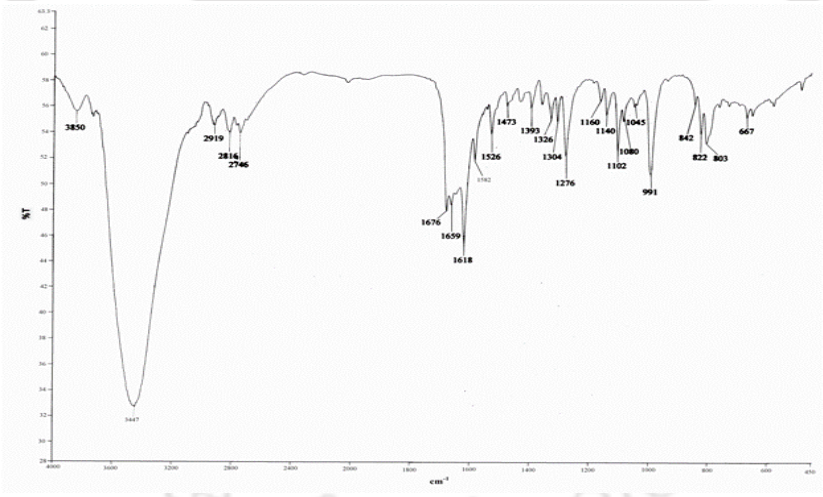

Figure 3.29: FT-IR (KBr, cm^{-1}) spectra of **3.2**.

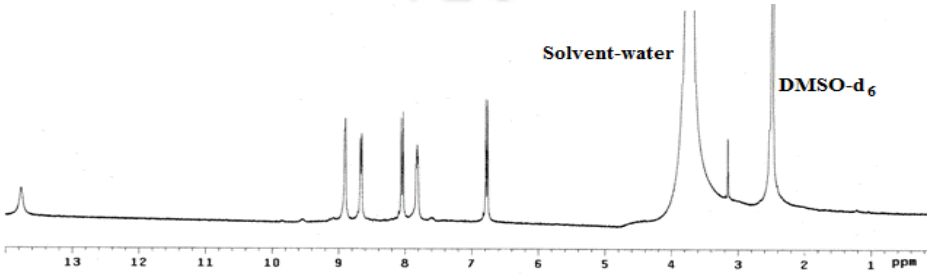

Figure 3.30: ^{1}H-NMR (400 MHz, DMSO-d_6) spectra of **3.2**.

Synthesis of 3.3:

The bromide salt of **3.1** was prepared by reacting **3.1** (0.173 g, 1 mmol) in DMF (15 mL) with 1mL of hydrobromic acid. On standing the bromide salt crystallizes. Yield ~ 90%. IR (KBr, cm^{-1}): 3437 (s), 2920 (w), 2825 (w), 1676 (m), 1638 (m), 1617 (m), 1582 (w), 1526 (w), 1324 (w), 1304 (w), 1276 (w), 1101 (w), 991 (w), 820 (w), 804 (w), 786 (w), 665 (w). ^{1}HNMR (DMSO-d_6, 400MHz), 13.75 (s, 1H), 8.94 (q, J = 1.6Hz, 1H), 8.79 (d, J =8.4Hz, 1H), 8.09 (q, J = 4.8 Hz, 1H), 7.92 (d, J = 10.4 Hz, 1H), 6.84 (d, J = 10.4 Hz, 1H), 3.12 (s,1H).

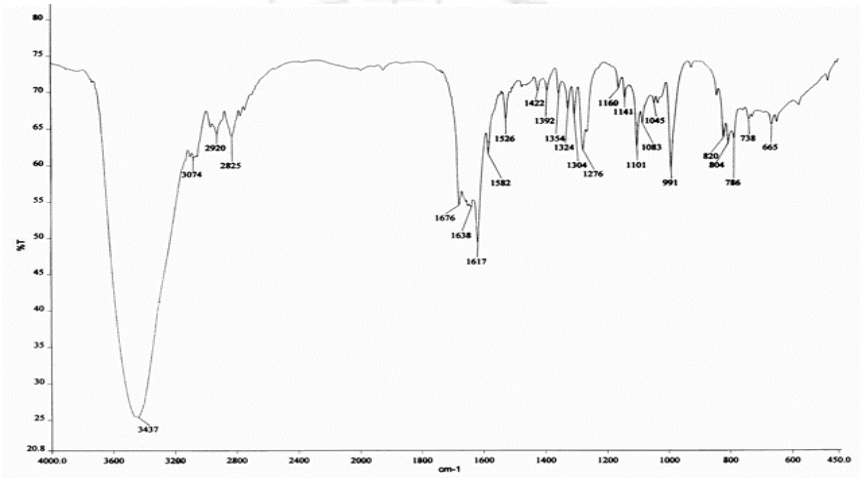

Figure 3.31: FT-IR (KBr, cm^{-1}) spectra of **3.3**.

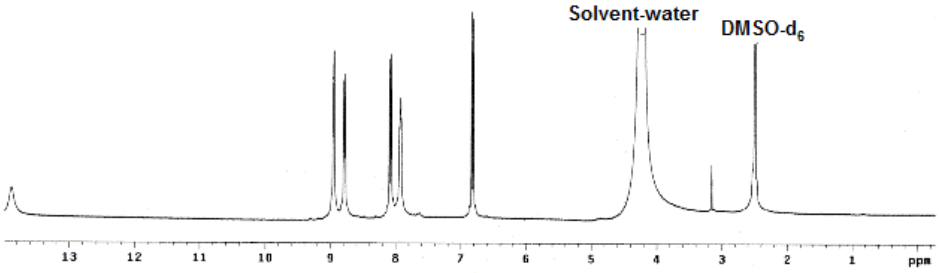

Figure 3.32: ^{1}H-NMR (400 MHz, DMSO-d_6) spectra of **3.3**.

Synthesis of 3.4:

The perchlorate salts of **3.1** was prepared by reacting **3.1** (0.173 g, 1 mmol) in DMF (15 mL) with 1 mL of perchloric acid. On standing the nitrate salt crystallizes. Yield ~ 84%. IR (KBr, cm^{-1}): 3447 (w), 3050 (m), 2921 (m), 2831(m), 2773 (w), 1678 (m), 1617 (m), 1582 (w), 1526 (w), 1423 (w), 1393 (w), 1355 (w), 1325 (w), 1304 (w), 1277 (m), 1142 (s), 1115 (s), 1102 (s), 1089 (s), 1046 (w), 991 (s), 820 (w), 805(w), 785 (w), 665 (w), 648 (w), 636 (w), 626 (w). ^{1}HNMR

(DMSO-d_6, 400MHz),13.75 (s, 1H), 8.87(q, *J* = 1.6Hz, 1H), 8.62 (d, *J* =8.4Hz, 1H), 8.02 (q, *J* = 4.8 Hz, 1H), 7.78 (d, *J* = 10.4 Hz, 1H), 6.76 (d, *J* = 10.4 Hz, 1H), 3.12 (s,1H).

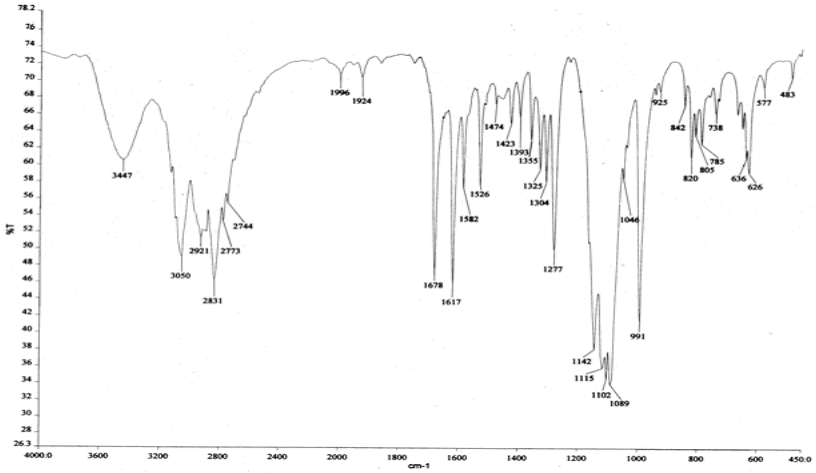

Figure 3.33: FT-IR (KBr, cm^{-1}) spectra of **3.4**.

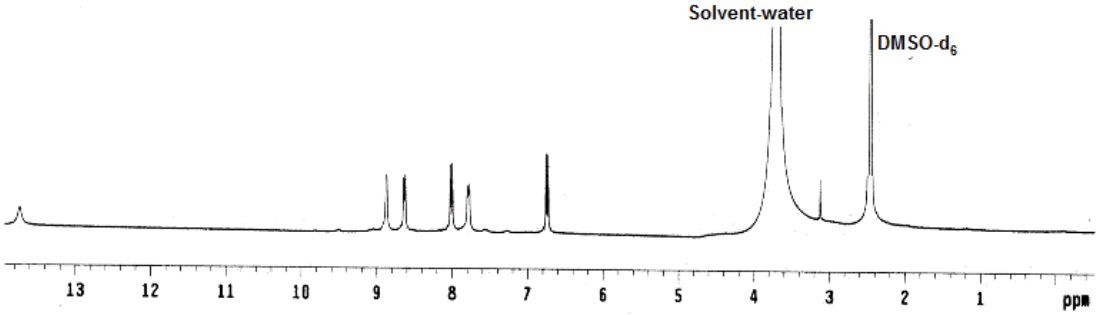

Figure 3.34: ^{1}H-NMR (400 MHz, DMSO-d_6) spectra of **3.4**.

Synthesis of 3.5:

The nitrate salt of **3.1** was prepared by reacting **3.1** (0.173 g, 1 mmol) in DMF (15 mL) with 1 mL of nitric acid. On standing the nitrate salt crystallizes. Yield ~ 86%. IR (KBr, cm^{-1}): 3445 (m), 3050 (m), 2923 (w), 2832 (m), 2772 (w), 1677(m), 1661 (m), 1617 (m), 1582 (w), 1526 (w), 1384 (s), 1356 (w), 1325 (w), 1304 (w), 1277 (w), 1101 (w), 1084 (w), 992 (m), 820 (w), 805(w), 785 (w), 665 (w). ^{1}HNMR (DMSO-d_6, 400MHz), 13.75 (s, 1H), 9.18 (q, *J* =1.6Hz, 1H), 9.03 (d, *J* = 8.4Hz, 1H), 8.51 (q, *J* = 4.4 Hz, 1H), 7.90 (d, *J* = 10.4, 1H), 7.21 (d, *J* = 10.4, 1H), 3.12 (s, 1H).

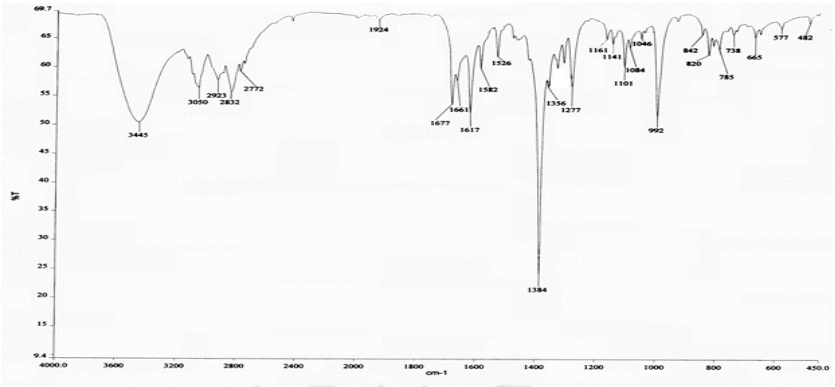

Figure 3.35: FT-IR (KBr, cm^{-1}) spectra of **3.5**.

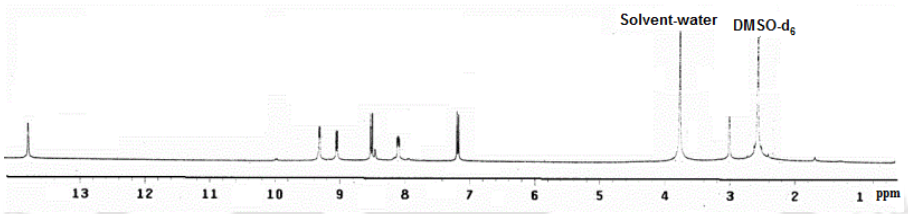

Figure 3.36: ^{1}H-NMR (400 MHz, DMSO-d_6) spectra of **3.5**.

Synthesis of 3.6:

The nitrate salt **3.6** was prepared by reacting 5-aminoquinoline (0.144 g, 1 mmol) in methanol (15 mL) with 1 mL of nitric acid. On standing the nitrate salt crystallizes. Yield: ~ 90%. IR (KBr, cm^{-1}): 3399 (s), 3086 (s), 2924 (s), 1764 (w), 1638 (m), 1590 (s), 1383 (bs), 1223 (m), 1033 (w), 826 (s). ^{1}HNMR (400MHz, DMSO-d_6): 13.10 (s, 1H), 8.76 (m, 1H), 7.87 (m, 1H) 7.25 (m, 3H), 7.05 (m, 1H), 4.62 (s, 2H).

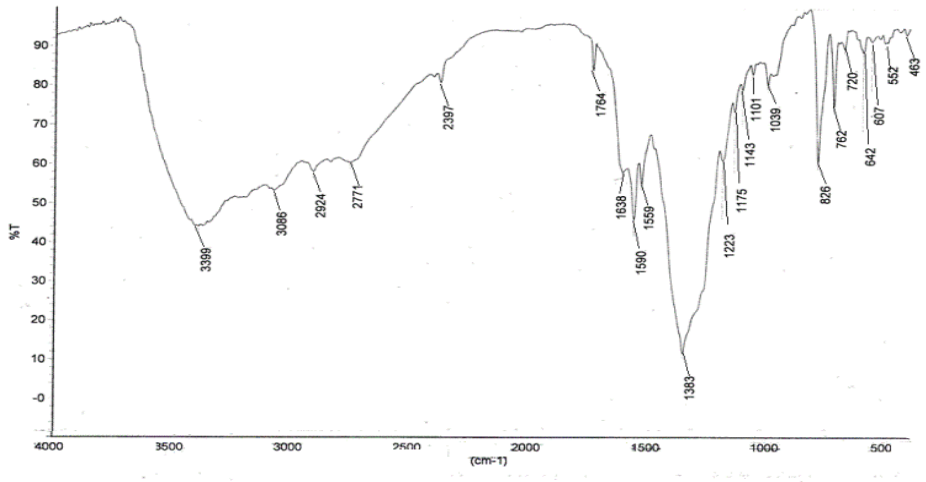

Figure 3.36: FT-IR (KBr, cm^{-1}) spectra of **3.6**.

Synthesis of 3.7:

The nitrate salt **3.7** was prepared by reacting 4-hydroxyquinoxaline (0.146 g, 1 mmol) in methanol (15 mL) with 1 mL of nitric acid. On standing the nitrate salt crystallizes. Yield ~ 96%. IR (KBr, cm^{-1}): 3431 (s), 3016 (s), 2804 (s), 1721 (s), 1652 (m), 1576 (w), 1384 (s), 1291 (w), 1227 (w), 824 9w), 773 (m). ^{1}HNMR (400 MHz, DMSO-d_6): 12.2 (s, 2H), 8.16 (t , J = 8.4 Hz, 2H), 7.81 (t, *J* = 8 Hz, 1H), 7.67 (d, *J* = 8.2 Hz, 1H), 7.50 (t, *J* = 8Hz).

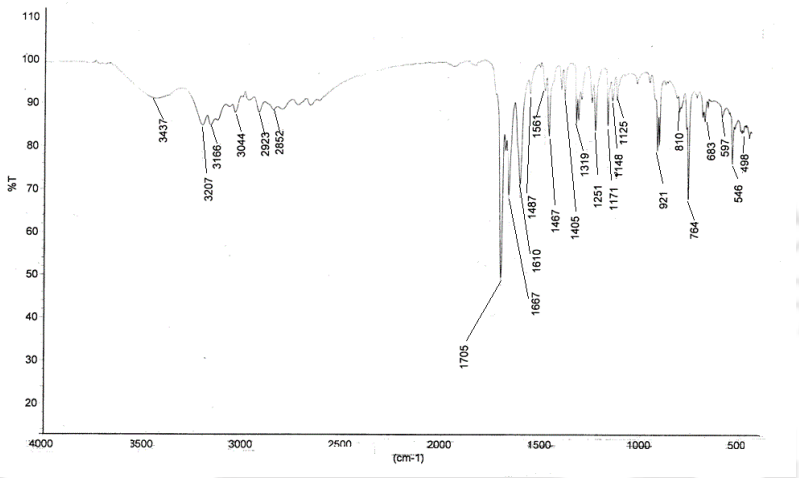

Figure 3.37: FT-IR (KBr, cm^{-1}) spectra of **3.7**.

Synthesis of 3.9:

Host-guest complex of TBAF with **3.1** was prepared by slow evaporation of a solution of TBAF and **3.1** in 1:1 molar ratio in dimethylsulphoxide and blue crystals could be obtained after 3 weeks. Yield ~ 56%. IR (KBr, cm^{-1}): 3442 (w), 1603 (s), 1573 (m), 1529 (s), 1488 (m), 1466 (w), 1380 (w), 1303 (w), 1129 (m), 1277 (s), 1105 (w), 1065 (w), 796 (w), 737 (w). ^{1}H-NMR (DMSO-d^6): 8. 78 (d, *J* = 8.0 Hz, 2H), 7.82 (d, *J* = 8.4 Hz, 1H), 7.67(t, *J* = 4.4 Hz, 1H), 6.55 (d, *J* = 10.4 Hz, 1H), 3.16 (t, *J* = 8.4 Hz, 2H), 1.56 (m, 2H), 1.31 (m, 2H), 0.92 (t, *J* = 7.6 Hz 3H). ^{13}C-NMR (DMSO-d_6): 182.73, 149.74, 146.80, 143.63, 131.55, 130.16, 127.50, 126.22, 122.93, 57.54, 23.05, 19.18, 13.44.

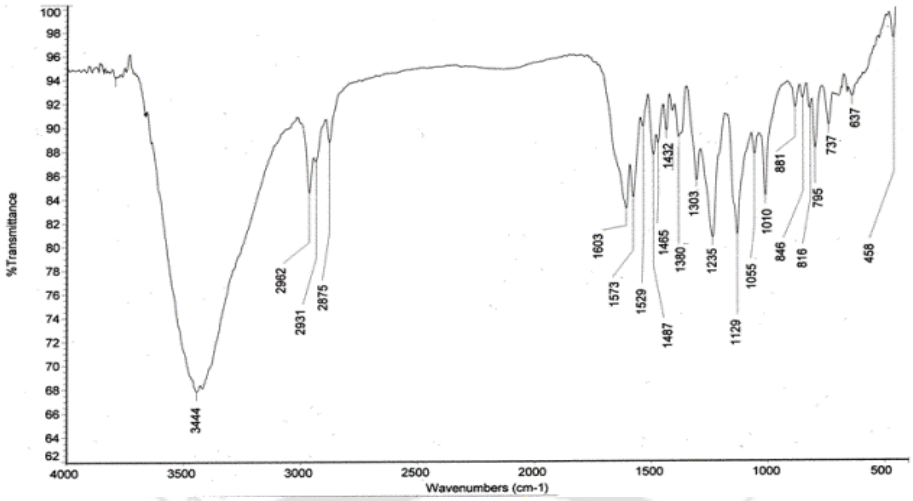

Figure 3.38: FT-IR (KBr, cm^{-1}) spectra of **3.9**.

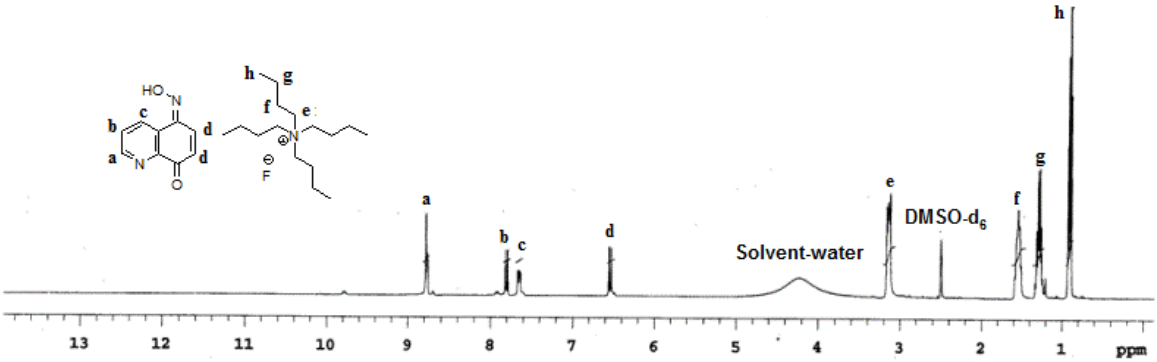

Figure 3.39: ^{1}H-NMR (400 MHz, DMSO-d_6) spectra of **3.9**.

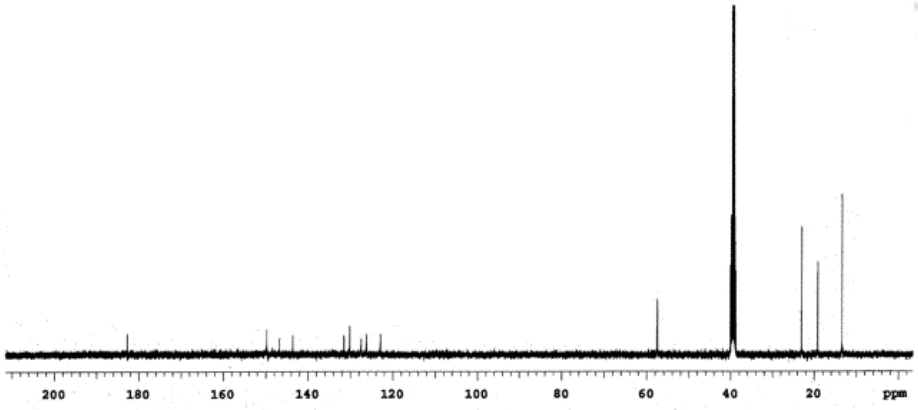

Figure 3.40:^{13}C-NMR (400 MHz, DMSO-d_6) spectra of **3.9**.

Synthesis of 3.10:

To a solution of 5-nitroso-8-hydroxyquinoline (0.348 g, 1mmol) in methanol, anhydrous zinc chloride (0.137 g, 1 mmol) was added and stirred for half an hour. A green precipitate obtained

was filtered and redissloved in dimethylformamide. Solution on standing for one week resukted dark green crystals of the zinc complex. Yield ~ 95 %. IR (KBr, cm^{-1}): 3204 (w), 1605 (s), 1577 (m), 1549 (s), 1529 (s), 1493 (m), 1444(w), 1411(w), 1375 (w), 1357 (w), 1305 (m), 1277 (s), 1244 (s), 1148 (s), 1106 (w) 1065 (w), 1027 (w), 819 (w), 796 (w), 741 (w), 692 (w), 502 (w), 473 (w).

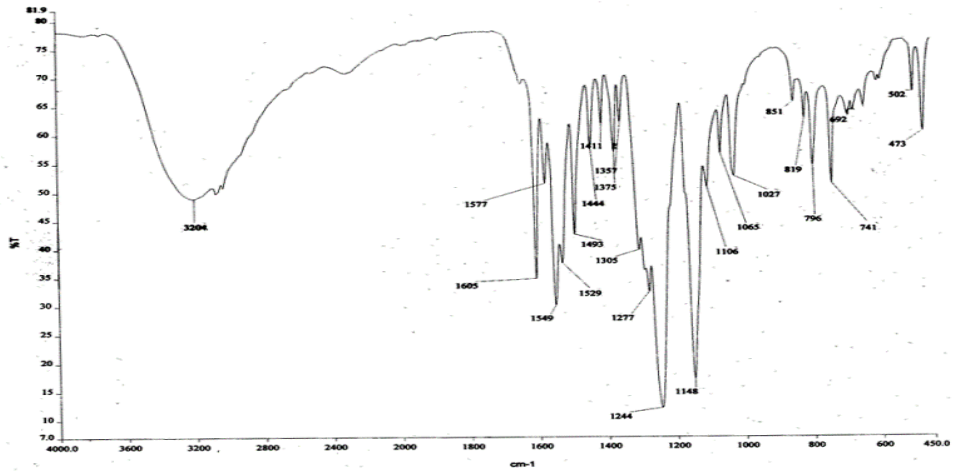

Figure 3.41: FT-IR (KBr, cm^{-1}) spectra of **3.10**.

3.6: Reference

1. L. J. Prins, D. N. Reinhoudt, P. Timmerman, *Angew. Chem. Int. Ed.*, 2001, **40**, 2382.
2. J. M. Rivera, T. Martin, J. Rebek Jr., *Science*, 1998, **279**, 1021.
3. N. Paul, G. F. Joyce, *Curr. Opin. Chem. Biol*., 2004, **8**, 634;
4. J. -M. Lehn, *Proc. Natl. Acad. Sci. USA*, 2002, **99**, 4763.
5. M. Crego-Calama, P. Timmerman, D. N. Reinhoudt, *Angew. Chem. Int. Ed*., 2000, **39**, 755.
6. F. Ortega-Caballero, C. Rousseau, B. Christensen, T. E. Petersen, M. Bols, *J. Am. Chem. Soc*., 2005, **127**, 3238.
7. R. Cacciapaglia, S. Di Stefano, L. Mandolini, *Acc. Chem. Res*., 2004, **37**, 113.
8. V. van Axel Castelli, A. Dalla Court, L. Mandolini, D. N. Reinhoudt, L. Schiaffino, *Chem. Eur. J*., 2000, **6**, 1193.
9. T. W. Bell, N. M. Hext, *Chem. Soc. Rev*., 2004, **33**, 589.
10. C. P. Collier, E. W. Wong, M. Belohradsky, F. M. Raymo, J. F. Stoddart, P. J. Kuekes, R. S. Williams, J. R. Heath, *Science*, 1999, **285**, 391.

11. A.V. Jentzch, D. Emery, J. Mareda, P. Metrangolo, G. Resnati, S. Matile, *Angew. Chem. Int. Ed. Eng*., 2011, **50,** 11657.
12. S. Guha, F. S. Goodson, L. J. Corson, S. Saha, *J. Am. Chem. Soc*., 2012, **134,** 13679.
13. B. M. Hay, *Chem. Soc. Rev*., 2010, **39,** 3700.
14. S. Deeshko, S. Dechert, F. Meyer, *J. Am. Chem. Soc*., 2004, **126,** 4508.
15. B. L. Schottel, H. T. Chifotides, K. R. Dunbar, *Chem. Soc. Rev*., 2008, **37**, 68.
16. R. E. Dawson, A. Hennig, D. P. Weimann, D. Emery, V. Ravikumar, J. Montenegro, T. Takeuchi, S. Gabutti, M. Mayor, J. Mareda, C. A. Schalley, S. Matile, *Nature Chem*., 2010, **2,** 533.
17. J. T. Davis, *Nature Chem*., 2010, **2**, 516.
18. A. S. Singh, S. -S. Sun, *RSC Adv*., 2012, **2,** 9502.
19. X. -P. Bao, L. Wang, L. Wu, Z. -Y. Li, *Supramolecular Chem*., 2008, **20,** 467.
20. P. Mateus, N. Bernier, R. Delgado, *Coord. Chem. Rev*., 2010, **254,** 1726.
21. K. Bowman-James, *Acc. Chem. Res*., 2005, **38,** 671.
22. K. Choi, A. D. Hamilton, *J. Am. Chem. Soc*., 2001, **123,** 2456.
23. S. O. Kang, R. A. Begum, K. Bowman-James, *Angew. Chem., Int. Ed. Eng*., 2006, **45,** 7882.
24. P. A. Gale, *In Encyclopedia of Supramolecular Chemistry J L Atwood and J W Steed (Eds.) (New York: Marcel Dekker)*, 2004.
25. J. L. Sessler, D. -G. Cho, V. Lynch, *J. Am. Chem. Soc*., 2006, **128,** 16518.
26. A. S. Singh, S. -S. Sun, *RSC Adv*., 2012, **2**, 9502.
27. N. Okabe, M. Akita, *Acta Crystallogr*., 1997, **53C**, 1324.
28. A. A. Isaev, I. I. Lomovskii, K. G. Korolev, R. K. Karimov, *Chem. Heterocyclic Compd*., 2005, **41**, 1027.
29. J. K. Nath, J. B. Baruah, *New J. Chem*., 2013, **37,** 1509.
30. A. Frontera, F. Saczewski, M. Gdaniec, E. Dziemidowicz- Borys, A. Kurland, P. M. Deya, D. Quinonero, C. Garau, *Chem. Eur. J*., 2005, **11,** 6560.
31. H. Casellas, C. Massera, F. Buda, P. Gamez, J. Reedjik, *New. J. Chem*., 2006, **30,** 1561.
32. D. -X. Wang, M. -X. Wang, *J. Am. Chem. Soc*., 2013, **135,** 892.
33. M. Albrecht, C. Wessel, M. de Groot, K. Rissanen, A. Luchow, *J. Am. Chem. Soc*., 2008, **130**, 4600.

34. L. Vlaencia, R. Bastda, E. Gracia-Espana, J. V. de Julian-Ortiz, J. M. Llinares, A. Macias, P. P. Lourido, *Cryst. Growth Des*., 2010, **10,** 3418.
35. S. Hazra, B. Sarkar, S. Naiya, M. G. B. Drew, A. Ghosh, *Polyhedron,* 2012, **46,** 8.
36. W. -S. Loh, M. Hemamanlini, H. -K. Fun, *Acta Crystallogr*., 2010, **66E,** o2907.
37. L. Adriaenssens, C. Estarellas, A. V. Jentzsch, M. M. Belmonte, S. Matile, P. Ballester, *J. Am. Chem. Soc*., 2013, **135**, 8324.
38. P. U. Maheswari, B. Modec, A. Pevec, B. Kozlevcar, C. Massera, P. Gamez, J. Reedijk, *Inorg. Chem*., 2006, **45**, 6637.
39. M. Zaccheddu, C. Filippi, F. Buda, *J. Phys. Chem. A*., 2008, **112**, 1627.
40. M. M. Watt, L. N. Zakharov, M. M. Haley, D. W. Johnson, *Angew. Chem. Int. Ed*., 2013, **52**, 10275.
41. D. Quinonero, C. Garau, C Rotger, A. Frontera, P. Ballester, A. Costa, P. M. Deya, *Angew. Chem. Int. Ed*., 2002, **41**, 3389.
42. H. A. Benesi, J. H. Hildebrand, *J. Am. Chem. Soc*., 1949, **71,** 2703.
43. K. H. Lee, H. -Y. Lee, D. H. Lee, J. -I. Honga, *Tetrahedron Lett*., 2001, **42**, 5447.
44. D. H. Lee, K. H. Lee, J. -I. Hong, *Org. Lett*., 2001, **3**, 5.
45. K. L. Kirk, *Biochemistry of the halogens and inorganic halides, Plenum, New York*, 1991, 58.
46. M. Kleerekoper, *Endocrinol. Metab. Clin. North Am*., 1998, **27**, 441.
47. T. Jentsch, *Curr. Opin. Neurobiol*., 1996, **6**, 303.
48. J. A. Varner, K. F. Jensen, W. Horvath, R. L. Isaacson, *Brain Res*., 1998, **784**, 284.
49. S. Yun, H. Ihm, H.G. Kim, C. -W. Lee, B. Indrajit, K. S. Oh, Y. J. Gong, J. W. Lee, J. Yoon, H. C. Lee, K. S. Kim, *J. Org. Chem*., 2003, **68**, 2467.
50. E. B. Bassin, D. Wypij, R. B. Davis, *Cancer Causes Control*, 2006, **17**, 421.
51. S. -X. Wang, Z. -H. Wang, X. -T. Cheng, J. Li, Z. -P. Sang, X. -D. Zhang, L. -L. Han, X. Y. Qiao, Z. -M. Wu, Z. -Q. Wang, *Environ. Health Perspect*., 2006, **115**, 643.
52. F. Hinterholzinger, B. Ruhle, S. Wuttke, K. Karaghiosoff, T. Bein, *Sci. Rep.,* 2013, **3**, 2562.
53. C. Caltagirone, P. A. Gale, *Chem. Soc. Rev*., 2009, **38**, 520.
54. S. Y. Kim, J. I. Hong, *Org. Lett*., 2007, **9**, 3109.
55. R. Hu, J. Feng, D. Hu, S. Wang, S. Li, Y. Li, G. Yang, *Angew. Chem. Int. Ed*., 2010, **49**, 4915.

56. R. Dutzler, E. B. Campbell, M. Cadene, B.T. Chait, R. MacKinnon, *Nature*, 2002, 415, 287.
57. S. Devaraj, D. Saravanakumar, M. Kandaswamy, *Tetrahedron Lett*., 2007, **48**, 3077.
58. V. Luxami, S. Kumar, *Tetrahedron Lett*., 2007, **48**, 3083.
59. D. A. Jose, P. Kar, D. Koly, B. Ganguly, W. Thiel, H. N. Ghosh, A. Das, *Inorg. Chem*., 2007, **46**, 5576.
60. V. Amendola, L. Fabbrizzi, *Chem. Commun*., 2009, 513.
61. Z. Guo, I. Shin, J. Yoon, *Chem. Commun*., 2012, **48**, 5956.
62. C. B. Rosen, D. J. Hansen, K.V. Gothelf, *Org. Biomol. Chem*., 2013, **11**, 7916.
63. B. Taner, O. Alici, P. Deveci, *Supramol. Chem*., 2014, **26**, 119.
64. A. Tarai, J. B. Baruah, *CrystEngComm*., 2015,**17**, 2301.
65. R. S. Sujith, G. N. Rao, C. Janadhana, *Spectrochim. Acta*., 2006, **65A**, 565.
66. T. Balaji, H. Matsunaga, *Anal. Sci*., 2005, **2**, 973.
67. Q. Wang, Y. Xie, Y. Ding, X. Li, W. Zhu, *Chem. Commun*., 2010, **46**, 3669.
68. P. E. Jackson, *Trends Anal. Chem*., 2001, **20**, 320.
69. K. O. Christe, W. W. Wilson, *J. Fluorine Chem*., 1990, **46**, 339.
70. C. Caltagirone, P. A. Gale, *Chem. Soc. Rev*., 2009, **38**, 520.
71. J. Jiang, H. Jiang, X. Tang, L. Yang, W. Dou, W. Liu, R. Fang, W. Liu, *Dalton Trans*., 2011, **40**, 6367.

Chapter 4

Synthesis, characterization and structural study of polymorphs and salts of 4-nitro-N-(quinolin-8-yl)benzamide

McCrone[1] defined polymorphism as the ability of a substance to crystallize in different crystal forms. The physical properties of different polymorphs such as solubility, spectroscopic properties, thermal properties and electrical properties differ. Specially, the solubility and drug activities of polymorphic drugs require special attention to make them effective active pharmaceutical ingredient.[2-7]

From the crystallographic point of view the polymorphism is divided in to two classes: a) Conformational polymorphism[8-9] and b) Packing or orientational polymorphism.[10-11] Conformational polymorphism is associated with molecular flexibility and related to differences in molecular conformation in the crystal phase.[9] Whereas the orientational polymorphism occurs due to the molecules packing in different manners while maintaining the same conformation. Thus, such systems show different crystal structures in which the unit cells have more than one molecule. Number of symmetry independent molecules per unit cell is described by Z′; higher Z′ value provides more avenues to form orientational polymorphs. In the case of the molecules with flexible structure both the conformational and the orientational polymorphism may occur. There are also examples of flexible molecules that are present in the same conformation in different crystal structures.[12-14] Due to obvious reason of conformational rigidity in structurally rigid molecules, only the packing polymorphism is observed. The strong hydrogen bonds such as O-H···O, N-H···O or O-H···N which have energies in the range of 4-15 kcal mol^{-1} are often the main cause to contribute to different packing patterns. But the role of weak interactions ranging from 1-4 kcal mol^{-1} associated with interactions such as C-H···O, C-H···N, and N-H···π interactions are of definite importance contributing to stability of a particular packing patterns.[15-16] From

theoretical point of view polymorphs can be infinite numbers, but only few of them can be isolated or practically feasible.

Polymophism is observed in many quinoline derivatives, for example Kahlau *et al.* reported[17] dimorphism shown by 2-methyl quinoline and 3-methyl quinoline. Thermal analysis on the four polymorphic forms of 2-quinolinecarboxaldehyde[18-19] shows clear melting points for each polymorph. But so far only three polymorphic forms of this compound have been structurally established. Five polymorphs, two solvates and a monohydrate of a quinoline derivative dehydro-aripiprazole, an active metabolite of aripiprazole are reported in literature.[20]

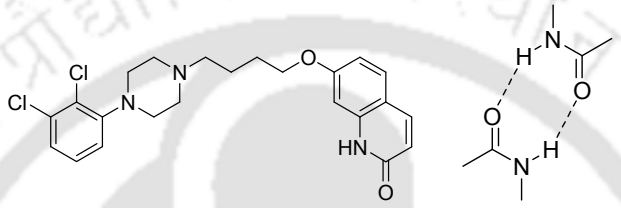

(a) (b)

Scheme 4.1: (a) Dehydro-aripiprazole and (b) homomeric synthons found in the self-assemblies of different polymorphs.

These polymorphs are designated as polymorph **I-V**, arises from different conformationally stabilized in their crystal structures. Among these polymorphic forms, polymorph **V** is thermodynamically stable at ambient temperature whereas the polymorph **I** is the stable form at temperature ≥70 °C, Polymorphs **I**, **II**, **III**, and **IV** have monotropic relationship that means they do not show reversible transformations below their melting points; on the other hand, enantiotropic relationship is referred to reversible solid to solid transformations at a transition temperature.

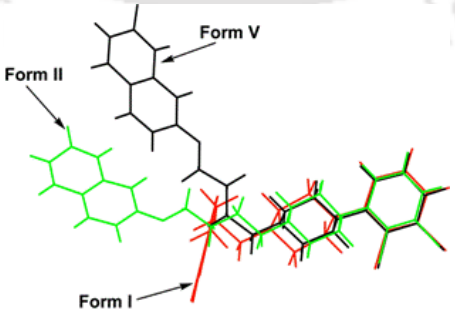

Figure 4.1: Overlay of the structures of the polymorphs **I**, **II** and **V** of Dehydro-aripiprazole illustrating the difference in the conformations.

Enantiotropic relationship is observed among the polymorphs **I** and **V**, as well as between **II** and **V**. In these polymorphs the orientation of the one end differs with respect to the other end kept fixed as illustrated in Figure 4.1.

Crystal structures of the polymorphs **I, II, V** show that the dehydro-aripiprazole molecules form dimeric motifs with N-H···O=C of amides (scheme 4.1). These dimeric units are comprised of different conformers contributing to the packing patterns of the polymorphs. There are also examples of compounds with possibilities of partial bonds rotation to give rise to polymorphs. For instance, 2-(phenylamino)nicotinic acid shows four polymorphs (Figure 4.2a).[21] On the other hand, 2-acetamidobenzamide (Figure 4.2b) shows polymorphs from the partial rotation of the amide bonds.[22] Hence combination of amide bond with quinoline moiety has definite potential to prepare compounds which would throw light on understanding of conformational polymorphism.

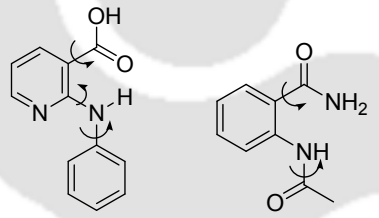

(a) (b)

Figure 4.2: Rotatable bonds in (a) 2-(phenylamino)nicotinic acid and (b) 2-acetamidobenzamide which helps to generate polymorphic forms.

4.1: Polymorphs of 4-nitro-N-(quinolin-8-yl)benzamide (4.1)

To bring about different polymorphic structures from quinoline amide derivatives we examined crystallization of a series of amide derivatives listed in scheme 4.2. Among these compounds our study to crystallize 4-nitro-N-(quinolin-8-yl)benzamide (**4.1**) from different solvents have yielded four different polymorphs. On the other hand, we could not obtain crystals from a solution of 2-nitro-N-(quinolin-8-yl)benzamide (**4.2**), but obtained crystals of only one type (monoclinic, $P2_1$ space group) from 3-nitro-N-(quinolin-8-yl)benzamide (**4.3**). These compounds were prepared by reacting 8-aminoquinoline with 4-nitrobenzoyl chloride for the compound **4.1**, 2-nitrobenzoyl chloride for **4.2** and 3-nitrobenzoyl chloride for compound **4.3** in the presence of triethylamine in tetrahydrofuran. The compounds in each case were characterized by various spectroscopic tools. The compound **4.1** gave four different types of crystals depending on

solvents among which one of the polymorph was reported in literature.[23] Based on the crystals obtained from particular solvent they are named as Polymorph **VI**, Polymorph **VII** Polymorph **VIII** and Polymorph **IX** whose crystal morphologies are shown in Figure 4.3.

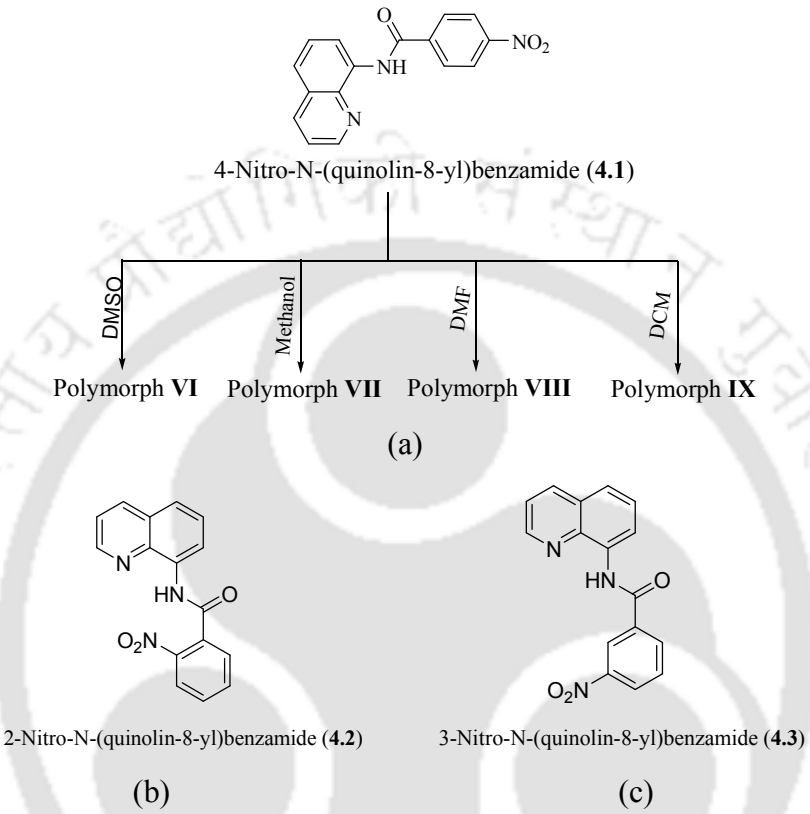

Scheme 4.2: (a) Three forms of the polymorphs of **4.1**, (b) compound **4.2** and (c) compound **4.3**.

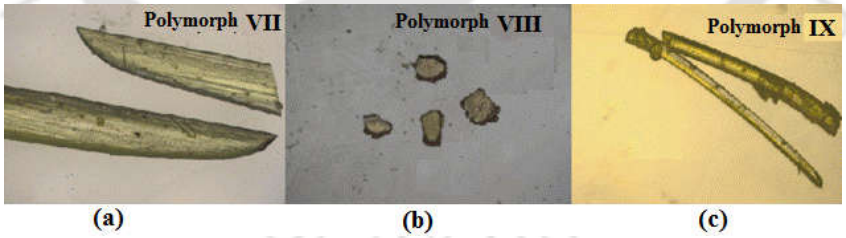

Figure 4.3: The optical micrograph of the crystals of the polymorphs (a) **VII** (b) **VIII** and (c) **IX**.

The crystal structures of all the polymorphic forms are determined. The polymorph (Polymorph **VI**) reported earlier belongs to monoclinic space group $P2_1/c$, which was obtained upon crystallization from dimethylsulphoxide. The crystals of the polymorph **VII** belongs to monoclinic space group $P2_1/c$. In the crystal packing it has a chain like structure with cyclic

$R^2_2(10)$ type[24] hydrogen bond motifs (Figure 4.4a). These $R^2_2(10)$ type hydrogen bond motifs are formed with the aid of the C15-H···O1 and C12-H···O3 interactions (Table 4.1).

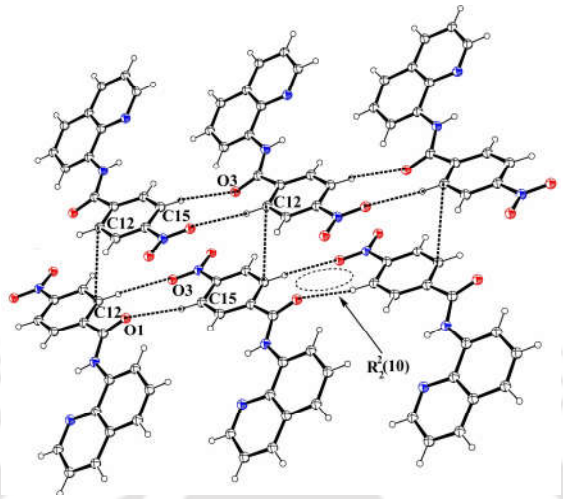

(a)

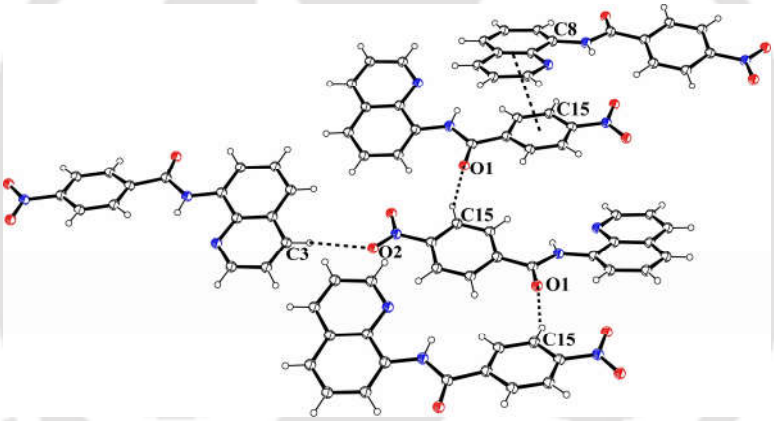

(b)

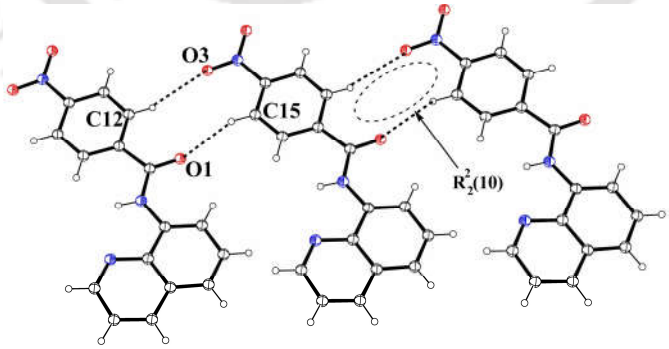

(c)

Figure 4.4: Weak interactions among the molecules in crystal lattices of polymorph (a) **VII**, (b) **VIII** and (c) **IX** (ORTEPs are drawn with 35 % thermal ellipsoids).

In the crystal lattice, the neighboring molecules interact through hydrogen bonds leading to chain like structures. The hydrogen bonded chains are arranged in two layers by π···π interactions[25] between the phenyl rings ($d_{\pi}\ldots_{\pi}$, 3.351 Å). Overall there are two parallel chains, these chains are repeated as units, in the lattice these molecules are arranged slightly offset to each other. The molecules in one of the chains are linked by C-H···O interactions[26] along the a-axis. The molecules present on the other chain are related to the molecules of this chain by 2_1 screw axis. These adjacent double chains are related to each other by inversion symmetry. When viewed along a pair of the interacting chains, the parent molecules appear to be organized in head to head arrangements. However, when the two molecules across the two layers of non-interacting chains are compared, they appear to be organized in head to tail arrangements across the two layers.

The crystals of the polymorph **VIII** belong to monoclinic space group $P2_1/c$. This polymorph in its lattice has molecules that form chain like structures with head to tail arrangements. One of the oxygen atoms of the nitro group involved in C3-H···O2 ($d_{D}\ldots_{A}$, 2.50 Å) interactions; such interactions result in the formation of chain like structure (Figure 4.4b). The carbonyl oxygen atom of amide group is engaged in C15-H···O1 interactions with neighboring molecules (Table 4.1). The phenyl and quinoline rings are nearly parallel to each other and have favorable geometry to have π···π interactions ($d_{\pi}\ldots_{\pi}$, 3.36 Å) as they are in favorable proximity to have such interactions.

Table 4.1: Hydrogen bond parameters of polymorphs **VII**, **VIII** and **IX**.

Compound No.	D-H···A	$d_{D\text{-}H}$(Å)	$d_{H\cdots A}$(Å)	$d_{D\cdots A}$(Å)	∠ D-H···A(º)
Polymorph **VII**	C12-H···O3 [1+x,y,z]	0.93(3)	2.45(2)	3.35(3)	164(2)
	C15-H···O1 [-1+x,y,z]	0.93(3)	2.41(4)	3.29(6)	160(3)
Polymorph **VIII**	C3-H···O2 [-1+x,1/2-y,1/2+z]	0.93(5)	2.50(3)	3.42(6)	171(3)
	C15-H···O1 [2-x,-1/2+y,1/2-z]	0.93(3)	2.40(7)	3.27(3)	158(3)
Polymorph **IX**	C12-H···O3 [-1/2+x,1/2+y,z]	0.93(3)	2.53(4)	3.42(5)	160(2)
	C15-H···O1 [1/2+x,-1/2+y,z]	0.93(3)	2.42(5)	3.29(5)	156(5)

The crystals of the polymorph **IX** belong to monoclinic, *Cc* space group. The packing patterns of the polymorphs **VII** and **IX** are almost identical; both have chain type of arrangements of molecules in respective lattice. The polymorph **IX** has also chain-like structure that can be distinguished from the chains in polymorph **VII** or **VIII**. The chains in **IX** are arranged in such a way that the molecules in the first chain are related by a diagonal translation (related as C-

centering) and the molecules in the second chain are related to the first by a glide-plane. These double chain-like structures are repeated as pairs and neighboring pairs of chains are related by C-centering. Both the polymorphs **VII** and **IX** have C12-H···O3 and C15-H···O1 interactions. Presence of these interactions in the lattice of **VIII** result in the formation of $R^2_2(10)$ motifs. All the aromatic rings positioned on one side of the chain have similar orientation. Thus, a one dimensional chain-like structure extended through $R^2_2(10)$ hydrogen bond motifs (Figure 4.4c) are observed. Interestingly, when we check the morphology of these three polymorphs, three polymorphs have different morphology from each other as shown in Figure 4.3; optical micrograph of these polymorphs.

The compound **4.1** has two planes namely aminoquinoline plane and nitro-phenyl plane which are connected through an amide bond. Thus, there is a probability to change the torsion angle between these two planes by changing conditions of crystallization or by formation of salts (Figure 4.5). As a result we obtained three polymorphs of **4.1** on crystallizing from three different solvent systems, namely polymorph **VII**, polymorph **VIII** and polymorph **IX** from methanol, dimethylformamide (DMF) and dichloromethane (DCM) respectively. Moreover concomitant polymorph of polymorph **VIII** and polymorph **IX** was obtained from a solvent mixture of DMF and *tert*-butanol.

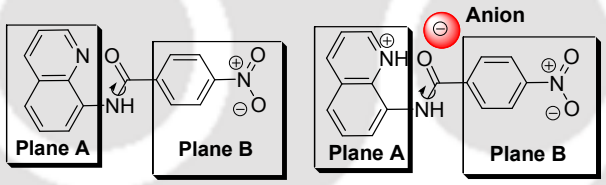

(a) (b)

Figure 4.5: (a) The two aromatic planes in the **4.1** and (b) The salts of **4.1**, showing that the position of an anion can influence the torsion angle of protonated **4.1**.

4.1.1: Differential scanning calorimetry study

Differential scanning calorimetry (DSC) has been used[27-28] to understand thermal behaviors of the different polymorphs. The DSC plots of the polymorphs in the range of 30-200 ºC were recorded for two heating cycles (Figure 4.6). While heating polymorph **VII** showed two endothermic peaks and on cooling it showed one exothermic peak (Figure 4.6a).

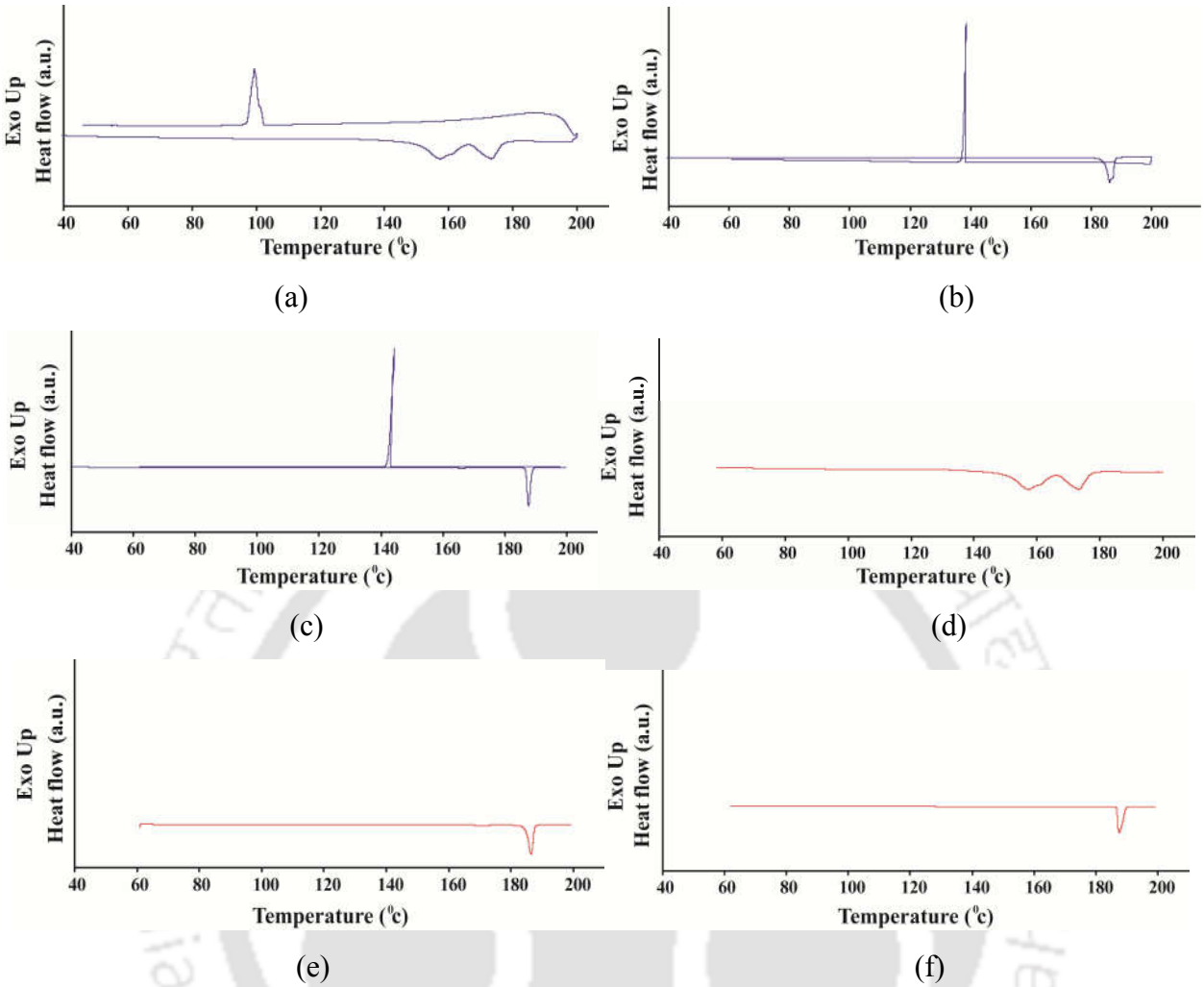

Figure 4.6: DSC plots obtained for heating and cooling at a rate of 3 ºC /min of the polymorph (a) **VII**, (b) **VIII** and (c) **IX**. The DSC plots of second time heating at 3 ºC/min after first cycle of heating and cooling of polymorphs (d) **VII**, (e) **VIII** and (f) **IX**.

The endothermic peak appearing at 157 ºC with the onset temperature of 151 ºC corresponds to melting of the polymorph **VII** and the presence of a second endothermic peak with an onset temperature of 167 ºC and peak at 173 ºC; suggests the polymorph **VII** have liquid crystal like property. Thus, on checking the morphology changes of the polymorph **VII** while heating it under hot stage microscope with a heating rate 3 ºC/min under inert atmosphere, we observed that polymorph **VII** became milky hazy liquid above 157 ºC as shown in Figure 4.7. While cooling, appearance of exothermic peak with onset temperature of 101 ºC and peak at 99 ºC is attributed to the recrystallization of the melt.

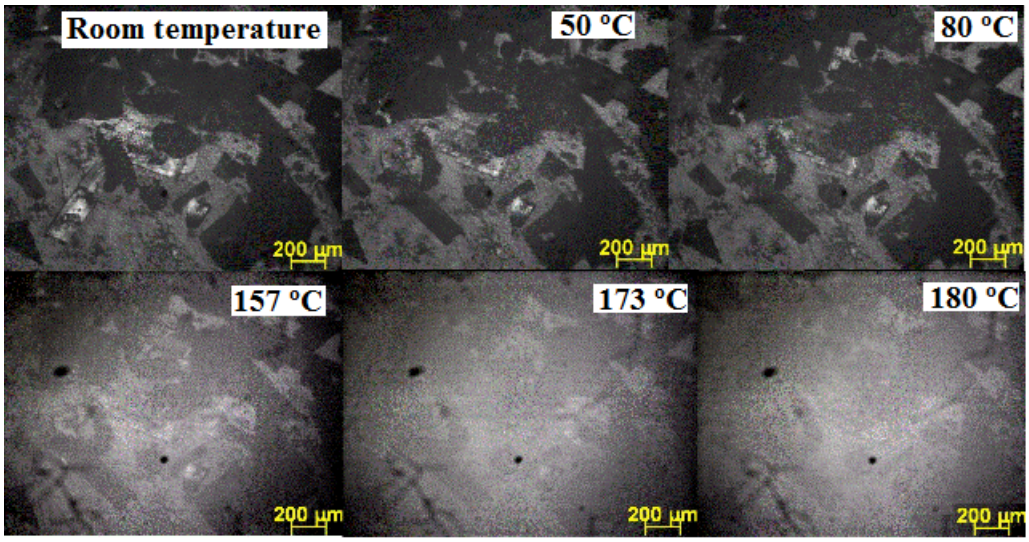

Figure 4.7: The images of crystalline sample of the polymorph **VII** heated at different temperatures.

In the case of the polymorphs **VIII** and **IX,** each show one endothermic peak on heating, corresponding to their respective melting and subsequent cooling gave one exothermic peak of recrystallization in each case. In the DSC plots of the polymorph **VIII**, endothermic peak appeared with onset temperature of 184 ºC and peak at 186 ºC, and the exothermic peak was observed at a temperature 138 ºC as shown in the Figure 4.7b. Similarly, the polymorph **IX** shows an endothermic peak with onset temperature of 186 ºC and peak at 187 ºC. While, cooling it showed an exothermic peak at 144 ºC which is attributed to recrystallization (Figure 4.7c). The enthalpy of melting for polymorph **VII**, polymorph **VIII** and polymorph **IX** are 15.50 J/g, 75.64 J/g and 65.12 J/g respectively. Similar DSC plot to that of the first heating was observed when the samples of polymorphs used for the first cycle of heating were heated for the second time. Endothermic peak corresponding to melting appeared at same temperature on second heating cycle for each polymorph as illustrated in Figure 4.7d-f. It is a general fact that polymorphs of amides interconvert among themselves, which were reflected in their DSC curves.[29] However, in such studies slight differences in the melting temperature of individual polymorphs in each form were observed.[30] In our case, there was no thermal conversion between the polymorphs. Accordingly, the second cycle heating of the polymorphs showed almost identical profiles as that of the first cycles. These show that there were no noticeable changes of structures within the

temperature where DSC were recorded. It could be one of the reasons that polymorph **VII** having suitable alignments of molecules to exhibit liquid crystal like properties shows two endothermic peaks. From crystallography it is already shown that the molecules of polymorph **VII** are arranged in chain like arrangements. The crystal densities of three polymorphs are 1.453 g/cm^3, 1.436 g/cm^3 and 1.477 g/cm^3, which are comparable to each other. From DSC study it was observed that the polymorphs were in monotropic relationships as there is no inter conversion among the polymorphs before their melting temperatures.

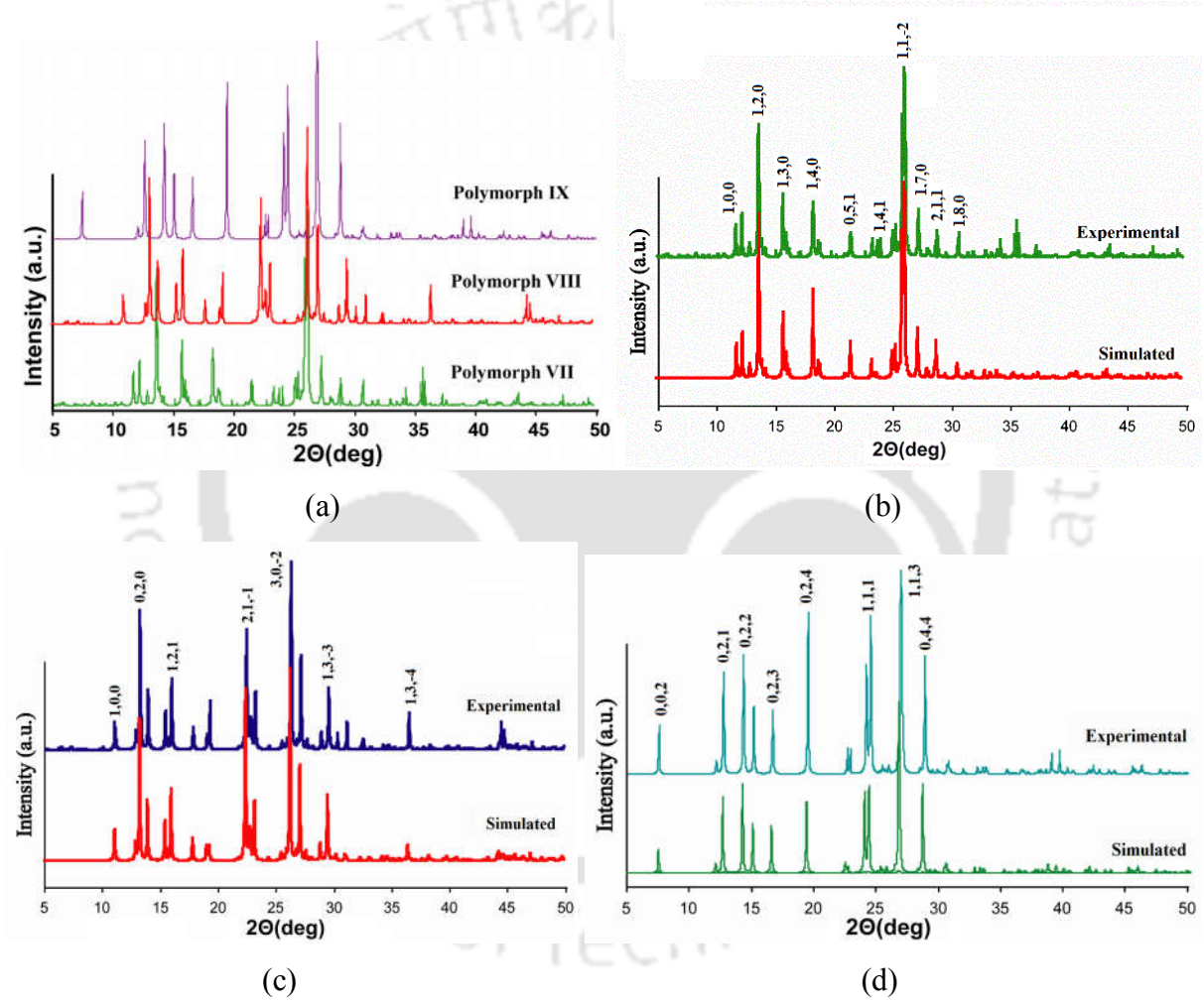

Figure 4.8: (a) The comparison experimental powder X-ray diffraction patterns of the three polymorphs **VII**, **VIII** and **IX**. The comparison of simulated and experimental powder X-ray diffraction patterns of polymorphs (b) **VII** (c) **VIII** and (d) **IX**.

The polymorphs **VII**, **VIII** and **IX** have characteristic PXRD patterns (Figure 4.8a), which are well distinguishable from each other, hence in a mixture of crystals of these polymorphs can be

easily analyzed. Moreover, the simulated powder-XRD patterns obtained from the single crystal x-ray diffraction data are found to be resembled with the experimental ones, which confirmed the purity of the bulk samples of the polymorphs (Figure 4.8b-d).

As mentioned above, the three polymorphs were obtained from three different solvents and a concomitant polymorph of polymorph **VIII** and polymorph **IX** were obtained from a mixture of solvents. Moreover, it is reported in literature that, solvent[31-33] and anion[34-35] can guide crystallization or transformation of crystals. To see the influence of different solvents in the crystallization process, crystallization of **4.1** was carried out from the solution of different solvents systems. We have chosen methanol, DMF, DCM, dioxane as solvents to crystallize **4.1** by taking their binary mixtures at different proportions. The powder X-ray diffractions of the crystals obtained from complete evaporation of solvents after several days at ambient conditions were analyzed (Figure 4.9).

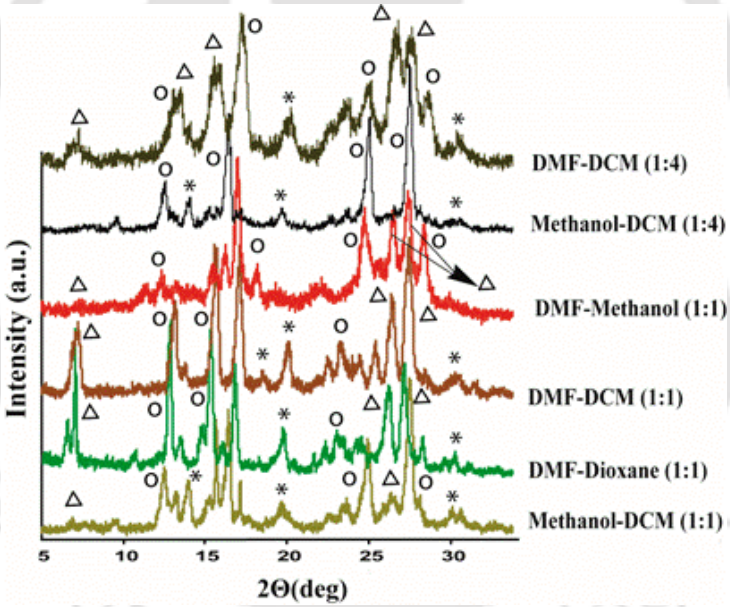

Figure 4.9: Powder XRD patterns of the mixture of polymorphs of **4.1** crystallized from different mixture of solvents (the peaks represented by '*' are from polymorph **VII**, 'o' are from polymorph **VIII** and 'Δ' are from polymorph **IX,** respectively.

We find that PXRD patterns of the crystals obtained from the crystallization of **4.1** from an equal volume of mixed solvent comprising of *tert*-butanol and dimethylformamide show the PXRD peaks of polymorphs **VIII** as well as that of polymorph **IX** (Figure 4.10). This suggests that simultaneous crystallization of polymorphs **VIII** and **IX** can be done from mixed solvents. The

use of 1:1 ratio of methanol and DCM led to a mixture of **VII** and **VIII** with minor amount of **IX**, whereas use of same combination of solvents in 1:4 ratio yielded **VII** and **VIII**; it shows that the methanol has

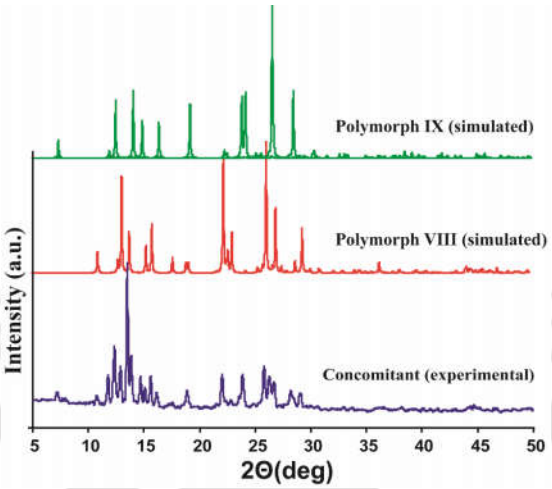

Figure 4.10: The comparison of experimental powder-XRD pattern of the concomitant polymorph with simulated patterns of individual polymorphs.

a higher tendency to control the crystallization process over the dichloromethane. The use of DMF and methanol in 1:1 mixture led to the formation of **VII** and **VIII** as the major components and polymorph **IX** as the minor component. The trend supports the preferential crystallization of the polymorph **VII** from methanol and the polymorph **VIII** from DMF independently. In binary mixed solvent, the two solvents compete independently to guide crystallization of the selective polymorph or mixture of polymorphs. Analogously, a mixture of DMF and DCM in 1:1 ratio led to crystals of polymorphs **VIII** and **IX** predominantly with trace amount of crystals of polymorph **VII**; however, changing the ratio of DMF:DCM to 1:4 resulted in the crystallization of polymorphs **VII**, **VIII** and **IX** but lesser quantity of crystals of polymorph **IX** was obtained with respect to the other two polymorphs. However, when 1:1 mixture of DMF-dioxane was used as solvent of crystallization, polymorphs **VII** and **IX** were found to be major product with trace amount of polymorph **VIII**. Thus, to a large extent the binary mixture of solvents did not alter the signature or proportion of the crystals of the polymorphs from the ones that were independently crystallized from the constituent solvents. However, from above observation it can be suggested that solvents have definite role in stabilization of a particular polymorph. Different polymorphs obtained from different solvent mixtures are listed in Table 4.2.

Table 4.2: different polymorphs obtained from different solvent systems.

Solvent system	Polymorph
Methanol : DCM (1:1)	**VII** + **VIII** + **IX***
Methanol : DCM (1:4)	**VII** + **VIII**
DMF : methanol (1:1)	**VII** + **VIII**
DMF : DCM (1:1)	**VIII** + **IX** + **VII***
DMF : DCM (1:4)	**VII** + **VIII** + **IX***
DMF : dioxane (1:1)	**VII** + **IX** + **VIII***
DMF : *tert*-butanol	**VIII** + **IX**

'*' represents minor amount

In case of 3-nitro-N-(quinolin-8-yl)benzamide (**4.3**), we could obtained only one type of polymorph. The crystal belongs to monoclinic space group $P2_1$.

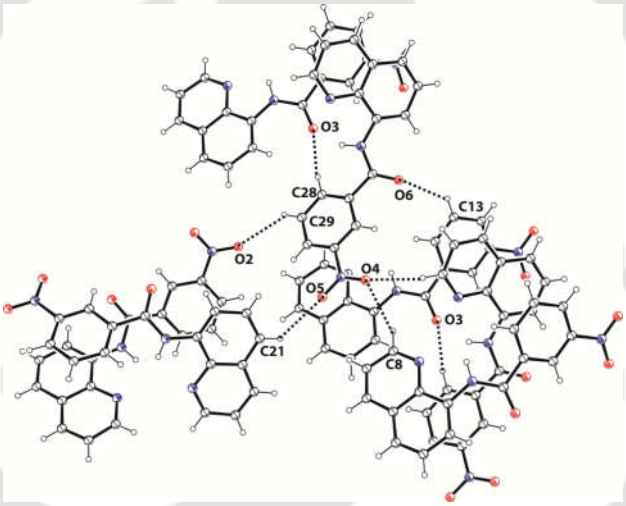

Figure 4.11: The weak interactions among the molecules in crystal lattices of **4.3** (ORTEP drawn with 35 % thermal ellipsoids).

In its crystal lattice, the molecules are held each other by weak C-H···O interactions. The one of the oxygen atom of the nitro group, O4 involves in a bifurcated hydrogen bond with two C8-H bonds from the two independent molecules (Figure 4.11). The oxygen atom, O5 anchors another molecule through C-H···O5 interaction. Thus, each nitro group holds three molecules of **4.3** to hold a network of five molecules. The amide group also contributes to the assembly through oxygen atom O3 interacting with C28-H bond of the nitro phenyl ring.

Besides above mentioned derivatives, we also studied polymorphism in ethyl ester derivative ethyl-4-(2-oxo-2-(quinolin-8-ylamino)ethoxy)benzoate (**4.4**) shown in Figure 4.12a. This

compound shows two polymorphs when crystallized in different solvent systems. One form (Polymorph **X**) was obtained from methanol and crystals belong to triclinic *P-1* space group,

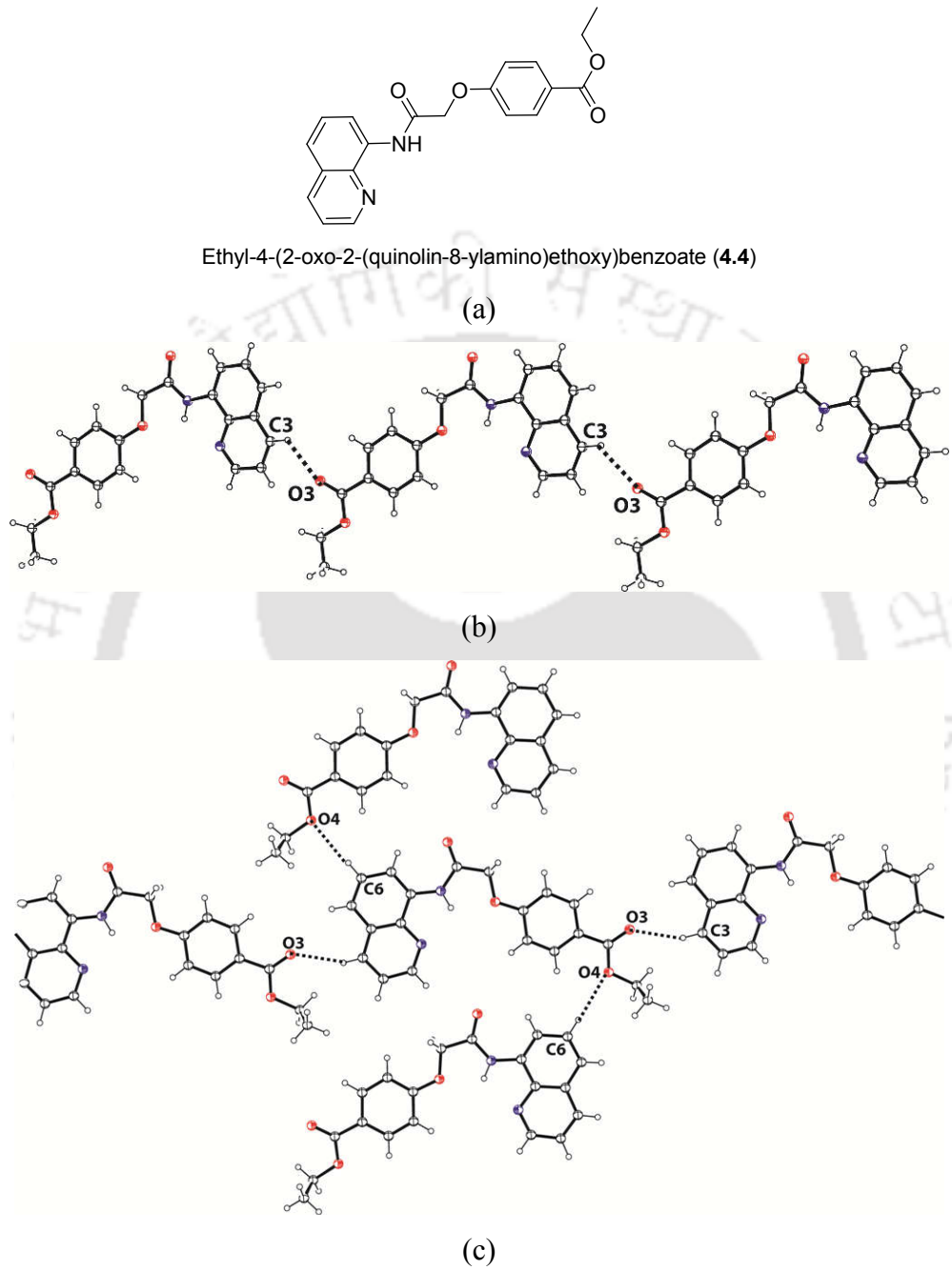

Figure 4.12: (a) Compound **4.4**; weak interactions among the molecules in crystal lattices of (b) Polymorph **X** and (c) Polymorph **XI** (ORTEP drawn with 35 % thermal ellipsoids).

which has a simple packing pattern. In the crystal lattice a layer of molecules extends, where the molecules are linked to each other by weak C3-H···O3 hydrogen bonds (Figure 4.12b). Whereas,

the second form (Polymorph **XI**) crystallized in monoclinic $P2_1$ space group and it was obtained from tetrahydrofuran. In this case both the oxygen atoms of the ester group participate in hydrogen bond formation to give a sheet of molecules. These sheets of molecules are held by π···π interactions (Figure 4.12c). In both the polymorphs planarity between the quinoline ring and the phenyl ring was retained. However, the positions of the ethyl group attached to the ester moiety were different.

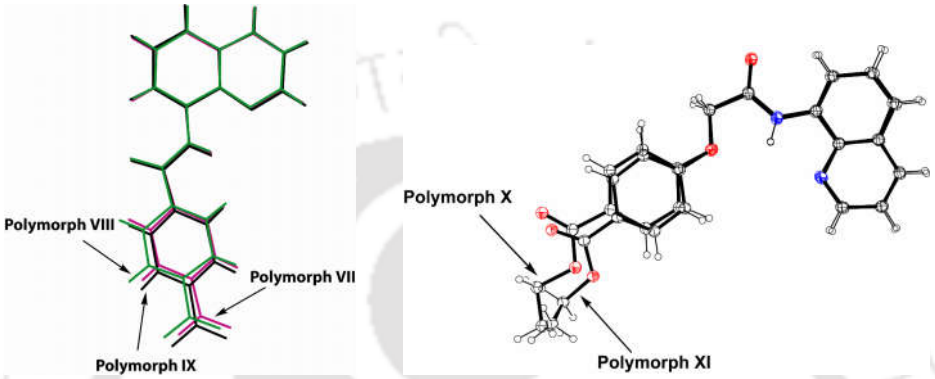

(a) (b)

Figure 4.13: Overlay of the (a) polymorphs **VII-IX** and (b) polymorphs **X-XI**.

Thus the two polymorphs of compound **4.4** differ in the orientation of ethyl group. But, interesting point among the two sets polymorphs (**4.1** and **4.4)** is that former set is due to the orientation across the amide bond (Figure 4.13a), whereas the latter set has similar orientations of amide group but the due to differences in orientations of ethyl group caused polymorphism (Figure 4.13b). This clearly indicates that a substituent at a remote site can contributes to the stabilization of conformational polymorph through participation in the weak interactions schemes. Slight different arrangements in the conformers lead to the polymorphs.[36-37] However in compound **4.4** ethyl group insignificantly contributes to the interaction schemes but can adopt different orientation to construct tight packed structures.

4.2: Salts of 4-nitro-N-(quinolin-8-yl)benzamide (4.1)

As we have seen that solvents have definite impact on the crystallization of compound **4.1** resulting to different polymorphs upon changing the solvent of crystallization. Thus, to check the effect of protonation of the quinoline nitrogen and the role of counter anion on structure of protonated species we prepared three salts of **4.1**. The salts were prepared by adding mineral

acids namely sulphuric acid, hydrobromic acid and nitric acid to the solution of **4.1** as illustrated by Scheme 4.3.

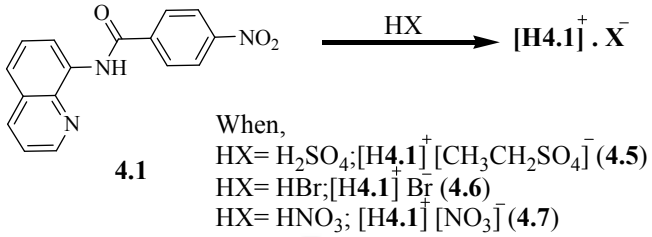

Scheme 4.3: Synthesis of salts of **4.1**.

The salt **4.5** with a composition of $[H\mathbf{4.1}]^{+}[CH_3CH_2SO_4]^{-}$ was obtained from reacting **4.1** with sulphuric acid in ethanol. This salt has ethylsulphate anion, which was generated *in-situ* from the reaction of sulphuric acid with ethanol in the presence of **4.1**. Generation of ethyl sulphate *in situ* may be as a consequence of reaction of ethanol with sulphuric acid as shown in equation 4.1.

$$H_2SO_4 + CH_3CH_2OH \rightleftharpoons CH_3CH_2OSO_3H + H_2O$$

Equation 4.1: Reaction of ethanol with sulphuric acid.

In-situ generation and stabilization of ethylsulphate anions by various supramolecular assemblieshas been well studied.[38-39] However, we observe formation of such species in the presence of an amide bond containing molecule, which is easy to synthesize as compared to many complex receptors reported earlier. In the crystal lattice of this salt, there are two oxygen atoms from the anion involved in bifurcated hydrogen bonds stabilize the packing. The oxygen atom, namely the atom O5 interacts with C1-H bond and C2-H bond whereas, the atom O6 interacts with N2-H bond as well as with C13-H bond (Figure 4.14a). The atom O4 forms strong hydrogen bond with N1-H bond (Table 4.3). Both the oxygen atoms O2 and O3 of the nitro group are involved in C-H···O interactions with C7-H and C2-H bonds respectively. Apart from these, phenyl ring is almost perpendicular to quinoline ring in the cationic part, this occurs to accommodate the ethylsulphate anions in the lattice.

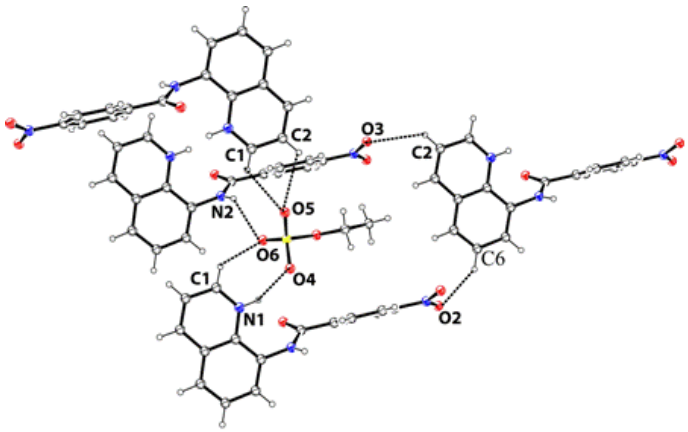

(a)

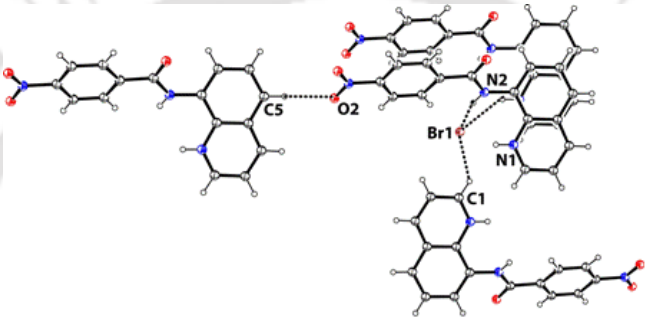

(b)

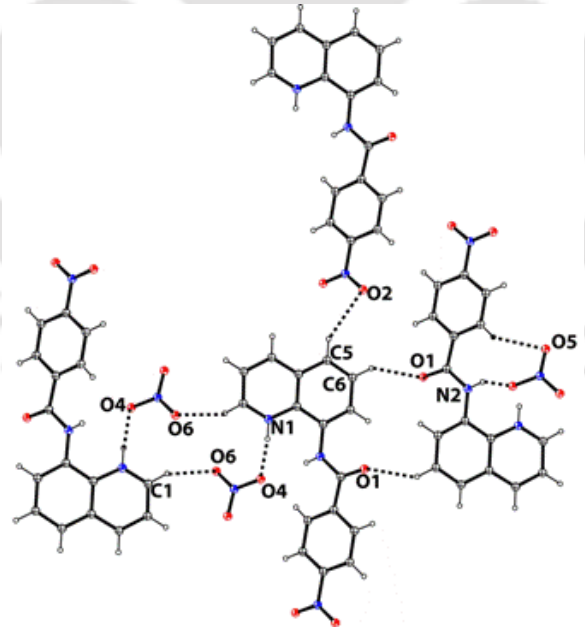

(c)

Figure 4.14: Weak interactions among the molecules in crystal lattices of (a) **4.5**, (b) **4.6** and (c) **4.7** (ORTEPs are drawn with 35 % thermal ellipsoids).

The bromide salt **4.6** crystallizes in triclinic *P-1* space group. In comparison to the structure of **4.1**, the plane of the phenyl ring in the bromide salt is significantly away from the plane containing quinoline ring. The crystal lattice is stabilized by strong electrostatic N-H···Br interactions (Figure 4.14b). Each bromide ion is held by four prominent interactions, two of them are N2-H···Br interactions and other interactions are C1-H···Br and C16-H···Br interactions (Table 4.3). The bromide ions are generally known to adopt spherically symmetric coordinating supramolecular environment.[40] There are also examples of bromide ions having T-shaped environments.[41] Whereas, the bromide ions in the crystal lattice of the salt **4.6** has distorted tetrahedron environment.

Table 4.3: Hydrogen bond parameters of salts **4.5-4.7**.

Compound No.	D-H···A	d_{D-H}(Å)	$d_{H\cdots A}$(Å)	$d_{D\cdots A}$(Å)	∠ D-H···A(º)
4.5	N1- H···O4 [-x,1-y,1-z]	0.86	1.97	2.76(3)	153
	N2 - H···O6 [1-x,1-y,1-z]	0.86	2.29	2.90(3)	129
	C1 - H···O5 [-1+x,y,-1+z]	0.93	2.47	3.11(4)	127
	C5 - H···O1 [-x,-y,-z]	0.93	2.59	3.41(3)	147
	C7- H···O2 [1-x,1-y,1-z]	0.93	2.59	3.23(4)	127
	C13-H···O6	0.93	2.58	3.46(4)	160
4.6	N1 - H ··· Br1 [-1+x,y,z]	0.86	2.43	3.21(9)	152
	N2 - H···Br1	0.86	2.62	3.37(11)	148
	C1 - H···Br1 [-x,1-y,-z]	0.93	2.87	3.60(13)	138
	C16 -H···Br1	0.92	2.98	3.89	165
	C5-H···O2	0.93	2.66	3.52	153
4.7	N1-H1A···O4[1-x,1-y,1-z]	0.86	1.94	2.75(6)	157
	N2-H2A···O4 [-x,1-y,1-z]	0.83(6)	2.09(6)	2.84(6)	149(5)
	C1-H1···O6 [1+x,1+y,z]	0.93	2.42	3.24(7)	147
	C1-H1···O6 [1-x,1-y,1-z]	0.93	2.57	3.19(8)	125

In the self assembly of the nitrate salt **4.7**, two oxygen atoms are involved in C-H···O interactions namely the atom O5 interact with C16-H and O6 with C1-H (Figure 4.14c). Similar C-H···O interactions are observed with the carbonyl oxygen atom O1 with C6-H and that of the O2 with C5-H. The nitrate oxygen atom O4 is involved in a strong hydrogen bond with N1-H (Table 4.3). The nitrate salt is highly porous as it is obvious from a spacefill model diagram of the packing of the molecules in the crystal structure viewed along a-axis (Figure 4.15). The analysis of the packing pattern of the salt shows void with dimension 114.8 $Å^3$ (13.5 %) per unit cell having volume 853.4 $Å^3$.

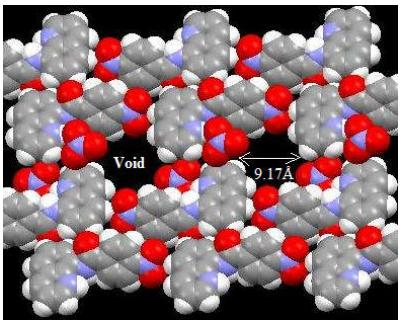

Figure 4.15: A spacefill model showing the voids in the packing pattern of the nitrate salt **4.7** (viewed along a-axis).

Generally porous structures are obtained as isomorphic desolvate. By definition desolvates have three dimensional structures of their parent solvates formed upon loss of solvent molecules. Such desolvates were demonstrated by Stephenson *et al*.[42] in spirapril hydrochloride. In the present case the bromide and nitrate salts (**4.6** and **4.7**) are air stable as well as not hygroscopic. However, close analysis reveals that the packing patterns of the nitrate and bromide salts have similar principal weak interactions between the hosts. But differences arise between these two cases is the interactions of the protonated parent compound with the anions. Bromide ions are spherical whereas the nitrate ions are planar. Size-wise nitrate is smaller than bromide, hence solvent might have been present in the nitrate salt as filler molecules to make a tight packed structure to make arrangement of anions and solvent in space comparable to size occupied by bromide ions. Such solvent molecules might have got lost of the nitrate salt during crystallization, causing formation of an isomorphic desolvate having a porous structure.

As we have mentioned, there are possibilities of partial bond rotation between the quinoline ring and phenyl ring which may be insisted by solvent molecule on neutral **4.1** or by counter anion on protonated **4.1** (Figure 4.5). Thus, it is interesting to look at the torsion angles as defined in Figure 4.16a; a) C7-C8-N2-C10, b) C8-N2-C10-O1, c) O1-C10-C11-C16 and d) C13-C14-N3-O2 in each case. The differences in the torsion angle C7-C8-N2-C10 in each case show the dissimilar projection of the carbonyl group of amide across the quinoline ring. The differences in torsions defined as ‘a’, ‘b’ and ‘c’ vary the planarity between quinoline ring and phenyl ring among the three polymorphs (Figure 4.13a). The differences in torsion angles of the three polymorphs can be attributed to the formation of different packing patterns in the three polymorphs. The origin of the differences in the geometries of the polymorphs arises from the

synergic effects of partial rotation of the amide bond and resonance effect of the nitro group. In none of the case we could isolate solvate, where one could have anticipated large variation of torsion angles by strong interactions of solvent molecules with the parent molecules. The torsion angles of the polymorphs are listed in Table 4.4.

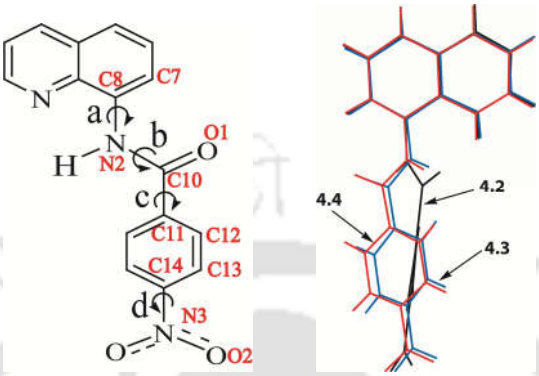

(a) (b)

Figure 4.16: (a) Atom numbering to describe the torsion angles of **4.1**; (b) overlay of the protonated cations of the salts **4.5**-**4.7**.

Large changes in the C7-C8-N2-C10 torsion angles with respect to the parent compound (**4.1**) could be brought about in the salts of **4.1**. In addition to size differences between a bromide and a nitrate anion, bromide ion has spherical charge distribution whereas the nitrate ion has charge distributed among the three oxygen atoms. On the other hand, the relatively larger ethylsulphate anion is nonplanar and has multiple sites for weak interactions. These factors affect the packing patterns in each case. Accordingly, the twist between the two planes; torsions between the quinoline ring plane and the phenyl ring plane of the cations differ (Figure 4.16b). It is found that the projections of carbonyl group with respect to the nitrogen atom of the quinoline ring in the structure of ethylsulphate salt (**4.5**) and in bromide salt (**4.6**) are opposite to each other. Thus, differences in the shape, size and weak interaction of the anions cause the differences in the torsion angles of the cationic counterparts (Table 4.4).

Table 4.4: Torsion angles in the polymorphs and salts of **4.1**.

Polymorph **VII**	Torsion angle	Polymorph **VIII**	Torsion angle	Polymorph **IX**	Torsion angle
C7-C8-N2-C10	- 4.6	C7-C8-N2-C10	- 6.4	C7-C8-N2-C10	- 3.5
C8-N2-C10-O1	1.7	C8-N2-C10-O1	- 4.4	C8-N2-C10-O1	- 1.9
O1-C10-C11-C16	158.4	O1-C10-C11-C16	164.3	O1-C10-C11-C16	175.6
C13-C14-N3-O2	-1.3	C13-C14-N3-O2	7.3	C13-C14-N3-O2	- 9.3

Ethylsulphate salt	Torsion angle	Bromide salt	Torsion angle	Nitrate salt	Torsion angle
C7-C8-N2-C10	112.3	C7-C8-N2-C10	- 42.8	C7-C8-N2-C10	-38.6
C8-N2-C10-O1	7.0	C8-N2-C10-O1	- 0.29	C8-N2-C10-O1	-1.7
O1-C10-C11-C16	148.4	O1-C10-C11-C16	177.5	O1-C10-C11-C16	-179.2
C13-C14-N3-O2	- 15.0	C13-C14-N3-O2	- 4.0	C13-C14-N3-O2	-4.0

Thus, on analyzing these three salts it was found that the twist between the two planes is guide by the bulkiness of the corresponding counter ion. In case of salt **4.5** the phenyl ring with respect to quinoline ring is almost perpendicular to each other, this happens to accommodate the ethylsulphate anions in the lattice which has a relatively bigger size. Among the bromide salt **4.6** and nitrate salt **4.7** the twist between the quinoline and the phenyl rings is found to be more in **4.6**. Since bromide ion is more spherically bulkier with higher charge density whereas the nitrate ion is planer and charge is distributed among the three oxygen atoms. This can be thought of as supramolecular machine where the twist of two parts of guest molecule can be controlled by selecting proper size and shape of the guest molecule.[43-44] The sequence of magnitude of the twist between the two planes was **4.5** > **4.6** > **4.7**.

4.3: Conclusion

In conclusion, four conformational polymorphs **VI-IX** of **4.1** and also a concomitant polymorph of polymorph **VII** and **IX** were prepared by crystallization in different solvent systems. Highly ordered structures are observed in each case, comprising of molecules with different orientations arranged in their respective lattice. The differential scanning calorimetry analysis established that the three polymorphs **VII-IX** have monotropic relationship. The dihedral angles of aromatic plane across the amide bond of protonated **4.1** are dependent on the size and shape of the counter anions.

4.4: Experimental

The detailed synthetic methodologies for synthesis of the metal complexes are described. Analytical data are provided with each complex. The instrumental details and crystallographic parameters are provided in Appendix.

Synthesis of 4.1:

8-Aminoquinoline (0.288 g, 2 mmol) was dissolved in 20 mL of dry THF to this triethylamine (0.277 mL, 2 mmol) was added and stirred for 15 minutes, followed by addition of 4-nitrobenzoylchloride (0.371 g, 2 mmol) solution in dry THF. The resulting mixture was stirred for 5 hours at room temperature. Completion of the reaction was checked with TLC, solvent was removed under reduced pressure to obtain a pale yellow solid of compound **4.1**. Elemental analysis calculated for $C_{16}H_{11}N_3O_3$, C: 65.53 %, N: 14.33 %, H: 3.78 %; found C: 65.35 %, N: 13.86 %, H: 3.19 %. Yield ~ 75%. IR (KBr, cm^{-1}): 3441 (s), 3331 (s), 2925 (w), 2853 (w), 1676 (s), 1601 (m), 1519 (s), 1480 (w), 1426 (w), 1386 (m), 1341 (m), 1263 (w), 1179 (w), 1112 (w), 851 (w), 827 (w), 794 (w), 684 (w), 602 (w), 456 (w). ^{1}HNMR (400MHz, DMSO-d_6): 10.78 (s, 1H), 8.98 (q, J = 1.6 Hz, 1H), 8.69 (d, J = 7.6 Hz, 1H), 8.47 (q, J = 1.2 Hz, 1H), 8.43 (d, J = 8.8 Hz, 2H), 8.27 (d, J = 8.4 Hz, 2H), 7.80 (d, J = 8.0 Hz, 1H) 7.70 (m, J = 4.0 Hz, 2H). ESI mass: [M + H] calculated for $C_{16}H_{12}N_3O_3$, 294.0879; found 294.1329.

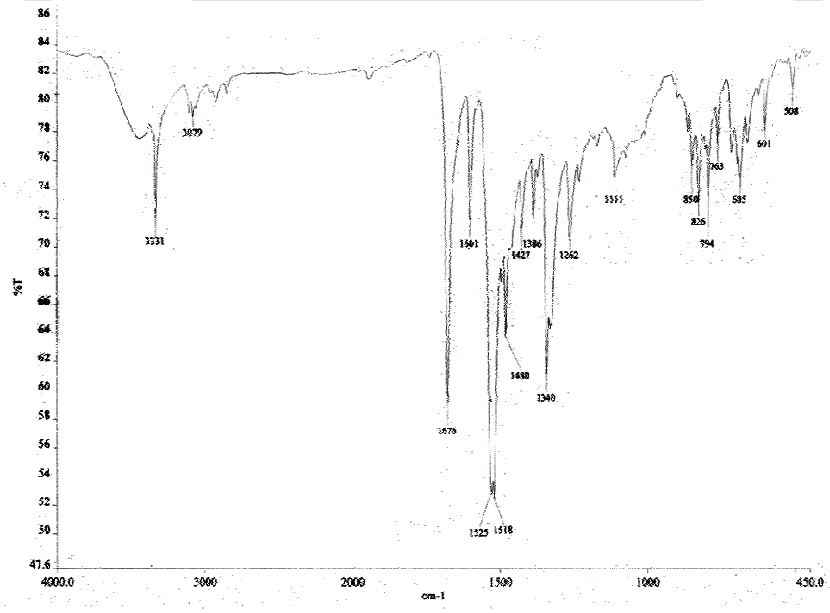

Figure 4.17: FT-IR (KBr, cm^{-1}) spectra of **4.1**.

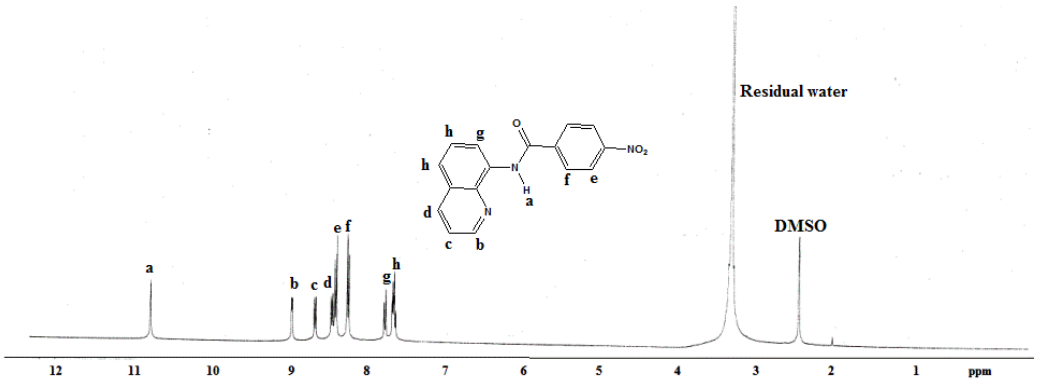

Figure 4.18: ^{1}H-NMR (400MHz, DMSO-d_6) spectra of **4.1**.

Synthesis of 4.2:

8-Aminoquinoline (0.288 g, 2 mmol) was dissolved in 20 mL of dry THF to this triethylamine (0.277 mL, 2 mmol) was added and stirred for 15 minutes, followed by addition of 2-nitrobenzoylchloride (0.371 g, 2 mmol) solution in dry THF. The resulting mixture was stirred for 5 h at room temperature. Completion of the reaction was checked with TLC, solvent was removed under reduced pressure to obtain a pale yellow solid of compound **4.2**. Elemental analysis calculated for $C_{16}H_{11}N_3O_3$, C: 65.53 %, N: 14.33 %, H: 3.78 %; found C: 65.31 %, N: 13.93 %, H: 3.13 %. Yield ~ 71%. IR (KBr, cm^{-1}): 3445 (m), 3301 (m), 3085 (w), 2924 (w), 1670 (s), 1616 (m), 1526 (s), 1484 (w), 1418 (m), 1348 (s), 1326 (m), 1238 (m), 1135 (w), 1073 (w), 822 (w), 796 (m), 762 (m), 762 (m), 717 (m), 598 (w). ESI mass: [M + H] calculated for $C_{16}H_{12}N_3O_3$, 294.0879; found 294.0254.

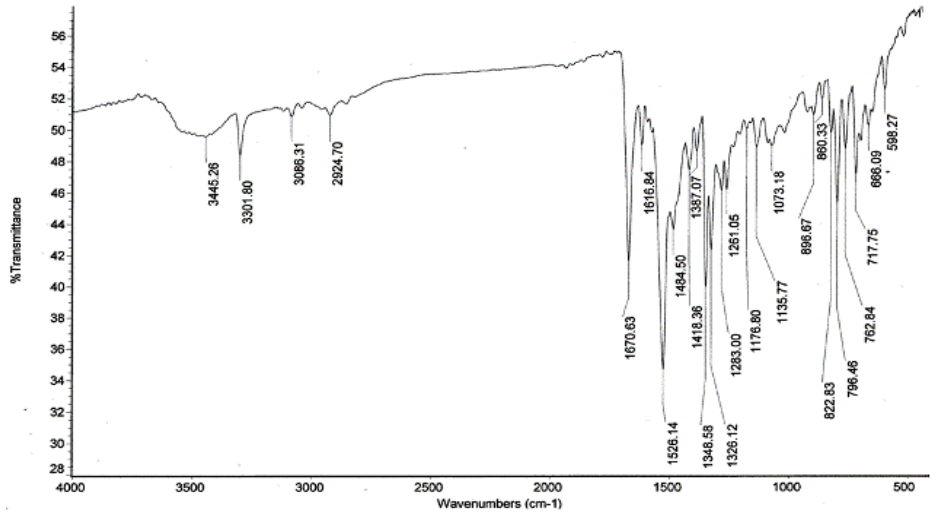

Figure 4.19: FT-IR (KBr, cm^{-1}) spectra of **4.2**.

Synthesis of 4.3:

8-aminoquinoline (0.288 g, 2 mmol.) was dissolved in 20 mL of dry THF to this triethylamine (0.277 mL, 2 mmol.) was added and stirred for 15 minutes, followed by addition of 3-nitrobenzoylchloride (0.371 g, 2 mmol.) solution in dry THF. The resulting mixture was stirred for 5 hours at room temperature. Completion of the reaction was checked with TLC, solvent was removed under reduced pressure to obtain a pale yellow solid of compound **4.3**. Elemental analysis calculated for $C_{16}H_{11}N_3O_3$, C: 65.53 %, N: 14.33 %, H: 3.78 %; found C: 65.33 %, N: 13.72 %, H: 3.86 %. Yield ~ 78%. IR (KBr, cm^{-1}): 3444 (s), 3302 (s), 2923 (m), 2854 (w), 1670 (s), 1616 (m), 1526 (s), 1483 (m), 1421 (m), 1384 (w), 1348 (s), 1327 (m), 1260 (m), 1126 (w), 1019 (w), 923 (w), 823 (m), 792 (m), 761 (m), 719 (m), 666 (w), 597 (w). ESI mass: [M + H] calculated for $C_{16}H_{12}N_3O_3$, 294.0879; found 294.1501.

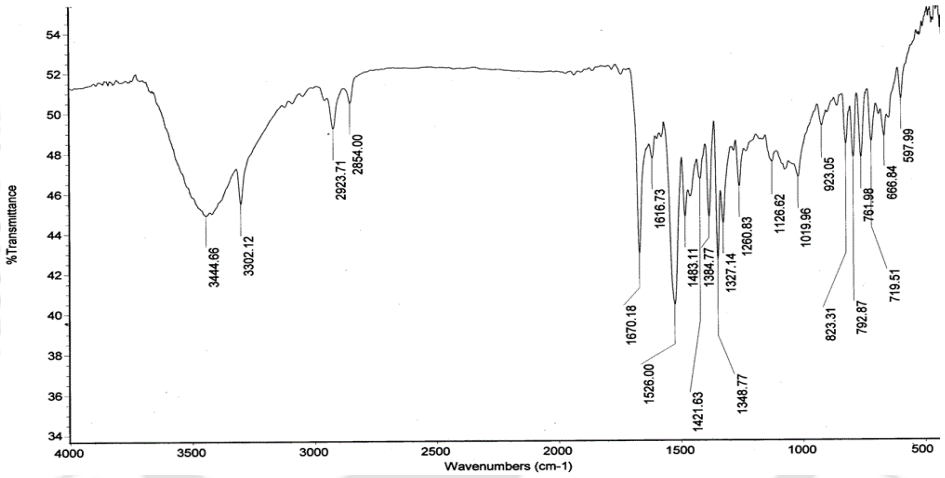

Figure 4.20: FT-IR (KBr, cm^{-1}) spectra of **4.3**.

Synthesis of 4.4:

To a solution of 8-aminoquinoline (0.72 g, 5 mmol) in dry dichloromethane (20 mL), triethylamine (0.71 mL, 5 mmol) was added. Solution was stirred at 0ºC for 15 mins, followed by which bromoacetyl bromide (0.52 mL, 6 mmol) was added. Reaction mixture was then stirred overnight and filtered. Filtrate was washed with water (10 mL), dried over anhydrous sodium sulphate and then the solvent was removed under reduced pressure. Product was obtained as a brown solid that was purified by recrystallisation from dichloromethane. Amide obtained from above reaction (0.53 g, 2 mmol), ethyl 4-hydroxybenzoate (1.66 g, 10 mmol) and potassium carbonate (1.07 g, 7 mmol) were added to dry acetone (20 mL) under nitrogen and the reaction

mixture was stirred at 60 ºC for 9 hrs. After completion of reaction solvent was removed under reduced pressure to obtain a pale yellow solid which was recrystallized from methanol. IR (KBr, cm^{-1}): 3430 (m), 3323 (m) 2977 (w), 1701(s), 1691(s), 1607 (s), 1544 (s), 1507 (m), 1485 (m), 1427 (w), 1388 (w), 1367 (w), 1330 (w), 1318 (w), 1301 (w), 1279 (m), 1248(s), 1167 (m), 1107 (m), 1055 (m), 841(w), 823 (w), 791 (m), 764 (w), 755 (w), 686 (w), 638 (w), 567 (w), 500 (w). ^{1}H-NMR (400MHz, $CDCl_3$): 10.88 (s, 1H), 8.82 (q, *J* = 1.6 Hz, 1H), 8.78 (t, *J* = 4.4 Hz, 1H), 8.14 (dd, *J* = 1.6 Hz, 1H), 8.05 (dd, *J* = 2.0 Hz, 2H), 7.52 (d, *J* = 4.0 Hz, 2H), 7.44 (q, *J* = 4.0 Hz, 1H), 7.11 (d, *J* = 8.8 Hz, 2H), 4.76 (s, 2H), 4.35 (q, *J* = 7.2 Hz, 2H), 1.37 (t, *J* = 7.2 Hz, 3H). ESI mass: [M + H] calculated for $C_{20}H_{19}N_2O_4$, 351.1345; found 351.0266.

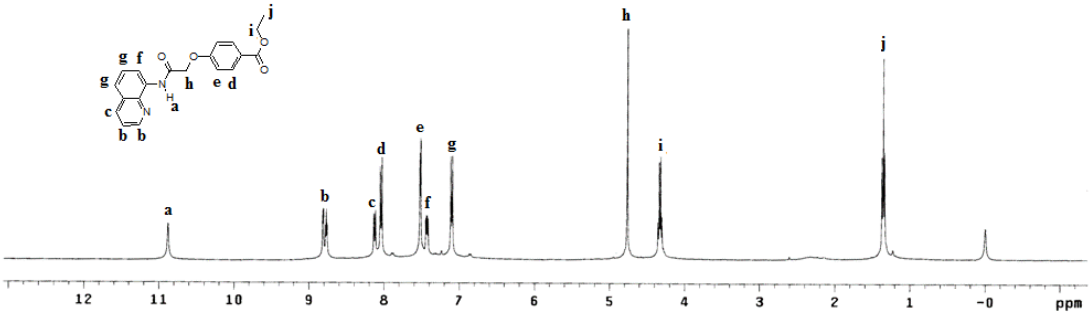

Figure 4.21: ^{1}H-NMR (400MHz, $CDCl_3$) spectra of **4.4**.

Synthesis of 4.5:

The ethylsuphate salt of 4-nitro-N-(quinolin-8-yl)benzamide was prepared also by reacting **4.1** (0.29 g, 1 mmol) in ethanol (15 mL) by addition of few drops of conc. H_2SO_4. White crystals crystallize upon standing. Yield ~70%. IR (KBr, cm^{-1}): 3433(s), 3097(w), 1674 (s), 1634 (m), 1594 (m), 1556 (m), 1518 (s), 1483 (m), 1416 (w), 1377 (w), 1345 (m), 1259 (s), 1218 (s), 1064 (w), 1011 (m), 923 (m), 825 (w), 766 (w), 570 (w). ^{1}HNMR (400MHz, DMSO-d_6): 10.94 (s, 1H), 9.10 (q, *J* = 1.6 Hz, 1H), 8.81 (d, *J* = 8.8 Hz, 1H), 8.51 (q, *J* = 7.6 Hz, 2H), 8.44 (t, *J* = 6.8 Hz, 1H), 8.30 (t, *J* = 6.8 Hz, 2H), 8.02 (d, *J* = 8.4Hz, 1H) 7.89 (m, *J* = 4.8 Hz, 2H) 7.83(t, *J* = 8.0 Hz, 1H), 3.47 (m, *J* = 2.0 Hz, 2H), 1.06 (m, *J* = 2.0 Hz, 3H).

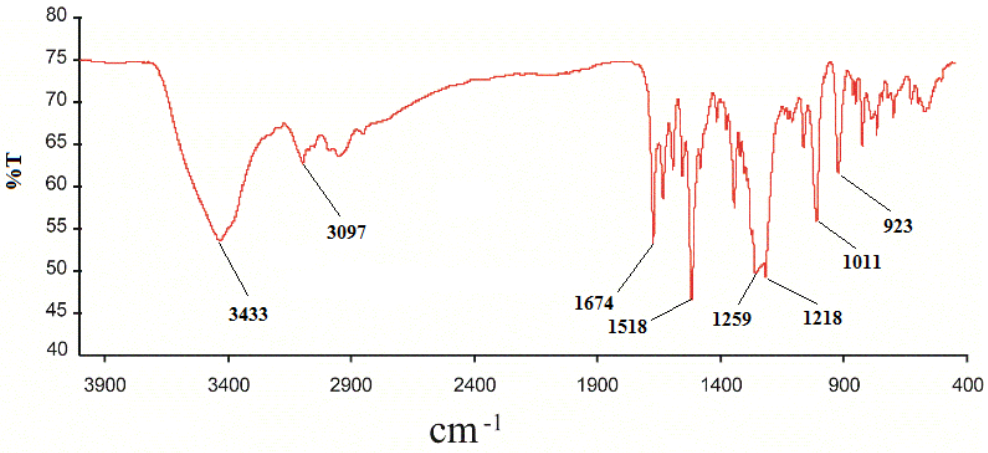

Figure 4.22: FT-IR (KBr, cm^{-1}) spectra of **4.5**.

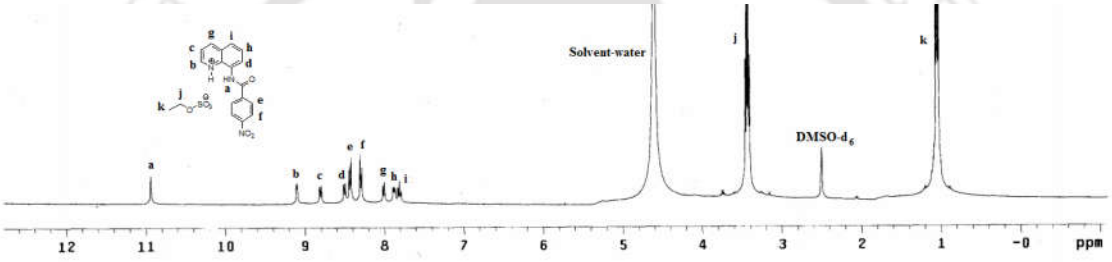

Figure 4.23: ^{1}H-NMR (400MHz, DMSO-d_6) spectra of **4.5**.

Synthesis of 4.6:

The bromide salt of 4-nitro-N-(quinolin-8-yl)benzamide was prepared by reacting 4-nitro-N-(quinolin-8-yl)benzamide (0.29 g, 1 mmol) in a mixed solvent of methanol and DMF (9:1, 10 mL) with 1mL of HBr. On standing the bromide salt crystallizes. Yield ~ 90%. IR (KBr, cm^{-1}): 3451 (s), 2925 (w), 2851 (w), 1681 (m), 1630 (m), 1602 (m), 1556 (m), 1520 (m), 1484 (w), 1374 (w), 1344 (w), 1259 (w), 1218 (w), 1051 (w), 850 (w), 823 (w), 760 (w), 711 (w), 600 (w).

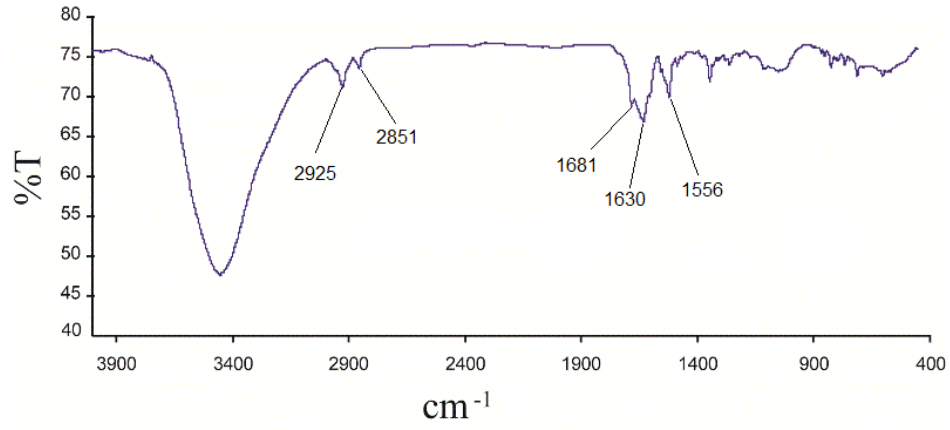

Figure 4.24: FT-IR (KBr, cm^{-1}) spectra of **4.6**.

Synthesis of 4.7:

The nitrate salt of 4-nitro-N-(quinolin-8-yl)benzamide was prepared by reacting 4-nitro-N-(quinolin-8-yl)benzamide (0.29 g, 1 mmol) in a mixed solvent of methanol and DMF (9:1, 10 mL) with 1mL of HNO_3. On standing the nitrate salt crystallizes. Yield ~ 90%. IR (KBr, cm^{-1}): 3427 (s), 2919 (w), 2849 (w), 1682 (m), 1631 (m), 1599 (m), 1535 (m), 1519 (m), 1384 (s), 1345 (m), 1310 (m), 1278 (w), 1258 (w), 1218 (w), 1102 (w), 1021 (w), 833 (w), 824 (w), 710 (w), 597 (w).

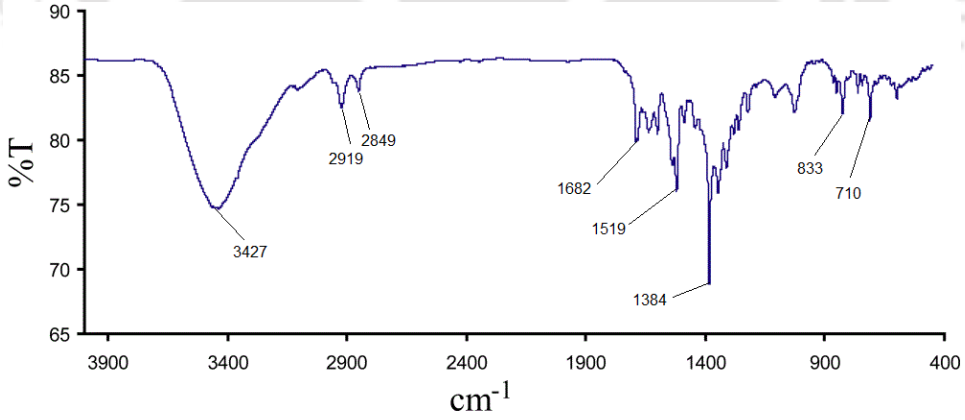

Figure 4.25: FT-IR (KBr, cm^{-1}) spectra of **4.7**.

4.5: Reference

1. W. C. McCrone, Polymorphism. In *Physics and Chemistry of the Organic Solid State*; D. Fox, M. M. Labes, A. Weissberger Eds.; Wiley-Interscience: New York, 1965, Vol. **2**, pp 725.

2. J. D. Dunitz, *Pure Appl. Chem.,* 1991, **63**, 177.
3. J. D. Dunitz, J. Bernstein, *Acc. Chem. Res.,* 1995, **28**, 193.
4. J. D. Dunitz, *Acta Crystallogr., Sect. B.,* 1995, **51**, 619.
5. J. Bernstein, R. J. Davey, J. -O. Henck, *Angew. Chem. Int. Ed.,* 1999, **38**, 3441.
6. J. Bernstein, *Polymorphism in Molecular Crystals*; Oxford University Press: Oxford, 2002.
7. R. J. Davey, *Chem. Commun.,* 2003, 1463.
8. *Solid-State Characterization of Pharmaceuticals*; A. Zakrzewski, M. Zakrzewski, Eds. Assa International Inc.: Danbury, CT, USA, 2006.
9. *Polymorphism in the Pharmaecutical Industry*; R. Hilfiker, Ed. Wiley-VCH: Weinheim, Germany, 2006.
10. G. R. Desiraju, *Cryst. Growth Des.*, 2008, **8**, 3.
11. A. D. Bond, R. Boese, G. R. Desiraju, *Angew. Chem., Int. Ed.,* 2007, **46**, 615.
12. A. D. Bond, R. Boese, G. R. Desiraju, *Angew. Chem., Int. Ed.,* 2007, **46**, 618.
13. A. D. Bond, R. Boese, G. R. Desiraju, *Am. Pharm. Rev.* 2007, May/June, 1.
14. J. Bernstein, Organic Solid State Chemistry, Elsevier, Amsterdam, 1978.
15. A. Nangia, *Acc. Chem. Res.,* 2008, **41**, 595.
16. D. J. W. Grant, Theory and origin of polymorphism, in: H. G. Brittain (Ed.), Polymorphism in Pharmaceutical Solids, Marcel Dekker Inc., New York, 1999, p. 1.
17. R. Kahlau, T. Gnutzmann, F. Emmerling, K. Rademann, E. A. Rossler, *J. Chem. Phys.,* 2012, **137**, 054505, 1.
18. W. M. Motswainyana, M. O. Onani, *Acta Crystallogr. Sect. E.,* 2011, **67**, O2573.
19. T. M. R. Maria, M. E. S. Eusebio, J. A. Silva, A. J. F. N. Sobral, C. Cardoso , J. A. Paixao, M. R. Silva, *J. Mol. Struct.*, 2012, **1030**, 67.
20. T. A. Zeidan, J. T. Trotta, R. A. Chiarella, M. A. Oliveira, M. B. Hickey, O. Almarsson, J. F. Remenar, *Cryst. Growth Des.*, 2013, **13**, 2036.
21. S. Long, S. Parkin, M. A. Siegler, A. Cammers, T. Li, *Cryst. Growth Des.,* 2008, **8**, 4006.
22. J. M. Kelleher, M. T. McAuliffe, H. A. Moynihan, N. D. Mullins, *ARKIVOC.*, 2007, **16**, 209.
23. G. Lei, L. -H. Jing, L. Zhou, *Acta Crystallogr.,* 2008, **E64**, o2401.
24. M. C. Etter, *Acc. Chem. Res.*, 1990, **23**, 120.
25. C. R. Martinez, B. L. Iverson, *Chem. Sci.*, 2012, **3**, 2191.

26. G. R. Desiraju, T. Steiner, *The weak hydrogen bond in structural chemistry and biology, Oxford University Press, Oxford,* 1999.
27. K. Kawakami, *J. Pharm. Sci*., 2007, **6**, 982.
28. G. W. H. Hohne, W. Hemminger, H. -J. Flammersheim, *Differential Scanning Calorimetry, second rev. ed., Spinger-Verlag Publisher, Berlin, Heidelberg*, 2003.
29. A. L. Grzesiak, M. Lang, K. Kim, A. J. Matzger, *J. Pharm. Sci*., 2003, **92**, 2260.
30. R. J. Sarma, J. B. Baruah, *Solid State Sci*., 2008, **10**, 580.
31. W. M. Bloch, C. J. Sumby, *Chem. Commun*., 2012, **48**, 2534.
32. Z. Duan, Y. Zhang, B. Zhang, D. Zhu, *Cryst. Eng. Comm*., 2011, **13**, 680.
33. Z. -Y. Liu, E. -C. Yang, L. -L. Li, X. -J. Zhao, *Dalton Trans*., 2012, **41**, 6827.
34. A. Aijaz, P. Lama, P. K. Bharadwaj, *Inorg. Chem*., 2010, **49**, 5883.
35. X. Cui, A. N. Khlobystov, X. Chen, D. H. Marsh, A. J. Blake, W. Lewis, N. R. Champness, C. J. Roberts, M. Schroder, *Chem. Eur. J*., 2009, **15**, 8861.
36. S. Venugopalan, S. N. Prasad, *J. Chem. Phys*., 1980, **72**, 4153.
37. S. K. Nayak, K. N. Venugopala, D. Chopra, T. N. Guru Row, *CrystEngComm*., 2011, **13**, 591.
38. S. G. Bott, A. W. Coleman, J. L. Atwood, *J. Am. Chem. Soc*., 1988, **110**, 610.
39. A. J. Blake, P. Hubberstey, U. Suksangpanya, C. L. Wilson, *J. C. S. Dalton Trans*., 2000, 3873.
40. C. A. Ilioudis, K. S. B. Hancock, D. G. Georganopoulou, J. W. Steed, *New J. Chem*., 2000, **24**, 787.
41. C. Tamuly, R. J. Sarma, A. S. Batsanov, A. Goeta, J.B. Baruah, *Acta Crystallogr*., 2005, **61C**, 0324.
42. G. A. Stephenson, E. G. Groleau, R. L. Kleemann, W. Xu, D. R. Rigsbee, *J. Pharm. Sci*., 1998, **87**, 536.
43. V. Balzani, J. F. Stoddart, *Angew. Chem*., 2000, **112**, 3484.
44. J. S. Hannam, S. M. Lacy, D. A. Leigh, C. G. Saiz, A. M. Z. Slawin, S. G. Stitchell, *Angew. Chem*., 2004, **43**, 3260.

Chapter 5

Synthesis, characterization and anti-malarial study of quinoline derivatives, salts and cocrystal

Quinolines based molecules are used as drugs.[1-9] Many quuinoline derivatives are used as antimarial agents and quinoline based antimalarial drugs are of special interest because of their ability to form inclusion compound by forming stacked structures with β-hematin.[10-11] β-Hematin is a constituent of blood has a carboxylate group containing arm that coordinates to a iron ion to form dinuclear structure. The dinuclear nature of hematin has an important role to provide the space for stacking interactions to accommodate quinoline based drug molecules.[10] Moreover, formation of polymorph or salts/cocrystals of a drug molecule may change the effectiveness of drugs activities. This is due to the fact that salts or cocrystals formation enhance solubility, stability, bioavailability of active pharmaceutical ingredients (API). Hence, it would be of interest to look at the binding of quinoline derivatives with another drug related molecule such as hydroxycarboxylic acids; to look at their possible packing interactions among the host and guest molecules.[12-19] Further, such a study would help to understand the potential of a cocrystal or salt to act as a drug.[20-23] Structural study have established the salt formation ability of 4-aminopyridine with hydroxycarboxylic acids, namely 2- and 4-hydroxybenzoic acid and 3,4,5-trihydroxybenzoic acid.[24] Based on such available data we set to study formation salts and cocrystal of structural isomers of aminoquinolines with different hydroxyaromatic carboxylic acids. 5-Aminoquinoline has some structural similarities with 4-aminopyridine, but the directional properties by virtue of the positions of the donors and acceptors in this molecule make a difference. Later molecule has multiple numbers of rings making it more potential candidate for stacking effect. On the other hand, 8-aminoquinoline has nitrogen atom in the ring and an amino group that may contribute to weak interactions, whereas 5-aminoquinoline is expected to generate linear structures. Another interest to study on the structure of such salts or cocrystals would be to ascertain the role of quinoline to retain intramolecular hydrogen bonds of

hydroxy groups next to a carboxylic acid group in a salt or cocrystal partner. The salts and cocrystal of quinolines and hydroxyaromatic carboxylic acids were tested for their antimalarial activities and such with neutral compounds derived from aminoquinoline. The salts and cocrystal investigated in this study are listed in Chart 5.1.

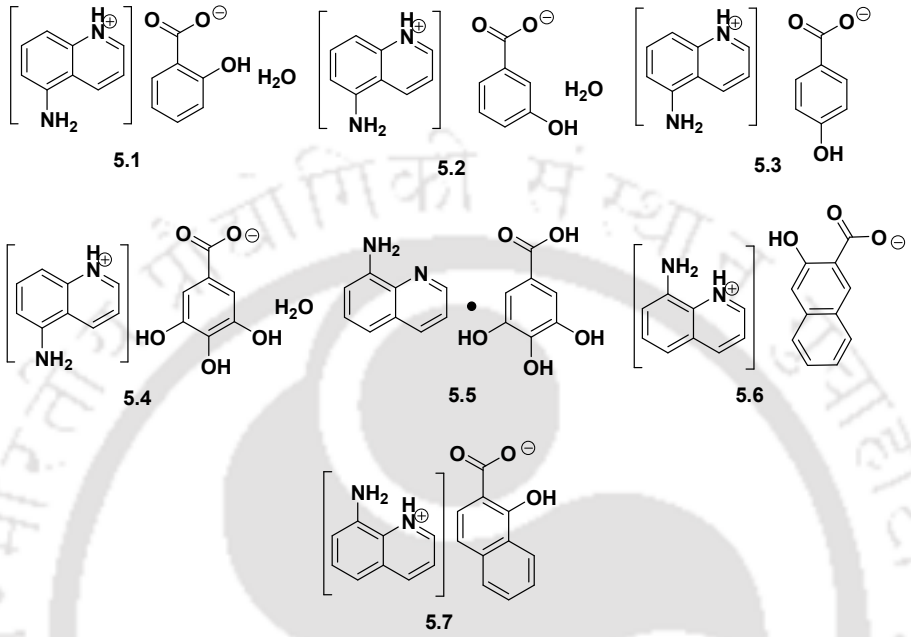

Chart 5.1: Salts and cocrystal of aminoquinolines with hydroxyaromatic acids.

5.1: Structural features of salts and cocrystal

When a carboxylic acid interact with a nitrogen containing molecule it can form a cocrystal by sharing the hydrogen atom of the acid with base counterpart, or it may form a salt by a complete proton transfer from acidic part to nitrogen atom of the Lewis base. Childs *et al*. reported that location of the proton of acid-base adduct can be distinguished from their Δp*K*a values; formation of salt or cocrystal is determined by Δp*K*a value between a base and acid. If Δp*K*a (Δp*K*a = p*K*a (base) - p*K*a (acid)) is greater than 2 or 3 forms salt while smaller Δp*K*a values forms cocrystal.[20] It is also reported that parameter is inappropriate for accurately predicting salt formation in the solid state when Δp*K*a is between 0 and 3.[21]

The salt formed from the reaction between 5-aminoquinoline and 2-hydroxybenzoic acid was 5-aminoquinolinium 2-hydroxybenzoate monohydrate (**5.1**). The salt **5.1** crystallizes in orthorhombic $P2_12_12_1$ space group. It is comprised of one 2-hydroxybenzoate anion, one 5-aminoquinolinium cation and a water molecule as solvent of crystallization in the crystal lattice

(Figure 5.1a). 2-hydroxybenzoic acid and 5-aminoquinoline have Δp*Ka* value greater than 2.[25-29] In the crystal lattice of **5.1**, the 2-hydroxybenzoate anion are present as discrete units and they possesses intramolecular hydrogen bond formed between the hydroxy group and one of the oxygen atom of carboxylate group. The anions are nearly in same plane; they are arranged along *c*-crystallographic axis in a sheet like arrangement. The 5-aminoquinolinium cations are present perpendicular to these layers and they are anchored by hydrogen bonds with the carbonyl group of anions and also through electrostatic interactions of $^{+}$N-H with the anions (Figure 5.1b). The salt has intramolecular hydrogen bond similar to the parent acid. They are further held by N-H···π interactions [N1-H···π; $d_{D\cdots A}$, 3.523Å]. The larger polarizing ability of -NH_2 group compared to an -OH group and due to the strong electrostatic interactions operating in the packing pattern facilitates such N-H···π interactions.

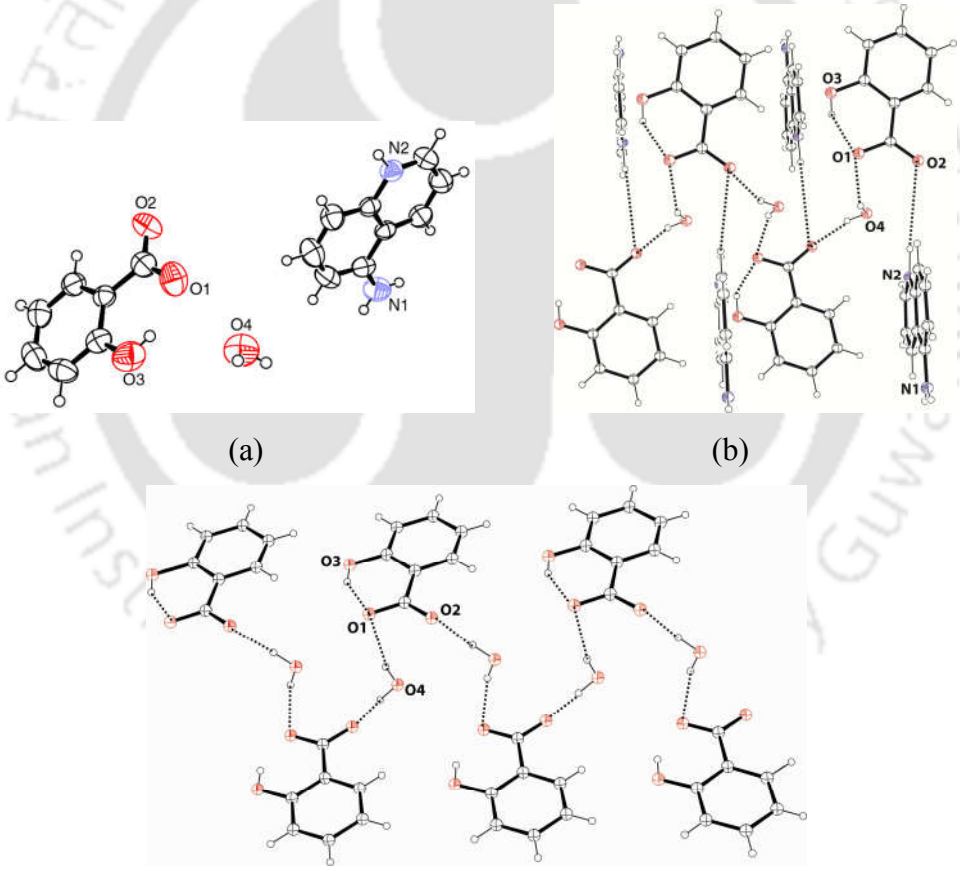

Figure 5.1: (a) Structure of **5.1** (ORTEP drawn with 35 % thermal ellipsoid), (b) Hydrogen bonds in **5.1** and (c) The arrangement of the 2-hydroxybenzoate anions in the crystal lattice of **5.1** after exclusion of 5-aminoquinolinium actions.

It was earlier suggested that the polarisability of electrons plays a crucial role in such systems.[24] Thus, the protonation on the nitrogen atom of quinoline and availability of an appropriate π-cloud in the vicinity is responsible to have the N-H···π interactions in salt **5.1**. The water molecules act as support to hold the quinolines and carboxylic acids. The quinoline molecules interact with oxygen atoms of water molecules through C13-H···O4 interactions; whereas both the O-H bonds of water molecules are held to oxygen atoms of carbonyl groups of two independent molecules from two layers (figure 5.1c). The strong hydrogen bond interactions make the acidic OH group unavailable to interact with another anion. Thus, the anions form supramolecular assembly assisted by water molecules. Various water assisted assemblies of salts of hydroxycarboxylic acids with aromatic amines were earlier shown and their packing patterns were found to be guided by the substituent on the aromatic rings.[30] From a CSD analysis it was also pointed out that the pyridine carboxylates have higher tendency to form hydrated salts.[31] In our case the water molecules do not interact with the quinolinium cations through N-H···O interactions, but interact through C-H···O interactions (weakest among the H-bonds discussed), suggests that the water molecules acts as filler molecules in the crystal lattice.

The asymmetric unit of the crystal structure of the salt **(5.2)** of 3-hydroxybenzoic acid and 5-aminoquinoline has symmetry non-equivalent molecules of two 3-hydroxybenzoate anions along with the 5-aminoquinolinium cations (figure 5.2a). The cations and anions form stacked arrangements. The cations are in head to tail arrangement (i.e. facing opposite dipoles) to meet the energetically favorable geometry for the dipolar interactions between them. The layer like structures of the cations is separated by 3-hydroxybenzoate anions. The anions are responsible to form a stable packing pattern by interacting with two cations through $^{+}$N-H···O and N-H···O interactions (figure 5.2b). One set of 5-aminoquinolinium cations are held by hydrogen bonds between the N-H bonds and carbonyl oxygen atoms (Table 5.1).

Table 5.1: Hydrogen bond parameters in **5.1-5.3.**

Compound No.	D-H···A	$d_{D\text{-}H}$(Å)	$d_{H\cdots A}$(Å)	$d_{D\cdots A}$(Å)	∠ D-H···A(º)
5.1	N2-H···O2 [1-x,-1/2+y,3/2-z]	1.06(3)	1.69(3)	2.73(3)	169(3)
	O3-H···O1	0.82	1.77	2.50(3)	148
	O4-H···O1 [1/2-x,1-y,-1/2+z]	0.83(6)	2.16(6)	2.96(4)	165(5)
	O4-H···O2 [x, y,-1+z]	0.94(4)	1.89(4)	2.80(4)	168(4)
	C13-H···O4 [1/2+x,1/2-y,1-z]	0.93	2.58	3.26(3)	131

5.2	N1-H···O8 [1-x,-y,1-z]	0.86	2.21	2.96(14)	145
	N1-H···O2 [1-x,1-y,1-z]	0.86	2.15	2.93(16)	152
	N2-H···O1	0.86	1.80	2.66(13)	177
	N3-H···O7	0.86	2.20	2.98(14)	152
	N3-H···O4 [-x,y,1/2-z]	0.86	2.18	2.92(18)	145
	O3-H···O4 [x,1-y,-1/2+z]	0.82	1.88	2.63(16)	153
	N4-H···O5 [x,2-y,-1/2+z]	0.86	1.82	2.68(19)	179
	O6-H6···O2	0.82	1.96	2.70(18)	150
5.3	N1-H···O2 [x,1+y,z]	0.96	1.75	2.65(4)	157
	N2-H···O2	0.86	2.23	3.04(4)	159
	N2-H···O1 [-x,-y,-z]	0.86	2.08	2.91(4)	163
	O3-H···O1 [1-x,1/2+y,1/2-z]	0.80	1.90	2.64(4)	153

Close examination shows that the neighboring symmetry non-equivalent 3-hydroxybenzoate anions are hydrogen bonded to each other through hydroxy group of one anion with carboxylate group of another; they make spiral arrangement in the packing pattern as illustrated in figure 5.2c.

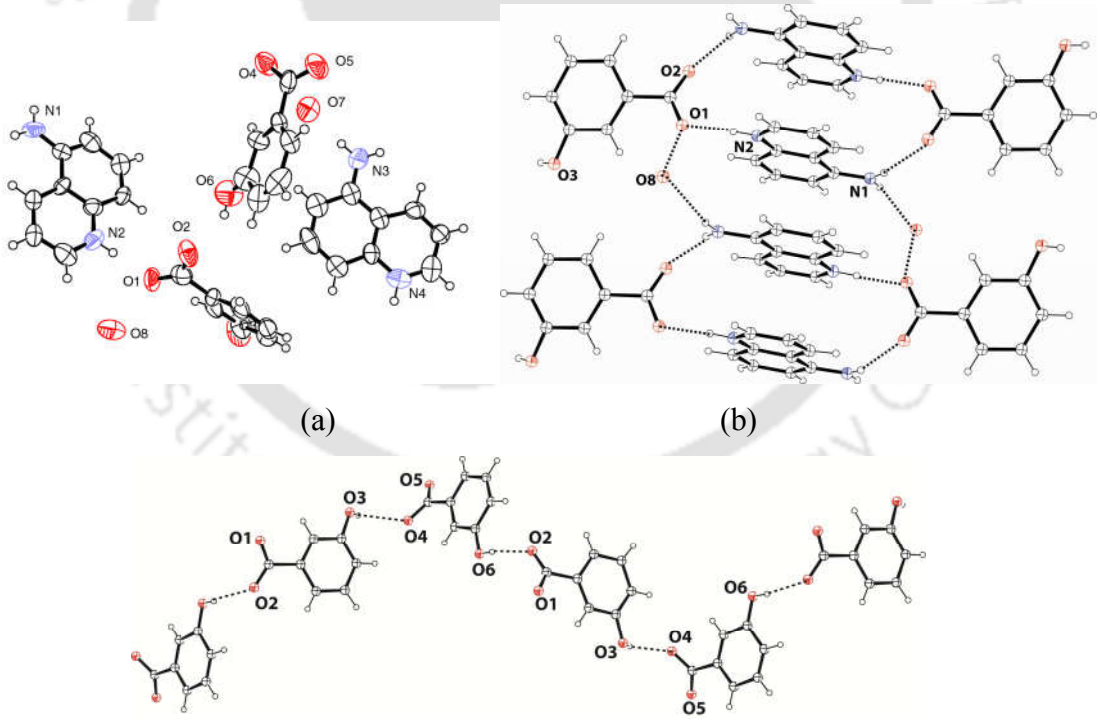

Figure 5.2: (a) Structure of **5.2** (ORTEP drawn with 35 % thermal ellipsoid), (b) Hydrogen bond interactions in **5.2** showing two symmetry non-equivalent molecules in two different colors and (c) Arrangement of carboxylate anions in the lattice.

The neighboring cations are not in one plane and they are twisted with respect to each other. This could be one of the reasons to make them symmetry non equivalent. Difference in the structural pattern of **5.2** in comparison with **5.1** is that in former case the water molecules are associated with O-H···O and N-H···O interactions with the cations and anions to make the self-assembled structure, whereas in later case it is through O-H···O and C-H···O interactions.

The Δp*K*a value of 4-hydroxybenzoic acid with 5-aminoquinoline is nearly 1, accordingly the 4-hydroxybenzoic acid reacted with 5-aminoquinoline to form salt **5.3** in anhydrous form.[25-29] The salt **5.3** has a relatively simple structure (figure 5.3a). Spiral chain-like assemblies are formed among the anions by intermolecular hydrogen bonds between hydroxy groups and carboxylate groups (figure 5.3b) of these anions. The spiral chains are held together by hydrogen bond interactions of amino group and $^{+}$N-H groups of the cations as illustrated in figure 5.3c. The hydrogen bond parameters are listed in Table 5.1.

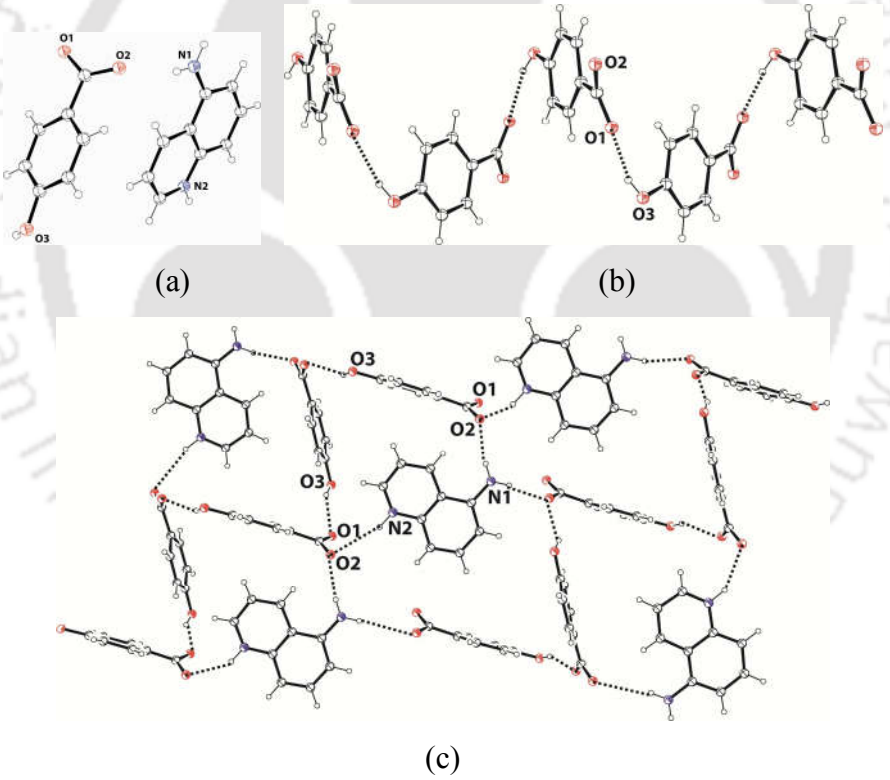

Figure 5.3: (a) Structure of the **5.3**, (b) Arrangements of 4-hydroxybenzoate anions in the lattice and (c) Hydrogen bond interactions in **5.3**.

In the case of the 3,4,5-trihydroxybenzoic acid, which is also known as gallic acid and 5-aminoquinoline the Δp*K*a is less than 1,[25-29] here too we obtained a monohydrated salt, (**5.4**).

The unit cell of salt **5.4** contains two gallate anions and two 5-aminoquinolinium cations. Out of these, there is a pair of highly disordered cation and anion as shown in the figure 5.4a. We have resolved this disorder, as the two overlapping structures. We have to accommodate two different groups at opposite sites namely a carboxylic acid and hydroxy groups. This is to be done by 180º rotation of a molecule on top of another molecule in which later is hold fixed.

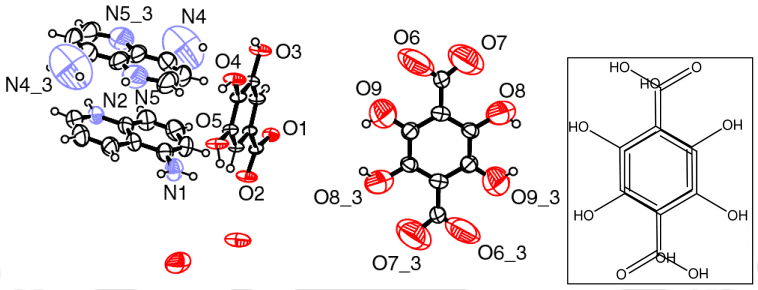

(a)

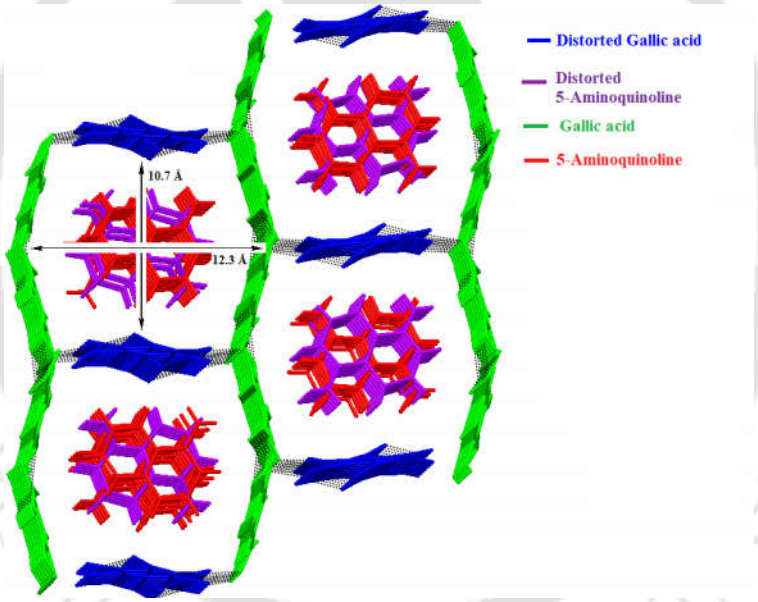

(b)

Figure 5.4: (a) Structure of salt **5.4** (ORTEP drawn with 35 % thermal ellipsoids). Inset is showing the type of disorder observed due to tumbling of two molecules of gallic acid. (b) The channels showing the encapsulation of cations.

The 5-aminoquinolinium cations are held in the channels formed by the gallate anions as illustrated in figure 5.4b. Since electrostatic interactions assisted the formation of channel like structure in this salt, the cations within the channels adopt disordered structure. The cations adopt

disordered structure due to two rotational structures that can be put up-side down parallel on the top of each other. To adopt such disordered structure a combination of two orientations are required (inset of figure 5.4a). The packing pattern of the salt shows the formation of two layers from the self assembly of gallate anions in which partitions are from the disordered gallate anions. The cations are held as layers one on the top of the other in a sequence of 5-aminoquinolinium cations which are not disordered followed by disordered one. The observed disorder is thus attributed to the non-rigidity caused by electrostatic interactions in an unsymmetrical molecule to adopt two optional orientations across the aromatic heterocyclic ring. Similarly, we attempted to get crystalline products from the reactions of 8-aminoquinoline with gallic acid, 2-hydroxy-3-naphthoic acid and 1-hydroxy-2-naphthoic acid but, we could obtain cocrystal in case of 8-aminoquinoline with gallic acid (**5.5**). The cocrystal formation in this case is attributed to the difference in p*K*a values between 8-aminoquinoline and gallic acid, which is less than zero (Figure 5.5a).[25-29] It is interesting to note that the $R^2_2(8)$ type of cyclic hydrogen bond motifs among carboxylic acid group is observed which gives dimeric units. The dimers are arranged in one dimension so that all the hydroxy groups are pointing towards each other from two different dimeric units (figure 5.5b).

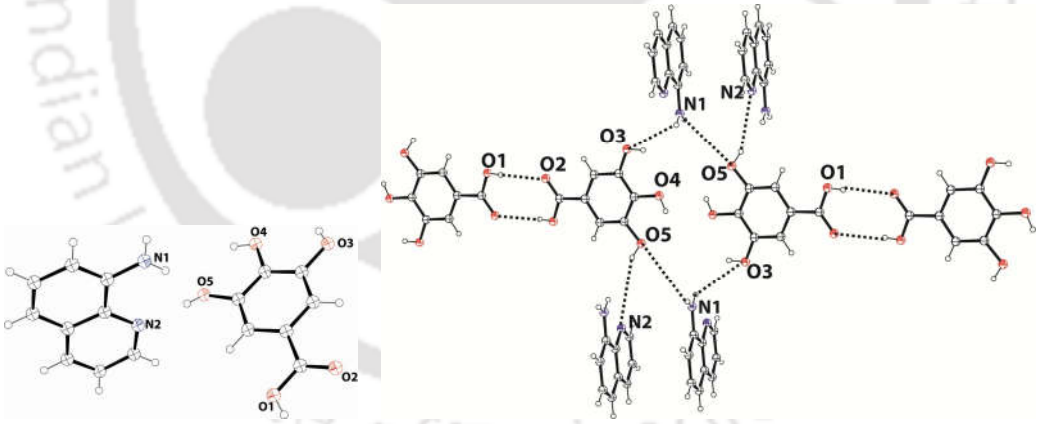

(a) (b)

Figure 5.5: (a) The structure of cocrystal **5.5** (ORTEP drawn with 35 % thermal ellipsoids) and (b) Hydrogen bond interactions.

The dimers are bridged by amino group of the 8-aminoquinoline to make cyclic type of hydrogen bonded units. The hydrogen bond parameters are listed in Table 4.2. The structure of gallic acid monohydrate is comprised of hydrogen bonded dimers extending in one plane as polymeric

chain.[32] Furthermore, in the extended structure each gallic acid molecule is linked by bridging water molecule.[32] The amino group of 8-aminoquinoline plays a similar role in the structure of **5.5** as that of the role of water molecule in the structure gallic acid monohydrate. But due to the presence of two nitrogen binding sites in 8-aminoquinoline (namely N-atom and amine group) it does not allow the formation of sheets. Thus, in the structure of the cocrystal **5.5** the sheet-like structure is segregated to a chain like structure among the gallic acids.

Table 5.2: Hydrogen bond parameters of **5.5-5.7**.

Compound No.	D-H····A	d_{D-H}(Å)	$d_{H\cdots A}$(Å)	$d_{D\cdots A}$(Å)	< D-H····A(º)
5.5	O1-H···O2 [-x,-y,1-z]	0.82	1.83	2.65(3)	179
	N1-H···O3 [x,y,-1+z]	0.86	2.37	3.17(3)	154
	N1-H···N2	0.86	2.46	2.77(3)	102
	O3-H···O4	0.82	2.35	2.76(2)	113
	O3-H···N1 [1+x,y,1+z]	0.82	2.01	2.77(3)	156
	O4-H···O5	0.82	2.20	2.65(3)	115
	O5-H···N2 [1-x,-y,1-z]	0.82	1.94	2.73(3)	162
	C11-H···O2 [x,1/2-y,-1/2+z]	0.93	2.59	3.44(4)	152
	C14-H···O3 [-1+x,1/2-y,-1/2+z]	0.93	2.58	3.29(4)	134
5.6	N1-H···O1 [-x,-y,1-z]	0.96	1.69	2.64	173
	N2-H···O1 [-x,-y,1-z]	0.95	2.09	2.98	154
	N2-H···O2 [-1/2-x,1/2+y,1/2-z]	0.81	2.38	3.16	163
	O3-H···O2	0.82	1.79	2.52	149
	C1-H···O2 [-x,-y,1-z]	0.93	2.37	3.09	134
	C2-H···O3 [1/2+x,1/2-y,1/2+z]	0.93	2.39	3.28	161
	C19-H···O1	0.93	2.48	2.80	100
5.7	O1-H···O2	0.82	1.90	2.55	135
	N2-H···O5 [-1+x, y, -1+z]	0.89	2.12	2.98	161
	N2-H···N1	0.89	2.39	2.82	110
	N2-H···O2 [-1+x, y, z]	0.89	2.17	2.95	148
	N4-H···O3	0.89	2.39	2.89	116
	N4-H···O6 [-1+x, y, -1+z]	0.89	2.15	3.01	165
	C14-H···O5	0.93	2.44	2.75	100
	O1-H···O2	0.82	1.90	2.55	135

Similarly, the difference p*Ka* values between 2-hydroxy-3-naphthoic acid and 8-aminoquinoline is less than 2,[25-29] as expected they form a salt **5.6** in 1:1 ratio (figure 5.6a). In the structure of the salt of 2-hydroxy-3-naphthoic acid with 8-aminoquinoline, there are two bifurcated hydrogen bonds, first one is associated with the O2 atom of carboxylic acid group to hold two independent

quinolinium cations. This bifurcated hydrogen bond occurs by interactions of the amino group and C1-H bond with O2-atom as shown in figure 5.6c. The second bifurcated hydrogen bond involves O1 atom, it holds one quinoline molecule through interactions with amino group and $^{+}$N-H bond.

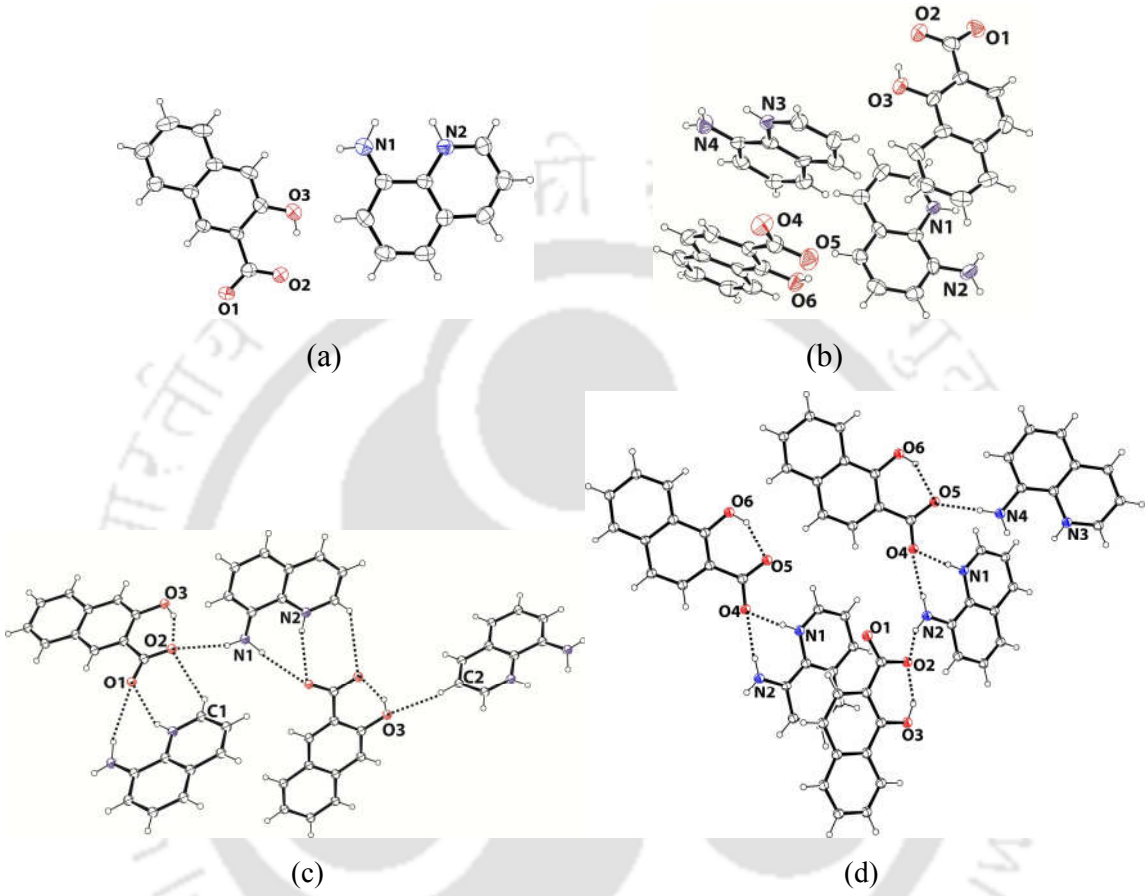

Figure 5.6: structure of (a) salt **5.6** and (b) salt **5.7** (ORTEP each drawn with 35 % thermal ellipsoids). Hydrogen bond interactions in salts (c) **5.6** and (d) **5.7**.

The quinoline nitrogen atom within the ring is protonated, while the hydroxy group of the 2-hydroxynapthoate remains undisturbed. There is an intramolecular hydrogen bond between the hydroxy group and carboxylate group.

Again, a salt was obtained in the case of reaction of 1-hydroxy-2-naphthoic acid with 8-aminoquinoline with Δp*K*a value less than 2.[25-29] The structure of the salt **5.7** so formed is shown in figure 5.6b. The salt **5.7** also has intramolecular hydrogen bond between hydroxy group and carboxylate anion as illustrated in figure 5.6d. Bifurcated hydrogen bonds between O4 with N2-

H and $^{+}$N1-H bonds in one pair of symmetry non-equivalent of cation and anion as well as $^{+}$N3-H···O1 and N4-H···O1in another pair are observed.

The packing patterns of **5.6** as well as **5.7** have contributions from the π···π interactions among the rings of the cationic and anionic counterparts. In these cases a small portion of the rings positioned parallel is on top of each other hence the π···π interactions are oblique type interactions, which is a frequently observed in aromatic stacking interactions. [33]

To find the differences between cocrystal and salts which formed by sharing of proton or proton exchange respectively, IR spectra of the OH region (2000 cm^{-1} to 4000 cm^{-1}) and carbonyl stretching region (1400 cm^{-1} to 1800 cm^{-1}) of salt **5.4** and cocrystal **5.5** are compared with gallic acid. It is found that OH stretching region of gallic acid and cocrystal **5.5** are have resemblances (figure 5.7a), whereas salt **5.4** shows stretching frequencies at 3458 cm^{-1}, 3348 cm^{-1} and

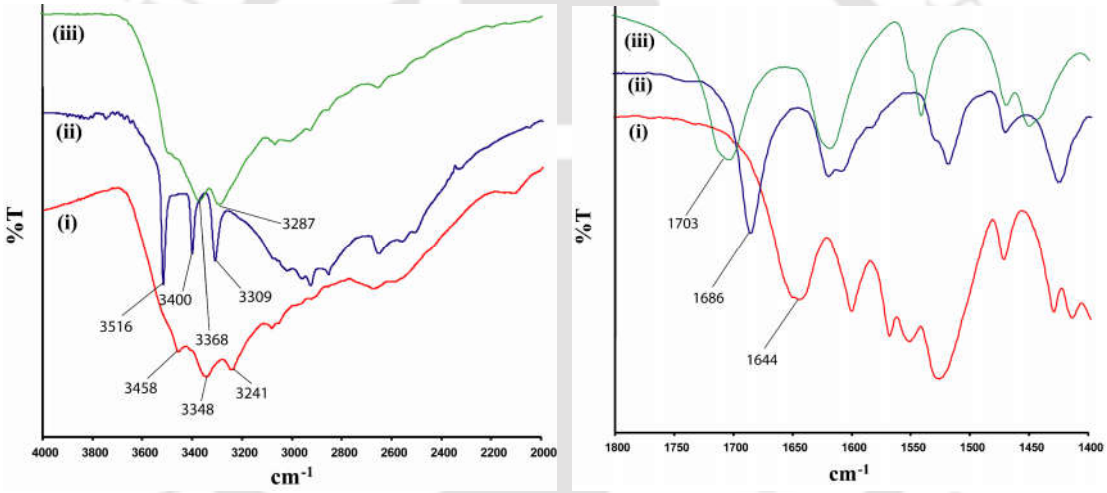

(a) (b)

Figure 5.7: FT-IR spectra of salts/cocrystal (a) in range 2000 cm^{-1} to 4000 cm^{-1} (i) Salt **5.4**, (ii) adduct **5.5** and (iii) Gallic acid; and (b) in the range 1400 cm^{-1} to 1800 cm^{-1} of (i) Salt **5.4**, (ii) Adduct **5.5** and (iii) Gallic acid.

3241 cm^{-1}; which shows structural differences occurred due to proton transfer to form the salt in case of **5.4**. On the other hand the carbonyl stretching of gallic acid appears at 1703 cm^{-1}, such stretching appear at 1644 cm^{-1} and 1686 cm^{-1} respectively (figure 5.7b) in the salt **5.4** and in the cocrystal **5.5**. As it can be seen that C=O stretching of gallic acid in salt has shifted to lower frequency compared to stretching in cocrystal, suggesting the deprotonated carboxylic group of

gallate in salt **5.4**. We have confirmed that there is no overlapping peaks from the quinoline counter part with the stretching of carboxylic counterpart in the 1400 cm^{-1}-1800 cm^{-1} region.

5.2: Antimalarial study

After establishing the structures of the salts and cocrystal we have studied antimalarial properties of the salts andcocrystal to compare such properties with covalently linked derivatives of quinoline. We have sorted out a few compounds derived from aminoquinolines derivatives. The structural compositions of the salts, cocrystal and derivatives of aminoquinoline taken up for antimalarial study are shown in figure 5.8.

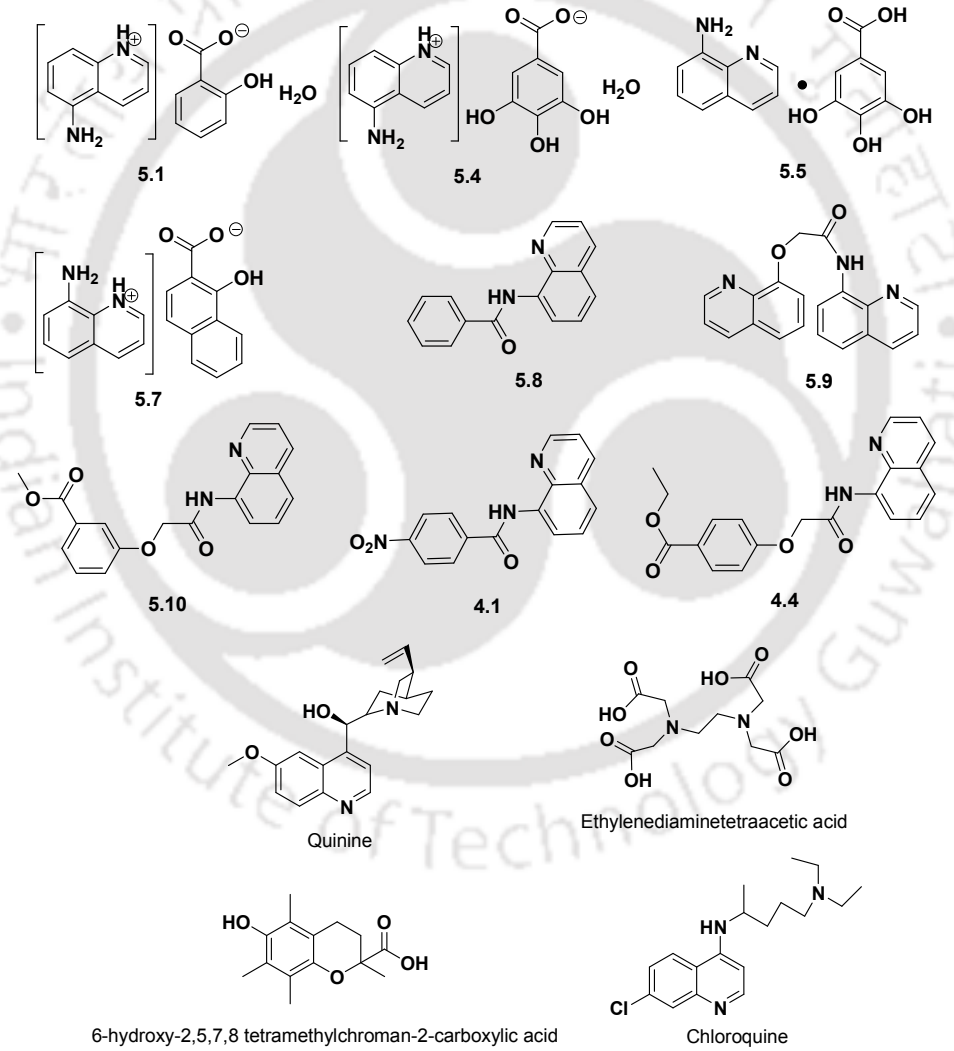

Figure 5.8: Salts, cocrystal and derivatives of aminoquinoline.

Among the five aminoquinoline derivatives those were tested for animalarial activity, compounds **5.8**[34] and **5.9**[35] were reported in literature. Each salt **5.1, 5.4** and **5.7** as well as cocrystal **5.5** showed antimalarial activity with IC_{50} values in 6-20 μM range for the chloroquine-resistant strain, but was four fold less active against the chloroquine-sensitive strain (Table 5.3).

Table 5.3: Antimalarial activities of different salts, cocrystal and compounds.

Compound name	Antimalarial activity IC_{50} ± S.D. (μM) (% Parasite growth at 50 μM)		% β-Haematin formation inhibition at 50 μM	% Iron chelation at 50 μM	% Free radical scavenging activity at 50 μM	% Red blood cell lysis at 50 μM
	FCR-3 strain	3D7 strain				
Salt **5.1**	9.34 ± 2.10	34.6 ± 3.19	0.1 ± 0.01	0.1 ± 0.01	21.4 ± 0.62	3.64 ± 1.2
Salt **5.4**	5.91 ± 1.12	25.1 ± 1.30	10.8 ± 1.86	0.1 ± 0.01	18.5 ± 3.71	1.29 ± 0.67
Cocrystal **5.5**	14.18 ± 3.12	75.4 ± 5.12	0.1 ± 0.01	0.1 ± 0.01	5.22 ± 0.26	1.01 ± 0.33
Salt **5.7**	20.33 ± 3.82	104.1 ± 16.5	0.1 ± 0.01	0.1 ± 0.01	6.12 ± 0.90	0.15 ± 1.58
Compound **5.8**	n.d.	> 50 (80.9 ± 3.44%)	0.1 ± 0.01	0.1 ± 0.01	0.1 ± 0.01	0.38 ± 0.25
Compound **5.9**	12.52 ± 2.07	25.2 ± 3.62	0.1 ± 0.01	22.4 ± 4.96	2.02 ± 0.16	3.67 ± 0.30
Compound **5.10**	n.d.	> 50 (76.7 ± 4.48%)	0.1 ± 0.01	21.4 ± 4.29	0.1 ± 0.01	0.85 ± 1.10
Compound **4.1**	n.d.	> 50 (95.4 ±2.36%)	0.1 ± 0.01	18.6 ± 4.64	0.1 ± 0.01	0.06 ± 0.24
Compound **4.4**	n.d.	> 50 (76.5 ± 6.34%)	0.1 ± 0.01	13.6 ± 1.77	0.1 ± 0.01	0.85 ± 0.26
Quinine	0.17 ± 0.03	0.09 ± 0.01	n.d.	n.d.	n.d.	8.22 ± 2.17
Chloroquine	0.12 ± 0.01	0.0065 ±0.001	43.6 ± 13.0	n.d.	n.d.	2.09 ± 0.59
Ethylenediaminetetraacetic acid (EDTA)	n.d.	n.d.	n.d.	24.8 ± 1.59	n.d.	n.d.
Trolox™ (6-hydroxy-2,5,7,8 tetramethylchroman-2-carboxylic acid)	n.d.	n.d.	n.d.	n.d.	19.1 ± 1.14	n.d.

n.d = Not done

The activity was slightly less when compared to the quinine standard. 8-Aminoquinoline and 5-aminoquinolin[36] shows IC_{50} values greater than 10μM. On the other hand, 6-(8′-pentadecenyl)-salicylic acid[37] has an IC_{50} value of 10.1μM, 3,5-dihydroxy 2-naphthoic acid[38] has IC_{50} value 25 μM and gallic acid[39] has an IC_{50} value of 71.5 μM. Thus, IC_{50} values for salts and cocrystal are much less than individual components. This clearly indicates the combine effect of two active components changes their effective anti-malarial activities. Derivatisation of aminoquinoline did not enhance antimalarial activity, but instead displayed minimal antimalarial activity at 50 μM when tested against the chloroquine-sensitive strain (Table 5.3). Aminoquinoline compounds are known to chelate metals such as iron with potential free radical scavenging activity,[40] but these properties were not retained with these salts, cocrystal and derivatives of aminoquinolines. None of these were able to inhibit β-haematin or haemozoin formation as a mechanism of action, as has been shown for 2-amino-8-hydroxyquinoline.[41] Among the individual quinoline derivatives the bis-quinoline derivative **5.8** is a good chelator for iron, shows antimalarial activities comparable to the salts.

All the tested compounds retained a good safety profile and did not affect the membrane integrity of the red blood cell.[42] Salts of gallic acid have low IC_{50} values. Cooperative effects of two substrates provide extra potency to such compositions. However, use of poly-hydroxyaromatic carboxylic acid as one component, they not only enhance water solubility but helps to maintain neutral condition by neutralizing quinoline counterpart. In order to gain support towards importance of salt over a covalent compound we studied the antimalarial activity of compound **5.8-5.10** (Table 5.3). IC_{50} value of **5.4** is less than **5.5**, as in these cases the gallic acid is a common component. Thus quinoline counterpart changes antimalarial activities.

5.3: Conclusion

It is established that from the *p*Ka differences of the partner compounds the salt and cocrystal were formed in a predictive manner in the case of different combinations of aminoquinolines and hydroxyaromatic carboxylic acids. Water assisted anionic assemblies are observed in the case of the hydrated salt. A channel like structure was observed in the salt of gallic acid with 5-aminoquinoline. It is seen that salts and adduct of quinoline with hydroxy-aromatic acid enhance antimalarial activities over parent compounds. Enhanced nature could be attributed to the increase in hydrophilicity of these salts and adducts through proton sharing or proton transfer

between the two counterparts. The tested amides of aminoquinolines were not potent. Moreover, antimalarial actions on the parasites by the salt **5.4** are comparable with safety profile to chloroquine and independent of iron chelation as well as haemozoin formation.

5.4: Experimental

The detailed synthetic methodologies for synthesis of the metal complexes are described. Analytical data are provided with each complex. The instrumental details and crystallographic parameters are provided in Appendix.

Synthesis of 5.1:

The salt **5.1** was prepared from 1:1 (molar ratio) mixture of *5*-aminoquinoline with 2-hydroxybenzoic acid dissolved together in methanol and were kept undisturbed for crystallization. After 3-4 days obtained crystals of salt **5.1**. Yield ~ 90 %. IR (KBr, cm^{-1}): 3444 (s), 3321(m), 3082 (w), 1627 (s), 1589 (s), 1566 (m), 1482 (m), 1454(m), 1432 (w), 1384 (m), 1361(m), 1330 (m), 1305 (w), 1252 (w), 1138 (w), 1028 (w), 859(w), 787 (m), 702 (w), 664 (w). ^{1}H-NMR (400 MHz, DMSO-d_6): 8.79 (d, J = 4.0 Hz, 1H), 8.59 (d, J = 8.4 Hz, 1H), 7.79 (d, J = 7.6 Hz, 1H), 7.49 (m, 2H), 7.41 (q, J = 4.0 Hz, 1H), 7.19 (d, J = 8.4 Hz, 1H), 6.93 (d, J = 8.0 Hz, 2H), 6.73 (d, J = 8.0 Hz, 2H), 4.18 (s, 2H), 2.53 (s, 2H).

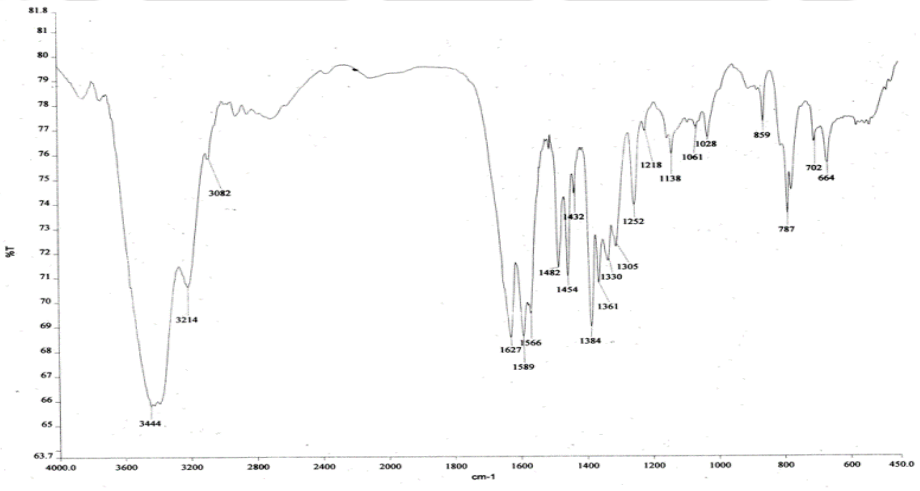

Figure 5.10: FT-IR (KBr, cm^{-1}) spectra of salt **5.1**.

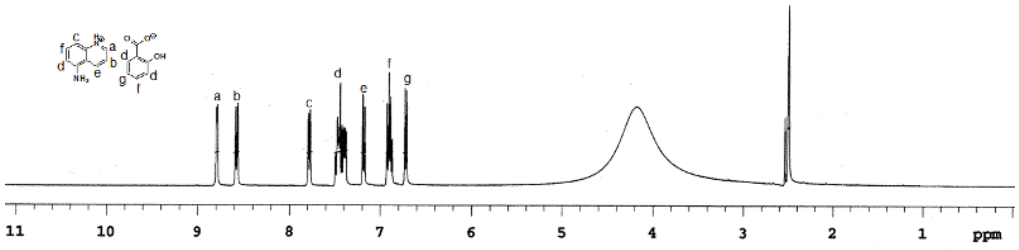

Figure 5.11: ^{1}H-NMR (400 MHz, DMSO-d_6) spectra of salt **5.1**.

Synthesis of 5.2:

The salt **5.2** was prepared from 1:1 (mole ratio) mixture of *5*-aminoquinoline with 3-hydroxybenzoic acid dissolved together in methanol and were kept undisturbed for crystallization. After 3-4 days obtained crystals of salt **5.2**. Yield ~ 90 %. IR (KBr, cm^{-1}): 3388 (s), 3227 (m), 2923 (w), 1665 (w), 1599 (w), 1537 (w), 1473 (w), 1431 (w), 1395 (s), 1364 (s), 1312 (w), 1227 (m), 1177(w), 1149 (w), 931(w), 889 (w), 795 (m), 777 (m), 702 (w).

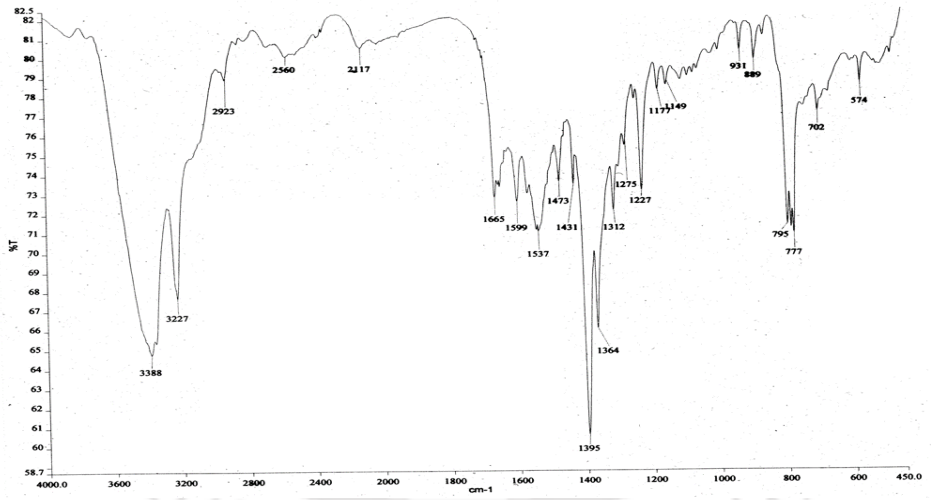

Figure 5.12: FT-IR (KBr, cm^{-1}) spectra of salt **5.2**.

Synthesis of 5.3:

The salt **5.3** was prepared from 1:1 (mole ratio) mixture of *5*-aminoquinoline with 4-hydroxybenzoic acid dissolved together in methanol and were kept undisturbed for crystallization. After 3-4 days obtained crystals of salt **5.2**. Yield ~ 92 %. IR (KBr, cm^{-1}): 3445 (s), 3171 (m), 2925 (w), 1635 (m), 1599 (s), 1530 (w), 1506 (w), 1434 (w), 1360 (m), 1311 (w), 1281 (m), 1248 (w), 1164 (w), 848 (w), 788 (m), 703(w), 614(w).

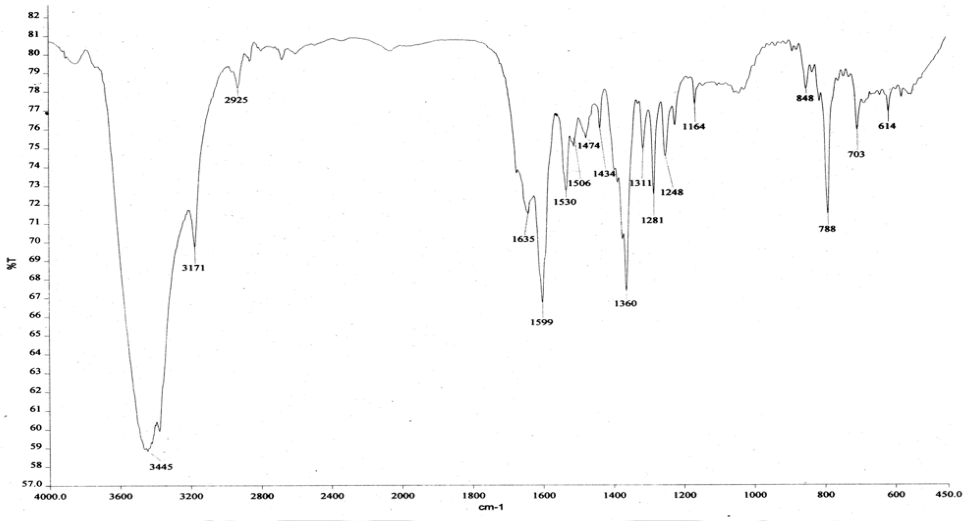

Figure 5.13: FT-IR (KBr, cm^{-1}) spectra of salt **5.3**.

Synthesis of 5.4:

The salt **5.4** was prepared from 1:1 (mole ratio) mixture of *5*-aminoquinoline with gallic acid dissolved together in methanol and were kept undisturbed for crystallization. After 3-4 days obtained crystals of salt **5.4**. Yield ~ 88 %. IR (KBr, cm^{-1}): 3458 (s), 3348 (s), 3241 (m), 3076 (w), 2671 (w), 1644 (w), 1599 (w), 1526 (m), 1471 (w), 1360 (s), 1307 (m), 1228 (m), 1179 (w), 1102 (w), 1035 (m), 886 (w), 786 (m), 746 (w), 703(w), 575(w). ^{1}H-NMR (400 MHz, DMSO-d_6): 9.23(s, 1H), 8.76(d, J = 4.0 Hz, 1H), 8.53 (d, J = 8.4 Hz, 1H), 7.43 (t, J = 8.0 Hz, 2H), 7.36 (q, J = 4.0 Hz, 1H), 7.19(d, J = 8.0 Hz, 1H), 6.94(s, 3H), 6.72(d, J = 7.6 Hz, 2H), 5.9(s, 2H).

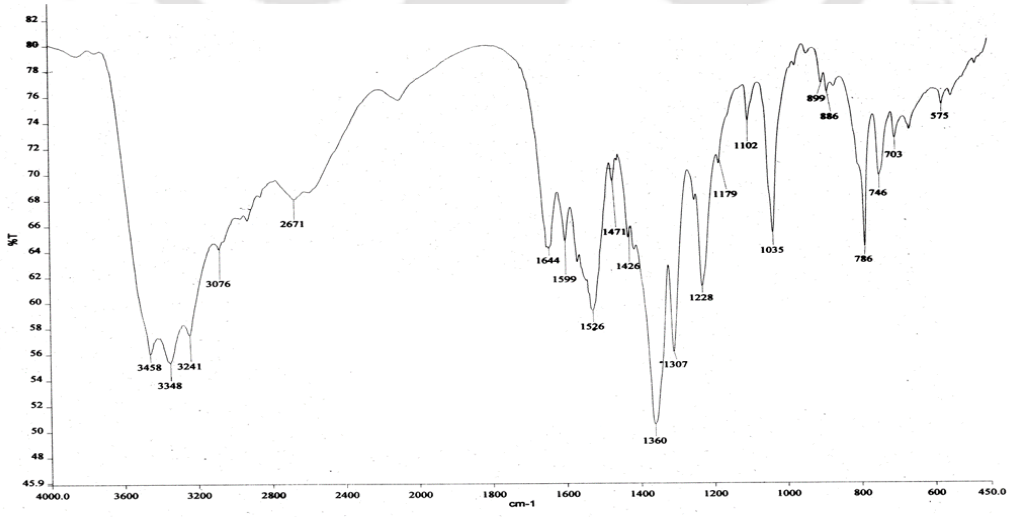

Figure 5.14: FT-IR (KBr, cm^{-1}) spectra of salt **5.4**.

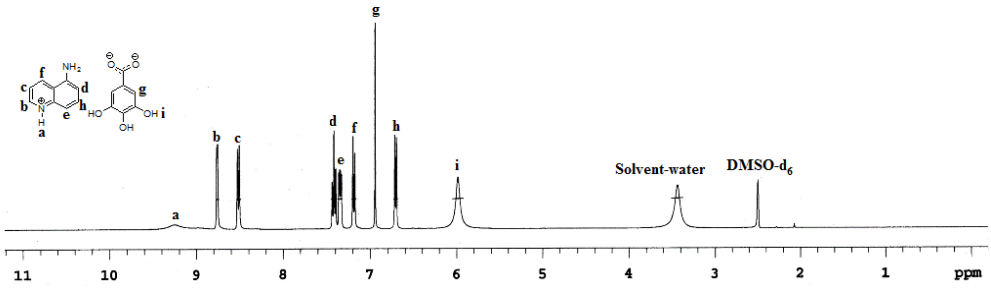

Figure 5.15: ^{1}H-NMR (400 MHz, DMSO-d_6) spectra of salt **5.4**.

Synthesis of 5.5:

The salt **5.5** was prepared from 1:1 (mole ratio) mixture of *8*-aminoquinoline with gallic acid dissolved together in methanol and were kept undisturbed for crystallization. After 3-4 days obtained crystals of salt **5.5**. Yield ~ 85 %. IR (KBr, cm^{-1}): 3516 (m), 3400 (m), 3309 (m), 1686 (s), 1620 (m), 1519 (w), 1425 (m), 1374 (w), 1324 (s), 1272 (w), 1188 (m), 1032 (m), 900 (w), 857 (w), 825 (w), 787 (w), 766 (w), 718 (w). ^{1}H-NMR (400 MHz, DMSO-d_6): 9.23(s, 1H),8.87(s, 1H), 8.71 (dd, *J* = 1.6 Hz, 1H), 8.17 (dd, *J* = 1.6 Hz, 1H), 7.46 (q, *J* = 4.0 Hz 1H), 7.30(t, *J* = 8.0 Hz, 1H), 7.06(dd, *J* = 0. 8 Hz, 1H), 6.91(s, 2H), 6.86(dd, *J* = 1.2 Hz, 1H), 5.90(s, 1H), 4.09(s, 3H).

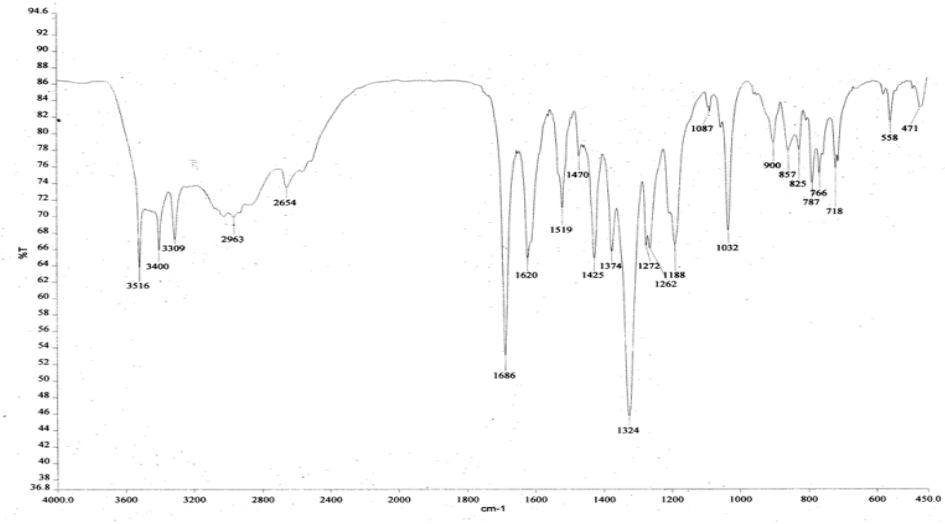

Figure 5.16: FT-IR (KBr, cm^{-1}) spectra of salt **5.5**.

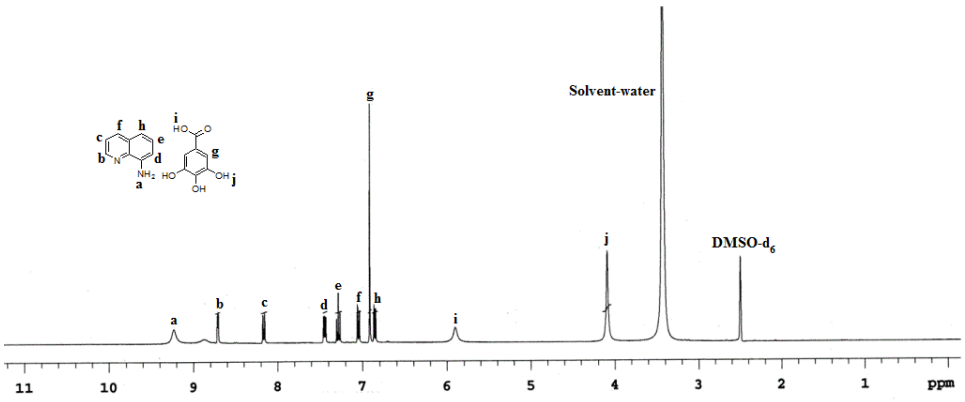

Figure 5.17: ^{1}H-NMR (400MHz, DMSO-d_6) spectra of salt **5.5**.

Synthesis of 5.6:

The salt **5.6** was prepared from 1:1 (mole ratio) mixture of *8*-aminoquinoline with *2*-hydroxy-*3*-naphthoic acid dissolved together in methanol and were kept undisturbed for crystallization. After 3-4 days obtained crystals of salt **5.6**. Yield ~ 89 %. IR (KBr, cm^{-1}): 3457 (m), 3378 (m), 3086 (w), 3043 (w), 1649 (s), 1595 (m), 1513 (s), 1465 (m), 1447 (m), 1370 (s), 1330 (m), 1316 (s), 1243 (m), 1209 (w), 1142 (w), 868 (w), 832 (m), 779 (w), 756 (w), 742 (w), 693 (w), 593 (w), 478 (w). ^{1}HNMR (400 MHz, DMSO-d_6), 8.73 (t, *J* = 2.4Hz, 1H), 8.54 (s, 1H), 8.18 (d, *J* = 8.4 Hz, 1H), 7.97 (d, *J* = 8 Hz, 1H), 7.77 (d, *J* = 8.4 Hz, 1H), 7.54 (q, *J* =0.8 Hz, 1H), 7.52 (m, *J* = 0.8 Hz, 1H), 7.36 (m, *J* = 0.8 Hz, 4H), 7.08 (d, *J* = 8 Hz, 1H), 6.90 (q, *J* = 0.8 Hz, 1H).

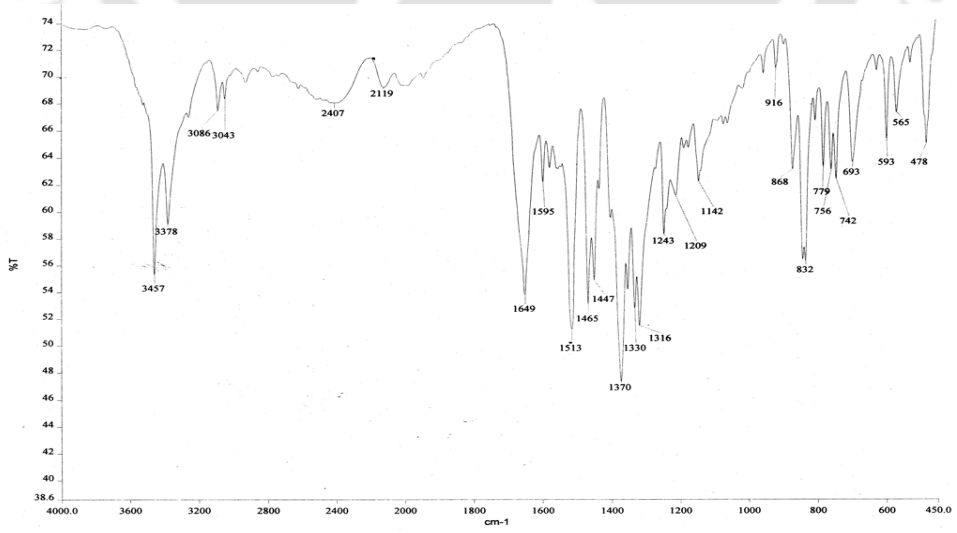

Figure 5.18: FT-IR (KBr, cm^{-1}) spectra of salt **5.6**.

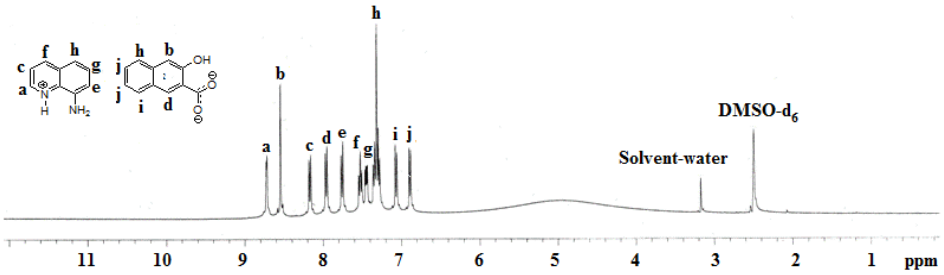

Figure 5.19: ^{1}H-NMR (400MHz, DMSO-d_6) spectra of salt **5.6**.

Synthesis of 5.7:

The salt **5.7** was prepared from 1:1 (mole ratio) mixture of *8*-aminoquinoline with 1-hydroxy-2-naphthoic acid dissolved together in methanol and were kept undisturbed for crystallization. After 3-4 days obtained crystals of salt **5.7**. Yield ~ 90 %. IR (KBr, cm^{-1}): 3424 (m), 3210 (m), 2923 (w), 1631 (m), 1582 (s), 1504 (m), 1467 (m), 1405 (s), 1377 (m), 1328 (m), 1309 (m), 1213 (w), 1017 (w), 863 (w), 815 (m), 795 (m), 771 (m), 693 (m). ^{1}HNMR (400 MHz, DMSO-d_6), 8.72 (d, *J* = 4Hz, 1H), 8.30 (d *J* = 8Hz, 1H), 8.17 (d, *J* = 8.4 Hz, 1H), 7.90 (d, *J* = 8 Hz, 1H), 7.76 (d, *J* = 8.8 Hz, 1H), 7.67 (t, *J* = 1.2, 1H), 7.59 (t, *J* = 8.4 Hz, 1H), 7.46 (q, *J* = 3.6 Hz, 1H), 7.39 (d, *J* = 8.4 Hz, 1H), 7.31 (t, *J* = 7.6 Hz, 1H), 7.07 (d, *J* = 8Hz, 1H), 6.89 (d, *J* = 7.6 Hz, 1 H).

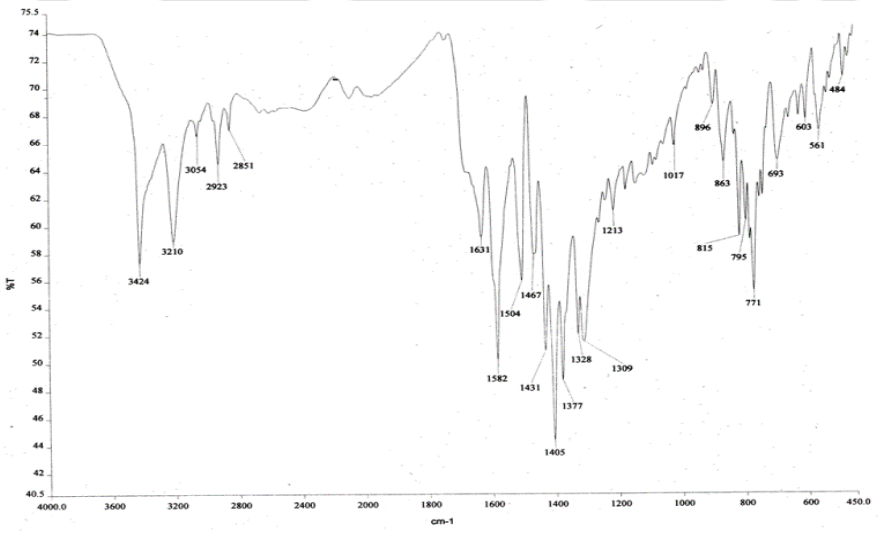

Figure 5.20: FT-IR (KBr, cm^{-1}) spectra of salt **5.7**.

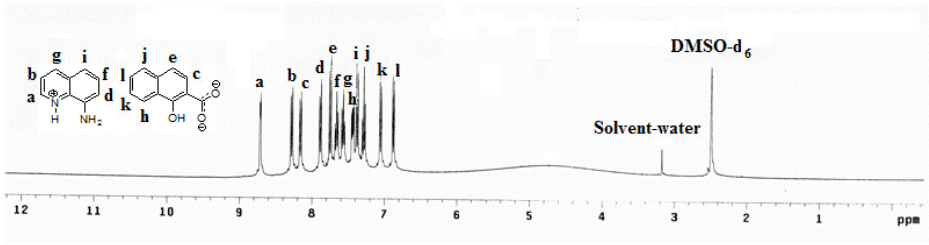

Figure 5.21: ^{1}H-NMR (400MHz, DMSO-d_6) spectra of salt **5.7**.

Synthesis of 5.8:

To a solution of 8-aminoquinoline (0.29 g, 2 mmol) in dry THF (20 ml) triethylamine (0.28 ml, 2 mmol) was added and stirred for 15 minutes. To this reaction mixture a solution of benzoyl chloride (0.29 g, 2 mmol) solution in dry THF (20 ml) was added. The resulting mixture was stirred for 5 h at room temperature. Solvent was removed in reduced pressure to obtain solid of **5.8**. Yield ~ 60 %. IR (KBr, cm^{-1}): 3383 (m), 3279 (m), 2361 (m), 2337 (w), 1656 (s), 1632 (w), 1597 (m), 1554 (m), 1514 (s), 1486 (m), 1452 (w), 1416 (w), 1376 (m), 1296 (m), 1276 (m), 1214 (m), 824 (s), 760 (m), 710 (s), 687 (w), 597 (w). ESI mass: [M + H] calculated for $C_{16}H_{13}N_2O$, 249.1028; found 249.3641.

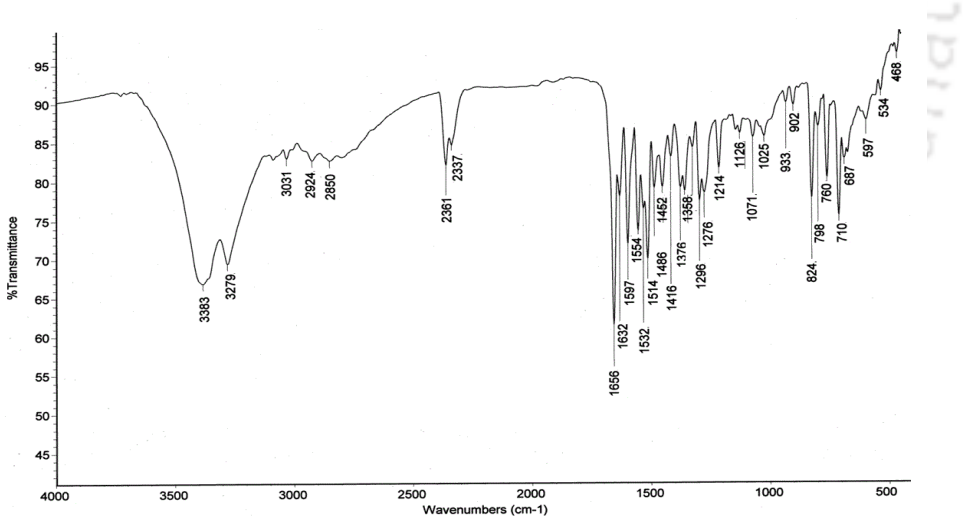

Figure 5.22: FT-IR (cm^{-1}, KBr) spectra of salt **5.8**.

Synthesis of 5.9:

Compound 5.9 was synthesized following reported procedure.[30] IR (KBr, cm^{-1}): 3316 (m), 3284 (w), 3253 (w), 3062 (w), 1651 (s), 1600 (m), 1542 (s), 1482 (m), 1441 (m), 1421 (w), 1380 (m),

1309 (m), 1246 (s), 1203 (m), 1103 (w), 891 (w), 818 (w), 788 (w), 744 (m), 725 (w), 688 (w), 556 (w), 496 (w). ESI mass: [M + H] calculated for $C_{20}H_{16}N_3O_2$, 330.1243; found 330.0165.

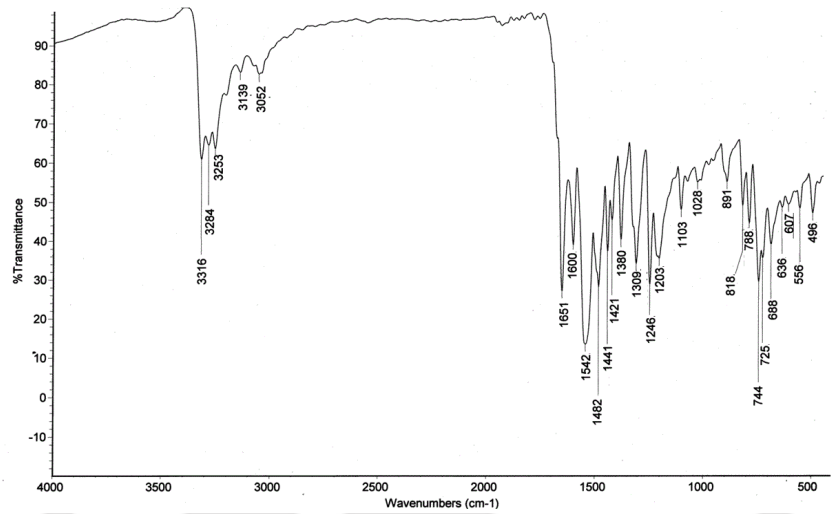

Figure 5.23: FT-IR (KBr, cm^{-1}) spectra of salt **5.9.**

Synthesis of 5.10:

8-Aminoquinoline (0.72 mg, 5 mmol) was dissolved in dry dichloromethane (20 ml) and triethylamine (0.71 ml, 5 mmol) was added to it. The solution was stirred at 0ºC for 15 min after which bromoacetyl bromide (0.52 ml, 6 mmol) was added dropwise to the stirred solution over a period of 30 min. The reaction mixture was then stirred overnight. Subsequently the reaction mixture was filtered to remove the hydrobromide salts, and the filtrate was collected. The filtrate was washed with water (10 ml), dried over sodium sulfate and then the solvent was removed under reduced pressure. The product was obtained as a brown solid that was purified by recrystallisation from dichloromethane.

The amide obtained from above reaction (0.53 gm, 3 mmol), methyl-3-hydroxybenzoate (0.45 mg, 3 mmol) and K_2CO_3 (1.07 gm, 7 mmol) were added to dry acetone (20 ml) in nitrogen atmosphere and the reaction mixture was stirred at 60 ºC for 9 h. (The reaction progress was monitored at regular intervals using TLC.) After completion of the reaction the solvent was removed under reduced pressure that gave a pale yellow solid. The product obtained was crystallized from methanol**.** IR (KBr, cm^{-1}): 3410 (m), 3332 (m) 3004 (w), 2916 (w), 1710 (s),

1684 (s), 1585 (w), 1541 (s), 1487 (m), 1459 (m), 1435 (m), 1388 (w), 1372(w), 1324(w), 1296 (s), 1284 (m), 1224 (w), 1189 (w), 1103 (m), 1075 (m), 990 (w), 890 (w), 828 (w), 794 (w), 758 (m), 734 (m), 680 (w), 602 (w), 579 (w), 554 (w). : ^{1}H-NMR (400 MHz, $CDCl_3$): 10.91 (s, 1H), 8.84 (q, *J* =1.2 Hz, 1H), 8.79 (t, *J* =4.4 Hz, 1H), 8.14 (dd, *J* =1.6 Hz, 1H), 7.74 (dd, *J* =1.2 Hz, 2H), 7.52 (d, *J* =4.4 Hz, 2H), 7.45 (m, 1H), 7.32 (dd, *J* =2.4 Hz, 2H), 4.76 (s, 2H). ESI mass: [M + H] calculated for $C_{19}H_{17}N_2O_4$ 337.1188; found 337.0094.

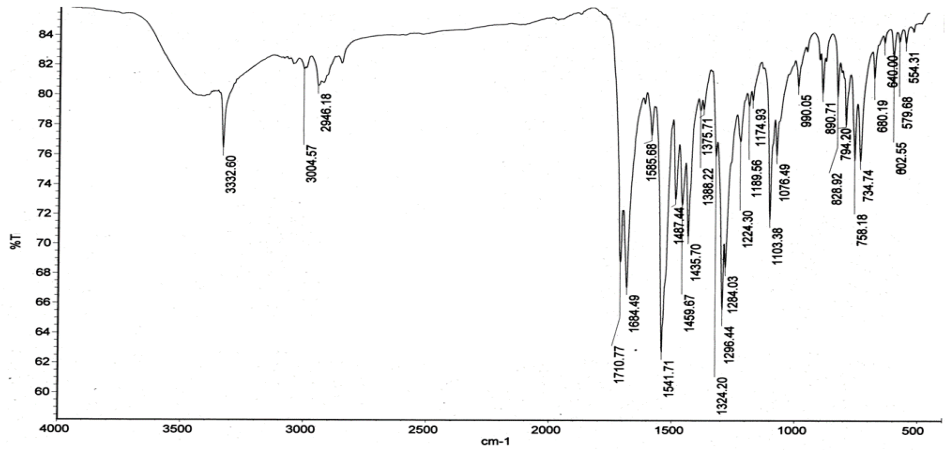

Figure 5.24: FT-IR (cm^{-1}, KBr) spectra of salt **5.10.**

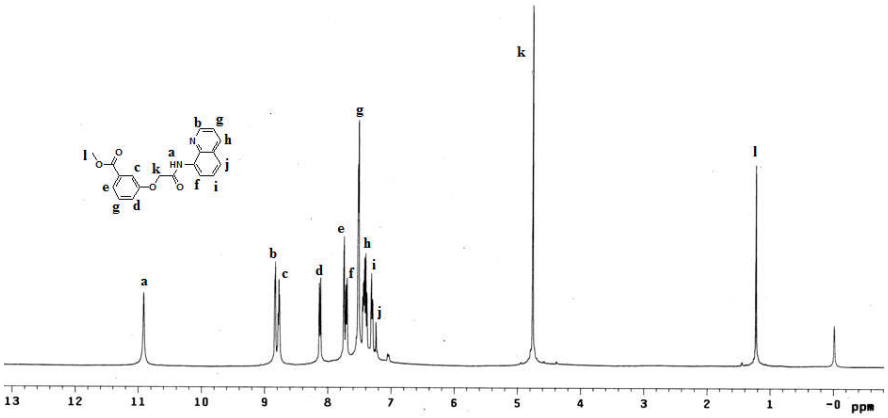

Figure 5.25: ^{1}H-NMR (400 MHz, $CDCl_3$) spectra of **5.10**.

5.5: In vitro antimalarial assay

Antimalarial activity of the compounds, against the chloroquine-resistant (FCR-3) and chloroquine-sensitive (3D7) strains of *P. falciparum,* was performed using the [^{3}H]-hypoxanthine incorporation assay.[43-44] The parasites were continuously maintained *in vitro* in

supplemented RPMI-1640 culture media and at a haematocrit of 5%. The culture was incubated at 37 °C in a gaseous atmosphere of 5 % CO_2, 3 % O_2, 92 % N_2 and synchronized at the ring stage with 5 % D-sorbitol before being adjusted to a final parasitaemia of 0.5 % and haematocrit of 1%.[45] This suspension (200 µL) was added to each well of the 96-well plate with the exception of four wells which received non-parasitized red blood cells. Stock solutions of the test compounds were made up in DMSO and serially diluted in culture medium in a 96-well microtiter plate. The microtiter plate was then incubated for 24 h. Following the incubation period, 25 µL of the radiolabeled [^{3}H]-hypoxanthine isotope (Amersham) at a concentration of 1.85 µCi/well was added to each well. Microtiter plate was then incubated for a further 24 h. The parasitic DNA was harvested onto glass fibre filter mats by use of a Titertek™ semi-automatic cell harvester. The mats were then transferred to sample bags containing scintillation fluid (Wallac®) and the β-radioactivity counted on the Wallac® 1205 Betaplate scintillation counter. Counts per minute (cpm) were generated and the % parasite growth calculated. The concentration required to inhibit parasite growth by 50% (IC_{50} value) was determined from log sigmoid dose response curves using the GraphPad Prism® 5.0 software. Chloroquine and quinine were used as the positive controls. Each experiment was repeated, at least, in triplicate.

5.6: Inhibition of β-haematin formation

To asceratain mechanism of action similar to that of chloroquine, the compounds were incubated with 1 mg/mL haemin (Sigma) solubilised in DMSO, with a final pH of 4.7 ensured by using a 0.5M acetate buffer.[40] The plates were then incubated for 24 hours before the unreacted haemin was removed from the β-haematin crystals by centrifugation. The β-haematin crystals were then quantitated by dissolving them in 2M NaOH. Absorbance at 405 nm was used to calculate the IC_{50} value at which β-haematin formation was inhibited using GraphPad Prism® 5.0 software. Chloroquine was used as positive control. Each experiment was repeated three times.

5.7: Haemolytic activity

The haemolytic activities of the compounds were evaluated in comparison to standard antimalarial agent, quinine.[46] Haematocrit (1%) of fresh human red blood cells was incubated with each test compound (50 µM) for 48 hours at 37^{o}C before the absorbance was read at 540

nm. Percentage of haemolysis was calculated using a 2.0% (v/v) TritonX100 solution as the 100% haemolytic control. Each experiment was repeated at least in triplicate.

5.8: Iron chelation assay

The ferrozine-iron chelation assay was used to determine the ferrous ion chelating properties of the derivatives.[46] The derivatives were incubated at room temperature with 0.48 mM $FeCl_2$ dissolved in 5% (w/v) ammonium acetate for 5 minutes before 1.2 mM ferrozine was added. The mixture was shaken vigorously before being incubated at room temperature in the dark for 30 minutes. Thereafter the absorbance was measured at 540 nm in an ELISA plate reader (Labsystems Multiskan RC) with Ascent Software (version 2.4). Percentage inhibition of ferrozine-Fe^{2+} complex formation was calculated with EDTA used as positive control.

5.9: Reference

1. S. N. Cohen, K. O. Phifer, K. L. Yielding, *Nature,* 1964, **202**, 805.
2. A. Dorn, S. R. Vippagunta, H. Matile, C. Jaquet, J. L. Vennrstrom, R. C. Ridley, *Biochem. Pharmacol.,* 1998, **55**, 727.
3. R. E. Bambury, *In Burger's Medicinal Chemistry, Part II. Wiley, New York*, 1979, p 41
4. H. Gershon, M. Gershon, D. D. Clarke, *Mycopathologia,* 2004, **158**, 131.
5. H. Gershon, R. Parmegiani, *Appl. Microbio.,* 1962, **10**, 348.
6. P. Hongmanee, K, Rukseree, B. Buabut, S Boontiwa, P. Prasit, *Antimicrob Agents Chemo.,* 2007, **51**, 1105.
7. J. Mao, H. Yuan, Y. Wang, B. Wan, M. Pieroni, Q. Huang, R. B. van Breemen, A. P. Kozikowski, S. G. Franzblau, *J. Med. Chem.*, 2009, **52**, 6966.
8. P. R. Verhoest, D. S. Chapin, M. Corman, K. Fonseca, J. F. Harms, X. Hou, E. S. Marr, F. S. Menniti, F. Nelson, R. O'Connor, J. Pandit, C. P. LaFrance, A. W. Schmidt, C. J. Schmidt, J. A. Suiciak, S. Liras, *J. Med. Chem.,* 2009, **52,** 5188.
9. G. X. Li, Z. Q. Liu, X. Y. Luo, *Eur. J. Med. Chem.,* 2010, **45**, 1821.
10. R. Buller, M. L. Peterson, O. Almarsson, L. Leiserowitz, *Cryst. Growth Des.,* 2002, **2,** 553.
11. T. J. Egan, *J. Inorg. Biochem.,* 2006, **100**, 916.
12. S. F. Alshahateet, R. Bishop, D. C. Craig, F. Kooli, M. L. Scudder, *CrystEngComm.,* 2008, **10**, 297.

13. R. F. Semeniuc, T. J. Reamer, M. D. Smith, *New J. Chem.,* 2010, **34**, 439.
14. A. Karmakar, R. J. Sarma, J. B. Baruah, *CrystEngComm.,* 2007, **9**, 378.
15. C. R. Bondy, P. A. Gale, S. J. Loeb, *J. Am. Chem. Soc.,* 2004, **126**, 5030.
16. M. H. Filby, J. W. Steed, *Coord. Chem. Rev.*, 2006, **250**, 3200.
17. A. Karmakar, J. B. Baruah, *Supramolecular Chem.*, 2008, **20**, 667.
18. A. Karmakar, R. J. Sarma, J. B. Baruah, *CrystEngComm.*, 2007, **9,** 378.
19. D. Kalita, H. Deka, S. S. Samanta, S. Guchait, J. B. Baruah, *J. Mol. Struct.,* 2011, **990**, 183.
20. S. L. Childs, G. P. Stahly, A. Park, *Mol. Pharmaceutics,* 2007, **4**, 323.
21. B. R. Bhogala, S. Basavoju, A. Nangia, *CrystEngComm.,* 2005, **7**, 551.
22. C. C. Seaton, K. Chadwick, G. Sadiq, K. Guo, R. G. Davey, *Cryst. Growth Des.,* 2010, **10**, 726.
23. E. A. Meyer, R. K. Castellano, F. Diederich, *Angew. Chem. Int Ed. Eng.,* 2003, **42**, 1210.
24. S. Vaupel, B. Brutschy, P. Tarkakeswar, K. S. Kim, *J. Am. Chem. Soc.*, 2006, **28**, 5416.
25. D. D. Perrin, B. Dempsey, E. P. Serjeant, *pK_a Prediction for Organic Acids and Bases*, Chapman & Hall, London, 1981.
26. D. D. Perrin, *Dissociation Constants of Organic Bases in Aqueous Solution*, Butterworths, London, 1965; Supplement, 1972.
27. E. P. Serjeant, B. Dempsey, *Ionization Constants of Organic Acids in Aqueous Solution*, Pergamon, Oxford, 1979.
28. R. N. Castle, *The Chemistry of Heterocyclic Compounds, Condensed Pyridazines Including Cinnolines and Phthalazines*, John Wiley & Sons, Science, 2009.
29. A. Albert, "*Ionization Constants of Heterocyclic Substances*", in A. R. Katritzky, Ed., *Physical Methods in heterocyclic Chemistry*, Academic Press, New York, 1963.
30. B. Sarma, N. B. Nath, B. R. Bhogala, A. Nangia, *Cryst. Growth Des.,* 2009, **9**, 1546.
31. D. A. Haynes, W. Jones, W. D. S. Motherwell, *CrystEngComm,* 2005, **7**, 342.
32. R. W. Jiang, D. -S. Ming, P. P. H. But, T.C.W. Mak, *Acta Cryst.,* 2000, **C56**, 594.
33. S. L. James, *Encyclopedia of Supramolecular Chemistry, Marcel Dekker, Inc, New-York*, 2004, pp 1093.
34. A. Richardson Jr., E. D. Amstutz, *J. Org. Chem.*, 1960, **25**, 1138.
35. D. Kalita, J. B. Baruah, *CrystEngComm*., 2010, **12**, 1562.

36. T. J. Egan, R. Hunter, C. H. Kaschula, H. M. Marques, M. Ashley, J. Walden, *J. Med. Chem.,* 2000, **43***,* 283.

37. I. M. Chung, S. H. Seo, E. Y. Kang, W. H. Park, H. I. Moon, *Malar. J.,* 2009, **8,** 151.

38. R. Conners, F. Schambach, J. Read, R. B. Sessions, L. Vivas, A. Easton, S. L. Croft, R. L. Brady, *Mol. Biochem. Parasitol.,* 2005, **142**, 137.

39. D. Ndjonka, B. Bergmann, C. Agyare, F. M. Zimbres, K. Lursen, A. Hensel, C. Wrenger, E. Liebau, *Parasitol. Res.,* 2012, **111,** 827.

40. S. M. Chemaly, C. T. Chen, R. L. van Zyl, *J. Inorg. Biochem*., 2007, **101**,764.

41. I. Gulcin, *Amino Acids,* 2007, **32***,* 431.

42. F. Hayat, E. Moseley, A. Salahuddin, R. L. van Zyl, A. Azam, *Eur. J. Med. Chem*., 2011, **46**, 1897.

43. R. L. van Zyl, S. T. Seatlholo, A. Viljoen, *South African J. Botany,* 2010, **76***,* 662.

44. R. E. Desjardins, C. J. Canfield, D. J. Haynes, J. D. Chulay, *Antimic. Agents Chemother,* 1979, **16**, 710.

45. N. Qiao, M. Li, W. Schlindwein, N. Malek, A. Davies, G. Trappitt, *Int. J. Pharm*., 2011, **419**, 1.

46. J. N. van Vuuren, R. L. van Zyl, *Basic Clin. Pharmacol. Toxicol*., 2014, **115(S1)**, 760.

Chapter 6

Synthesis, characterization and metal ion recognition by *bis*-quinoline amide derivatives

There are large numbers of examples of small fluorescent molecules which are used to detect metal ions.[1-8] Some of the examples were also discussed in the first chapter of the thesis. Some analytes show selective fluorescence emission response to two or more metal ions.[9-13] For instances 5-(4-nitrobenzene diazo)-8-benzenesulfonamidoquinaldine has been used to detect Zn^{2+} and Hg^{2+} ions in biological systems.[14] It shows 'ON' and 'OFF' fluorescence responses upon coordination to Zn^{2+} and Hg^{2+} ions respectively. Interestingly, in this system Hg^{2+} ions can replace coordinated Zn^{2+} ions to show ON-OFF response as depicted in Figure 6.1.

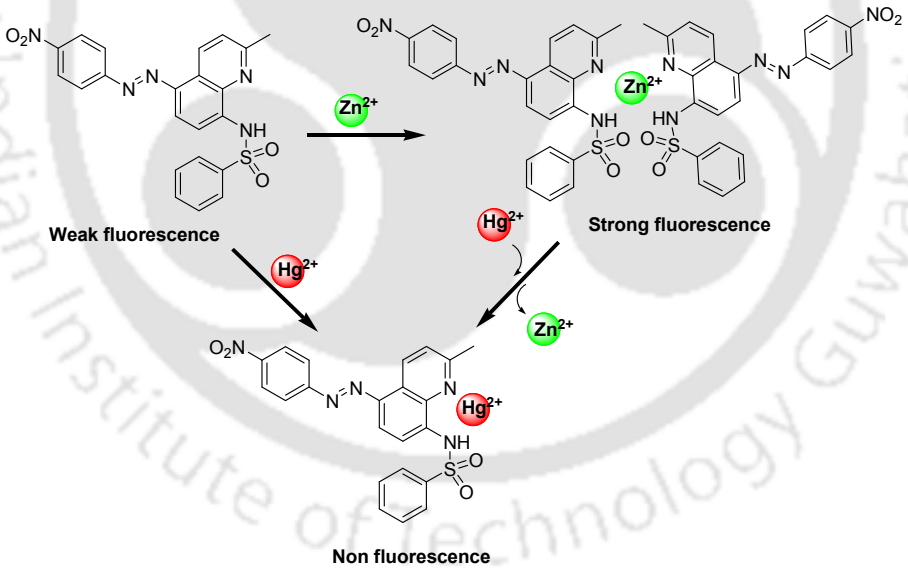

Figure 6.1: Coordination modes of Zn^{2+} and Hg^{2+} ions with 5-(4-nitrobenzene diazo)-8 benzenesulfonamidoquinaldine.

However, many fluorescence receptors developed so far for two metal ions detections fail to detect one type of ion in the presence of other ion or vis-versa.[15-32] Fluorescent sulphonamide derivatives of aminoquinolines have potential in imaging of zinc ions.[33] Water soluble quinoline

derivatives also have the ability to sense zinc ions under biological conditions.[34-35] Fundamental problems with such receptors is the interference of other metal ions present in the solution.[36] Such a problem was partly overcome by designing quinoline receptors which operates through internal charge transfer mechanism.[37] Lippard and his coworkers[38] developed very efficient quinoline based sensors for detection of zinc ions.

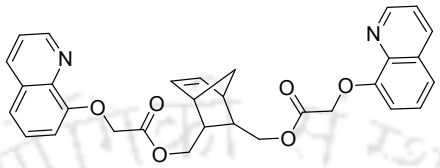

Figure 6.2: Hydroxyquinoline functionlized polynorbornene.

The receptors with two pendant arms bearing 8-aminoquinolines have higher efficiency over similar type of receptors with quinoline unit at one arm. Moreover, a hydroxyquinoline derivative of polynorbornene with two flexible arms to hold metal ions shows fluorescence turn-on upon coordination to Zn^{2+} and Cd^{2+} ions (Figure 6.2).[39]

From the above discussions it can be suggested that there exists opportunity to prepare receptors with multiple numbers of quinoline rings to hold metal ions in multiple numbers.

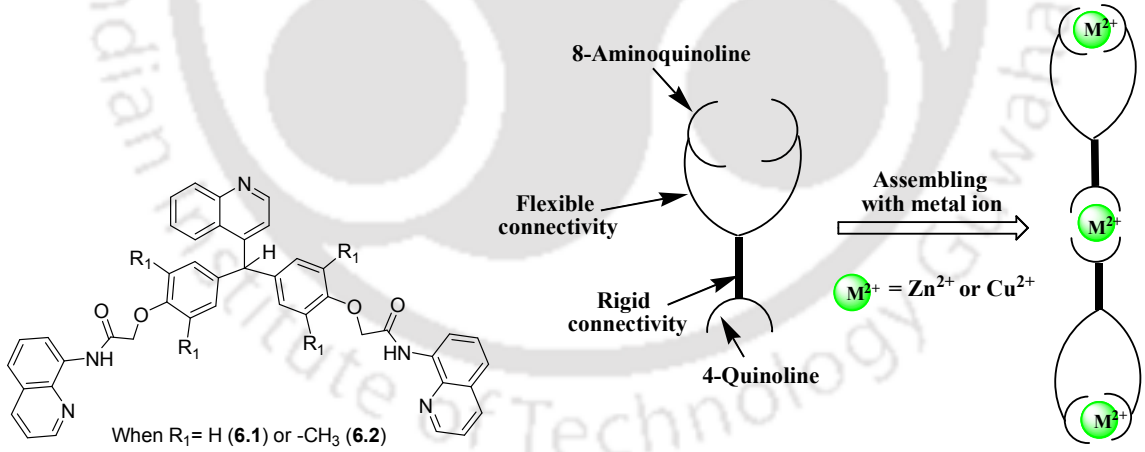

(a) (b)

Figure 6.3: (a) Compounds **6.1** and **6.2**; (b) design principle of assemblies of tri-quinoline receptor for binding metal ions.

Thus, keeping this in mind we prepared two tri-quinoline based compounds **6.1** and **6.2,** which have two flexible arms to hold metal ions and an openly projected 4-quinoline ring (Figure 6.3a).

Thus they will be suitable to form metal complexes as illustrated schematically in Figure 6.3b. Compounds **6.1** and **6.2** have *bis*-phenolate ether tethers connecting quinoline amide moieties. Additional 4-quinoline moiety provides a shape like a projectile with two open wings. The choice of these compounds also arises from the facts that the zinc[15-26, 13] and the copper ions[27-32] can change fluorescence emissions of quinoline derivatives with high specificity. Masking of fluorescence emission by copper ions of quinoline derivatives over the zinc ions[40] is not overcome so far in this class of receptors. *Bis*-8-aminoquinoline amide derivatives were shown to lose fluorescence response to zinc ions in the presence of copper ions.[41] There are reports on the steric and electronic effects contributing to stabilize different conformations of amides.[42-44] A substituent atom or group present at an appropriate position of some amide derivatives can change rotational barriers of *trans* or *cis* conformers of amides.[45] These factors also contribute to fluorescence emission occurring through twisted intramolecular charge transfer (TICT) mechanism of some amides derivatives.[46-47] On the other hand, compounds **6.1** and **6.2** have a portion of the structure which has pincer type of geometry and ligands of such geometrical features easily form copper and zinc complexes.[48-52]

The compounds **6.1** and **6.2** were synthesized by reacting 2-bromo-N-(quinolin-8- yl)acetamide with the corresponding bis-phenol (**6.1a** or **6.2a**) in dry acetone in the presence of anhydrous potassium carbonate (Scheme 6.1).

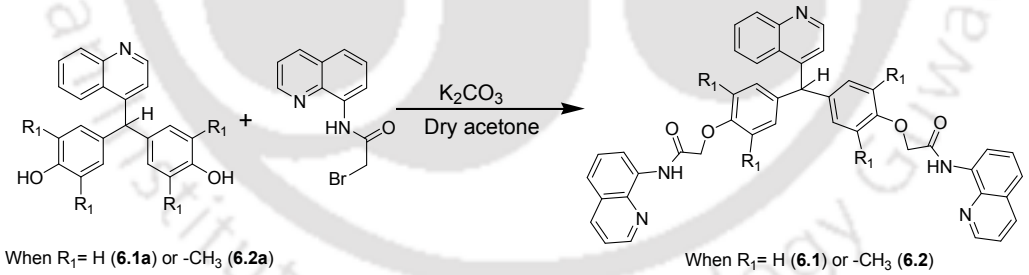

Scheme 6.1: Synthesis of compounds **6.1** and **6.2**.

The compounds **6.1** and **6.2** were characterised by by ^{1}H-NMR, IR and mass spectra. As there are multiple numbers of quinoline moieties in compounds **6.1** and **6.2**, protons on the quinoline units were assigned by analyzing the observed correlation between coupling patterns of typical two dimensional ^{1}H-HOMOCOSY spectra of compound **6.1** shown in Figure 6.4. The cross peak assigned as 'A' represents the coupling of H_m and H_n protons of 4-quinoline moiety. The 'B' represents coupling between H_f and H_e protons of hetero nuclear ring of 8-aminoquinoline. Cross

peaks 'C' and 'D' represent coupling of H_i-H_j and H_l-H_k protons of 4-quinoline ring. Cross peak 'E' and 'F' represents the coupling between H_d-H_c and H_a-H_b protons of 8-aminoquinoline ring.

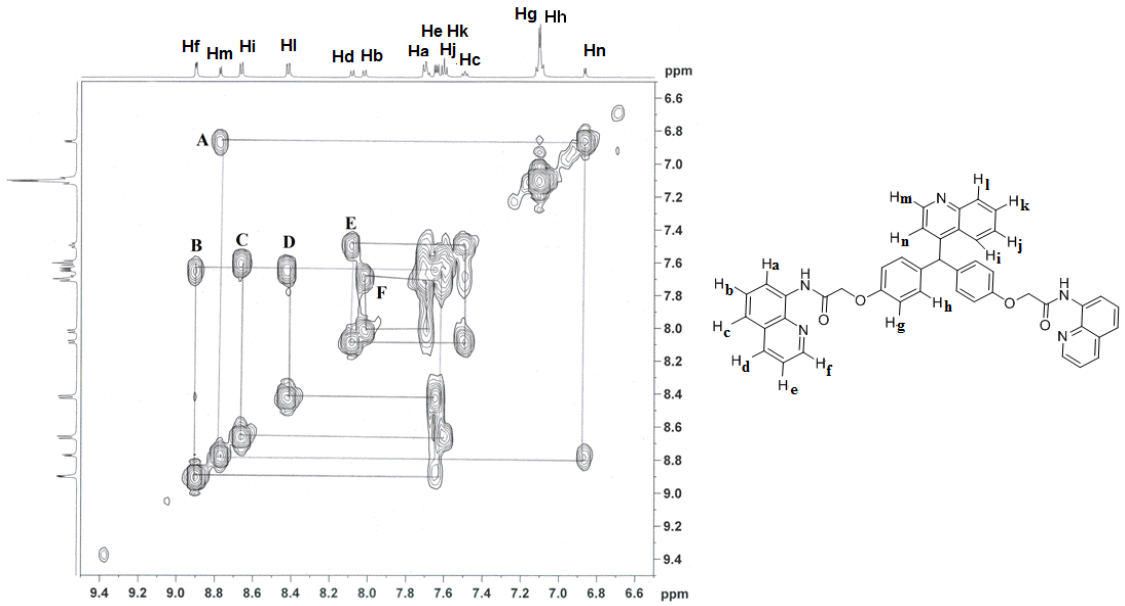

Figure 6.4: Assignment of peaks in the aromatic region of two-dimensional ^{1}H-HOMOCOSY (600 MHz, DMSO-d_6) of compound **6.1** (in range of 6.5 to 9.5 ppm).

The tri-quinoline derivatives **6.1** and **6.2** possess V-shape *bis*-phenolate ether linkage anchoring flexible methylene groups, such units are flexibile and suitable to adopt different orientations depending on conditions. Generally constraints provided by the substituent present in a flexible receptor enhances selectivity to bind to metal ions.[53-54] Differences in binding ability of metal ions to a receptor influences internal charge transfer which influences the position and the intensity of their fluorescence emissions of the receptor.[55] Since the compounds **6.1** and **6.2** have different substituent at two aromatic rings, hence their optical properties are expected to differ with coordination environments and electronic factors of different metal ions. Thus, we carried absorption and fluorescence emission titration of compounds **6.1** and **6.2** with various biological active metal ions.

6.1: Absorbance study

Intensities of the UV absorptions of the **6.1** present at 252 nm and 360 nm were increased upon the addition of a solution of Zn^{2+} ions (Figure 6.5a). These spectral changes took place at the cost of the absorption present at 303 nm. As a result of such changes three isobestic points at 245 nm,

280 nm and 331 nm had appeared. Similar spectral changes were observed upon the addition of a solution of Cu^{2+} ions to a solution of **6.1**.

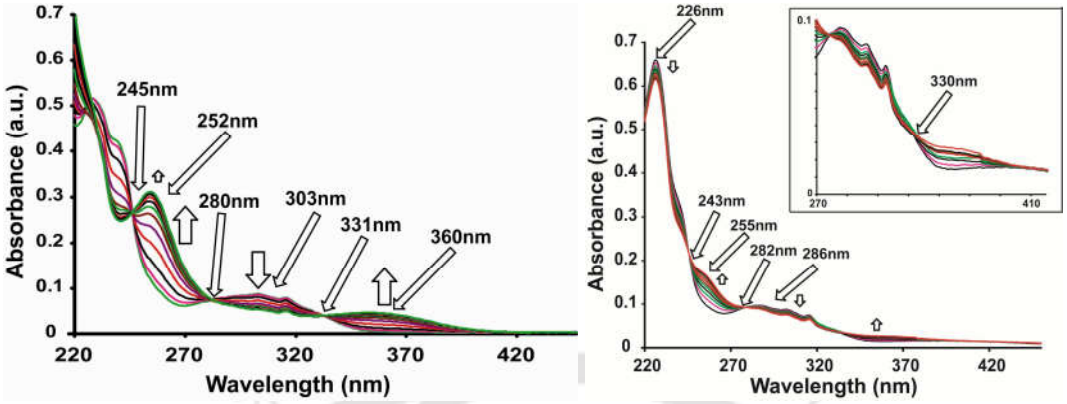

(a) (b)

Figure 6.5: Changes in the absorption spectra of (a) the compound **6.1** and (b) the compound **6.2**, on the addition of a solution of Zn^{2+} ions (in each case 0.033 equivalent from a solution of methanol in aliquots).

However, Zn^{2+} and Cu^{2+} ions were relatively less effective in changing the absorbance spectra of the **6.2** (Figure 6.5b) as compared to the compound **6.1**. Addition of a solution of Zn^{2+} ions to a solution of the **6.2,** the absorption peak appearing at 255 nm increased with a concomitant decrease in the absorption at 226 nm and 286 nm. These changes in absorptions passed through isosbestic points appearing at 243 nm, 282 nm and 330 nm.

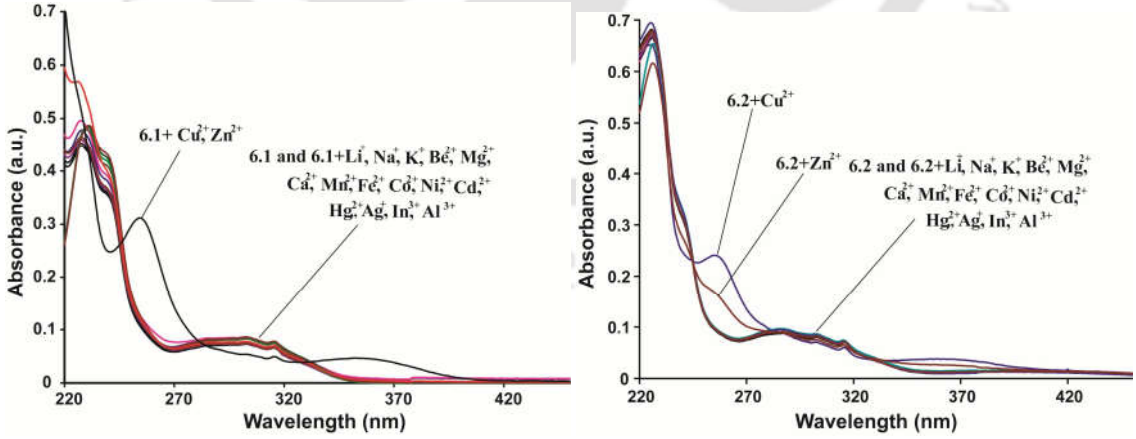

(a) (b)

Figure 6.6: Absorbance spectra of compounds (a) **6.1** and (b) **6.2** in the presence of various metal ions.

Similarly, when the titrations were carried out for other biologically active metal ions with compounds **6.1** and **6.2**, there were insignificant changes in their absorbance spectra as shown in the Figure 6.6. The extinction coefficients calculated from the absorbance at 303 nm of the methanol solution of the compounds **6.1** and **6.2** are 8753 cm^2mol^{-1} and 9671 cm^2mol^{-1} respectively. In cases of **6.1** and **6.2** addition of 0.33 μM of Zn^{2+} and Cu^{2+} ions causes observable changes in absorption, which is much lower than the limit of copper in drinking water (~20 μM) and the typical concentration of copper in blood (15.7-23.6 μM) of normal individual.[56] Detection limits from UV-visible spectroscopic titration for compound **6.1** were found to be 160.34 μM and 204.82 μM; for compound **6.2** these were 192.66 μM and 168.25 μM for Zn^{2+} and Cu^{2+} ions respectively.

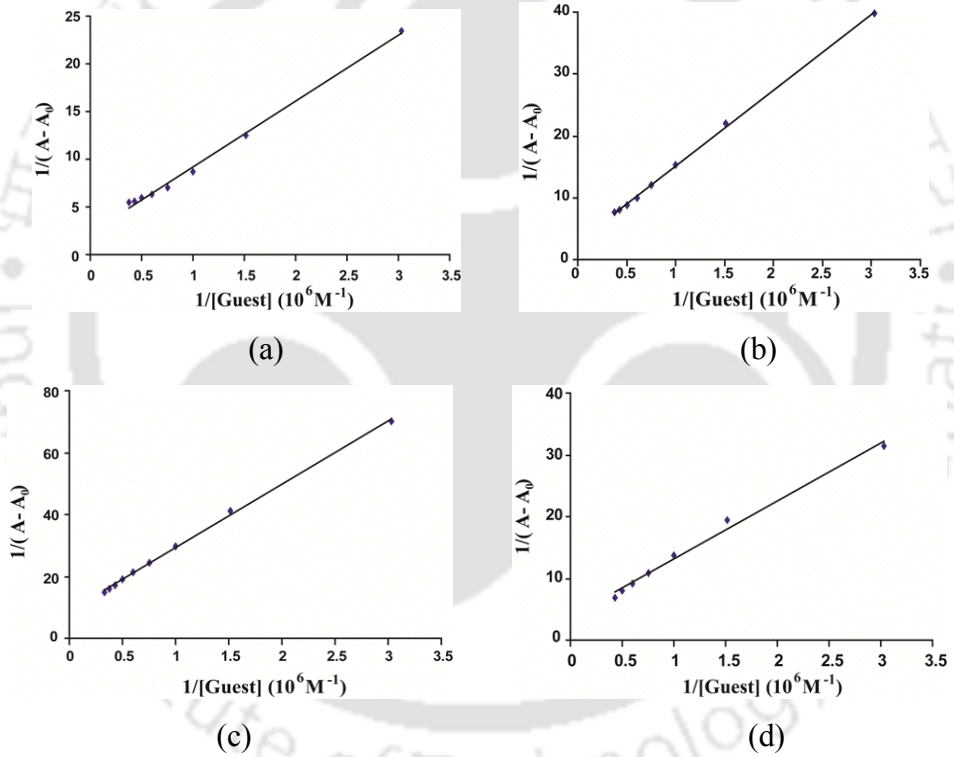

Figure 6.7: Binding constant plot (at 253 nm) of **6.1** with (a) Zn^{2+} and (b) Cu^{2+} ions; **6.2** with (c) Zn^{2+} and (d) Cu^{2+} ions.

By using Benesi and Hildebrand equation binding constants of compound **6.1** were found to be $11.66 \pm 2 \times 10^4\ M^{-1}$ and $13.53 \pm 2 \times 10^4\ M^{-1}$ with Zn^{2+} and Cu^{2+} respectively (Figure 6.7). Thus, logK of compound **6.1** with Zn^{2+} and Cu^{2+} are 5.07 and 5.13 respectively whereas for compound

6.2 binding constants were 6.86 (± 8) × 10^4 M^{-1} and 8.14 ± 3 × 10^4 M^{-1} and logK values are 4.84 and 4.91 respectively.

6.2: Fluorescence study

A methanol solution of compound **6.1** shows a broad fluorescence emission peak at 397 nm on excitation at 310 nm and on similar excitation a methanol solution of the compound **6.2** showed broad emission peak at 400 nm. Both the emission spectra have a shoulder at 340 nm. This emission peak could be from the quinoline ring, whereas broad and intense emission at 397 nm and 400 nm for the compounds **6.1** and **6.2** respectively are originate from the aminoquinoline rings. The positions of emission spectra of the compounds do not change with changes in concentrations, which suggest that there are no interactions between the aminoquinoline groups present in these compounds. These observations are conventional as *bis*-aminoquinoline derivatives show fluorescence emissions at similar wavelengths.[40-41]

The intensity of the fluorescence emission peak of the compound **6.1** present at 397 nm decreases upon addition of Zn^{2+} ions and a new emission peak at 493 nm appeared. As the concentration of the Zn^{2+} ions was increased the intensity of this peak was increased to reach a maximum point. Further addition of the Zn^{2+} ions, this emission peak at 493 nm splits up into two new independent emission peaks appearing at 451nm and 551 nm (Figure 6.8a). These two broad peaks formed by splitting of an emission peak spreads over range 430-580 nm is a unprecedented observation in quinoline system and resembles white light emission. This occurs at low concentrations of the Zn^{2+} ions with respect to the compound **6.1** which is at about 30:1 molar ratio. Based on the observation of such a phenomenon at a low concentration of zinc ions with respect to the receptor it can be suggested as to originate from a sensitization process caused by zinc ions on compound **6.1** rather than a conventional complex formation. This type of emission phenomenon can be projected as an exceptional observation as Stokes shift of 183 nm was observed with emission at 493 nm. When this emission changed to two wavelengths the Stokes shift associated with new peaks were 141 nm and 241 nm. In literature, a maximum Stokes shift of 199 nm was observed from an aminoquinoline derivative on interaction with zinc ions due to internal charge transfer (ICT) mechanism.[37] Thus, compound **6.1** is suitable to modulate fluorescence by changing concentrations of zinc ions. Similar fluorescence titrations were carried out with compound **6.1** by adding Li^+, Na^+, K^+, Be^{2+}, Mg^{2+}, Ca^{2+}, Ni^{2+}, Co^{2+}, Mn^{2+},

Cd^{2+} and Hg^{2+} ions. These ions showed insignificant changes in fluorescence emissions of compound **6.1**.

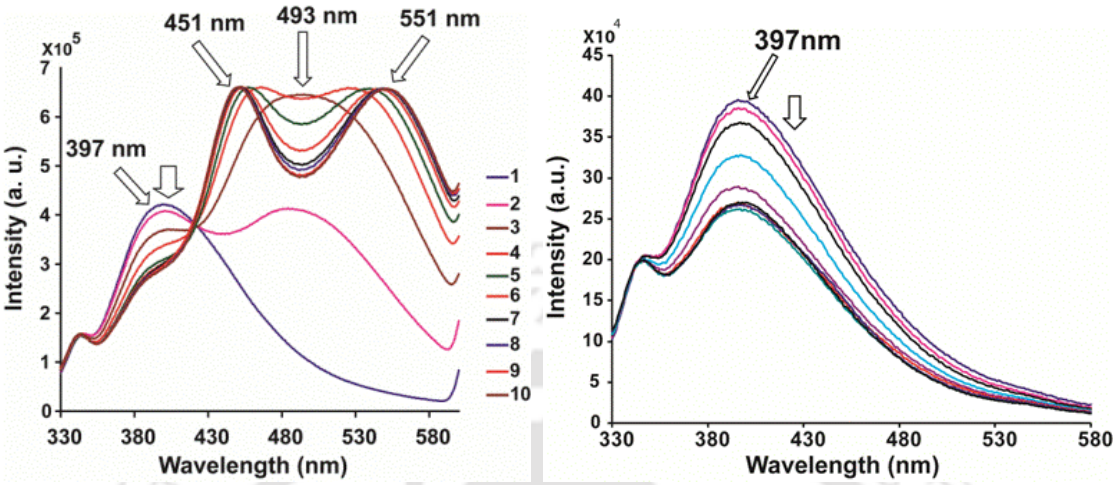

(a) (b)

Figure 6.8: The changes in the emission spectra of the compound **6.1** (10^{-5} M in methanol, 3 mL) upon excitation at 310 nm upon addition of the solutions of (a) Zn^{2+} ions and (b) Cu^{2+} ions (in each case 0.033 equivalent from a 10^{-4} M solution of methanol in aliquot).

We find that on addition of a solution of Cu^{2+} ions to a solution of compound **6.1** decreases the fluorescence emission at 397 nm (Figure 6.8b). Addition of Cu^{2+} ions decreases the enhanced fluorescence emission of **6.1** in the presence of Zn^{2+} ions. It was also observed that once fluorescence of the compound **6.1** was quenched by Cu^{2+} ions, the addition of zinc ions to such a solution could not recover the emission. The compound **6.2** is structurally more rigid derivative in comparison to the compound **6.1**, as it has two methyl groups attached to each aromatic ring of *bis*-phenolate groups. Analogous to **6.1**, on addition of Zn^{2+} ions to solution of **6.2** decreases its emission at 400 nm with appearance of new emission at 490 nm (Figure 6.9a). However, major difference between the fluorescence emissions of these two compounds on interactions with zinc ions is that at higher concentrations of zinc ions, splitting of fluorescence emission peak was not observed in the case of the compound **6.2**. Compound **6.2** showed single emission peak at 490 nm on addition of Zn^{2+} ions, and for this emission peak Stokes shift observed was 180 nm. On the other hand **6.2** also showed decrease in intensity of the emission at 400 nm upon addition of Cu^{2+} ions (Figure 6.9b).

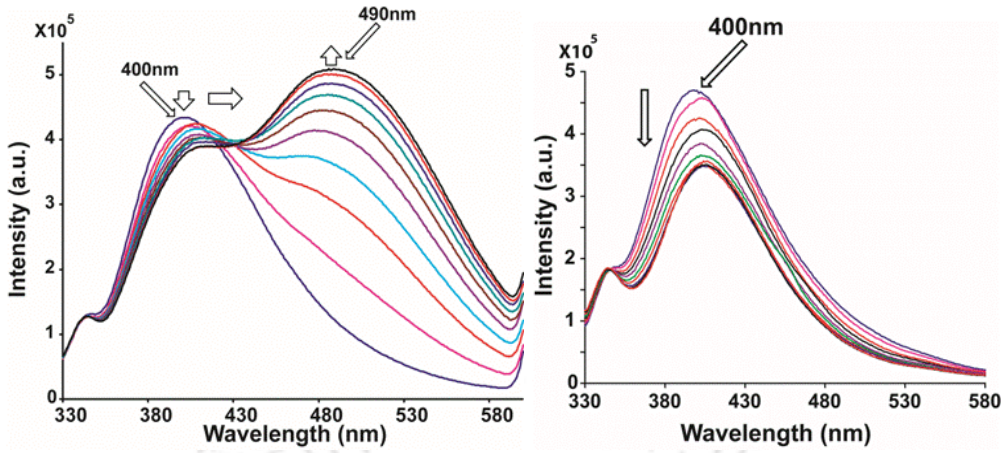

(a) (b)

Figure 6.9: Changes in emission spectra of the **6.2** (10^{-5} M in methanol, 3 mL) upon addition of (a) zinc chloride and (b) cupric chloride (in each case 0.033 equivalent of methanol solution in aliquot).

In both the cases emission spectra were not affected by metal ions other than Zn^{2+} and Cu^{2+} ions as Figure 6.10. These observations show the selectivity of compound **6.1** and **6.2** for Zn^{2+} and Cu^{2+} ions over other biologically active metal ions studied.

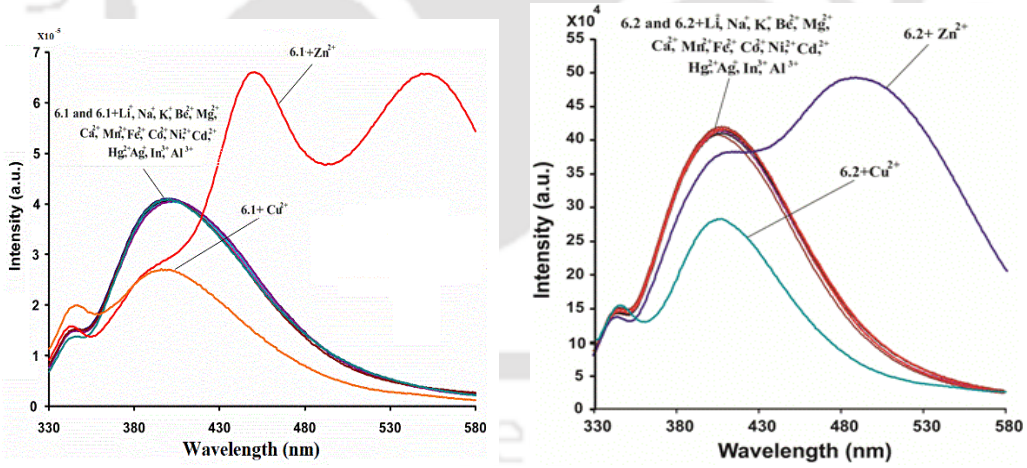

(a) (b)

Figure 6.10: Fluorescence emission of (a) **6.1** and (b) **6.2** in the presence of various metal ions.

Notable observation in compound **6.2** is that the quenching caused by addition of solution of Cu^{2+} ions to a solution of **6.2** can be recovered by adding a solution of Zn^{2+} ions; thus both of these metal ions can be detected by fluorescence technique independently in the presence of each

other. Reversible change in the fluorescence emission of compound **6.2** by two the metal ions was established by carrying out a series of competitive experiments. To do so, we added equivalent amount of cupric chloride to a solution of the compound **6.1**, this decreased the fluorescence emission at 400 nm to a lowest level. To this solution, a methanol solution of zinc chloride was added in 0.033 mole equivalent aliquot. We observed that the fluorescence emission at 490 nm increased as concentrations of zinc ions were increased (Figure 6.11a). In an another experiment a fluorescence titration was carried out by adding a methanol solution of zinc chloride solution to a solution of the compound **6.2**, addition continued till there was no further increase in fluorescence at 490 nm took place.

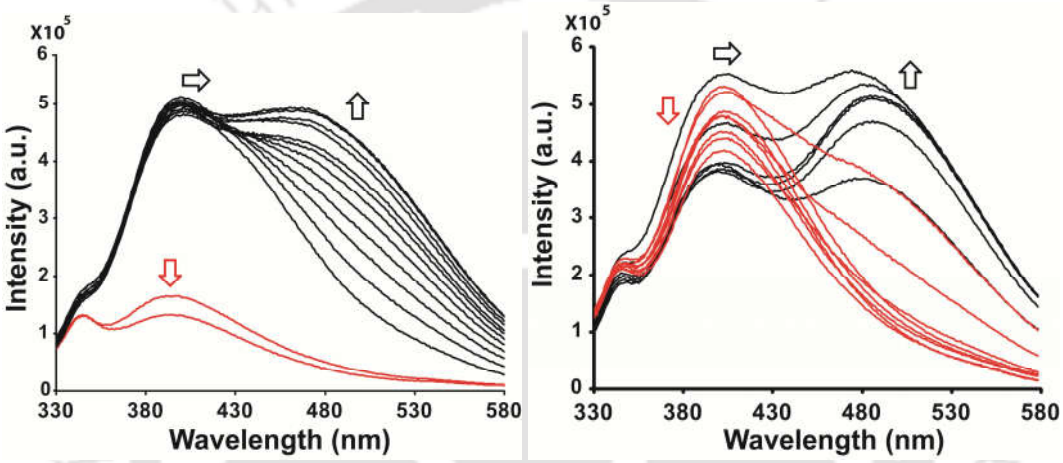

Figure 6.11: (a) Changes in fluorescence of a solution of **6.2** (10^{-4} M in methanol) containing 1 equivalent cupric chloride (red lines), followed by addition of a solution of zinc chloride in 0.033 equivalent in aliquot (black lines). (b) Changes in fluorescence of a solution of **6.2** on addition of zinc chloride 0.033 equivalent (six times, black lines) followed by addition of cupric chloride in 0.033 equivalent aliquots (red lines).

After reaching this point, a solution of copper chloride was added, which resulted a decrease in fluorescence emission at 490 nm and emission continue to shift to show a fluorescence emission peak at 400 nm and after reaching this stage, fluorescence emission at the 400 nm decreases to a minimum on continuation of addition of cupric chloride solution (Figure 6.11b).

To prove competitive effect of these two ions, we have carried out a series of experiments by changing sequence of addition of zinc and copper ions to respective receptor solution. The changes in normalized fluorescence intensities from different control experiments are shown in

Figure 6.12. As it can be seen from Figure 6.12a, addition of the solution of cupric chloride quenched the fluorescence emission of the compound **6.1** at 397 nm; when a zinc chloride solution was added to such a solution, the original fluorescence of the compound **6.1** could not be recovered. However, when a solution of zinc chloride (circles in Figure 6.12b) was added, the fluorescence emission increased to a particular concentration. But due to splitting of the fluorescence emission beyond this critical concentration as discussed earlier there was an apparent decrease in the fluorescence emission.

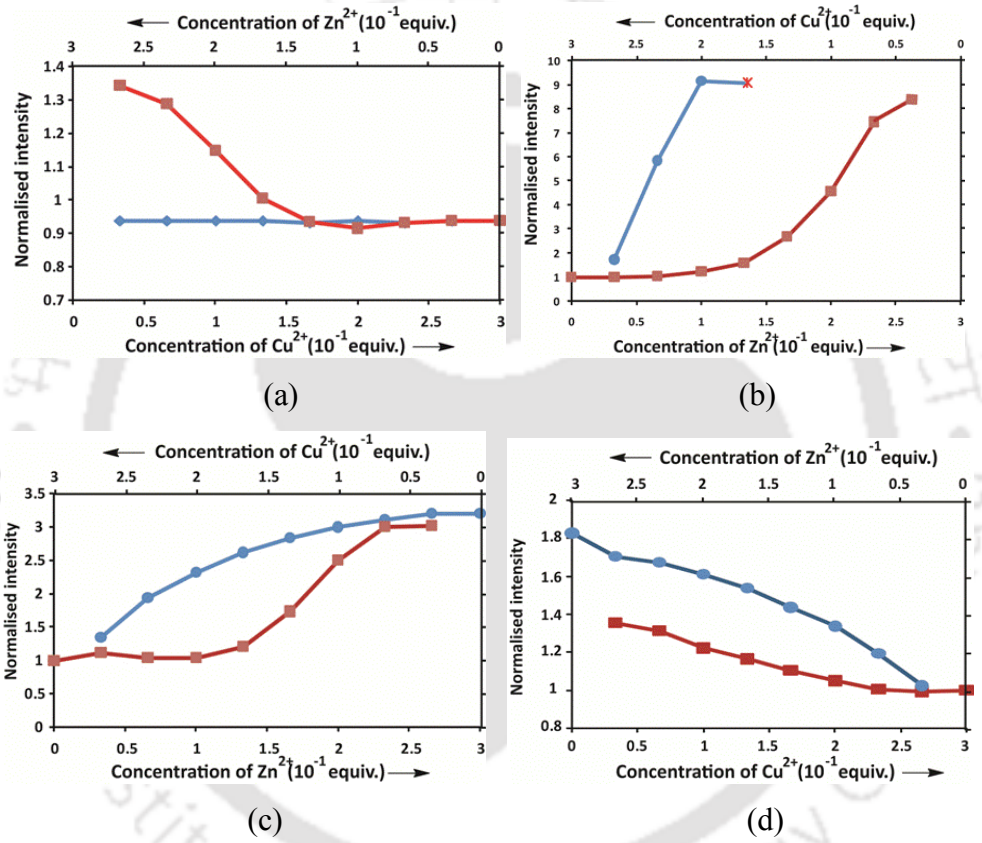

Figure 6.12: Competitive fluorescence titration showing changes in fluorescence emission of a solution of **6.1** on addition of solution of (a) cupric chloride (squares) followed by solution of zinc chloride (filled circles). (b) Zinc chloride (filled circles) followed by addition of cupric chloride (squares); compound **6.2** on addition of (c) Zinc chloride (filled circles) followed by solution of Cupric chloride (squares). (d) Cupric chloride (filled circles) followed by addition of Zinc chloride (squares), (in each case ligand 10^{-5} M in 3 mL in methanol).

Hence to avoid confusion, intensity changes beyond this point are not shown in this Figure. When a solution of cupric chloride was added to this solution, the fluorescence got quenched

(squares in Figure 6.12b). These data clearly established the fact that the quenching in the fluorescence emission of compound **6.1** caused by copper ions could not be retrieved, however the reverse case was possible. On the other hand, similar experiments carried out with compound **6.2** (Figure 6.12c and 6.12d) have revealed that fluorescence quenching at 400 nm caused by the cupric chloride could be retrieved by adding a solution of zinc chloride, and fluorescence enhancement caused by zinc ion could be quenched by cupric chloride. Thus, from the above experiment it was observed that changes in fluorescence emission of compound **6.2** on addition of metal ions was reversible unlike the case of compound **6.1**.

6.3: Isothermal calorimetry

We carried out independent isothermal calorimetry titration of compound **6.1** with zinc chloride and with copper chloride. Binding isotherms were obtained by integrating raw data which was fitted to a "one-site" model (Figure 6.13). We found the number of binding sites as 1.31 and 1.37 per ligand for Zn^{2+} and Cu^{2+} ions respectively.

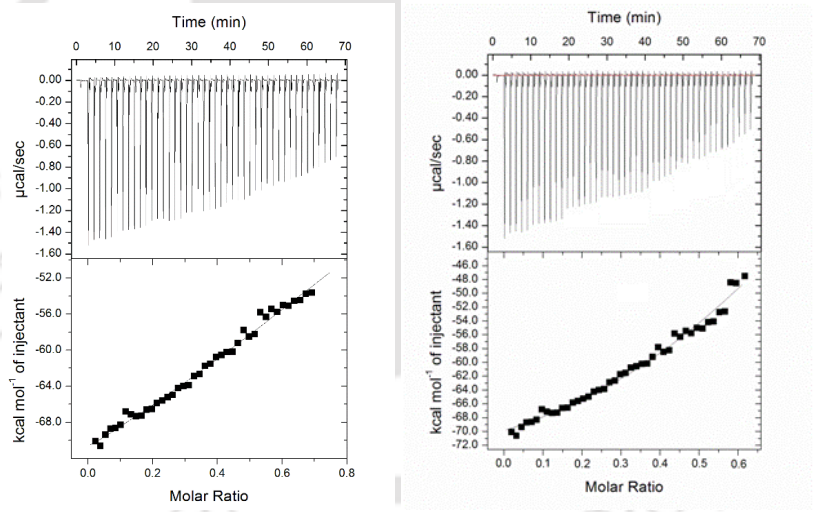

(a) (b)

Figure 6.13: Isothermal calorimetric titration of 5×10^{-5} M of compound **6.1** (1% DMSO in water) with (a) $ZnCl_2$ and (b) $CuCl_2$ (in each case 2×10^{-4} M in 1% DMSO in water) at 25 ºC.

These suggest that in each case three ligands are associated with four metal ions in complexes formed in solution. Based on this we propose structure of the aggregate with divalent copper or zinc as shown in Figure 6.14, generated through GaussView. Binding constant (K) with zinc ion is 2.67×10^4 M^{-1} and with copper is 3.47×10^4 M^{-1}; whereas enthalpy changes in case of Zn^{2+}

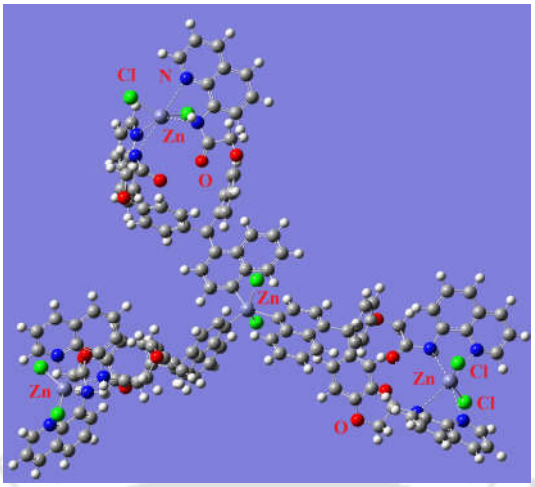

Figure 6.14: Proposed ball and stick model of aggregate of **6.1** with Zn^{2+} ions.

and Cu^{2+} ions are -9.239 cal/mol and -7.843 cal/mol and respectives entropy changes are -289 cal/mol/° and -239 cal/mol/°.

6.4: ^{1}H-NMR titration

^{1}H-NMR titration of compound **6.1** with $ZnCl_2$ showed appearance of a new set of peaks other than the ones that were observed from parent compound **6.1**. These new signals were similar to signals of parent compound in terms of coupling constants but appeared at different positions. Thus, in solution there is equilibration between the free and the bound compound **6.1** with Zn^{2+} ions. New signals were appeared as a result of the complex formation, which are marked with asterisk (Figure 6.15). Important point from NMR titration observed is the identification of duplicate set of new signals in addition to the signals of the compound **6.1**. This clearly indicated that only one type of complex was formed by compound **6.1** with Zn^{2+} ions in solution. On the other hand, it is seen that the chemical shift positions of the protons of the three quinoline rings were shifted; hence the zinc complex in solution was formed through participation of all the three quinoline rings. Signal at 7.12 ppm is attributed to phenylene protons of the *bis*-phenolate unit. This assignment is based on a comparison of ^{1}H-NMR of compound **6.1** with compound **6.2**; latter does not show this particular signal as this position is occupied partially by methyl groups. At higher concentrations of the zinc ion the aromatic proton signal appearing at 7.12 ppm splits suggesting that chelation of the 8-aminoquinoline part to Zn^{2+} ion. On the other hand, it is observed that at low concentrations of the Zn^{2+} ions NH signal of the compound **6.1** is not

affected, but new signal for NH is observed at higher concentrations of Zn^{2+} ions, this suggests that further coordination of the initially formed complex with Zn^{2+} ion affects the amide hydrogen.

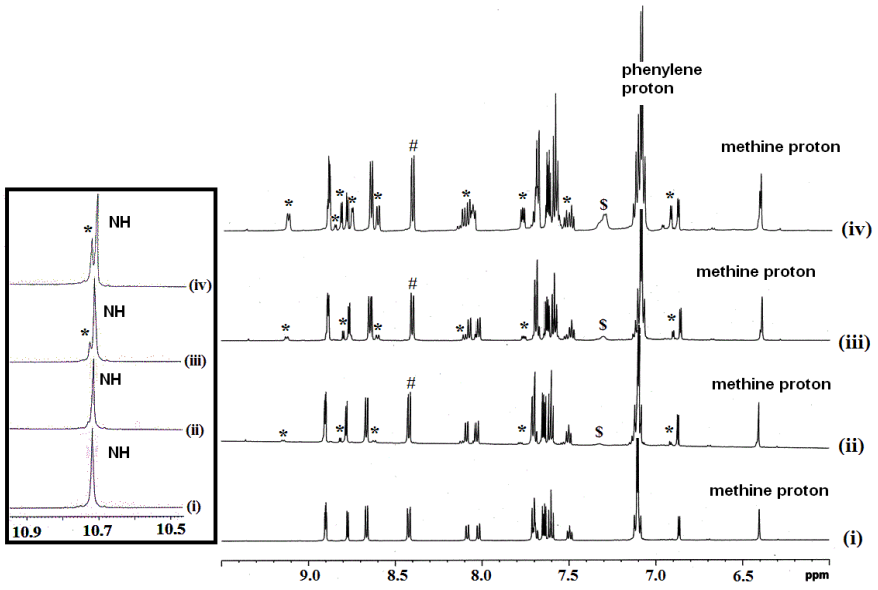

Figure 6.15: ^{1}H-NMR (600MHz, DMSO-d_6) spectra (aromatic region) of (i) **6.1**; and in the presence of (ii) 0.5 equivalent, (iii) 1.0 equivalent and (iv) excess amounts of zinc chloride dissolved in DMSO-d_6. Peaks marked by # are from compound **6.1**; whereas peaks marked as * are from compound **6.1** bound to zinc ions. Inset is the expansion in the NH protons appearing in off-set region.

Some signals of quinoline ring protons appear up-field with respect to parent signals on interaction with Zn^{2+} ions, which may be attributed to formation of planar geometry by occupying equatorial positions by nitrogen in the chelate, in which ring current may be causing such a shift. However, such up-field shifts observed from protons on quinoline rings coordinating to Zn^{2+} ions[57] was suggested to arise from restricted bond rotation and/or π-stacking interactions for coordination between the pendant quinoline moieties.[58]

Thus, we carried reaction between zinc chloride and compound **6.1** in methanol which gave the precipitate of zinc complex of compound **6.1**. When recorded ^{1}H-NMR spectrum of the precipitate obtained from the above reaction, it is observed that peaks of the parent compound are shifted in the complex (Figure 6.16).

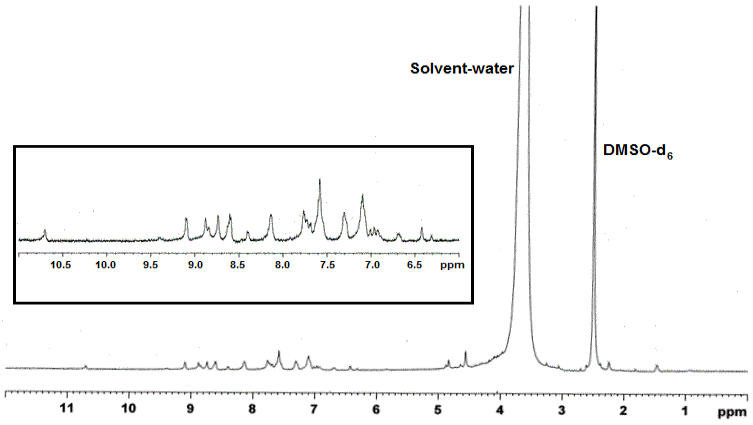

Figure 6.16: 1H-NMR (600 MHz, DMSO-d_6) spectra of zinc complex of compound **6.1**.

6.5: DFT study

To understand fluorescence emissions, we have analyzed the highest occupied molecular orbital (HOMO) and lowest unoccupied molecular orbital (LUMO) of the **6.1** and **6.2** by DFT calculation using B3LYP basis set. HOMO of **6.1** spreads over the 8-aminoquinoline amide and phenyl moiety of one arm; however LUMO spreads only on the 8-aminoquinoline amide moiety of another arm. While in case of **6.2**, HOMO and LUMO are localized on 8-aminoquinoline located at alternate arms of the skeleton (Figure 6.17). HOMO and LUMO gap of both are comparable; 0.154 eV in **6.1** and 0.153 eV in **6.2**. Since, in the compounds **6.1** and **6.2,** electrons are localized on 8-aminoquinoline amide moiety in ground state and excited states, the intervening part has no significant contribution to emission and absorption of these compounds under normal situation.

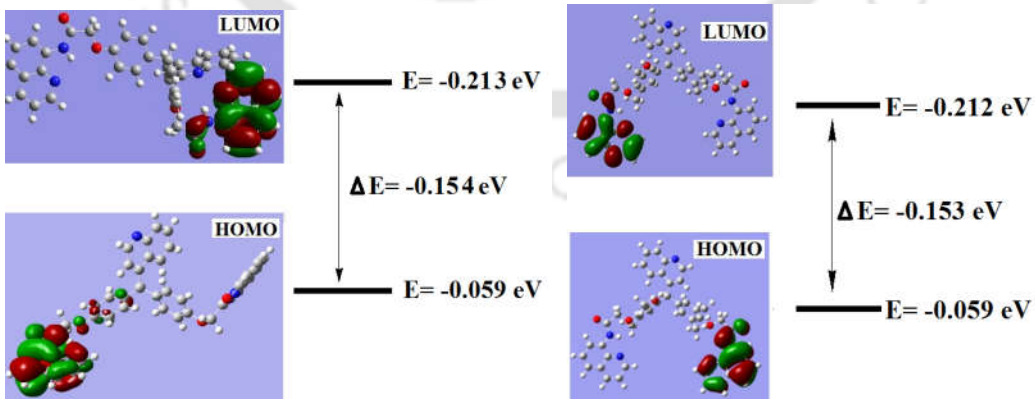

(a) (b)

Figure 6.17: HOMO and LUMO of (a) **6.1** and (b) **6.2** (calculated gas phase energies are not scaled).

Increase in the intensity of the fluorescence emissions of compounds **6.1** and **6.2** by Zn^{2+} ions can be explained by formation of a chelated complex initially, which self assembles with additional amount of zinc ions. At low concentration of Zn^{2+} ions, a mixed mechanism involving excited state proton transfer facilitated by Zn^{2+} ions and a twisted intramolecular charge transfer mechanism at high concentrations is operative in the case of compound **6.1**. Zn^{2+} ions initially participate in excited state proton transfer to show emission at higher wavelength in conventional manner as depicted earlier for analogous compounds;[13] But significant difference in the present case is the dual fluorescence emission at relatively low concentration of Zn^{2+} ions. As the concentration of Zn^{2+} ions increase compound **6.1** forms assembly by coordinating to Zn^{2+} ions through 4-quinoline moiety to adopt two different orientations across amide units (I and II in Figure 6.18). Such conformations in simple amide containing fluorescent molecules essentially causes dual fluorescence due to twisted intramolecular charge transfer (TICT) process.[42-47] Thus, compound **6.1** when coordinates to zinc ions shows dual fluorescence. Dual fluorescence generally occurs in flexible structures through twisted internal charge transfer process.[25] On the other hand, addition of Cu^{2+} ions to a methanol solution of compound **6.1**, reduce the intensity of emission at 397 nm (Figure 6.8b) and during the process no shift in emission peak was observed. Reduction in intensity of fluorescence of quinoline derivatives routinely occurs;[41] analogously, as a result of electron and energy transfer from excited state of **6.1** to a low lying empty d-orbital of paramagnetic Cu2+ ions quenching occurs. Various metal ions except Cu^{2+} ions, such as Li^{+}, Na^{+}, K^{+}, Be^{2+}, Mg^{2+}, Ca^{2+}, Ni^{2+}, Co^{2+}, Mn^{2+}, Cd^{2+}, Hg^{2+} and with Zn^{2+} ions, did not interfere in the zinc ions sensing. Effect of the substituent group such as methyl group causing equilibration of conformational isomers of metal complexes were reported eralier.[26] Based on such precedence it is suggested that due to steric factor of methyl groups in compound **6.2**, only excited state proton transfer mechanism operates. This fact is also suggested from the observation on localization of HOMO strictly on 8-aminoquinoline moiety in the case of compound **6.2**. Thus, the methyl groups present in compound **6.2** enforces relatively higher rigidity to the aggregate due to which only excited state proton transfer (III of Figure 6.18) takes place to show single emission peak at longer wavelength. Secondly, due to steric reasons the sensitivity of zinc ions to mask the detection of the copper ions and vice versa decreases in the compound **6.2**. This makes

a comparable sensitivity differences caused by these two metal ions. Hence, zinc and copper ions can be detected reversibly in this system.

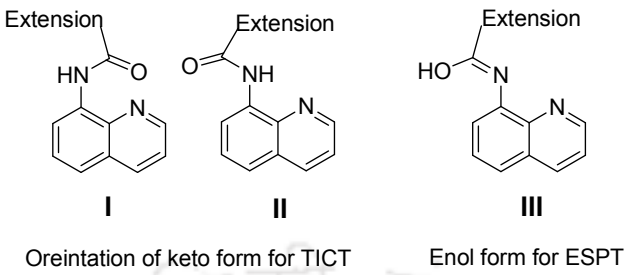

Figure 6.18: I and II are orientations of keto form for TICT; III is planar enol form for ESPT.

6.6: Conclusion

This study has established some novel and unprecedented fluorescence emission properties of aggregates formed by a tri-quinoline based receptors on interactions with Zn^{2+} ions. Methyl groups present on the aromatic ring of the connecting part of a particular tri-quinoline make distinct impact on fluorescence changes by the zinc ions to make them unique examples to show either single or dual fluorescence at different concentrations of Zn^{2+} ions. Masking effect of fluorescence emission by Cu^{2+} ions of quinoline derivatives have been overcome in a tri-quinoline receptor having methyl substituted *bis*-phenolate tether, enabling reversible modulation of the fluorescence intensities by sequential addition of Cu^{2+} and Zn^{2+} ions and vice versa. Substituent changing the emission properties of the receptors in presence of Zn^{2+} ions to show dual fluorescence makes new avenues to explore similar system and utilize them as optical materials. Compound **6.1** showing a Stokes shift of a value higher than 200 nm and also showing fluorescence spreading over a wide range of visible spectra intermittent concentration of Zn^{2+} ions requires definite attention to make new optical materials.

6.7: Experimental

The detailed synthetic methodologies for synthesis of the metal complexes are described. Analytical data are provided with each complex. The instrumental details and crystallographic parameters are provided in Appendix.

Synthesis of 2-Bromo-N-(quinolin-8-yl)acetamide:

2-Bromo-N-(quinolin-8-yl)acetamide was prepared by reported procedures.[59]

Synthesis of 6.1a:

4-Quinolinecarboxaldehyde (0.785 g, 5 mmol) and phenol (0.941 g, 10 mmol) were dissolved in acetic acid (20 mL) and the solution was stirred for half an hr in an ice bath. A mixture of concentrated sulphuric acid and glacial acetic acid (in 1:2 ratio, 10 mL, v/v) was drop-wise added to the reaction mixture. After stirring for half an hr, the mixture was kept in a deep freeze for one week. After one week, ice cold water (10 mL) was added to the reaction mixture; a white precipitate appeared. Reaction mixture was filtered and the precipitate was washed with aqueous sodium bicarbonate solution (20 %, 25 mL). The product was then dried in air. Yield ~ 75 %. ^{1}H-NMR (400 MHz, DMSO-d_6): 6.19 (s, 1H), 6.68 (d, J = 9.2Hz, 4H), 6.89 (d, J = 8.8Hz, 4H), 7.52 (t, J = 7.2Hz, 1H), 7.70 (t, J = 7.2 Hz, 1H), 8.00 (d, J = 7.6Hz, 1H), 8.08 (d, J = 8.8Hz, 1H), 8.80 (d, J = 4.8Hz, 1H), 9.34 (s, 2H). ESI mass: [M + H] Calculated for $C_{22}H_{18}NO_2$ 328.3838; found 328.0075.

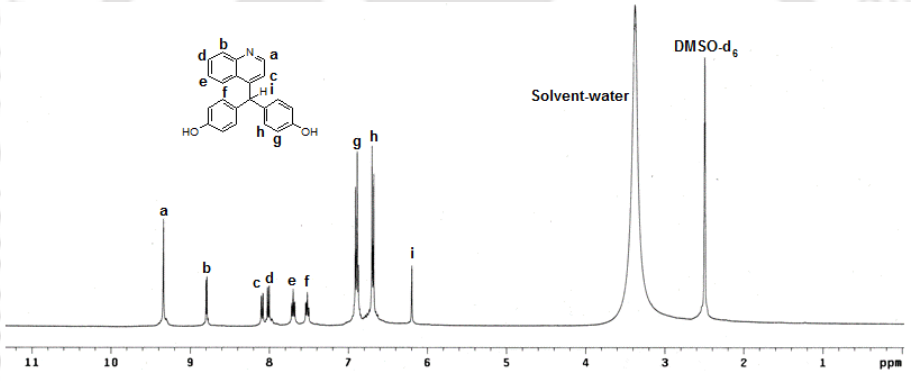

Figure 6.19: ^{1}H-NMR (400 MHz, DMSO-d_6) spectra of **6.1a**.

Synthesis of 6.2a:

Similar to compound **6.1a**, 4-quinoline-2, 6-dimethyl-bis-phenol (**2a**) was prepared by reported procedure. Yield ~ 80 %. ^{1}H-NMR (400 MHz, DMSO-d_6): 2.06 (s, 12H), 6.04(s, 1H). 6.64 (s, 4H), 6.91(d, J = 4.4 Hz, 1H), 7.51(t, J = 8 Hz, 1H), 7.68(t, J = 8 Hz, 1H), 7.99 (d, J = 8 Hz, 1H), 8.05 (d, J = 8.8Hz, 1H), 8.13 (s, 2H), 8.78 (d, J = 4.4 Hz, 1H). ESI mass: $[M-H]^-$ Calculated for $C_{26}H_{24}NO_2$ 381.4663; found 328.0075 381.8339.

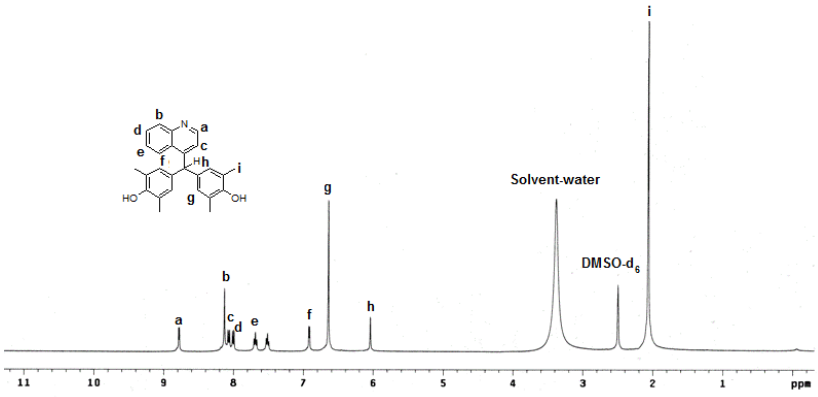

Figure 6.20: ^{1}H-NMR (400 MHz, DMSO-d_6) spectra of **6.2a**.

Synthesis of 6.1:

2-Bromo-N-(quinolin-8-yl)acetamide (1.06 g, 4 mmol), bis-phenol **6.1a** (0.67 g, 2 mmol) and anhydrous potassium carbonate (1.11 g, 8 mmol) were added to dry acetone (20 mL) in nitrogen atmosphere and the reaction mixture was stirred at 60 °C for 10 h. (Progress of the reaction was monitored at regular intervals using TLC). After completion of the reaction, solvent was removed under reduced pressure to obtain a pale yellow solid. Solid was washed with dilute sodium hydroxide solution (5%), and water; then extracted with dichloromethane. Subsequent removal of solvent and purification by chromatography (silica gel; hexane/ethyl acetate 3:2) gave compound **6.1**. The solid crude product was crystallized from methanol/DMF (4:6) solvent mixture. Yield ~ 60 %. Melting point: 183 ºC. IR (cm^{-1}): 3360 (s), 3339 (s), 2924 (m), 1638 (s), 1598 (m), 1539 (s), 1505 (s), 1425 (m), 1384 (m), 1326 (m), 1237 (s), 1217 (m), 1174 (m), 1055 (m), 826 (m), 786 (m), 754 (m), 603 (m), 513 (w).^{1}H-NMR (600 MHz, DMSO-d_6): 10.71(s, 2H), 8.90 (dd, J = 0.8 Hz, 2H), 8.77 (d, J = 3.2 Hz, 1H), 8.67 (d, J = 5.6 Hz, 2H), 8.42 (dd, J = 0.8 Hz, 2H), 8.09 (d, J = 5.6 Hz, 1H), 8.02 (d, J = 6.0 Hz, 1H), 7.71 (m, 3H), 7.65 (d, J=2.8 Hz, 2H), 7.61 (t, J = 5.2 Hz, 2H), 7.50 (t, J = 5.6 Hz, 1H), 7.12 (m, 8H), 6.86 (d, J = 3.2 Hz, 1H), 6.40 (s, 1H) 4.86 (s, 4H). ^{13}C-NMR (600 MHz, DMSO-d_6): 166.84, 156.56, 150.38, 149.91, 148.82, 139.01, 136.44, 136.25, 133.90, 130.47, 129.25, 128.21, 127.46, 126.93, 124.35, 122.48, 122.13, 121.92, 117.05, 115.63, 68.47, 51.37. ESI mass: [M + H] calculated for $C_{44}H_{34}N_5O_4$ 696.7719; found 696.2676.

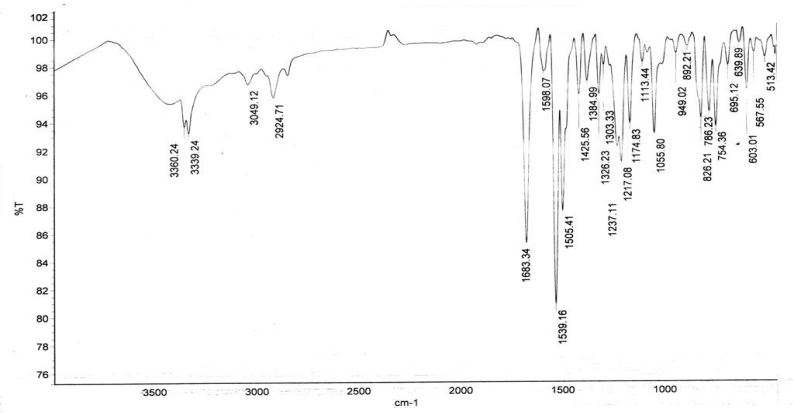

Figure 6.21: FT-IR (KBr, cm^{-1}) spectra of **6.1**.

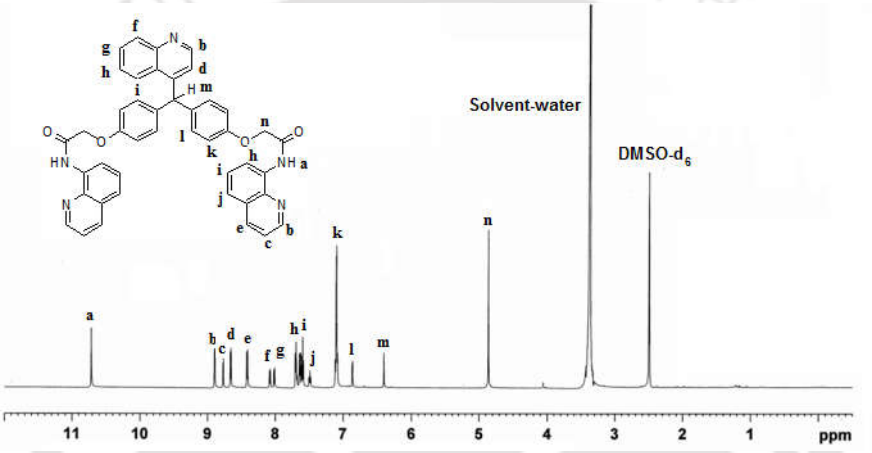

Figure 6.22: ^{1}H-NMR (600 MHz, DMSO-d_6) spectra of **6.1**.

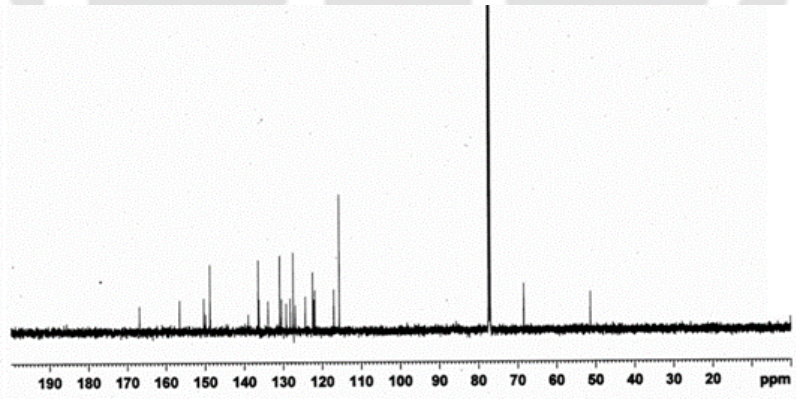

Figure 6.23: ^{13}C-NMR (600 MHz, DMSO-d_6) spectra of **6.1**.

Synthesis of 6.2:

Compound **6.2** was synthesized by a similar procedure as for **6.1** where **6.2a** was used instead of **6.1a.** The compound **6.2** was obtained as solid crude product with a yield ~ 40 %. Melting point: 157 ºC. IR (cm^{-1}): 3328 (s), 2922 (s), 2852 (m), 1676 (s), 1591(m), 1536 (s), 1483 (s), 1425 (m),

1384 (m), 1323 (m), 1203 (s), 1145 (s), 1047 (m), 952 (w), 824 (m), 791(m), 748 (m), 663 (w), 595 (w), 555 (w), 506 (w). ^{1}H-NMR (600 MHz, DMSO-d_6): 11.23 (s, 2H), 8.86 (t, *J* = 3.6 Hz, 3H), 8.83 (d, *J* =1.2 Hz, 2H), 8.18 (d, J =1.2 Hz, 1H), 8.17 (dd, J =1.2 Hz, 2H), 8.00 (d, J = 8.4 Hz, 1H), 7.70 (t, J = 6.0 Hz, 1H), 7.58 (m, 3H), 7.51 (t, J = 6.0 Hz, 1H), 7.47 (q, J = 4.2 Hz, 2H), 7.26 (s,1H), 6.98 (t, J = 4.2 Hz, 1H), 6.81 (s, 4H), 6.09 (s, 1H), 4.56 (s, 4H) 2.35 (s, 12H). ^{13}C-NMR (600 MHz, $CDCl_3$): 167.43, 153..92, 150.43, 148.83, 139.12, 183.64, 136.41, 134.13, 131.27, 130.41, 130.24, 129.28, 128.27, 127.53, 127.47, 127.02, 124.37, 122.42, 122.28, 121.91, 117.03, 71.44, 51.84, 29.91, 16.99. ESI mass: [M + H] calculated for $C_{48}H_{42}N_5O_4$ 752.8782; found 752.3273.

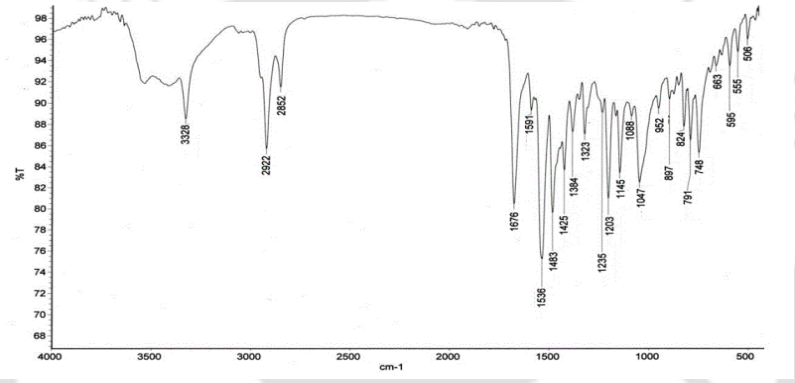

Figure 6.24: FT-IR (KBr, cm^{-1}) spectra of **6.2**.

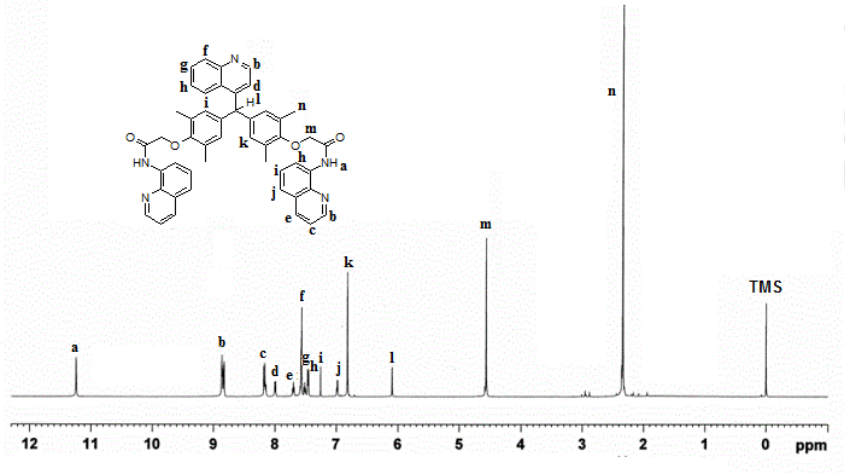

Figure 6.25: ^{1}H-NMR (600 MHz, $CDCl_3$) spectra of **6.2**.

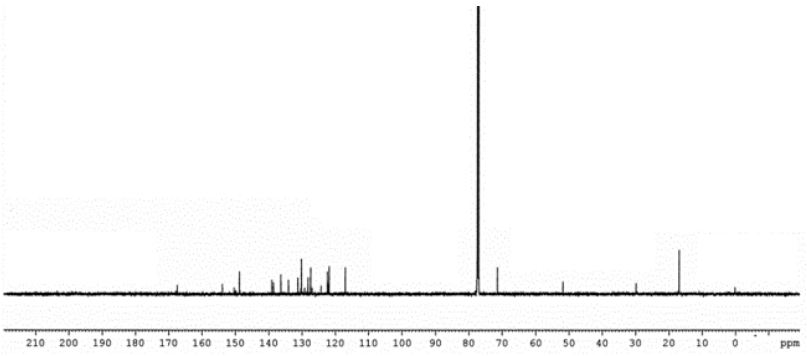

Figure 6.26: ^{13}C-NMR (600 MHz, $CDCl_3$) spectra of **6.2**.

6.8: Reference

1. X. J. Feng, P. Z. Tian, Z. Xu, S. F. Chen, M. S. Wong, *J. Org. Chem*., 2013, **78**, 11318.
2. M. H. Lee, J. S. Kim, J. L. Sessler, *Chem. Soc. Rev*., 2015, **44**, 4185.
3. J. R. Askim, M. Mahmoudia, K. S. Suslick, *Chem. Soc. Rev*., 2013, **42**, 8649.
4. S. Pal, N. Chatterjee, P. K. Bharadwaj, *RSC Adv*., 2014, **4**, 26585.
5. A. P. de Silva, H. Q. N. Gunaratne, T. Gunnlaugsson, A. J. M. Huxley, C. P. McCoy, J. T. Rademacher, T. E. Rice, *Chem. Rev*., 1997, **97**, 1515.
6. B. Kuswandi, Nuriman, W. Verboom, D. N. Reinhoudt, *Sensors*, 2006, **6**, 978.
7. B. Valeur, I. Leray, *Coord. Chem. Rev*., 2000, **205**, 3.
8. J. S. Kim, D. T. Quang, *Chem. Rev*., 2007, **107**, 3780.
9. H. Komatsu, D. Citterio, Y. Fujiwara, K. Minamihashi, Y. Araki, M. Hagiwara, K. Suzuki, *Org. Lett*., 2005, **7**, 2857.
10. M. Schmittel, H.W. Lin, *Angew. Chem. Int. Ed*., 2007, **46**, 893.
11. N. Singh, R. C. Mulrooney, N. Kaur, J. F. Callan, *Chem. Commun*., 2008, 4900.
12. H. J. Jung, N. Singh, D. Y. Lee, D. O. Jang, *Tetrahedron Lett*., 2010, **51**, 3962.
13. J. -F. Zhu, H. Yuan, W. -H. Chan, A. W. M. Lee, *Org. Biomol. Chem*., 2010, **8**, 3957.
14. J. W. Lee, H. S. Jung, P. S. Kwon, J. W. Kim, R. A. Bartsch, Y. Kim, S. -J. Kim, J. S. Kim, *Org. Lett*., 2008, **10**, 3801.
15. L. Xue, H. -H. Wang, X. -J. Wang, H. Jiang, *Inorg. Chem*., 2008, **47**, 4310.
16. L. Xue, C. Liu, H. Jiang, *Chem. Commun*., 2009, 1061.
17. C. C. Woodroofe, S. J. Lippard, *J. Am. Chem. Soc*., 2003, **125**, 11458.

18. E. M. W. M. van Dongen, L. M. Dekkers, K. Spijker, E. W. Meijer, L. W. J. Klomp, M. Merkx, *J. Am. Chem. Soc*., 2006, **128**, 10754.
19. G. K. Walkup, S. C. Burdette, S. J. Lippard, R. Y. Tsien, *J. Am. Chem. Soc*., 2000, **122**, 5644.
20. Y. Shiraishi, C. Ichimura, T. Hirai, *Tetrahedron Lett*., 2007, **48**, 7769.
21. D. A. Pearce, N. Jotterand, I. S. Carrico, B. Imperiali, *J. Am. Chem. Soc*., 2000, **123**, 5160.
22. X. -M. Meng, M. -Z. Zhu, L. Liu, Q. -X. Guo, *Tetrahedron Lett*., 2006, **47**, 1559.
23. S. Mizukami, S. Okada, S. Kimura, *Inorg. Chem*., 2009, **48**, 7630.
24. K. Komatsu, Y. Urano, H. Kojima, T. Nagano, *J. Am. Chem. Soc*., 2007, **129**, 13447.
25. M. M. Henary, Y. Wu, C. J. Fahrni, *Chem. Eur. J*., 2004, **10**, 3015.
26. T. Hirano, K. Kikuchi, Y. Urano, T. Nagano, *J. Am. Chem. Soc*., 2002, **124**, 6555.
27. X. H. Wang, J. Cao, C. F. Chen, Chinese J. Chem., 2010, **28**, 1777.
28. T. Moriuchi- Kawakami, J. Sato, Y. Shibutani, *Anal. Sci*., 2009, **25**, 449.
29. G. -K. Li, Z. -X. Xu, C. -F. Chen, Z. -T. Huang, *Chem. Commun*., 2008, 1774.
30. V. Dujols, F. Ford, A. W. Czarnik, J. Am. Chem. Soc., 1997, **119**, 7386.
31. E. Ballesteros, D. Moreno, T. Gomez, T. Rodriguez, J. Rojo, M. Garcia-Valverde, T. Torroba, *Org. Lett*., 2009, **11**, 1269.
32. A. C. Burdette, S. J. Lippard, *Proc. Nat. Acad. Sci. USA*, 2003, **100**, 3605.
33. C. J. Frederickson, E. J. Kasarskis, D. Ringo, R. E. Frederickson, *J. Neurosci. Meth*., 1987, **20**, 91.
34. P. D. Zalewski, I. J. Forbes, R. Borlinghaus, W. H. Betts, S. F. Lincoln, A. D. Ward, *Chem Biol*., 1994, **1**, 153.
35. P. D. Zalewski, S. H. Millard, I. J. Forbes, O. Kapaniris, A. Slavotinek, W. H. Betts, A. D. Ward, S. F. Lincoln, I. Mahadevan, *J. Histochem. Cytochem*., 1994, **42**, 877.
36. L. Xue, H. -H. Wang, X. -J. Wang, H. Jiang, *Inorg. Chem*., 2008, **47**, 4310.
37. L. Xue, C. Liu, H. Jiang, *Chem. Commun*., 2009, 1061.
38. E. M. Nolan, J. Jaworski, K. -I. Okamoto, Y. Hayashi, M. Sheng, S. J. Lippard, *J. Am. Chem. Soc*., 2005, **127**, 16812.
39. P. -S. Yao, Z. Liu, J. -Z. Ge, Y. Chen, Q. -Y. Cao, *Dalton Trans*., 2015, **44**, 7470.
40. X. Y. Zhou, B. R. Yu, Y. L. Guo, X. L. Tang, H. H. Zhang, W. S. Liu, *Inorg. Chem*., 2010, **49**, 4002.

41. J. Jiang, H. Jiang, X. Tang, L. Yang, W. Dou, W. Liu, R. Fang, W. Liu, *Dalton Trans*., 2011, **40**, 6367.
42. H. Kagechika, T. Himi, E. Kawachi, K. Shudo, *J. Med. Chem*.,1989, **32**, 2292.
43. Y. Toriumi, A. Kasuya, A. Itai, *J. Org. Chem*., 1990, **55**, 259.
44. A. Itai, Y. Toriumi, N. Tomioka, H. Kagechika, I. K. Azumaya, *Tetrahedron Lett*., 1989, **30**, 6177.
45. I. Azumaya, H. Kagechika, Y. Fujiwara, M. Itoh, K. Yamaguchi, K. Shudo, *J. Am. Chem. Soc*., 1991, **113**, 2833.
46. J. Kim, T. Morozumi, N. Kurumatani, H. Nakamura, *Tetrahedron Lett*., 2008, **49**, 1984.
47. J. Kim, T. Morozumi, H. Nakamura, *Tetrahedron*, 2008, **64**, 10735.
48. G. Ambrosi, M. Formica, V. Fusi, L. Giorgi, A. Guerri, M. Micheloni, P. Paoli, R. Pontellini, P. Rossi, *Inorg. Chem*., 2007, **46**, 4737.
49. A. Anichini, L. Fabbrizzi, P. Paoletti, R. M. Clay, J. Chem. Soc., *Dalton Trans*., 1978, 577.
50. P. Dapporto, M. Formica, V. Fusi, L. Giorgi, M. Micheloni, P. Paoli, R. Pontellini, P. Rossi, *Inorg. Chem*., 2001, **40,** 6186.
51. G. Ambrosi, M. Formica, V. Fusi, L. Giorgi, A. Guerri, S. Lucarini, M. Micheloni, P. Paoli, P. Rossi, G. Zappia, *Inorg. Chem*., 2007, **46**, 309.
52. G. Ambrosi, M. Formica, V. Fusi, L. Giorgi, A. Guerri, S. Lucarini, M. Micheloni, P. Paoli, P. Rossi, G. Zappia, *Inorg. Chem*., 2005, **44**, 3249.
53. J. S. Kim, D. T. Quang, *Chem. Rev*., 2007, **107**, 3780.
54. S. Patra, D. Maity, R. Gunupuru, P. Agnihotri, P. Paul, *J. Chem. Sci*., 2012, **124**, 1287.
55. Y. Chen, C. Zhu, Z. Yang, J. Li, Y. Jiao, W. He, J. Chen, Z. Guo, *Chem. Commun*., 2012, **48**, 5094.
56. H. S. Jung, P. S. Kwon, J. W. Lee, J. I. Kim, C. S. Hong, J. W. Kim, S. Yan, J. Y. Lee, J. H. Lee, T. Joo, J. S. Kim, *J. Am. Chem. Soc*., 2009, **131**, 2008.
57. P. -S. Yao, Z. Liu, J. -Z. Ge, Y. Chen, Q. -Y. Cao, *Dalton Trans*., 2015, **44**, 7470.
58. Q. -Y. Cao, Z. -C. Wang, M. Li, J. -H. Liu, *Tetrahedron Lett*., 2013, **54**, 3933.
59. A. Karmakar, R. J. Sarma, J. B. Baruah, *CrystEngComm*., 2007, **9**, 379.

Conclusion

The products from various reactions between zinc chloride and 8-hydroxyquinoline in 1:1 molar ratio in different solvents were guided by the solvent. The different solvates of tetranuclear zinc-oxyquinolate complexes, hydroxyquinolium tetrachlorozincate complex and zinc oxyquinolate molecular complex could be prepared by changing the solvent have shown the sensitivity of formation of products on reaction conditions. The tetranuclear zinc-oxyquinolate complexes showed reversible absorption of atmospheric moisture on standing at room temperature which are reflected on the changes in the color of these metal complexes. A composite material of zinc oxide within the matrix of metal complex was prepared by taking the advantage hydrolytic instability of zinc chloride in the presence of hydroxyquinoline. A unique example of a molecular complex of two mono nuclear zinc-oxyquinolate complexes in 3-methylpyridine having metal centers with different coordination environments is unearthed. Tetranuclear cobalt (II) and manganese (II) complexes are used as building blocks to construct their respective decanuclear metal clusters by trapping carbonate ions formed *in situ.* Thus, this reaction provides avenue to construct new clusters. Tetranuclear cobalt (II) complex as well as decanuclear clusters of cobalt (II) and manganese (II) showed strong anti-ferromagnetic property, which opens possibilities for synthesis of new magnetic materials with analogous ligands.

Electron deficiency in the protonated nitroso derivative of 8-hydroxyquinoline helped to place the counter anions at suitable positions to show anion-π interactions. In all the salts perching type of anion-π interactions were observed; where the cations and anions were placed in alternate positions. The nitrate anion was observed to occupy oblique with respect to cation, which is a rare example. The anion-π interaction between nitrate and quinolinium ion showed exceptionally shorter distance compared to the conventional anion-π distances. These salts remain as strong ion pairs in solution. Thus, anion-π interactions are too weak to make distinctions in binding constants due to large electrostatic interactions contributing to the salts in solutions.

The deprotonation of oxime moiety present in the quinoline derivative by fluoride anion visually distinguished it from other analogous anions in slightly acidic pH. However, the acetate ions were found to interfere in the detection fluoride ions as it decreases the fluorescence intensity of the compound. Sharp enhancement in the fluorescence intensity of the 8-hydroxyquinoline

derivative on complexation with zinc ion enabled selective detection of zinc ion over other metal ions. The difference in the colors of the parent compound from the host-guest complex with fluoride salt or the zinc complex enabled detection of fluoride anion or zinc ion in solution as well as in solid state.

Taking advantage of possible partial bond rotation across the amide bond of 8-aminoquinoline derivative, four conformational polymorphs were prepared by crystallization from solutions in different solvents. Highly ordered structures were observed in each case, comprising of molecules with different orientations. The monotropic relationship between the three polymorphs was established by differential scanning calorimetry analysis. The dihedral angles of aromatic plane across the amide bond of the protonated 8-aminoquinoline derivative were dependent on the size and shape of the counter anions.

The formation of salt or co-crystal in various combinations of aminoquinolines and hydroxyaromatic carboxylic acids were determined by the differences in p*Ka* values of the partner compounds. In hydrated salt, the anionic assemblies were observed to be assisted by water molecules. A channel like structure was observed in the salt of gallic acid with 5-aminoquinoline. The salts and cocrystal formation enhanced the antimalarial activities over their respective individual parent compounds. Enhanced activity could be attributed to the increase in hydrophilicity of these salts and adducts through proton sharing or proton transfer between the two counterparts. The covalently linked simple amide derivatives of aminoquinolines were not potent. Moreover, antimalarial actions on the parasites by the salt of 5-aminoquinoline with gallic acid was comparable with safety profile to chloroquine and independent of iron chelation as well as haemozoin formation.

The aggregates formed between a tri-quinoline based receptors with or without zinc ions showed novel and unprecedented fluorescence emission properties. Presence or absence of substituent on the aromatic ring of the connecting part of a particular *tri*-quinoline receptor exhibited either single or dual fluorescence at different concentrations of zinc ions. Masking effect of fluorescence emission by Cu^{2+} ions have been suppressed in one of the *tri*-quinoline receptor having methyl groups in the *bis*-phenolate moiety, enabling reversible modulation of the fluorescence intensities by sequential addition of Cu^{2+} and Zn^{2+} ions and vice versa. The ability of substituent to modulate the emission properties of the receptors in presence of zinc ions to

show dual fluorescence makes new avenue to explore similar systems and utilize them as optical materials. *Tri*-quinoline based receptor showing a Stokes shift of a value higher than 200 nm and fluorescence emission spreading over a wide range of visible spectra at intermittent concentration of zinc ions requires definite attention to make new optical materials.

Appendix

Details of the analytical instruments:

X-Ray Crystallography:

X-ray diffraction data were collected on Bruker 3-circle diffractometers with CCD area detectors ProteumM APEX or SMART 6000 or Bruker Nonius Apex 2, using graphite-monochromated Mo-$K\alpha$ radiation (λ = 0.71073 Å) from a 60W microfocus Bede Microsource® with glass polycapillary optics or a sealed tube.

X-ray diffraction data for crystals were collected using Bruker SMART software. This software was also used for indexing and determination of the unit cell parameters. Some of the crystal diffraction data were collected on Oxford SuperNova diffractometer. Data refinement and cell reductions were carried out by CrysAlisPro. The structures were solved by direct methods and refined by full-matrix least squares against F^2 of all data, using SHELXTL software. The CIF of all the compounds synthesized and characterized are included in the soft copy.

All non-H atom were refined by full-matrix least squares in anisotropic, all H atoms in isotropic approximation, against F^2 of all reflections. All non-H atoms were refined by full-matrix least squares in the anisotropic approximation and the hydrogen atoms attached to these atoms were treated as 'riding' in calculated positions and in some of the cases the hydrogen atoms have been located on the difference Fourier maps. In all cases the hydrogen atoms attached to polar atoms such as O and N were located on the difference Fourier maps and refined in the final structure in isotropic approximation. The crystallographic tables for all the compounds are given at the end of this section, which includes the crystal parameters and the refinement factors.

Powder X-ray diffraction (XRD) patterns were recorded out on a Bruker D8 Advance (Germany) diffractometer with Cu Kα (1.542 Å) radiations operated at 40 kV and 40 mA on a glass surface of an air-dried sample.

IR Spectroscopy, UV-visible Spectroscopy and Fluorescence Spectroscopy:

IR spectra were recorded on a Perkin-Elmer Spectrum One FT-IR spectrometer with KBr pallet in the range 4000-400 cm-1. UV-Vis spectra data were recorded using Perkin-Elmer Lambda

750 UV-Vis spectrophotometer. Fluorescence emission spectra were recorded on a Horiba Jobin Yvon Fluoromax-4 spectrofluorimeter.

NMR Spectroscopy

The NMR spectra were recorded in a Bruker 400 MHz spectrometer and Oxford 600 MHz NMR spectrometer. The chemical shifts in the NMR spectra are all given in ppm and tetramethylsilane as the internal standard.

Differential scanning calorimetry and Thermogravimetric study:

Differential scanning calorimetry (DSC) were performed on a TA Instruments Q20 differential scanning calorimeter and SDT Q600 analyzer under nitrogen atmosphere from 35 to 350^0C with a heating rate of 10^0C. The thermogravimetric studies were carried out using a Mettlar Teledo TGA/STDA 851 thermal analyzer and also with TA instrument with model no. SDT Q600.

EPR spectroscopy, Surface analysis and Hot stage microscope:

Solid state X band electron paramagnetic resonance spectrum was recorded on a JES-FA200 ESR spectrometer and DPPH was used as internal standard. The surface analysis was carried out by using a Quantachrome, Model: Autosorb-IQ MP surface analyser. An optical microscope (BX-51, Olympus, Japan) equipped with a CCD camera (XC10) was used to take images of the crystal morphology.

Isothemal calorimetry and mass spectroscopy:

Thermodynamic parameters of the binding constants were determined by iTC 200 Microcalorimeter at 20 °C. ESI-mass spectra were recorded on a micro mass Q-TOF (Waters) mass spectrometer using acetonitrile / formic acid matrix.

DFT calculation:

Energy level calculations were carried out using the hybrid B3LYP functional under the density functional theory framework with the Gaussian 04 program package.

Bond parameters of complex **2.4**

Bond	Length (Å)	Bond angle	Angle (°)
Zn1-Br1	2.43(7)	Br1-Zn1-O1	108.23(7)
Zn1-O1	2.01(4)	Br1-Zn1-O2	106.31(7)
Zn1-O2	2.28(2)	Zn1-O2-Zn2a	171.71(7)
Zn1-O3	2.01(3)	Br1-Zn1-O3	106.45(13)
Zn1-N3	2.12(4)	Br1-Zn1-N3	97.20(9)
Zn2-O1	2.10(2)	Zn1-O3-Zn2	96.36(9)
Zn2-O3	2.13(3)	Zn1-O3-Zn2a	97.27(10)
Zn2-N1	2.07(4)	Zn2-O3-Zn2a	100.16(11)

Crystallographic data and refinement parameters for the compounds:

Compound No.	**2.1**	**2.2**	**2.3**	**2.4**
Formulae	$C_{60}H_{50}Cl_2N_8O_8Zn_4$	$C_{62}H_{54}Cl_2N_8O_8Zn_4$	$C_{58}H_{48}Cl_2N_6O_8S_2Zn_4$	$C_{60}H_{50}Br_2N_8O_8Zn_4$
Mol. wt.	1343.46	1371.51	1353.52	1432.38
CCDC No	960180	960179	960181	960177
Crystal system	Triclinic	Triclinic	Triclinic	Triclinic
Space group	*P-1*	*P-1*	*P-1*	*P-1*
Temperature (K)	296 (2)	296 (2)	296 (2)	296 (2)
Wavelength (Å)	0.71073	0.71073	0.71073	0.71073
a (Å)	11.4278(7)	11.2931(7)	11.5945(6)	11.3662(7)
b (Å)	12.5311(6)	12.6163(8)	12.4479(9)	12.5613(8)
c (Å)	12.6744(7)	12.7410(7)	12.5482(10)	12.6119(8)
α (°)	101.688(4)	102.346(5)	99.560(7)	101.500(5
β (°)	110.189(5)	111.205(5)	114.464(7)	109.660(6)
γ (°)	112.178(5)	109.004(5)	109.975(6)	111.242(6)
V ($Å^3$)	1457.18(14)	1482.62(15)	1445.71(18)	1470.82(16)
Z	1	1	1	1
Density/gcm^{-3}	1.531	1.536	1.555	1.617
Abs. Coeff. /mm^{-1}	1.780	1.751	1.863	3.031
Abs. correction	Multi-scan	None	Multi-scan	Multi-scan
F(000)	684	700	688	720
Total no. of reflections	5259	5364	5231	5323
Reflections, $I > 2\sigma(I)$	4012	4054	3572	3993
Max. 2θ (°)	50.50	50.50	50.50	50.50
Ranges (h, k, l)	$-13 \le h \le 13$ $-15 \le k \le 11$ $-15 \le l \le 15$	$-13 \le h \le 13$ $-15 \le k \le 15$ $-15 \le l \le 15$	$-13 \le h \le 13$ $-14 \le k \le 14$ $-15 \le l \le 15$	$-13 \le h \le 13$ $-15 \le k \le 14$ $-15 \le l \le 13$
Completeness to 2θ (%)	0.999	0.999	0.999	0.999

Data/ Restraints / Parameters	5259 / 0 / 372	5364 / 32 / 382	5231 / 0 / 363	5323 / 0 / 372
Goof (F^2)	1.035	1.034	1.049	1.028
R indices [$I > 2\sigma(I)$]	0.0422	0.0548	0.0615	0.0421
R indices (all data)	0.0610	0.0751	0.0936	0.0638

Compound No.	**2.5**	**2.6**	**2.7**	**2.10**
Formulae	$C_{18}H_{16}Cl_4N_2O_2Zn$	$C_{78}H_{68}N_{10}O_9Zn_3$	$C_{54}H_{36}Cl_2N_6O_{14}Co_4$	$C_{121}H_{94}N_{15}O_{27.5}Co_{10}$
Mol. wt.	499.50	1485.53	1171.51	2787.41
CCDC No	960182	960178	1025061	1022853
Crystal system	Monoclinic	Monoclinic	Monoclinic	Cubic
Space group	*C2/c*	*P2/c*	*P21/n*	*Pa-3*
Temperature (K)	296(2)	296(2)	296(2)	296(2)
Wavelength (Å)	0.71073	0.71073	0.71073	0.71073
a (Å)	15.2315(10)	22.9887(12)	11.0742(4)	28.1201(4)
b (Å)	8.1375(9)	8.3971(4)	13.6865(5)	28.1201(4)
c (Å)	16.742(2)	18.0997(8)	17.0032(7)	28.1201(4)
α (°)	90.00	90.00	90.00	90.00
β (°)	91.413(9)	93.958(4)	105.997(3)	90.00
γ (°)	90.00	90.00	90.00	90.00
V ($Å^3$)	2074.5(4)	3485.6(3)	2477.33(16)	22235.7(6)
Z	4	2	2	8
Density/gcm^{-3}	1.599	1.415	1.742	1.665
Abs. Coeff. /mm^{-1}	1.715	1.091	1.503	1.538
Abs. correction	Multi-scan	None	Multi-scan	Multi-scan
F(000)	1008	1536	1312	11320
Total no. of reflections	1870	6301	4992	7035
Reflections, $I > 2\sigma(I)$	1126	4013	3194	4024
Max. 2θ (°)	50.48	50.50	52.74	51.31
Ranges (h, k, l)	$-18 \le h \le 9$ $-9 \le k \le 9$ $-20 \le l \le 8$	$-27 \le h \le 27$ $-10 \le k \le 7$ $-21 \le l \le 20$	$-13 \le h \le 13$ $-17 \le k \le 17$ $-21 \le l \le 21$	$-34 \le h \le 34$ $-34 \le k \le 34$ $-34 \le l \le 34$
Completeness to 2θ (%)	0.992	0.998	0.986	0.998
Data/ Restraints / Parameters	1870 / 0 / 128	6301 / 7 / 467	4992 / 384 / 409	7035 / 62 / 486
Goof (F^2)	1.043	1.052	1.048	1.067
R indices [$I > 2\sigma(I)$]	0.0413	0.0647	0.0521	0.0679
R indices (all data)	0.0663	0.1058	0.0942	0.1348

Compound No.	**2.11**	**3.2**	**3.3**	**3.4**
Formulae	$C_{121}H_{94}N_{15}O_{27.5}Mn_{10}$	$C_9H_7N_2O_2Cl$	$C_9H_7N_2O_2Br$	$C_{18}H_{14}N_4OCl_2$
Mol. wt.	2747.51	210.62	255.08	565.23

CCDC No	1022854	914800	914799	914803
Crystal system	Cubic	Monoclinic	Monoclinic	Monoclinic
Space group	*Pa-3*	$P2_1/m$	$P2_1/m$	$C2/c$
Temperature (K)	296(2)	296(2)	296(2)	296(2)
Wavelength (Å)	0.71073	0.71073	0.71073	0.71073
a (Å)	28.2948(3)	7.7196(4)	7.7467(8)	14.2720(9)
b (Å)	28.2948(3)	6.5230(3)	6.7200(9)	7.3529(3)
c (Å)	28.2948(3)	9.1079(5)	9.2752(10)	21.2213(12)
α (°)	90.00	90.00	90.00	90.00
β (°)	90.00	96.577(3)	94.889(8)	96.845(4)
γ (°)	90.00	90.00	90.00	90.00
V ($Å^3$)	22652.7(7)	455.61(4)	481.09(10)	2211.1(2)
Z	8	2	2	4
Density/gcm^{-3}	1.611	1.535	1.761	1.698
Abs. Coeff. /mm^{-1}	1.160	0.391	4.245	0.375
Abs. correction	Multi-scan	None	Multi-scan	Multi-scan
F(000)	11160	216	252	1152
Total no. of reflections	7709	890	894	1996
Reflections, $I > 2\sigma(I)$	3366	784	704	1816
Max. 2θ (°)	52.72	50.46	49.46	50.50
Ranges (h, k, l)	$-35 \leq h \leq 35$ $-35 \leq k \leq 35$ $-35 \leq l \leq 35$	$-8 \leq h \leq 9$ $-7 \leq k \leq 7$ $-10 \leq l \leq 10$	$-9 \leq h \leq 9$ $-7 \leq k \leq 7$ $-10 \leq l \leq 10$	$-17 \leq h \leq 17$ $-8 \leq k \leq 8$ $-24 \leq l \leq 25$
Completeness to 2θ (%)	0.998	0.994	0.999	0.996
Data/ Restraints / Parameters	7709 / 59 / 486	890 / 0 / 85	894 / 0 / 85	1996 / 0 / 182
Goof (F^2)	1.025	1.023	1.039	1.046
R indices [$I > 2\sigma(I)$]	0.0844	0. 0380	0.0552	0.0870
R indices (all data)	0.1927	0. 0415	0.0708	0.0919

Compound No.	**3.5**	**3.6**	**3.7**	**3.9**
Formulae	$C_9H_7N_3O_5$	$C_9H_9N_3O_3$	$C_8H_7N_3O_4$	$C_{50}H_{82}F_2N_6O_7$
Mol. wt.	237.18	207.19	209.17	917.22
CCDC No	914801	944122	944121	1024294
Crystal system	Monoclinic	Monoclinic	Monoclinic	Monoclinic
Space group	$P2_1/c$	$P2_1/c$	$P2_1/c$	$P2_1/c$
Temperature (K)	296(2)	296(2)	296(2)	296(2)
Wavelength (Å)	0.71073	0.71073	0.71073	0.71073
a (Å)	10.1679(3)	9.0298(8)	5.2491(4)	22.5699(14)
b (Å)	6.8254(2)	4.9832(7)	10.7683(7)	9.4519(7)
c (Å)	14.2890(5)	20.8468(19)	16.3714(18)	26.9700(17)
α (°)	90.00	90.00	90.00	90.00

β (°)	95.034(2)	93.080(9)	95.572(9)	104.307(3)
γ (°)	90.00	90.00	90.00	90.00
V (Å^3)	987.83(5)	936.70(17)	921.01(14)	5575.0(6)
Z	4	4	4	4
Density/gcm^{-3}	1.595	1.469	1.508	1.093
Abs. Coeff. /mm^{-1}	0.133	0.113	0.124	0.077
Abs. correction	None	None	None	Multi-scan
F(000)	488	432	432	1992
Total no. of reflections	1785	1673	1664	9788
Reflections, $I > 2\sigma(I)$	1592	939	1145	5598
Max. 2θ (°)	50.48	50.48	50.48	50.00
Ranges (h, k, l)	-12 ≤ h ≤ 12 -8 ≤ k ≤ 8 -17 ≤ l ≤ 17	-10 ≤ h ≤ 6 -3 ≤ k ≤ 5 -21 ≤ l ≤ 25	-6 ≤ h ≤ 6 -12 ≤ k ≤ 12 -19 ≤ l ≤ 12	-26 ≤ h ≤ 26 -11 ≤ k ≤ 11 -32 ≤ l ≤ 32
Completeness to 2θ (%)	1.000	0.991	0.998	0.998
Data/ Restraints / Parameters	1785 / 0 / 155	1673 / 0 / 172	1664 / 0 / 140	9788 / 3 / 583
Goof (F^2)	1.065	1.140	0.917	1.351
R indices [$I > 2\sigma(I)$]	0.0426	0.0508	0.0420	0.0933
R indices (all data)	0.0466	0.1027	0.0667	0.2050

Compound No.	**3.10**	**Polymorph VII**	**Polymorph VIII**	**Polymorph IX**
Formulae	$C_{18}H_{14}N_4O_6Zn$	$C_{16}H_{11}N_3O_3$	$C_{16}H_{11}N_3O_3$	$C_{16}H_{11}N_3O_3$
Mol. wt.	447.70	293.28	293.28	293.28
CCDC No	983710	902577	902578	902579
Crystal system	Triclinic	Monoclinic	Monoclinic	Monoclinic
Space group	*P-1*	$P2_1/c$	$P2_1/c$	*Cc*
Temperature (K)	296(2)	296 (2)	296 (2)	296 (2)
Wavelength (Å)	0.71073	0.71073	0.71073	0.71073
a (Å)	7.2755(9)	7.5561(8)	10.2024(10)	3.8313(3)
b (Å)	7.9392(9)	25.171(3)	13.3545(12)	14.6334(7)
c (Å)	8.4103(9)	7.1509(8)	12.6962(13)	23.5223(13)
α (°)	74.394(10)	90.00	90.00	90.00
β (°)	64.840(11)	99.671(7)	128.364(6)	90.851(6)
γ (°)	87.012(10)	90.00	90.00	90.00
V (Å^3)	422.41(8)	1340.7(2)	1356.3(2)	1318.63(14)
Z	1	4	4	4
Density/gcm^{-3}	1.760	1.453	1.436	1.477
Abs. Coeff. /mm^{-1}	1.503	0.104	0.102	0.105
Abs. correction	Multi-scan	None	None	None

F(000)	228	608	608	608
Total no. of reflections	1533	2304	2342	1615
Reflections, $I > 2\sigma(I)$	1297	1128	1209	1457
Max. 2θ (°)	50.50	50.00	50.00	50.00
Ranges (h, k, l)	$-8 \le h \le 8$ $-8 \le k \le 9$ $-8 \le l \le 10$	$-8 \le h \le 8$ $-29 \le k \le 27$ $-8 \le l \le 8$	$-12 \le h \le 11$ $-15 \le k \le 15$ $-23 \le l \le 24$	$-4 \le h \le 4$ $-15 \le k \le 16$ $-27 \le l \le 25$
Completeness to 2θ (%)	0.998	0.975	0.988	0.998
Data/ Restraints / Parameters	2304 / 0 / 199	2304 / 0 / 199	2342 / 0 /199	1615 / 2 / 199
Goof (F^2)	0.924	1.027	1.024	1.029
R indices [$I > 2\sigma(I)$]	0.0417	0.0542	0.0461	0.0427
R indices (all data)	0.0539	0.1247	0.1148	0.0474

Compound No.	**4.3**	**Polymorph X**	**Polymorph XI**	**4.5**
Formulae	$C_{16}H_{11}N_3O_3$	$C_{20}H_{18}N_2O_4$	$C_{20}H_{18}N_2O_4$	$C_{18}H_{17}N_3O_7S$
Mol. wt.	293.28	350.36	350.36	419.41
CCDC No	1417843	1417845	1417844	902580
Crystal system	Monoclinic	Monoclinic	Triclinic	Triclinic
Space group	$P2_1$	$P2_1/n$	*P-1*	*P-1*
Temperature (K)	296 (2)	296 (2)	296 (2)	296 (2)
Wavelength (Å)	0.71073	0.71073	0.71073	0.71073
a (Å)	7.5262(6)	10.1836(13)	7.8618(6)	7.550(3)
b (Å)	23.9065(19)	15.7803(16)	8.3966(7)	10.677(3)
c (Å)	7.5360(5)	10.9900(14)	13.2455(11)	12.235(5)
α (°)	90.00	90.00	88.121(5)	107.628(16)
β (°)	91.955(5)	99.124(14)	89.539(5)	95.921(19)
γ (°)	90.00	90.00	85.062(5)	94.540(11)
V ($Å^3$)	1355.13(18)	1743.8(4)	870.64(12)	928.6(6)
Z	4	4	2	2
Density/gcm^{-3}	1.438	1.335	1.336	1.500
Abs. Coeff. /mm^{-1}	0.102	0.094	0.094	0.223
Abs. correction	None	None	None	None
F(000)	608	736	368	436
Total no. of reflections	4851	3151	3011	3289
Reflections, $I > 2\sigma(I)$	2791	1896	2279	2433
Max. 2θ (°)	50.48	50.50	50.00	50.48
Ranges (h, k, l)	$-9 \le h \le 9$ $-28 \le k \le 28$ $-9 \le l \le 9$	$-12 \le h \le 11$ $-18 \le k \le 18$ $-13 \le l \le 13$	$-9 \le h \le 9$ $-9 \le k \le 9$ $-15 \le l \le 15$	$-8 \le h \le 9$ $-12 \le k \le 12$ $-9 \le l \le 14$
Completeness to 2θ (%)	1.000	0.998	0.982	0.983

Data/ Restraints / Parameters	4851 / 1 / 397	3151 / 1 / 240	3011 / 3 / 236	3289 / 0 / 263
Goof (F^2)	1.022	1.128	1.070	1.100
R indices [$I > 2\sigma(I)$]	0.0484	0.1628	0.1872	0.0452
R indices (all data)	0.1192	0.1896	0.2046	0.0553

Compound No.	**4.6**	**4.7**	**5.1**	**5.2**
Formulae	$C_{16}H_{12}N_3O_3Br$	$C_{16}H_{12}N_4O_6$	$C_{16}H_{16}N_2O_4$	$C_{32}H_{30}N_4O_7$
Mol. wt.	374.20	356.30	300.31	582.60
CCDC No	902576	956990	842527	842528
Crystal system	Triclinic	Triclinic	Orthorhombic	Monoclinic
Space group	*P-1*	*P-1*	$P\ 2_12_12_1$	*P2/c*
Temperature (K)	296 (2)	296 (2)	296 (2)	296 (2)
Wavelength (Å)	0.71073	0.71073	0.71073	0.71073
a (Å)	4.0181(6)	3.7660(3)	10.8806(14)	22.106(3)
b (Å)	13.900(2)	14.0013(13)	19.061(2)	7.0550(8)
c (Å)	15.185(2)	16.2728(15)	6.9842(9)	21.103(2)
α (°)	93.052(8)	94.951(7)	90.00	90.00
β (°)	90.676(8)	92.379(7)	90.00	118.030(6)
γ (°)	93.453(8)	92.182(7)	90.00	90.00
V ($Å^3$)	845.3(2)	853.37(13)	1448.5(3)	2905.1(6)
Z	2	2	4	4
Density/gcm^{-3}	1.470	1.387	1.377	1.332
Abs. Coeff. /mm^{-1}	2.448	0.109	0.100	0.095
Abs. correction	Multi-scan	None	None	None
F(000)	376	368	632	1216
Total no. of reflections	2985	3014	1795	5044
Reflections, $I > 2\sigma(I)$	1438	1799	1518	3281
Max. 2θ (°)	50.48	50.00	44.08	50.00
Ranges (h, k, l)	$-4 \le h \le 4$ $-15 \le k \le 13$ $-16 \le l \le 16$	$-4 \le h \le 4$ $-16 \le k \le 16$ $-19 \le l \le 19$	$-12 \le h \le 12$ $-22 \le k \le 22$ $-8 \le l \le 8$	$-26 \le h \le 25$ $-8 \le k \le 8$ $-23 \le l \le 24$
Completeness to 2θ (%)	0.975	0.998	1.000	98.100
Data/ Restraints / Parameters	2985 / 0 / 208	3014 / 0 / 243	1795 / 0 / 212	5044 / 0 /390
Goof (F^2)	1.102	1.073	1.052	1.165
R indices [$I > 2\sigma(I)$]	0.0741	0.0753	0.0340	0.0836
R indices (all data)	0.1428	0.1202	0.0464	0.1176

Compound No.	**5.3**	**5.4**	**5.5**	**5.6**
Formulae	$C_{16}H_{14}N_2O_3$	$C_{48}H_{42}N_8O_{24}$	$C_{16}H_{14}N_2O_5$	$C_{20}H_{16}N_2O_3$
Mol. wt.	282.29	1114.90	314.29	332.35

CCDC No	843764	843765	842526	870032
Crystal system	Monoclinic	Monoclinic	Monoclinic	Monoclinic
Space group	$P2_1/c$	$P2_1/c$	$P2_1/c$	$P2_1/n$
Temperature (K)	296 (2)	296 (2)	296 (2)	296 (2)
Wavelength (Å)	0.71073	0.71073	0.71073	0.71073
a (Å)	13.602(4)	10.5148(4)	4.6357(4)	11.5532(10)
b (Å)	8.503(2)	10.7588(4)	23.366(2)	10.7257(8)
c (Å)	13.366(3)	22.1402(9)	13.4953(12)	13.8662(10)
α (°)	90.00	90.00	90.00	90.00
β (°)	116.823(8)	102.719(2)	99.715(6)	110.941(5)
γ (°)	90.00	90.00	90.00	90.00
V ($Å^3$)	1379.6(6)	2443.19(16)	1440.8(2)	1604.8(2)
Z	4	2	4	4
Density/gcm^{-3}	1.359	1.516	1.449	1.376
Abs. Coeff. /mm^{-1}	0.096	0.124	0.110	0.094
Abs. correction	None	None	Multi scan	None
F(000)	592	1156	656	696
Total no. of reflections	2667	5944	3566	16063
Reflections, $I > 2\sigma(I)$	1120	4657	1562	1020
Max. 2θ (°)	52.00	56.76	56.70	55.00
Ranges (h, k, l)	$-16 \le h \le 16$ $-10 \le k \le 10$ $-16 \le l \le 16$	$-13 \le h \le 13$ $-14 \le k \le 14$ $-29 \le l \le 28$	$-6 \le h \le 5$ $-28 \le k \le 30$ $-16 \le l \le 16$	$-13 \le h \le 13$ $-12 \le k \le 12$ $-16 \le l \le 16$
Completeness to 2θ (%)	0.981	0.970	0.994	1.000
Data/ Restraints / Parameters	2667 / 0 / 190	5944 / 3 / 420	3566 / 0 / 212	2899 / 2 / 239
Goof (F^2)	0.934	1.455	0.939	0.921
R indices [$I > 2\sigma(I)$]	0.0651	0.1577	0.0626	0.0476
R indices (all data)	0.1380	0.1416	0.1637	0.2038

Compound No.	**5.7**	**6.1**	**6.2**
Formulae	$C_{20}H_{16}N_2O_3$	$C_{44}H_{33}N_5O_4$	$C_{48}H_{41}N_5O_5$
Mol. wt.	332.35	695.75	767.86
CCDC No.	870031	1045039	1045040
Crystal system	Monoclinic	Triclinic	Triclinic
Space group	$P2_1$	*P-1*	*P-1*
Temperature (K)	296 (2)	296 (2)	296 (2)
Wavelength (Å)	0.71073	0.71073	0.71073
a (Å)	7.7707(9)	7.7358(9)	10.332(3)
b (Å)	22.233(3)	12.270(2)	11.304(3)
c (Å)	9.2354(11)	18.895(3)	20.260(13)
α (°)	90.00	102.694(12)	103.43(4)

β (°)	90.105(7)	90.092(10)	102.41(4)
γ (°)	90.00	99.123(9)	95.43(2)
V (Å^3)	1595.6(3)	1726.4(4)	2221.7(16)
Z	4	2	2
Density/gcm^{-3}	1.384	1.338	1.148
Abs. Coeff. /mm^{-1}	0.094	0.087	0.075
Abs. correction	None	Multi-scan	None
F(000)	696	728	808
Total no. of reflections	5051	6246	8052
Reflections, $I > 2\sigma(I)$	3499	2693	2955
Max. 2θ (°)	50.50	50.50	50.50
Ranges (h, k, l)	$-9 \le h \le 9$ $-26 \le k \le 26$ $-11 \le l \le 10$	$-9 \le h \le 9$ $-14 \le k \le 14$ $-22 \le l \le 22$	$-12 \le h \le 12$ $-13 \le k \le 13$ $-21 \le l \le 24$
Completeness to 2θ (%)	0.940	0.999	0.998
Data/ Restraints / Parameters	5051 / 1 / 455	6246 / 0 / 478	8052 / 0 / 515
Goof (F^2)	1.266	1.676	1.283
R indices [$I > 2\sigma(I)$]	0.1305	0.2525	0.1225
R indices (all data)	0.1532	0.3420	0.2376

List of Publication

1. **P. Khakhlary**, J. B. Baruah, Polymorphs and salts of 4-nitro-N-(quinolin-8-yl)benzamide. *J. Mol. Struc*., 2014, **1078**, 188.
2. **P. Khakhlary**, J. B. Baruah, Selective interactions of 5-(hydroxyimino)quinolin-8-one with tetra butyl ammonium fluoride and zinc (II) ions. *RSC Adv*., 2014, **4**, 64643.
3. **P. Khakhlary**, J. B. Baruah, Anion-π interactions in layered structures of salts of 5-(hydroxyimino) quinolin-8-one and related salts. *J. Chem. Sci*., 2015, **127**, 215.
4. **P. Khakhlary**, C. Anson, A. Mondal, A. Powell, J. B. Baruah, Structural and magnetic properties of oxyquinolinate clusters of cobalt (II) and manganese (II) and serendipitous intake of carbonate during synthesis. *Dalton Trans.*, 2015. **44**, 2964.
5. **P. Khakhlary**, J. B. Baruah, Studies on cluster, salt and molecular complex of zinc-quinolinate. *J. Chem. Sci*., 2015, **127**, 95.
6. **P. Khakhlary**, J. B. Baruah, Synthesis and characterization of tri-quinoline based receptors and study interactions with Zn^{2+} and Cu^{2+} ions. *Inorg. Chim. Acta*, 2016, **440**, 53.